Oxidative folding and early traffic of the human cystinuria transporter

Plegamiento oxidativo y tráfico intracelular del transportador humano defectuoso en cistinuria

Mònica Rius Radigales

Facultat de Biologia
Departament de Fisiologia i Immunologia
Programa de Doctorat de Biomedicina

Oxidative folding and early traffic of the human cystinuria transporter

Plegamiento oxidativo y tráfico intracelular del transportador humano defectuoso en cistinuria

Memòria per optar al grau de Doctora per la Universitat de Barcelona
presentada per:

Mònica Rius Radigales

El Director, La interessada,

José Julio Chillarón Chaves Mònica Rius Radigales

Barcelona, 2014

Contents

Abbreviations

4F2HC	surface antigen 4F2 heavy chain
APC	Amino acid polyamine and organic cation transporter superfamily
ATP	adenosine-5'-triphosphate
$b^{0,+}$AT	$b^{0,+}$ amino acid transporter
BiP	immunoglobulin-binding protein
BSA	bovine serum albumin
CFTR	cystic fibrosis membrane conductance regulator
CNX	calnexin
COPI	coat protein complex I
COPII	coat protein complex II
CRT	calreticulin
Cys	cysteine
DMEM	Dulbecco's modified Eagle' medium
dMNJ	deoxymannojirimycin
DMSO	dimethyl sulfoxide
DNA	deoxyribonucleic acid
DTT	dithiothreitol
ED	Edectodomain
EDEM	ER-degradation enhancing mannosidase-like protein
Endo H	Endoglycosidase H
ER	endoplasmic reticulum
ERAD	ER-associated protein degradation
ERGIC	ER Golgi intermediate compartment
FACS	fluorescence activated cel sorting
FBS	fetal bovine serum
GFP	green fluorescent protein
HA	hemagglutinin
HAT	Heteromeric amino acid transporter

HEPES	4-(2-hydroxyethyl)-1-piperazineethanesulfonic acid
HIV	human immunodeficiency virus
HSHAT	heavy subunit of the heteromeric amino acid transporter
HSP	heat-shock protein
IGF	insulin-like growth factor
kb	kilobase
kDA	kiloDalton
LAT	system L amino acid transporter
LDL	low-density lipoprotein
LPI	lysinuric protein intolerance
LSB	Laemmli sample buffer
LSHAT	light subunit of the heteromeric amino acid transporter
mPEG	mPEG5000-maleimide
NEM	N-ethylmaleimide
OST	oligosaccharyl-transferase
PBS	phosphate buffer saline
PCR	polymerase chain reaction
PDI	protein disulfide isomerase
rBAT	related to b0,+AT transporter
RT	room temperature
SDS	sodium dodecyl sulfate
SDS-PAGE	sds-polyacrylamide gel electrophoresis
SLC	Solute carrier
SRP	signal recognition particle
TCA	trichloroacetic acid
UGGT	UDP-glucose: glycoprotein-glucosyltransferase
UPS	ubiquitin-proteasom sustem
VSV	vesicular stomatitis virus
xCT	system xC- amino acid transporter
y^+LAT	system y^{+L} amino acid transporter

Introduction

Mammalian cells express more than 10,000 different protein species, which are synthesized on ribosomes as linear chains of up to several thousand amino acids. To function, these chains must generally fold into their native state. How this is accomplished and how cells ensure the conformational integrity of their proteome is one of the most fundamental and medically relevant problems in biology.

Several studies have yielded major advances in understanding fundamental principles underlying protein folding *in vitro* conditions that have contributed to understand the physicochemical principles of folding landscapes for small, single domain proteins. There has also been an increased research focusing on the key features of protein folding in the cell that differentiate it from *in vitro* folding, such as co-translational folding, chaperone-facilitated folding, and folding in crowded conditions with many weak interactions[1]. Chains may fold co-translationally before the entire chain has been made. In contrast, folding of proteins *in vitro* generally is initiated from an unfolded ensemble in which a population of full- length chains is subjected to folding conditions. This constitutes a major difference between the *de novo* folding reaction in the test tube and in a living organism. Furthermore, the presence of chaperones *in vivo* and other helping proteins avoids accumulation of aggregated proteins. experiments in vitro are done at high dilution. *In vivo*, macromolecule concentrations range from 200 to 400 mg/ml. The impact of crowding and the influence of protein-protein interactions must be taken into account. Folding events *in vivo* are spatially organized in a way that some interactions are preferred over others at different times. This does not occur *in vitro*, where folding takes place in a homogeneous environment. This point is key to the folding of membrane proteins. In fact, little is known on the folding of these type of proteins.

Protein quality control and the maintenance of proteome homeostasis are crucial for cellular and organismal health. This is achieved by an integrated network of several hundred proteins[2], including, most prominently, molecular chaperones and their regulators, which assist in *de novo* folding or refolding and the ubiquitin-proteasome system (UPS), that mediates the timely removal of irreversibly misfolded and aggregated proteins. Understanding these reactions will guide future efforts to define the proteostasis network as a target for pharmacological intervention in diseases of aberrant protein folding. A major challenge nowadays in the study of protein folding is to delucidate what and when chaperones are required for each protein.

1.1 Folding in the Endoplasmic Reticulum

The endoplasmic reticulum (ER) is the entry point for proteins to the secretory pathway. The ER provides an intracellular compartment distinct from the cytosol where post-translational modifications take place and provides a quality control on protein export allowing secretion of proteins that are folded and modified correctly. All polypeptides inserted into the ER are subject to quality control, including soluble and membrane proteins. The ER quality control machinery enables the retention of misfolded proteins within the ER lumen[3]. A signal sequence typically, but not exclusively found in the N terminus of the protein is recognized by the signal recognition particle (SRP)[4] with the resulting ribosome/nascent chain/SRP complex binding to the ER membrane *via* the SRP receptor and is then directed to the Sec61 translocon, which allows the translocation of the growing polypeptide chain across the membrane and into the ER. The rapid targeting of the nascent polypeptide chain to the ER ensures that translocation occurs co-translationally, meaning that the folding of the polypeptide chain will take place within the lumen of the ER. Several molecules including lectins, N-glycan processing enzymes, protein disulphide isomerases and molecular chaperones have been identified to participate in the quality control of the ER. Not all proteins use the same chaperones, some use more than one simultaneously or sequentially.

1.1.1 ER chaperones

Chaperones are involved in a multitude of cellular functions, including *de novo* folding, refolding of stress-denatured proteins, oligomeric assembly, intracellular protein transport and assistance in proteolytic degradation[5]. Members of these protein families are often known as stress proteins or heat-shock proteins (HSPs), as they are up-regulated under conditions of stress in which the number of protein aggregated folding intermediates increase. The ER contains chaperones from the Hsp70 and Hsp90 families[6]. They are multicomponent molecular machines that promote folding through ATP- and cofactor-regulated binding and release cycles. They typically recognize hydrophobic amino acid side chains exposed by non-native proteins and may functionally cooperate with ATP-independent chaperones, such as the small HSPs as Hsp60 in mammals and GroEl in yeast, which function as holdases, buffering aggregation[7].
Their range of substrates and roles in the ER are diverse. The ER Hsp70 family member is called BiP in metazoans or Kar2p in yeast. BiP is the most abundant

ER chaperone. It is usually the first chaperone to bind the nascent chain, and binds preferentially surfaces with alternating aromatic and hydrophobic amino acids[8]. The regions bound by BiP are predicted to exist quite frequently in protein sequences[9] allowing BiP to facilitate translocation of the nascent chain into the ER lumen[10]. J-domain proteins (Hsp40) binds to Hsp70 and stimulates its ATPase activity. While BiP associates with nascent chains immediately and transiently upon synthesis[11], its association with misfolded mutant proteins is prolonged[12]. This prolonged association might be a signal for degradation of the substrate protein, and evidence suggests that prolonged association to BiP of several misfolded substrates as ΔF508-CFTR leads to degradation[13].

A member of the Hsp90, GRP94, is an essential gene in metazoans as it is required for early developmental stages in mice, Arabidopsis, Drosophila, and C. elegans[14–17], yet many unanswered questions remain about its role in ER homeostasis and its mechanism of action. There are few confirmed substrates of GRP94 although it is one of the most abundant proteins of the ER. GRP94 participates in the folding of heavy and light chains of immunoglobulins[18]. The mammalian insulin-like growth factor (IGF)-I and -II also depend on GRP94 for their maturation[19,20]. Surprisingly the activity of GRP94 in unicellular organisms is not essential or in some cases such as yeast, it is even absent. The substrate-binding site for GRP94 has not yet been elucidated. This may be attributable to there being a large surface of interactions[21,22].

1.1.2 Oxidative folding in the ER

Newly synthesized proteins fold into functional 3-dimensional conformations stabilized by non-covalent interactions as van der Waals interactions, hydrogen bonds and the hydrophobic effect but also form disulfides, covalent bonds formed between the side chains of two cysteine residues. Disulfide bonds are crucial for the biosynthesis and function of many proteins. They promote structural stability, facilitate the assembly of multi-protein complexes and can modulate redox-dependent functions in response to changes in the cell[23]. Disulfide bonds can also mediate the formation of productive folding intermediates[24]. The formation of disulfides starts as the protein is being cotranslationally translocated into the ER[25]. However various proteins have been described to finalize their oxidative folding in a post-translational way[26–29]. Disulfide bonds can also be determinant for the functionality a proteins as has been described for the prokaryotic Cu,Zn-

superoxide dismutase that requires the formation of an intramolecular disulfide bond for is enzimatic activation[30].

Disulfide bond formation in the ER is catalyzed by the PDI family of dithiol-disulfide oxidoreductases[31]. PDI was the first ER oxidoreductase to be extensively characterized. It is an essential enzyme in yeast, and has been shown to function as a chaperone as well as introduce disulfide bonds into substrates[32–34]. About 20 proteins have been assigned to this family to date; with 15 members containing a thioredoxin-like fold, with characteristic CXXC motifs in their active site. These proteins catalyze thiol-disulfide exchange reactions by acting as electron acceptors during disulfide bond formation or as electron donors during breaking of disulfides. The PDI proteins also catalyze isomerization reactions by rearranging non-native to native disulfide[24]. One of the members of the PDI family, ERdj5, has been shown to break disulfides to facilitate the unfolding of proteins destined for degradation in the cytosol[35]. There is evidence that the diferent PDI proteins have substrate specificities and defined roles[36]. PDI contains a hydrophobic region that could help to inhibit aggregation of misfolded proteins, acting as a chaperone[37]. A study using as a model the 27th Ig domain that contains a single disulfide bond suggests that protein folding occurs prior to disulfide formation[38]. When PDI and other oxidoreductases introduce disulfides into newly synthesized proteins, their active sites have to be re-oxidized to allow for further rounds of disulfide formation. This function is fulfilled by specific ER-resident oxidases. These enzymes catalyze the first step in disulfide formation by transferring oxidizing equivalents to the PDI proteins, which then introduce these disulfides into nascent polypeptides[39–42]. The first of the ER oxidative pathways for *de novo* disulfide formation to be identified involves the ER oxidoreductin 1 protein (Ero1). This enzyme was initially characterized in yeast where it was shown to be essential for disulfide formation in PDIp[43,44]. Mammals and other vertebrates have two Ero1 paralogs: Ero1α which is present in all tissues and Ero1β which shows some tissue specific expression[45,46]. The Ero1 proteins use FAD as a cofactor to transfer electrons from PDI to molecular oxygen, forming hydrogen peroxide in the process[47,48].

During the folding of secretory pathway proteins, native intramolecular and intermolecular disulfide bonds can form co-translationally, before more C-terminal regions of the protein have entered the ER[25]. This can occur when the bonds form between adjacent cysteines[50,51] or when the protein is composed of autonomously

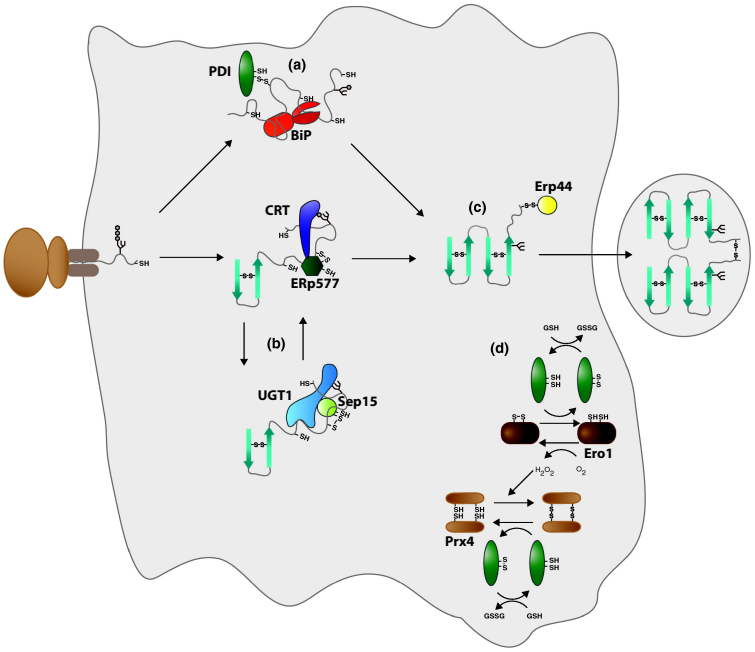

Figure 1.1. Overview of the oxidative folding in the ER. Proteins enter the ER co-translationally as unfolded polypeptide chains. (a) If they are non-glycosylated, they can bind BiP and PDI. (b) Glycoproteins interact with the CNX/CRT system. CRT interacts with the PDI family member ERp57. When folded, the proteins can leave the CNX/CRT cycle, if not, UGT1, which can cooperate with Sep15, another member of the PDI family, re-glucosylates the substrate allowing the protein to re-enter the CNX/CRT cycle. (c) Once folding is nearly complete, any free thiols remaining can covalently engage ERp44, avoiding premature transport to the Golgi until these thiols are buried or part of a disulfide bond. (d) PDIs can be oxidized by Ero1, which generates H_2O_2. This can be used indirectly to oxidize Prx4, which in turn oxidizes PDI generating two disulfide bonds per molecule of O_2. Figure adapted from Feige MJ and Hendershot LM 2011 [49].

folded domains [52]. Formation of non-native disulfides, also takes place, which need to be broken, and correct ones need to be formed so that the protein adquires its correct folding. Non-native disulfides could stabilize on-folding intermediates being therefore crucial for the efficient folding of some proteins. For example, a disulfide that forms between a cysteine residue within the prosequence of bovine pancreatic trypsin inhibitor greatly facilitates folding of this protein [53]. This disulfide is not present in the final native structure. In addition, the folding of the LDL receptor requires the formation of several non-native disulfides [54,55].

Another key element to understand is how do reductases distinguish between native disulfide bonds that need to be left untouched and nonnative disulfide bonds that need to be broken. It is possible that they are not able to distinguish them and that they reduce any disulfide bonds they encounter. The key may lie in the burial of native disulfides inside the folded protein. Native disulfide bonds may not

be accessible anymore, as illustrated by the high resistance to reducing agents of folded proteins[56]. Whereas disulfide-bond formation follows folding and does not drive protein folding directly, disulfide-stabilized folding intermediates do drive the equilibrium of the sequential folding steps forward, away from the unfolded state and toward the folded state of the newly synthesized protein.
Other disulfide bonds have been reported to form post-translationally. Influenza virus hemagglutinin (HA), for instance, does form its first two disulfide bonds during synthesis, but the subsequent set can form either during or after translation[25]. HA can even postpone disulfide formation completely until after chain termination[57]. In fact, various newly synthesized proteins tested can tolerate the postponing of disulfide bond formation until after chain termination and full translocation as vesicular stomatitis virus (VSV) G protein[58], low-density lipoprotein (LDL) receptor[54], tissue plasminogen activator[59], thyroglobulin[60], gp160 protein of HIV-1[61] and yeast carboxypeptidase Y.

1.1.3 Role of N-glycans in degradation and folding in the ER

The presence and location of bulky hydrophilic N-glycans within glycoproteins is thought to favor glycoprotein folding and transport[62,63]. N-glycans are highly flexible and hydrophilic structures that mask hydrophobic areas on proteins having an important effect in the protein folding process or the stability of the native glycoprotein conjugate[64,65]. The N-linked glycan is comprised of 2 N-acetyl glucosamines (GlcNAc) and 9 mannoses (Man) arranged in 3 branches with 3 glucoses (Glc) attached to the first branch mannose residue (Glc3Man9). Glycan processing starts immediately after its transfer from a dolichol-P-P derivative to Asn residues in nascent polypeptide chains entering the lumen of the ER by the oligosaccharyltransferase (OST) that is associated with the Sec61 translocon[66]. There are a number of lectins within the ER that show a remarkable range of glycan specificities. The first step is the removal of the outermost glucose unit from the glycan generated by the action of glucosidase II on the Glc2Man9 glycan after processing of Glc3Man9 by glucosidase I, or by the addition of a glucose moiety by UGGT. UGGT can act on misfolded glycoproteins in the ER and reglucosylate them so that they can rebind these lectin-like chaperones and undergo further folding cycles, ensuring that escape from the calnexin/calreticulin (CNX/CRT) cycle only takes place when folding is correct[67] (Figure . Binding and release are determined by monoglucosylation of the sugar chain[68]. The type 1 membrane protein CNX and the closely related ER luminal protein CRT both have specificity for the Glc1Man9 N-glycan[62,69]. CNX and CRT promote the efficient folding of gly-

coproteins by stabilizing folding events or slowing the folding process in a domain specific manner[68,70,71] and preventing aggregation and degradation[68,72]. They also retain non-native substrates in the ER to support additional attempts for proper folding[73] and facilitating disulfide bond formation through their association with the PDI ERp57[74–77].

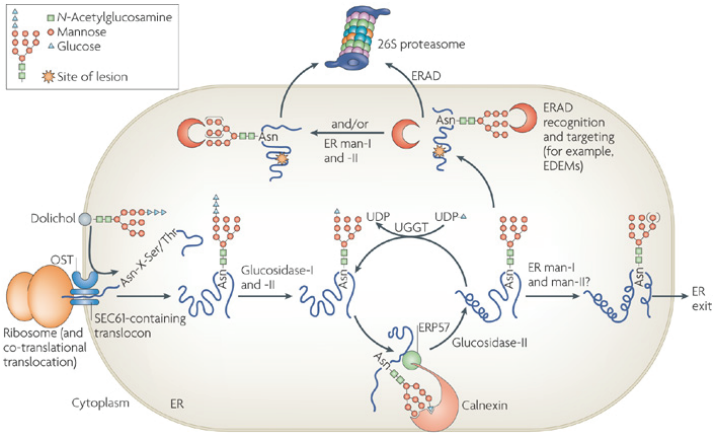

Figure 1.2. N-linked glycosylation and the degradation of glycosylated proteins. Figure adapted from Vembar et al. 2008[78].

The N-glycans present in a protein do not play equivalent roles in protein processing. Single glycans can play a major role in promoting the correct folding[79] but can also target misfolded glycoproteins for ER-associated degradation in yeast[80,81]. This has already been shown previously for some proteins as for the cystic fibrosis membrane conductance regulator (CFTR), a channel protein involved in the pathology of the cystic fibrosis[82]. In this case, glycans are required for CNX and ER-degradation enhancing mannosidase-like protein (EDEM) binding but not for the channel function, with the N900 glycan promoting folding and the N894 glycan supporting degradation. The simian virus 5 hemagglutinin-neuraminidase protein (HN), a model class II integral membrane glycoprotein contains 4 N-glycans. Alterations in the normal glycosylation pattern resulted in the impairment of HN protein folding and assembly which, in turn, affected the intracellular transport of HN. The consequences on HN maturation depended on both the number of deleted carbohydrate sites and their position in the protein. The study also shows that the N267 N-glycan plays a major role in promoting the correct folding of HN. Furthermore, the N110 N-glycan, which is not essential for the initial folding of HN, was found to play a role in preventing the aggregation of HN oligomers[79]. Another example is the yeast carboxipeptidase Y, a soluble glycoprotein with four N-linked glycans targeted through the Golgi to the yeast vacuole.

Only the C-terminal N-glycan drives the polypeptide into the degradation pathway, with the N-terminal glycans involved in efficient intracellular transport [80] [81].

1.1.4 Degradation of N-glycoproteins

A significant fraction of newly synthesized polypeptides entering the ER fails to acquire a native conformation [7]. The ER-associated protein degradation (ERAD), monitors the folding of membrane and secretory proteins whose biogenesis takes place in the ER [83]. The misfolded molecules are retained in the ER and eventually become substrates of the ERAD, a collection of quality-control mechanisms that clears the ER from these potentially harmful species. The removal of a number of ERAD components leads to embryonic lethality in mice, highlighting the importance of this process [84–86].
The features recognized on the misfolded proteins by these ERAD factors are largely unknown. A long ER residency, indicative of folding problems, results in the processing of the misfolded glycoproteins by Htm1, which generates a biochemical mark (α1,6-linked mannose) decoded by the lectin Yos9, an ERAD substrate recognition factor [87,88]. Both yeast Htm1 and its mammalian homologue EDEM are in complex with oxidoreductases (Pdi1 in yeast, Erdj5 in mammals), required for the stability of Htm1 and also for reducing disulfide bonds in misfolded proteins, which might affect subsequent ERAD steps [35,88].

The proteins are finally directed to ERAD generally by ubiquitinilation of the target proteins. The ubiquitin system mediates the covalent attachment of ubiquitin, a small 76-amino acid protein, to target proteins in the cytoplasm by the sequential action of activating (E1), conjugating (E2), and ligase (E3) enzymes [89]. Ubiquitin-modified proteins are then recognized and degraded by the proteasome. This pathway includes multiple elements that have distinct specificity for different classes of misfolded proteins [90–94]. The first step in the degradation of an ERAD substrate is the recognition of this substrate in the ER environment. Then the substrate is retrotranslocated back into the cytoplasm. On the cytosolic side of the ER membrane, the substrate is ubiquitinated by E3 ligase. Subsequently, the ubiquitinated substrate is extracted from the membrane in an ATP-dependent manner and released in the cytoplasm for degradation by the proteasome. These E3 ligase complexes a re best characterized in yeast where Doa10 [95] and Hrd1 [96,97] assemble into the Doa10 and the Hrd1 complexes, respectively, each responsible

for the degradation of a class of ERAD substrates[92]. Proteins with misfolded domains in the cytoplasmic side of the membrane (ERAD-C substrates) are degraded via the Doa10 complex; proteins with luminal (ERAD-L substrates) or intramembrane (ERAD-M substrates) misfolded domains are targeted to the Hrd1 complex[90–92]. In mammalian cells the best-studied E3 ligases are Hrd1 and Gp78. They are both homologous to yeast Hrd1 but assemble distinct E3 ligase complexes that preferably target different substrates[93,94,98–100]. Several more E3 ligases have been implicated in ERAD in mammalian cells (such as Rma1/Rnf5, Trc8, Rfp2, Rnf170, and Rnf185) but these are still poorly characterized[101–105].

1.2 Elements involved in the ER-exit of proteins

Secretory proteins contain sorting elements that are deciphered by the intracellular transport machinery at multiple stages to route proteins to their proper location. Clathrin and coat protein complexes I and II (COPI and COPII), have been described as multisubunit elements that recognize specific protein sorting signals and can selectively sort proteins into carrier vesicles. Direct binding interactions between coat subunits and specific cargo often determine inclusion into the forming carrier vesicle. However, adaptor proteins or transmembrane receptors are sometimes needed for efficient linkage of cargo to a coat protein complex. A robust quality control system operates in the ER to ensure that nascent cargo is retained and/or not recognized by the export machinery until the cargo is fully folded and assembled[78]. COPII efficiently recognizes and segregates vesicle cargo away from ER resident proteins for incorporation into budding vesicles[106,107]. Several studies have identified sorting signals displayed on cytosolic surfaces of transmembrane cargo that direct these proteins into COPII vesicles[108]. The Sec23-Sec24 complex associates with transmembrane cargo proteins in a sorting signal-dependent manner[109,110]. Structural studies on COPII have revealed multiple cargo recognition sites, within the Sec24p subunit, that bind to defined sorting signals[111,112]. Moreover, cells are endowed with multiple Sec24p isoforms to greatly expand the diversity of export signals that can be recognized by the COPII sorting machinery[113,114].

Several abundant membrane proteins have been identified that localized to early secretory compartments and to transport intermediates, which are potential receptor candidates, including the ERGIC-53 protein[115], the p24 proteins[116–118], and a set of ER vesicle (Erv) proteins[119–121]. ER sorting receptors are thought to

cycle between the ER and Golgi compartments in COPII-and COPI-derived vesicles, where the receptors would shuttle specific secretory cargo forward through cargo binding in the ER-followed by dissociation in the ERGIC or cis-Golgi compartments.
ERGIC-53 is an oligomeric single-pass transmembrane protein with a larger N-terminal lumenal domain and a short, cytoplasmically exposed 12 amino acid C-terminal tail sequence[122]. Overexpression of a dominant-negative ERGIC-53 mutation in cultured cells specifically blocks transport of the lysosomal glycoprotein cathepsin C[123]. Pulse-labeling experiments showed that nascent cathepsin Z-related protein bounds to ERGIC-53 in the ER and was dissociated in post-ER compartments[124] in accord with a cargo-receptor function. Additional studies demonstrated that cargo binding is pH dependent, that a conserved histidine residue at the carbohydrate-binding site of ERGIC-53 may serve as a pH sensor for cargo binding, and that elevation of lumenal pH *in vivo* specifically retards dissociation of cathepsin Z from ERGIC-53[125]. ERGIC-53 recognition of cargo relies on interactions with both N-linked carbohydrate as well as protein motifs. For procathepsin Z, a folded surface-exposed β-hairpin loop, which is next to the critical N-linked glycan site, was required for efficient binding[126]. It has been also described that ERGIC-53 loss of function caused inefficient ER export of the glycosylated coagulation factors V and VIII[127] and presumably reduces their secretion from hepatocytes into the plasma[128].
ERGIC-53 belongs to a family of related Ca^{2+}-dependent L-type lectins that are widespread in nature and include ERGL, VIP36, and VIPL proteins in animal cells[129]. Each of these L-type lectin family members has distinct binding activity toward high-mannose-type oligosaccharides[130].

The Erv proteins have also shown to recognize structural motifs[131,132]. Strains were any Erv is deleted display unfolded protein response pathway[121,133,134], indicating quality control issues in the ER. For example, the turnover rate of CPY$*$, a terminally misfolded ERAD substrate, is reduced in strains lacking Erv29p. Wild-type CPY normally depends on Erv29p for efficient export from the ER, and this stabilizing effect appears specific for CPY$*$ as other ERAD substrates are not influenced by erv29Δ[135].

1.3 Formation of conformational motifs and protein oligomerization in the ER

Protein subunits can play an important role in folding and/or exit of the ER. A particular heteromeric complex subunit may be necessary for the correct folding of other subunits of the same complex in other cases the folded subunits have to be assembled in order to be recognised by the ER-exit machinery.

Some protein complexes suffer *in vivo* post-assembly folding of selected subunits. DM α and β-chains of the HLA-DM, an heteromeric MHC molecule, fold, oxidize, and form a complex in the ER. Single DMα chains cannot fully oxidize without DMβ, while DMβ forms disulfide-linked homodimers without DMα. Correct oxidation and subsequent ER exit depend on the DMβ C25 and C35 residues. Another example is the TCRα subunit that is rapidly degraded in the ER when it is expressed in the absence of the other subunits[136].
Heteromeric cargo proteins can have an ER export signal only when the subunits are correctly folded and assembled. For example, a subfamily of mammalian inwardly rectifying potassium channels, Kir3, possesses four members that can combine in different permutations to yield active channels. Homotetramers of one member, Kir3.1, are not functional because these assemblies are retained in the ER. Kir3.1 lacks any ER export signals and therefore relies on signals found on its partners for efficient transport from the ER[137]. This may reflect an additional quality control step, such that only properly assembled complexes are selected for forward transport, leaving unassembled monomers behind to search for an appropriate partner or to interact further with the ER folding machinery.

1.4 Heteromeric amino acid transporters

The Heteromeric amino acid transporter family (HAT) belong to one of the 5 transporters superfamilies that have been described, the Amino acid, Polyamine and Organic Cation transporter superfamily (APC) that includes transporters in yeast, plants and animals[138,139]. They constitute one of the eleven families involved in amino acid transport across cell plasma membrane in mammals[140]. The amino acid transporters are classified according to their sequence homology and their functional properties as substrate specificity and transport mecanism. The HAT family is the only one that contains a heavy subunit (HSHAT) and a

light subunit (LSHAT) being the latter the one that confers substrate specificity and transport activity, assembled by a disulfide bridge which is conserved in all the family members[141–143]. A common feature of HATs is that they are obligatory exchangers, with the exception of system asc isoforms that also mediate facilitated diffusion[144].

1.4.1 Heavy subunits

This family, also known as Solute Carrier 3 (SLC3), is formed by 2 proteins: rBAT (related to $b^{0,+}$ amino acid transporter), also named SLC3A1, D2 and NBAT, and 4F2hc (SLC3A2, also named CD98hc and FRP). Heavy subunits are type II membrane N-glycoproteins with an intracellular N-terminus, a single transmembrane domain, and a bulky extracellular C-terminus[145]. These 2 heavy subunits share 30 % identity and 50 % similarity[146–149].The cysteine residue that forms the disulfide bridge with the corresponding light subunit is four to five amino acids away from the transmembrane domain. The bulky extracellular domain of SLC3 members has sequence and structural homology with insect maltases and bacterial α-glucosidases[145,150]. The crystal structure of the human ectodomain of 4F2hc has been solved at 2.1 $\dot{A}$ resolution. It contains the characteristic protein fold of these enzymes: a $(\beta\alpha)_8$ barrel (domain A) and a C-terminal, anti-parallel β $_8$ sandwich (domain C), but no domain B[145]. Despite this structural similarity, 4F2hc lacks the key catalytic residues necessary for glucosidase activity[145]. The atomic structure of the rBAT ectodomain (rBAT-ED) has not been solved, but sequence homology with glucosidases suggests that in addition to domains A and C, rBAT-ED has also domain B. No glucosidase-like activity has been described for rBAT. The heavy subunit is essential for trafficking of the holotransporter HAT to the plasma membrane, whereas the light subunit catalyzes the transporter function[151,152]. So far, heavy subunits have been described to be necessary for the arrival of the light subunit to the plasma membrane. It is still unknown if they perform any role in the amino acid transport specificity or the kinetics of the transporters. The specifc role of the large ectodomain of the heavy subunits of HATs remains largely unknown and no catalytic activity has yet been attributed to it[145].

rBAT (SLC3A1)

rBAT was the first identified subunit of HATs and was cloned as the result of functional expression assays in *Xenopus laevis* oocytes. rBAT expression induced

a high Na^+-independent uptake of dibasic and neutral amino acids[146,148]. Immunocytochemistry assays demonstrated that rBAT localizes in the brush border membranes of epithelial cells from small intestine and from renal proximal tubule, where rBAT expression increases from S1 to S3 segments[153–155]. No function besides targeting of $b^{0,+}$AT to the plasma membrane has been reported. The rBAT/$b^{0,+}$AT heterodimer oligomerizes into stable heterotetramers expressed in the brush bordermembranes of the epithelial cells from renal proximal tubule[156]. Chimerical fusion proteins of rBAT with 4F2hc-light subunits also show functional heterotetramers, suggesting that the heavy subunit dictates the oligomerization state[156]. Initial studies in the biogenesis of rBAT/$b^{0,+}$AT have shown that the co-expression of $b^{0,+}$AT and rBAT is required for the functional expression of system $b^{0,+}$ in the plasma membrane of non-polarized cells and in the apical membrane of polarized cells[157–159]. When expressed alone rBAT is retained and degraded by the ERAD[157]. Assembly of $b^{0,+}$AT with rBAT in the ER abolishes degradation of rBAT. Furthermore, the C-terminus of the light subunit $b^{0,+}$AT has an active contribution to the intracellular trafficking of the heterodimeric transporter[159]. Transport activity performed by the rBAT/$b^{0,+}$AT heterodimer constitutes the main apical reabsorption system for cystine in kidney[160]. Thus, mutations in either of the transporter subunits cause cystinuria (see Section 1.5).

4F2hc (SLC3A2)

4F2hc was found to share sequence similarity with rBAT. The synthetic 4F2hc RNA was tested in *Xenopus oocytes* and found to induce amino acid transport activity in this system. 4F2hc induced Na^+-independent uptake of cationic and Na^+-dependent uptake of large neutral amino acids high affinity transport. In the absence of Na^+, 4F2hc was also able to transport neutral amino acids with less affinity[147,149]. 4F2hc-associated transporters are ubiquitously expressed and is located in the basolateral plasma membrane in epithelial cells[140]. Besides being the heavy subunit of several amino acid transporters, 4F2hc is involved in a variety of cell functions. It mediates β-integrin signaling[161], cell fusion[162,163] and cell proliferation[164,165]. 4F2hc-associated transporters are overexpressed in cancers and in activated lymphocytic cells suggesting a role of 4F2hc and these transporters in cell growth[166–173]. 4F2hc-dependent β-integrin signaling might be at the basis of these roles in the case of 4F2hc, but how 4F2hc mediates integrin signaling is unknown[161,163].

1.4.2 Light subunits

HAT light subunits (LSHAT) are members of the Solute Carrier 7 family (SLC7)[138]. Until now, 10 light subunits have been identified in vertebrates. 6 of them assemble with 4F2hc: LAT-1, LAT-2, y^+LAT-1, y^+LAT-2, asc-1, xCT; 1 of them, $b^{0,+}$AT, with rBAT. Asc-2, AGT-1 and ArpAT are linked to an unknown heavy subunit. Light subunits are highly hidrophobic, non-glycosilated proteins of ∼50 kDa. LSHAT needs coexpression with its correspondant HSHAT to arrive to the plasma membrane, although the disulfide bond is not necessary for this function[141]. Cysteine-scanning mutagenesis studies support a 12-transmembrane-domain topology, with NH2 and COOH termini located inside the cell and with a reentrant-like structure in the intracellular loop IL2-3 for xCT, as a model for the light subunits of HATs[174]. They confer transport specificiy to the transporter: LAT-1 and LAT-2 transport large neutral amino acids[175–178], small (asc-1, LAT-2)[179]; negatively charged (xCT) and basic and neutral amino acids (y^+LAT-1, y^+LAT-2 and $b^{0,+}$AT)[155,180–184] (Table 1.1). The catalytic subunit $b^{0,+}$AT is functional in the absence of the heavy subunit rBAT[185]. Combinations amongst the different light and heavy subunits of HATs lead to a broad spectrum of amino acid transport systems. These systems provide the cell with the amino acids needed as well as with a mechanism that allows the cell to adapt and respond to changes in the environment.

Table 1.1. Heteromeric amino acid transporters

Heavy chain	Light chain	Gene	Amino acid transport	Inherited aminoaciduria
4F2hc		SLC3A2		
	y+LAT1	SLC7A7	y+L	LPI
	y+LAT2	SLC7A6	y+L	
	LAT1	SLC7A5	L	
	LAT2	SLC7A8	L	
	asc1	SLC7A10	asc	
	xCT	SLC7A11	xc-	
rBAT	SLC3A1	cystinuria		
	$b^{0,+}$AT	SLC7A9	$b^{0,+}$	cystinuria
?				
	AGT1	SLC7A13		
	asc2	SLC7A12	asc	

1.4.3 HATs structure

HSHATs structure

rBAT and 4F2hc have almost identical hydrophilicity profiles and contain an extracellular cysteine residue located four amino acids from their transmembrane regions. The amino acid sequence of the large ectodomains (∼50-60 kDa) of rBAT and 4F2hc share identity with bacterial α-amylases. In general, α-amylases are composed of three domains: a TIM barrel containing the active site residues and chloride ion-binding site (domain A), a long loop region inserted between the third β-strand and the third α-helix of domain A that contains calcium-binding sites (domain B, and a C-terminal β-sheet domain which, although presenting some variability in sequence and length between amylases, is always present in such proteins (domain C)[186].

It has not been possible, so far, to purify and crystallize whole 4F2hc or rBAT, thus, structure of heavy subunits remains unknown. However, the structure of the ectodomain of human 4F2hc has been solved (Figure 1.3)[145] and from there the ectodomain of rBAT was modelled.

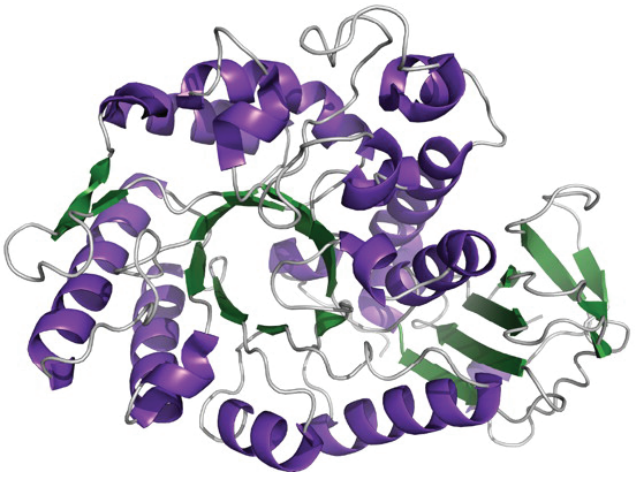

Figure 1.3. Structure of the 4F2hc ectodomain. Upper view of 4F2hc-ED structure. The structure is similar to that of α-glycosidases, including two domains: a TIM-barrel $(\beta/\alpha)_8$ and a C-terminal domain with eight antiparallel β-sheets.

The secondary and tertiary structure of rBAT has been predicted based on amino acid sequence similarity with 4F2hc (30 %) and with prokaryotic α-amylases (32 %)[187]. The human rBAT protein (685 amino acid residues) contains approximately 150 residues more than human 4F2hc (529 amino acid residues). The ectodomain of rBAT probably consists of three domains: A and C domains, as

in 4F2hc, and the B domain (a $\alpha 2\beta 3$ loop) characteristic of α-amylases. Because B domains of rBAT and oligo-1,6-glucosidase from Bacillus cereus (PDB: 1UOK) present high amino acid sequence identity (49 %) the B domain of rBAT was modeled using the structure of this α-amylase as a template. However, no α-glycosidase activity has been described for rBAT.

1.4.4 LSHATs structure

The structure of the bacterial APC transporters arginine/agmatine antiporter (AdiC)[188–191], H^+-coupled amino acid transporter (ApcT) ([192] and glutamate/GABA antiporter (GadC)[193] are the present structural models of the light subunits of HATs (Figure 1.4). These structures present low amino acid sequence identity with LAT transporters (∼18 %), however, they display topological features similar to them[174]. This suggested that they may share similar secondary and tertiary structures. The two solved APC transporters present the same 5+5 inverted symmetry motif fold. The two-fold-related 5+5 transmembrane repeat defines the fundamental machinery of transport. The two interior pairs of symmetry related helices (the TM1/TM6 domains and TM3/TM8 domains) define the central translocation pathway that contains the binding sites for substrate and ions in transporters sharing the 5+5 inverted repeat fold. Crystal structures of AdiC bound to its substrate L-arginine[190,191] show a substrate binding site similar to that of LeuT. Although direct evidence is lacking, the substrate binding site of LAT transporters is assumed to be similar, involving interaction of residues in TM1, TM3, TM6, and TM8, as indicated by Substituted-Cysteine Accessibility Method (SCAM) of SteT, a prokaryotic member of the LAT family[194].

Mutations in HATs are responsible for aminoacidurias such as cystinuria, caused by mutations in $b^{0,+}$AT or rBAT and Lysinuric Protein Intolerance (LPI) caused by mutations in y^+LAT1.

1.5 Cystinuria

Cystinuria (OMIM 20200) is an autosomal recessive disorder with an average prevalence of 1 in 7000 births, but it ranges from 1 in 2500 births in Jewish Israelis of Libyan origin to 1 in 100,000 in Sweden[195,196]. The hallmark of cystinuria is hyperexcretion of cystine and dibasic amino acids: lysine, arginine and ornithine into urine[195,197] due to the defective transport of these amino acids across the apical membrane of epithelial cells of the renal proximal tubule and small intes-

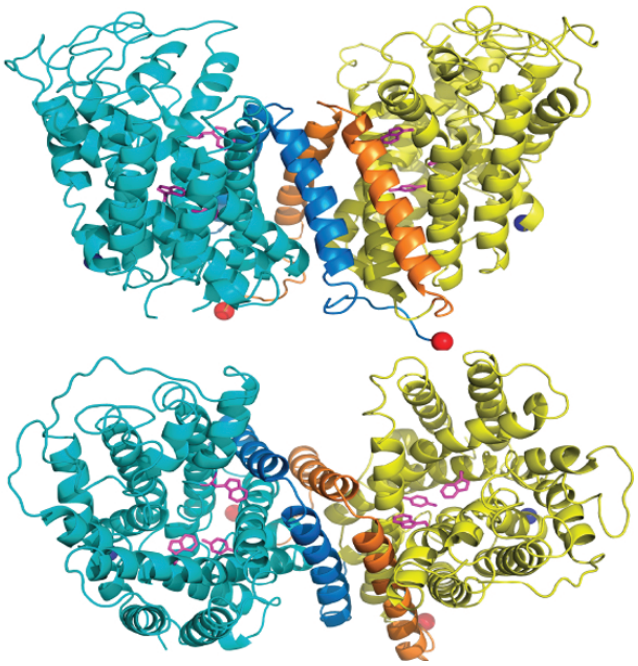

Figure 1.4. Structure of the AdiC. Ribbon diagrams of homodimer viewed from membrane, extracellular side up (top) and from extracellular solution (bottom). N- and C-termini are indicated by blue and red spheres, respectively.

tine[198–200]. The elevate concentrations of lysine, arginine and ornithine in urine do not cause any known disease. However, cystine, due to its low solubility, precipitates and forms renal cystine calculi (lithiasis) that can cause obstruction, infection and ultimately chronic kidney disease. Cystinuria patients do not suffer from malnutrition because the intestinal apical transporter solute carrier family 15 member 1 facilitates the apical absorption of dipeptides and tripeptides from dietary protein, which makes up for the loss of cysteine, lysine and arignine[201]. 50% of the patients suffer nefrolithiasis during the first 10 years of life[202,203]. Cystinuria causes 1-2% of all cases of renal lithiasis and 6-8% of renal lithiasis in pediatric patients[204]. These calculi are persistent: only 44% of patients remain free of stones after 3 months of their extraction[205].

At present, cystinuria treatment is focused in avoiding stones formation. Cystine excretion is reduced by restricting intake of dietary sodium[206–208] and animal proteins. As tubular cystine reabsorption is sodium-independent, the cause of the association of reduced cystine excretion with reduced sodium intake is unknown[206]. The reduction in the intake of animal protein reduces the intake of cystine and its precursor methionine[209], leading to alkalinization of the urine, which also increases cystine solubility. Among the methods used to increase cystine solubility in urine are increasing urine volume, increasing urine pH and reducing cystine to

cysteine which is more soluble. Increasing oral fluid intake should help to decrease the urine cystine concentration to <1 mmol/l, with 3-4 l of urine output required daily for the excretion of 1 g of cysteine per day. Cystinuria patients should maintain high urine flow rates throughout the day and consume fluids before bedtime in order to decrease the nocturnal aggregation of crystals.
An important determinant of cystine solubility is urine pH. The solubility of cystine in urine increases to ∼2 mmol/l at ⩾pH 7.5[210]. The most useful mean of achieving the increase in urine pH is by oral administration of potassium citrate and is not associated with the increase in cystine excretion that occurs after administration of sodium citrate[211]. Decreasing the intake of animal protein also decreases net acid excretion, increasing the urine pH and reducing the dose of potassium citrate required to alkalinize the urine. Acetazolamide has been recommended as an additional means to increase urine pH but it is not well tolerated and has not been shown to be superior to citrate[212]. The two most commonly agents commonly used are D-penicillamine and α-mercaptopropionylglycine, also known as tiopronin. These drugs work by reducing the disulfide bond between the two cysteines that form cystine. The thiol group of the drugs combines with cysteine to form a soluble cysteine-drug product. The solubility of the cysteine-penicillamine complex is up to 50-fold higher than that of cystine[213]. Often urological interventions are indicated for the management of cystine stones >5 mm in diameter. Cystine stones are less amenable to successful therapy with extracorporeal shock wave lithotripsy (SWL) than calcium oxalate stones[214]. Other cystine stones have a low degree of radiopacity and may not make easy targets for shock waves. For these reasons, ureteroscopy with a holmium laser may be the preferable modality of stone removal in patients with cystine lithiasis[215].

1.5.1 Classification of cystinuria

Three phenotype of cystinuria have traditionally described[216] on the basis of the urinary excretion of cystine and dibasic (lysine, arginine and ornithine) amino acids of the obligate heterozygous parent-type I, type II, and type III. Obligate heterozygotic relatives of patients with type I cystinuria have normal aminoaciduria, whereas obligate heterozygotic relatives of individuals with type II and III cystinuria had high or moderate hyperexcretion of cystine and dibasic amino acids, respectively. However, this classification correlates poorly with the extent of hyperaminoaciduria observed in heterozygotic indivi- duals who carry the same mutation, which has resulted in the classification of cystinuria being revised to type I, that includes patients formerly also classified as "type I", non-type I, that includes

the former type II and type III, and mixed type cystinuria, also known as type I/non-type I[181]. In type I cystinuria, both parents of affected individuals are type I heterozygotes, which means that they do not have hyperaminoaciduria (that is, the mode of inheritance is recessive). In non-type I cystinuria, patients inherit non-type I alleles from both parents. Non-type I heterozygous individuals have a variable degree of urinary hyperexcretion of cystine and dibasic amino acids; however, production of cystine calculi has been described very infrequently in these individuals[217]. Non-type I cystinuria should, therefore, be considered an autosomal dominant disease with incomplete penetrance for the cystine lithiasis trait. Patients with a mixed type cystinuria, who inherit type I and non-type I alleles from either parent have also been described[181,217,218]. Of the 97 phenotyped families from the International Cystinuria Consortium cohort, which includes mainly patients from Europe and Israel, 37 are type I, 46 are non-type I, and 14 are mixed type[217].

1.5.2 Genetics of cystinuria

Positional genetics[219] and mutational analysis[220] demonstrated that mutations in SLC3A1, the gene that encodes neutral and basic amino acid transport protein rBAT, cause cystinuria. However, genetic linkage studies indicated that not all cases of cystinuria were caused by mutations in this gene[221] and localized an additional gene linked to cystinuria to chromosome 19q13.1[222,223]. Mutational analysis of genes encoding proteins that comprise the light subunits of heteromeric amino acid transporters at 19q13.1 revealed that mutations in SLC7A9 also cause cystinuria[181].

Type I cystinuria

Type I cystinuria is predominantly caused by mutations in SLC3A1, but a small proportion of patients with type I cystinuria have two mutated SLC7A9 alleles[217]. 133 mutations in SLC3A1 have been described until now including nonsense, missense, splicing, frameshifts and large sequence rearrangements. 579 mutated alleles have been reported in patients from 23 countries, mainly from Europe, for this gene. The most common mutations among patients with cystinuria caused by known mutations in SLC3A1 are Met467Thr (26%), Thr216Met (12%), p.Glu298_Asp539dup (5%), and Arg270X (4%).

Functional studies of the cystinuria mutations M467T and M467K, suggested a

traffic defect when expressed in *Xenopus oocytes*, because function was recovered with higher protein expression, specially for the M467T mutant[224]. The R365W mutant had also an impaired traffic when expressed in HeLa cells[144]. The study of the biogenesis of type I cystinuria mutants localized in the TIM barrel showed that these mutants were unable to elicit any amino acid transport activity[157]. A decay of the rBAT signal co-precipitated with the anti-$b^{0,+}$AT antibody was observed for these TIM-barrel mutants, indicating that they are able to assemble efficiently with $b^{0,+}$AT but are subsequently directed to degradation, strongly suggesting that these mutations cause a misfolding of the extracellular domain (see section 3.1) The transmembrane domain mutant L89P does not heterodimerize with $b^{0,+}$AT and is degraded. However, the few heterodimers that are formed are stable, consistent with assembly, but not folding, defects[157].

Non-type I cystinuria

Almost all cases of non-type I cystinuria are caused by mutations in SLC7A9 with the exception of a few cases that involve a complex, inframe duplication of SLC3A1 p.Glu298_ Asp539dup (also referred to as dupE5-E9)[217]. 436 mutated SLC7A9 alleles have been reported in patients from 18 countries. Among patients with cystinuria caused by known SLC7A9 mutations, the most frequent mutations are Gly105Arg (21%), Pro482Leu (13%), c.614dupA (7%), Arg333Trp (6%), and Val170Met (4%). The mutation Pro482Leu is specific to Japan[225] (except for one allele identified in one Italian patient with cystinuria[226]. This mutation is present in 88% of Japanese patients with a mutation in SLC7A9 and in 76% of all Japanese patients with explained cystinuria. In Spanish patients with the SLC7A9 alleles, c.614dupA is the most frequent mutation (29%). The Val170Met mutation is exclusive to Jewish Israeli patients of Libyan origin (94% of patients) with the SLC7A9 alleles[181,217]. The Japanese and Israeli Jewish populations have less diversity in cystinuria mutations than other known populations.

The lack of genotype-phenotype correlation has led to the proposal of a novel classification for cystinuria based on genetics[202]. In this new classification, cystinuria is divided intro 3 different groups: type A if mutations are found in both SLC3A1 alleles, type B if mutations are found in both SLC7A9 alleles, and type AB if one mutation is found in each gene[202]. Individuals with heterozygous type AB have been identified[227], but cystin uric patients from families of such individuals have two mutated alleles in the same gene in addition to a mutated allele in the other

gene[217]. Since type AB double heterozygous individuals do not produce stones, and two mutations in the same gene were found in patients from these families , digenic inheritance of cystinuria was ruled out[217].

1.5.3 Cystinuria mouse models

Cystinuria has been described to occur naturally in cats[228], dogs[229] and maned wolves[230]. As these animal species are not suitable for genetic studies, two mouse model of cystinuria have been generated. Mutagenesis with N-ethyl-N-nitrosourea produced a mouse line (Peebles) that harbors a missense mutation (D140G) in SLC3A1 leading to Asp140Gly in rBAT, which parallels human type I cystinuria[231]. A knockout mice of SLC7A9 recapitulates the features of human non-type I cystinuria[232]. Both mouse models produce cystine stones at high rates and have morphological changes in kidney architecture that result from obstruction and inflammation.

Objectives

The general objective of this thesis is to describe mechanisms of biogenesis of the human cystinuria transporter rBAT-$b^{0,+}$AT, as a model for the study of membrane proteins.

Disulfides and N-glycans are crucial for the correct folding, assembly and traffic of proteins. Therefore the aims of this study were:

I. To identify the intramolecular disulfides and to describe the oxidative folding of rBAT-$b^{0,+}$AT.

II. To find the role of the rBAT disulfides in the biogenesis of the transporter.

III. To elucidate whether the light subunit $b^{0,+}$AT is or not required for the folding of rBAT.

IV. To identify the position of N-glycans in rBAT and to find their role in the biogenesis and function of the transporter.

As a consequence of the results obtained, a final aim was:

V. To analyse the role of the C-terminal loop of rBAT (residues 674-684) in folding and ER-exit of the transporter.

Results

3.1 Background

Previous studies in our group analysed the biogenesis of wild-type rBAT when expressed alone and in the presence of $b^{0,+}AT$, as well as the biogenesis of some cystinuria mutants, in MDCK and HeLa cells[157]. The study measured the degradaton and maturation half-times of the human subunits of the system $b^{0,+}$-like. It was shown that, without its partner, rBAT is rapidly degraded, while $b^{0,+}AT$ exhibited a much longer half life. The study also analysed some of the factors involved in rBAT degradation (Figure 3.5). The addition of the proteasome inhibitors MG132 and lactacystin delayed rBAT degradation. The ER-mannosidase inhibitor deoxymannojirimycin (dMNJ) had the same effect, revealing that rBAT disposal is mediated, at least in part, by the proteasome and the ER-mannosidase-dependent ERAD pathway[233,234]. It was also analysed if rBAT is a substrate of the calnexin/calreticulin chaperone cycle. These lectins reside in the ER and participate in the quality control of glycoproteins together with glucosidases I and II and UGGT (see Introduction). When glycoproteins are correctly folded they are no longer UGGT substrates; this precludes re-association with CNX/CRT and allow the proteins to exit the cycle[233,235]. Castanospermine inhibits glucose trimming mediated by the ER-glucosidases I and II, avoiding the generation of monoglucosylated N-glycans required for interaction with CNX/CRT. Addition of castanospermine accelerated rBAT disposal suggesting that the interaction with the calnexin chaperone system delays rBAT degradation[157].

Before degradation, unassembled rBAT displays a lag phase of ∼2 h in HeLa cells, where it may be retained by chaperones while waiting for its partner, the light subunit $b^{0,+}AT$. Actually, the assembly of rBAT with $b^{0,+}AT$ avoids the degradation of the heavy subunit. The heterodimer can then exit the ER and arrives to the Golgi apparatus were it acquires complex N-glycosylation. The maturation can be measured by Endoglycosidase H assays.

Some cystinuria mutants were also studied. All mutations in rBAT that cause type I cystinuria are localized in the extracellular domain of rBAT, except for the mutations L89P and I105R[236], that are in the transmembrane domain. The study analysed type I cystinuria rBAT mutants L89P, T216M, R365W, M467K and M467T (the last 4 mutants are in the TIM barrel domain) with or without $b^{0,+}AT$. T216M and M467T are the most common rBAT missense mutations, representing 6.4 and 26.4 % of the cystinuria alleles, respectively, of the International Cystinuria Consortium[217]. The transmembrane domain mutant L89P did not heterodimerize efficiently with $b^{0,+}AT$ and was degraded. However, the few heterodimers formed

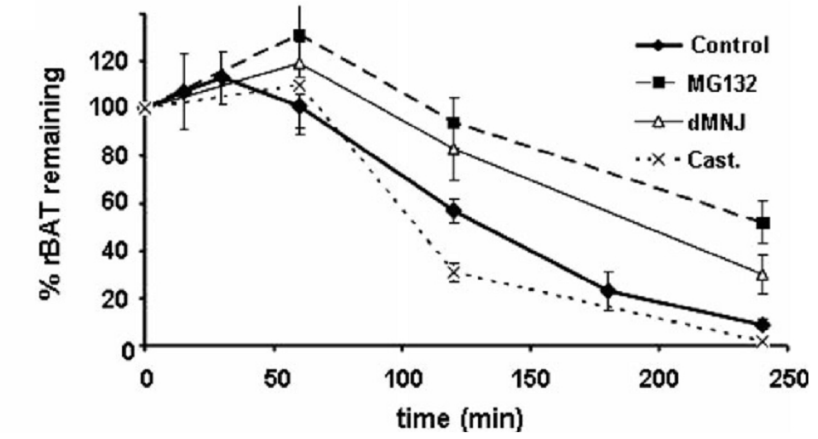

Figure 3.5. Degradation of rBAT in the absence of $b^{0,+}$AT. MDCK cells stably expressing human rBAT were labeled for 15 min with 35S-Met/Cys and chased with excess Met/Cys up to 4 h in presence of MG132, dMNJ or castanospermine. Equivalent amounts of radioactivity incorporated into protein were immunoprecipitated with the anti-rBAT antibody. The precipitates were run under reducing conditions. The quantifications (mean±SEM) of rBAT bands of at least three independent experiments for each condition are shown. The value at each point of the chase was divided by the value at point zero, which was set to 100. Figure extracted from Bartoccioni et al.[157] (see Appendix).

were stable, consistent with assembly, but not folding, defects.

Earlier functional studies of the cystinuria mutations M467T and M467K suggested a traffic defect when expressed in *Xenopus oocytes*, because function was recovered with higher protein expression, specially for the M467T mutant[224]. The R365W mutant had also an impaired traffic when expressed in HeLa cells[144]. The study of the biogenesis of type I cystinuria mutants localized in the TIM barrel showed that these mutants were unable to elicit any amino acid transport activity[157]. Moreover, none of them acquired complex N-glycosylation, consistent with retention in an intracellular location. A decay of the rBAT signal co-precipitated with the anti-$b^{0,+}$AT antibody was observed for these TIM-barrel mutants, indicating that they are able to assemble efficiently with $b^{0,+}$AT but are subsequently directed to degradation, strongly suggesting that these mutations cause misfolding of the extracellular domain (Figure 3.6).

Many human diseases are caused by mutation-induced misfolding of membrane proteins as cystic fibrosis[237], familial hypercholesterolemia[238], oculocutaneous albinism[239], cystinuria[157] and many others[240,241]. Our study and others evidence that knowledge of *in vivo* protein folding is important also to gain insight on the mechanisms of protein folding and misfolding, which are key issues in the

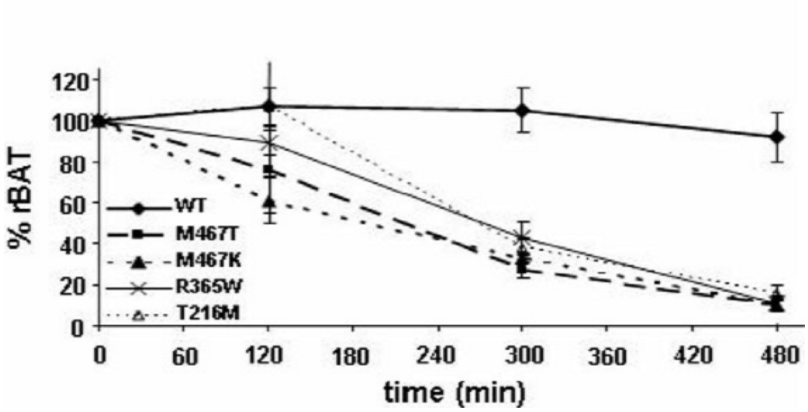

Figure 3.6. Quantification of post-assembly degradation of the extracellular domain rBAT mutants. HeLa cells transiently expressing $b^{0,+}AT$ together with wild-type or mutant rBAT were labelled for 30 min with 35S-Met/Cys and chased with excess Met/Cys up to 8 h. Equivalent amounts of radioactivity incorporated into protein were immunoprecipitated with the anti-rBAT antibody. The precipitates were run under reducing conditions. The quantifications (mean±SEM) of rBAT bands of at least three independent experiments for each condition are shown. The value at each point of the chase was divided by the value at point zero, which was set to 100. Figure extracted from Bartoccioni et al.[157] (see Appendix).

study of misfolding diseases.

The formation of disulfide bonds and the presence of N-glycans have an important role in the correct folding of glycoproteins[235]. Protein folding *in vivo* can be monitored by following the oxidation of disulfide bonds[56,57]. In order to study the early biogenesis of the human rBAT-$b^{0,+}AT$ heterodimer and the elements involved in the folding of rBAT, we studied the role of the cysteine residues and the N-glycans present in rBAT.

3.2 Role of the cysteine residues of rBAT in the presence/absence of $b^{0,+}AT$

Human rBAT contains eight cysteines. The first, cysteine 18, is cytosolic. The rest, cysteine 114 to cysteine 685, are extracellular (Figure 3.7). Cysteine 114 is disulfide-linked with human $b^{0,+}AT$[141,242], cysteines 242 and 273 are localized in the domain B, cysteine 571 is in domain C, and cysteines 666, 673 and 685 are in the C-terminal tail of rBAT[145]. Cysteine 685 is the C-terminal residue. Cysteines 114 to 685 are conserved in all orthologues except for cysteines 242 and 273 that are not conserved in the two urochordate rBAT orthologues (Figure 3.8).

The structure of rBAT has not been solved and therefore the intramolecular disul-

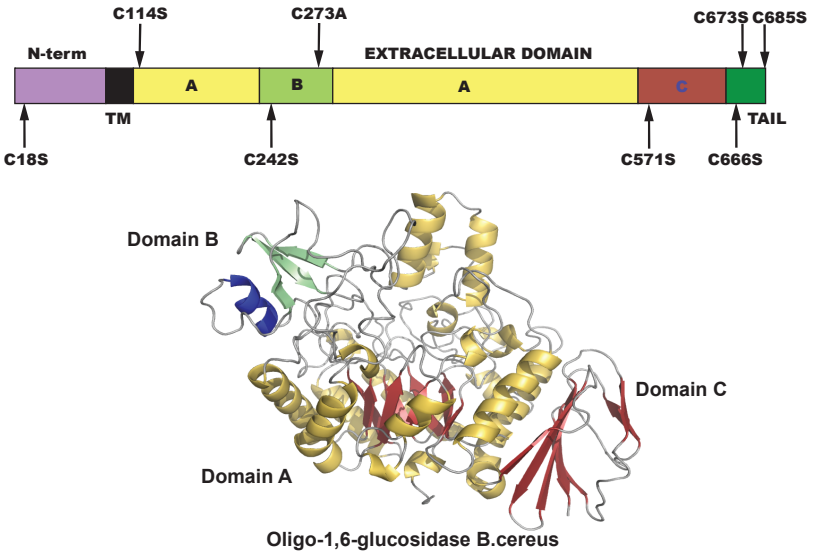

Figure 3.7. Cysteine residues in human rBAT. A scheme of human rBAT with the cysteine positions and the corresponding mutations is drawn to scale (top panel). A, B, and C, extracellular TIM barrel domain A, domain B, and domain C, respectively. The N-terminal cytoplasmic segment is shown in purple, the transmembrane domain is black, the domain A is depicted in yellow, the domain B is pale green, domain C is coloured in maroon and the C-terminal tail is dark green. The crystal structure of oligo-1,6-glucosidase from *Bacillus cereus* (PDB code 1UOK) [243] is shown to observe the opposite spatial position of domain B relative to domain C.

Homo sapiens	KG**C**QT	PK**C**LD	HD**C**TH	NQ**C**YF	WF**C**HL	DR**C**FV	TS**C**
Canis lupus	QA**C**RT	PR**C**LD	HD**C**TH	NQ**C**YF	WF**C**YL	DR**C**FV	SL**C**
Rattus norvegicus	KG**C**RT	PK**C**LD	HN**C**TH	KQ**C**YF	WF**C**LL	DK**C**FI	SS**C**
Mus musculus	KG**C**RT	PK**C**LD	HN**C**TH	KQ**C**YF	WF**C**LL	DR**C**FV	SS**C**
Gallus gallus	KGGVE	PK**C**LD	QD**C**VQ	KQ**C**YF	WM**C**SI	EN**C**FV	MN**C**
Xenopus laevis	KAGHE	PK**C**LD	HD**C**AQ	NQ**C**YL	WL**C**YT	DK**C**FI	SS**C**
Danio rerio	IDAVE	PR**C**MS	VN**C**--	QQ**C**YF	WF**C**YV	SQ**C**YV	Q-**C**
Takifugu rubripes	VDASE	PR**C**LS	AD**C**NQ	GQ**C**YL	WF**C**YI	DE**C**FI	T-**C**
Ciona intestinalis	QSTSF	PG**C**QE	VDS-K	KQFYY	YL**C**MV	GK**C**FT	--**C**
Human rBAT cysteines	C18	C114	C242	C273	C571	C673	C685

Figure 3.8. Alignment of cysteine residues in selected rBAT orthologues. The alignment of the cysteines of rBAT was performed in rBAT orthologues with the program CLUSTAL. A representative selection of rBAT orthologues is shown. In orange the cytosolic cysteine C18, in purple the cysteines that are completely conserved and in green the domain B cysteines, partially conserved. The position of human rBAT cysteines is shown.

fide connectivity is unknown. To analyse such connectivity we studied the free cysteines present in wild-type and cysteine rBAT mutants in the presence and absence of $b^{0,+}$AT. We used mass-tagging of accessible sulfhydryl (-SH) groups with mPEG5000-maleimide (mPEG) under denaturing conditions (Figure 3.9). mPEG is a membrane-impermeant reagent that has been used to study the topol-

ogy of some membrane proteins[244,245]. A molecule of mPEG attaches to a -SH group shifting the apparent molecular weight of the protein of interest by ∼5 kDa, which is easily detectable in SDS-PAGE. The actual shift can't be predicted with complete accuracy due to the fact that the PEG moiety does not bind SDS. The maleimide-thiol bond is stable under reducing conditions. According to the number of mPEGs attached to the protein, bands of different weights are obtained that correspond to the number of free cysteines present in the protein.

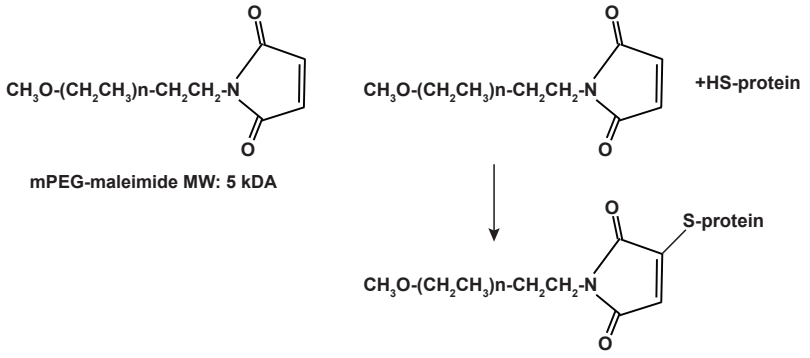

Figure 3.9. Structure of mPEG-maleimide and its attachment to thiol groups of proteins.

We first set up the method to find the optimal pegylation conditions for our protein. The anti-rBAT antibody recognizes an N-terminal fragment of rBAT close to C18[160]. In order to assure that the attachment of mPEG to C18 would not disturb the recognition of the epitope by anti-rBAT, we first used the cysteine mutant C18S, which is functionally indistinguishable from wild-type rBAT (see Section 3.2.1), to set up the pegylation conditions. Further experiments showed that wild-type rBAT was also immunoprecipitated with anti-rBAT antibody even when C18S was pegylated. Cells were lysed with denaturing buffer (see Materials and Methods) in the presence of different concentrations of mPEG. The samples were homogenized by pipetting and incubated at diverse times and temperatures (see Materials and Methods and Figure 3.10). In parallel, samples were incubated with the alkylating agent N-ethylmaleimide (NEM). As mPEG, NEM attaches to free cysteines, but it does not increase the rBAT molecular mass (MW of NEM, 0.125 kDa). The final condition used to analyse the pegylation of rBAT mutants was the incubation with 4 mM PEG at 30^{o}C for 30 min because it allowed a maximal pegylation of the sample. Just one of several experiments is shown. Other temperatures and incubation times were also analysed.

We also performed lysis of the cells with trichloroacetic acid (TCA) immediately after scrapping and prior to mPEG modification. Incubation of the samples with

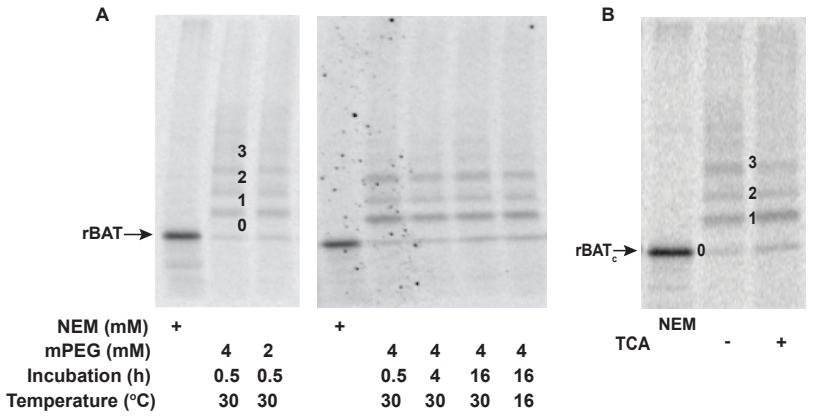

Figure 3.10. Pegylation of C18S rBAT mutant with different concentrations of mPEG, incubation times and temperatures. A, One experiment is shown where samples were treated with different mPEG concentrations, incubation times and temperatures. The numbers indicate the number of mPEGs attached to rBAT. NEM treatment is presented as a control. B, Pegylation pattern of samples with denaturing buffer: the samples were incubated (+) or not (-) with TCA prior to mPEG treatment. NEM treatment is presented as a control. The numbers indicate the number of mPEGs attached.

15% of TCA rapidly quench putative artifactual thiol-disulfide exchange reactions[246,247]. No significant difference in the pegylation of rBAT was observed between samples treated with or without TCA (Figure 3.10 B).

Once the optimal pegylation conditions were set up, we confirmed that the eight cysteines present in rBAT were accessible to mPEG under denaturing and reducing conditions. rBAT was synthesized in HeLa cells in the presence of [35S]Met/Cys and the reducing agent dithiothreitol (DTT). In these conditions rBAT remains core-glycosylated because of its presence in the ER[157] and is reduced because of the more reducing conditions in the ER lumen[56,57]. The cells were lysed in denaturing conditions with TSD buffer containing 4 mM mPEG without or with increasing concentrations of NEM. rBAT was immunoprecipitated with an antibody anti-human rBAT (see Materials and Methods), and the samples were ran in reducing SDS-PAGE. As expected, we detected an eight-step ladder (Figure 3.11), corresponding to the eight cysteines present in wild-type rBAT, confirming that under these conditions all rBAT cysteines are accessible to mPEG.

In order to study the disulfide bonds present in rBAT we performed an analysis of rBAT cysteine mutants. Single cysteine mutants of rBAT were generated by replacing cysteine to serine. Cysteine C273 was replaced by alanine, since the change for a serine creates a new, and used, N-glycosylation site (data not shown). The mutants and wild-type rBAT were expressed, together with $b^{0,+}$AT, in HeLa cells,

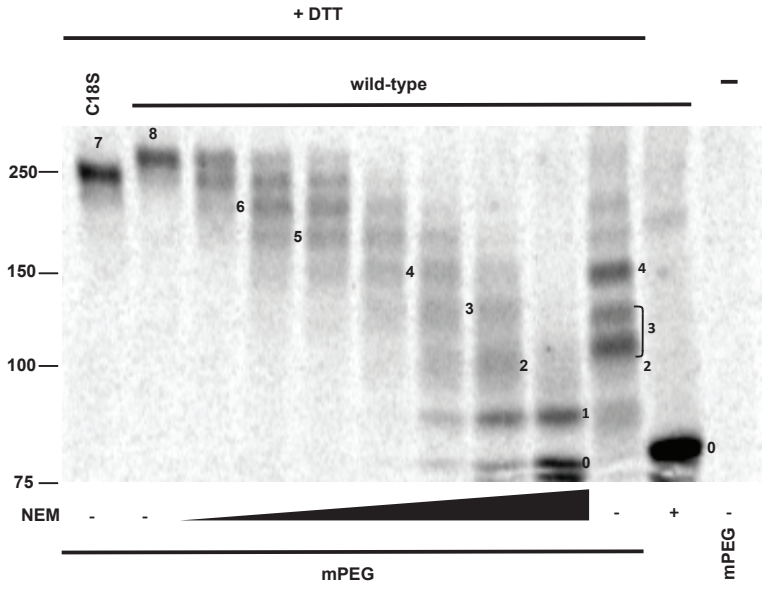

Figure 3.11. Accessibility of mPEG to rBAT cysteines. HeLa cells were transiently transfected with wild-type, C18S rBAT or with vector alone (-), and after 36 h the cells were labeled with [35S]Met/Cys in the absence or presence of 5 mM DTT (+ DTT). The cells were pelleted immediately and lysed in denaturing solution with either 4 mM mPEG (lanes 1 and 2), 20 mM NEM (lane 11), or 4 mM PEG with increasing concentrations (from 100 μM to 20mM) of NEM (black triangle, lanes 3 to 9). After incubation for 30 min at 30^{o}C, the lysates were immunoprecipitated with the anti-rBAT antibody and the precipitates run under reducing conditions. The numbers (0 to 8) point to the unpegylated (0) and pegylated (1 to 8) rBAT bands. Band 3 may appear as a smear or as a closely spaced doublet as in this figure (see Figures 3.20, 3.22, 3.24 and 3.25). A representative experiment is shown. This figure corresponds to the Supplementary Figure 1 of Rius et al.[248] (see Appendix)

and labelled with [35S]Met/Cys, pegylated under denaturing conditions, and immunoprecipitated with a specific antibody against $b^{0,+}AT$. For the C114S mutant the antibody against rBAT was used because, despite it associates with $b^{0,+}AT$ and is functionally similar to wild-type, it does not form a disulfide bond with $b^{0,+}AT$[141,242]. rBAT co-immunoprecipitation with anti-$b^{0,+}AT$ indicates that all cysteine mutants are able to assemble with $b^{0,+}AT$. As a control, parallel samples were alkylated with NEM. The precipitates were run in reducing SDS-PAGE and the pegylation pattern was studied (Figure 3.12).

Our starting hypothesis was that the rBAT ectodomain is fully oxidized in the presence of $b^{0,+}AT$. Taking into account that C18 is cytosolic and C114 is disulfide-linked with $b^{0,+}AT$, we expected only one mPEG bound to wild-type rBAT. In the most simple scenario, single mutants should be modified with two mPEGs (one attached to C18 and the second one to the now unpaired cysteine), except

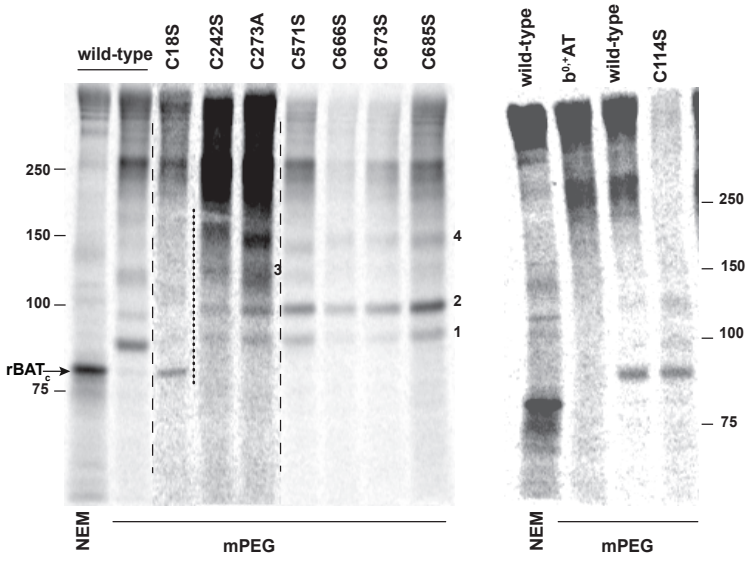

Figure 3.12. Pegylation of single cysteine rBAT mutants. HeLa cells were transfected with wild-type or cysteine rBAT mutants together with $b^{0,+}AT$, or $b^{0,+}AT$ alone. After 36 h the cells were labelled, pelleted, and lysed in denaturing solution with either 4 mM mPEG or 20 mM NEM (for clarity, only wild-type with NEM is shown. The results for the mutants were the same). Incubation and immunoprecipitation was performed as in Figure 3.11. C114S was immunoprecipitated with the anti-rBAT antibody. Numbers 0 to 4 highlight the more intense rBAT bands detected in each lane. $rBAT_c$, core-glycosylated rBAT. Dashed lines indicate that the Gray/Color Adjust tool of the View mode of the ImageQuant software (see Materials and methods) was used to linearly increase the intensity of lanes 3 to 5. Irrelevant lanes were removed between lanes 3 and 4 (dotted line). At least three independent experiments were performed with wild-type rBAT, the rBAT mutants, and $b^{0,+}AT$ alone.

for C18S (expected to be unmodified) and C114S (expected to be like the wild-type). The results agreed partially with this initial hypothesis. As observed in Figure 3.12, there was virtually no mPEG attached on C18S and one mPEG on the wild-type and the C114S mutant. This was consistent with the presence of 3 intramolecular disulfides within the rBAT ectodomain when rBAT is bound to $b^{0,+}AT$. For the other cysteine mutants we observed two different pegylation patterns: C571S, C666S, C673S and C685S showed mostly a band corresponding to two mPEG attached, although bands with 1, 3 and 4 mPEGs attached could be also observed. In contrast, the major bands present in the mutants C242S and C273A had 3 and 4 mPEGs attached. As the single mutants contain now 7 cysteines, the presence of a band with 4 mPEGs attached indicates that unpairing of cysteines C242 or C273 precludes formation of at least one of the other two disulfides. The fact that these two cysteine mutants show a similar pegylation pattern, different from the rest, also suggests that cysteines C242 and C273 could form a disulfide bond. However, this analysis did not help to elucidate the cysteine

connectivity from C571 to C685.

3.2.1 Biogenesis of single cysteine rBAT mutants

Next, we studied the biogenesis of these mutants. We performed pulse-chase experiments to address their stability and maturation in the presence and absence of $b^{0,+}$AT. When expressed alone in HeLa cells, wild-type rBAT is degraded with a half-time of ∼2 h after a lag phase of ∼2 h (see Figure 3.6). The cells were starved for 30 min and labelled with [35S]Met/Cys for 15 min [157]. The degradation was quantified at 5 h of chase (Figure 3.13). When expressed alone, rBAT remains core-glycosilated and can be observed as a ∼90 kDa band. No significant differences were observed compared to the degradation of wild-type rBAT.
We then did similar analysis in presence of $b^{0,+}$AT. The maturation half-time of wild-type rBAT in presence of $b^{0,+}$AT is ∼2 h. The cells were starved for 30 min and labelled for other 30 min. To assure that the rBAT measured was assembled with $b^{0,+}$AT, the samples were immunoprecipitated with the anti-$b^{0,+}$AT antibody.

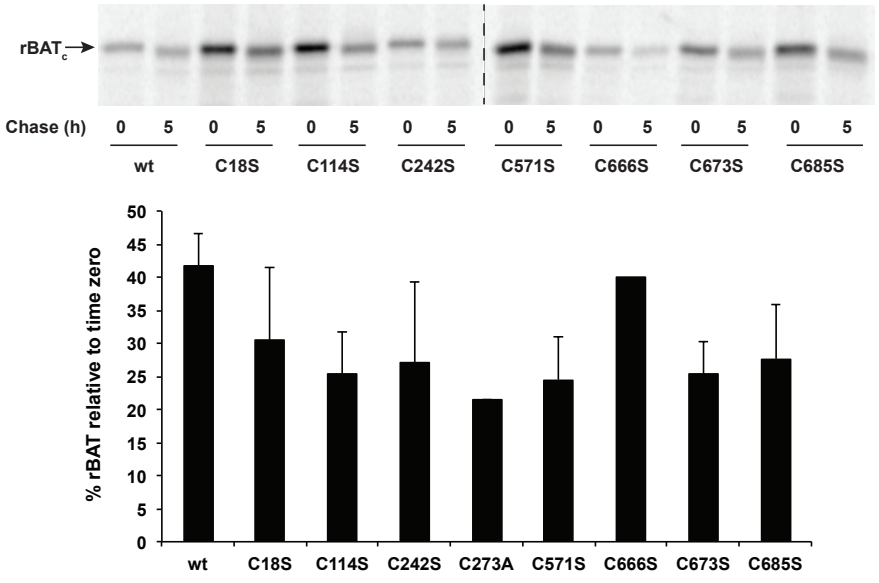

Figure 3.13. Degradation of cysteine rBAT mutants. HeLa cells transiently expressing rBAT mutants were starved for 30 min and labelled with [35S]Met/Cys for 15 min. The cells were chased for 5 h. Equivalent amounts of radioactivity incorporated into protein were immunoprecipitated with the anti-rBAT antibody. The precipitates were run under reducing conditions. $rBAT_c$, core-glycosylated rBAT. The dashed line indicates that irrelevant lanes were removed at that position. A representative experiment is shown. Quantification of the rBAT signal co-precipitated with the anti-rBAT antibody at time 5 h relative to time zero is shown. At least 3 experiments for each mutant were performed except for C273A and C666S (2 experiments performed).

rBAT at time zero appears as a band ∼90 kDa (rBAT core-glycosilated) while at 5 h of chase a smear may be observed (mature rBAT) due to N-glycans modification in the Golgi. The stability of wild-type and rBAT mutants was measured by quantification of the total rBAT (core-glycosilated and mature) at 5 h of chase relative to the amount of rBAT at time zero. Cysteine mutants C18S and C114S matured in a way similar to wild-type rBAT (Figure 3.14). A strong decrease in the rBAT signal co-precipitated with the anti-$b^{0,+}$AT antibody at 5 h of chase was observed for mutants C242S, C273A, C571S and C666S (between 20 and 35% of rBAT at 5 h of chase) (Figure 3.14 B) and no mature rBAT could be detected, indicating that these mutants are retained in the ER and suggesting a misfolding defect (similar to the cystinuria mutants previously studied[157]). In contrast, the mutants C673S and C685S able to mature (see the smear in Figure 3.14 A) albeit to a limited extent compared with wild-type rBAT (Figure 3.14 B, D, E and F). These 2 mutants were less stable than wild-type, but much more than mutants C242S to C666S (Figure 3.14 B).

Western Blots from total membranes were also performed (Figure 3.14 C). They confirmed the pulse-chase results. The mutants C242S to C666S showed only a band corresponding to immature rBAT, indicating that they do no exit the ER. The mutants C673S and C685S showed the smear corresponding to mature rBAT. In this case, differences can hardly be observed in the maturation of C673S and C685 (not shown) compared to wild-type. With the Western Blot we are not observing the fate of a small and recently synthesized population of protein but the total amount of protein expressed after ∼48 h of transfection. In this case, although C673S and C685S present a slower maturation rate, the amount of protein that has been able to arrive to the Golgi and beyond after 48 h of transfection is much higher than the amount of protein that it is still retained in the ER. This most likely reflects that the resident time of the protein in post-ER compartments is much higher that the time spent by the protein in the ER.

To accurately study the ER-to-Golgi traffic we monitored the maturation of the N-glycosilation of rBAT with Endoglycosidase H assays (Endo H). Endo H is able to cleave the N-glycans formed in the ER but not those modified in Golgi (see Materials and Methods). As we expected from the results of the pulse-chase experiments, mutants C18S and C114S showed an amount of Endo H sensitive band at 5 h of chase similar to wild-type rBAT (∼20%) (Figure 3.14 D and F). The mutants C242S to C666S showed no Endo H resistant band, confirming that none of these mutants are able to exit the ER and reach the Golgi apparatus

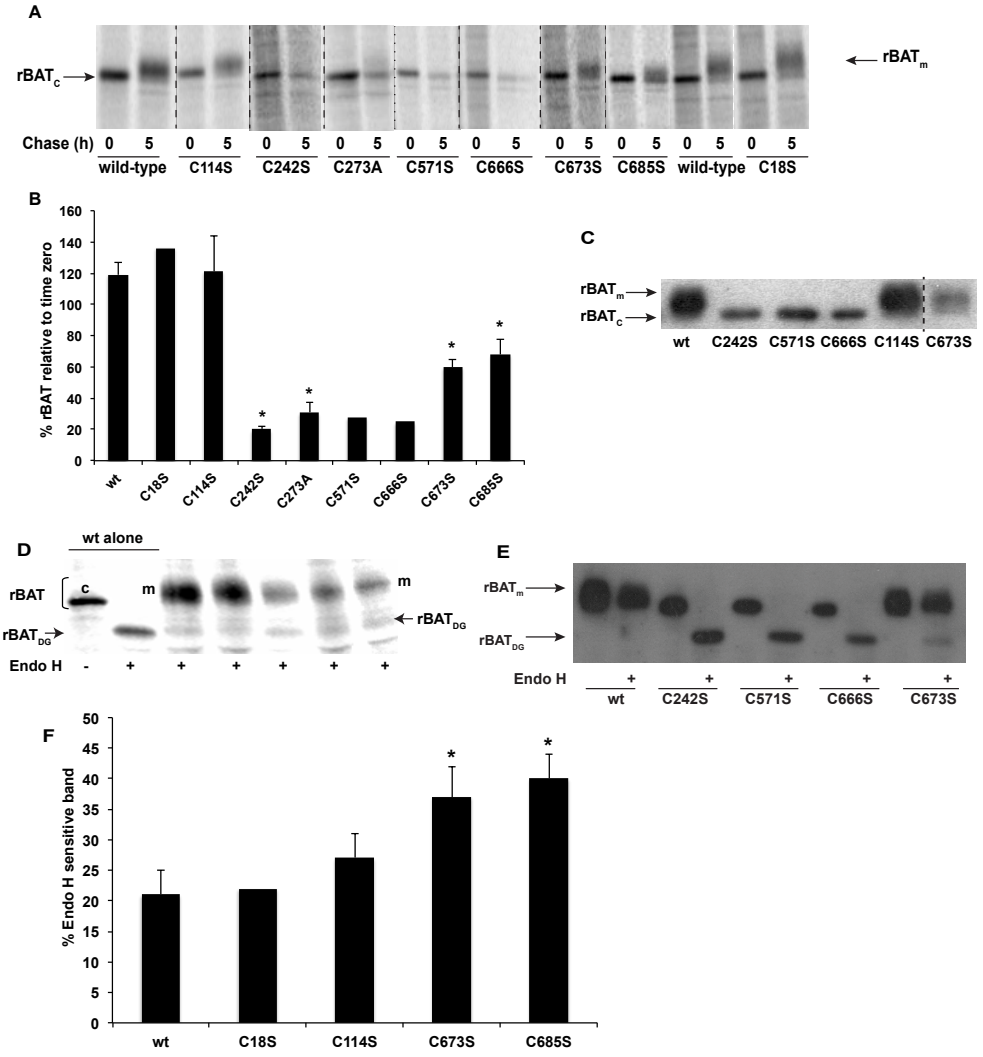

Figure 3.14. Stability and maturation analysis of cysteine rBAT mutants in the presence of $b^{0,+}AT$. A, HeLa cells transiently expressing $b^{0,+}AT$ together with wild-type and rBAT mutants were labelled and chased for 5 h. Equivalent amounts of radioactivity incorporated into protein were immunoprecipitated with the anti-$b^{0,+}AT$ antibody (except C114S, mutant, that was immunoprecipitated with anti-rBAT). The precipitates were run under reducing conditions. The results of a representative experiments is presented. $rBAT_c$, core-glycosylated rBAT; $rBAT_m$, mature rBAT. Dashed lines indicate that irrelevant lanes were removed. Dotted lines separate different gels. B, Quantification of rBAT signal co-precipitated with anti-$b^{0,+}AT$ antibody at 5 h relative to time zero is presented. Data are mean ± S.E. of at least three independent experiments for each rBAT species, unless no error bars are depicted (2 experiments performed). Shown are significant differences compared with the wild type (unpaired Student's t test). $*$, $p< 0.005$. C, Total membranes of transiently transfected HeLa cells were loaded for SDS-PAGE and analysed by western blot with anti-rBAT antibody. Dashed lines indicate that irrelevant lanes have been erased. D, Endo H analysis of cysteine rBAT mutants. HeLa cells were treated as in A and samples were incubated with Endo H for 30 min. Dashed lines indicate that the intensity of the lanes was linearly increased with ImageQuant. E, Total membranes were treated as in C. Samples were treated with Endo H. The result of a representative experiment is presented. $rBAT_{DG}$, deglycosylated rBAT; $rBAT_m$, mature rBAT. F, Quantification of the percentage of Endo H sensitive band was performed as follows: % Endo H sensitive rBAT=$100 \times \frac{rBAT_{DG}}{rBAT_{DG}+rBAT_m}$. Data are mean ± S.E. of at least three independent experiments unless no error bars are depicted (2 experiments performed). The asterisk indicates significant differences compared with the wild type (unpaired Student's t test). $p< 0.05$.

(Figure 3.14 E and C685S not shown). They display the same maturation defect as the cystinuria TIM-barrel mutants[157]. Although they are able to mature, cysteine mutants C673S and C685S showed a higher amount of Endo H sensitive band (∼35-40%) than wild-type rBAT (∼20%), indicating a slower maturation rate (Figure 3.14 F). Therefore, mutations in the extracellular domain cysteines C242 to C666 were retained in the ER. Mutations in the other two cysteines C673 and C685 presented a slightly reduced stability (Figure 3.14 D and F) and a maturation delay, showing for the first time a possible ER to Golgi traffic defect of the transporter.

We studied the transport activity of these mutants by measuring transport of L-cystine in HeLa cells expressing wild-type and cysteine rBAT mutants with $b^{0,+}$AT (Figure 3.15). The data were comparable between groups because of the similar transfection efficiency. As expected, all mutants that did not mature in pulse-chase experiments failed to elicit significant cystine transport. The mutants C18S and C114S had very similar transport activity compared with the wild-type; C673S and C685S were functional but showed less transport than wild-type rBAT.

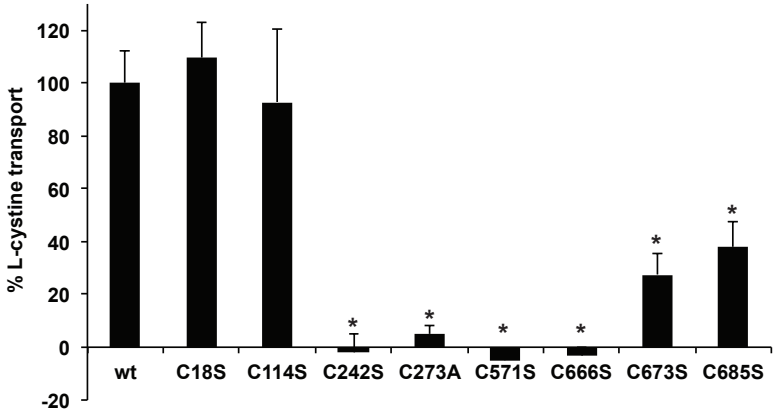

Figure 3.15. Transport activity of cysteine rBAT mutants. HeLa cells were transfected with $b^{0,+}$AT and the wild-type or rBAT mutants, and after 36 h L-cystine transport was measured for 2 min (see Materials and methods). Data were calculated as the difference between the uptake in each group minus the uptake in cells transfected with $b^{0,+}$AT alone (which was not different from the transport in vector-transfected cells). The percentage of transport activity compared with wild-type rBAT is shown. Data are the mean ± S.E. of at least 3 experiments. The asterisk, $*$, indicates significant differences compared with wild-type (unpaired Student's t test). $*$, $p<0.005$.

The study of the pegylation pattern of single cysteine mutants suggested that the rBAT ectodomain is fully oxidized and that one of the 3 intramolecular disulfides was C242-C273, but did not ascertain the disulfide connectivity between cysteines C571 to C685. Stability and maturation assays showed that cysteines C242 to C666 are retained in the ER and that cysteines C673 and C685 were able to exit the ER and mature, but at a slower rate than wild-type rBAT. The fact that these two cysteines showed a similar traffic defect suggested a possible disulfide bond between them. Therefore, the most probable disulfide connectivity in rBAT in the presence of $b^{0,+}$AT would be C242-C273, C571-C666 and C673-C685. With the aim of further supporting and trying to get more insight on the redox folding of rBAT, double rBAT cysteine mutants were generated and their pegylation pattern, stability and maturation were analysed.

3.2.2 Pegylation analysis and biogenesis of double cysteine mutants

Initially, the double mutants generated were the ones corresponding to the more likely native disulfide bonds (C242S-C273A, C571S-C666S and C673S-C685S), two double mutants that combined a domain B cysteine with domain C and the C-terminal tail (C242S-C571S and C242S-C666S); a double mutant combining the domain C cysteine with a C-terminal tail cysteine C571S-C673S; and finally the double mutant C666S-C685S. Later, we generated C666S-C673S, C242S-C673S and C571S-C685S. Therefore, 10 out of the 15 possible double mutants have been studied.

We first analysed the pegylation pattern of double cysteine mutants with $b^{0,+}$AT. These mutants contained 6 cysteines each. As cysteine 114 is disulfide linked with $b^{0,+}$AT, we could obtain bands from 1 mPEG attached, corresponding to the cytosolic cysteine 18, to 5 mPEGs attached if all the cysteines were free. The double mutants C242S-C273A, C571S-C666S and C673S-C685S as well as C571S-C673S and C666S-C685S showed up to three bands with a major band corresponding to one mPEG attached, as wild-type rBAT (Figure 3.16). Later experiments with mutants C571S-C685S and C666S-C673S gave the same pegylation pattern (not shown). Mutants C242S-C571S, C242S-C666S and C242S-C673S showed a different pegylation pattern with two major bands corresponding to 4 and 5 mPEGs attached. Considering that cysteine 18 is pegylated and that cysteine 114 is disulfide linked with $b^{0,+}$AT, these mutants mostly contained no intra-molecular disulfides (as the remaining 3-4 cysteines were pegylated, see Figure 3.16).

The fact that the double mutant C242S-C273A did not present bands correspond-

ing to 4 and 5 mPEGs attached (as in the single mutants, see Figure 3.12) suggested that it was not the absence of the C242-C273 disulfide *per se*, but the presence of unpaired C242 or C273 which was responsible for the impaired oxidation of the ectodomain. In fact, the double mutants containing one of these cysteines cause a major oxidative misfolding of the protein, reflected in an increase of the number of mPEG, attached (free thiol groups) (Figure 3.16, lanes 8 and 9). The fact that bands corresponding to 4 and 5 mPEGs do not appear when C242 and C273 are present, (Figure 3.16 lanes 6, 7, 10 and 11), suggests that these 2 cysteines are also sufficient for the formation of C242S-C273A (see also later and Figure 3.19). Assuming the formation of the B-domain disulfide, this implies the presence of non-native disulfides between the C-domain and the terminal tail in these mutants, at least in 1 mPEG band, as they all contain the same number of bands. It is also interesting to observe the different mobility of band 3 in the double mutants (see later). The data also suggested that any of the native disulfides could form in the absence of any of the other two as the pegylation pattern remains the same.

Next, we studied the maturation and stability of the double cysteine rBAT mutants. We performed pulse-chase experiments and quantified the maturation at 5 h of chase. Double mutants combining C242S to C666S with C242S to C685S showed a strong decrease in the rBAT signal co-precipitated with the anti-$b^{0,+}$AT antibody (Figure 3.17). The mutants were retained in the ER and no Endo H resistant band was detected. The stability of these mutants was highly compromised, similar to single mutants of cysteines C242 to C666. Strikingly, the double mutant C673S-C685S was the only one with a wild-type-like behaviour. As shown before, when only one of these two cysteines is mutated, the transporter displays an impaired stability and a slower maturation rate (Figure 3.14). These results further suggest that C673 and C685 form a disulfide bond. In this case, the double mutation supresses the damaging effects of the single mutants.

We analysed transporter function by measuring L-cystine uptake (Figure 3.18). Those double mutants that showed no maturation in pulse-chase analysis failed to elicit significant cystine transport. The C673S-C685S double mutant showed, as expected, a much higher activity. Note also that the activity of this double mutants is higher, as expected, than the one of the corresponding single mutants (Figure results:fig:cyssingletransport).

The results of the pegylation, stability and maturation of single and double mu-

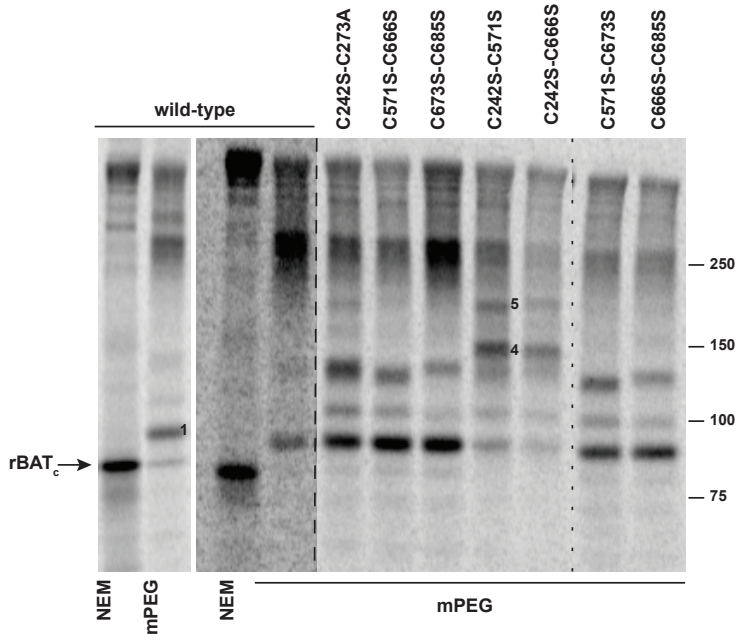

Figure 3.16. Pegylation of double cysteine rBAT mutants with $b^{0,+}$AT. The first gel (two lanes), from a different experiment, is shown to see more clearly the wild-type pegylation. This is also observed in the second gel, however, here the intensity of wild type lanes 1 and 2 was linearly increased with ImageQuant (dashed line). Dotted lines indicate that irrelevant lanes were removed. Numbers 4 and 5 highlight bands in C242S-C571S and C242S-C666S with four and five mPEGs attached. Number 1 marks the more intense rBAT band detected in all the other mPEG-treated samples. A representative experiment is shown from at least three for the wild type and each rBAT mutant. This figure corresponds to Figure 2B of Rius et al.[248] (see Appendix).

tants show that the single mutants C242S and C273S present a different pegylation pattern than the rest of the mutants, with more mPEGs attached, most likely reflecting more unfolded forms. Pulse-chase experiments showed that the cysteine mutants C673S and C685S present a traffic defect. Interestingly, the double mutants had a wild-type pegylation pattern for C242S-C273A and a wild-type maturation rate for C673S-C685S, suggesting that is the fact that a cysteine is impaired that cause these defects. In all, the results indicate that the disulfide bonds formed between the cysteines C242 to C666 are indispensable for biogenesis of the transporter. We concluded that the disulfides present in rBAT are: C242-C273, C571-C666, C673-C685. The pegylation data obtained suggest also that the disulfide bonds can form independently from each other, as the corresponding double mutants, with 1 mPEG as the major band.

We went further on this issue by generating rBAT mutants containing just the natively paired cysteines (C242-C273, DS1; C571-C666, DS2; C673-C685, DS3) as

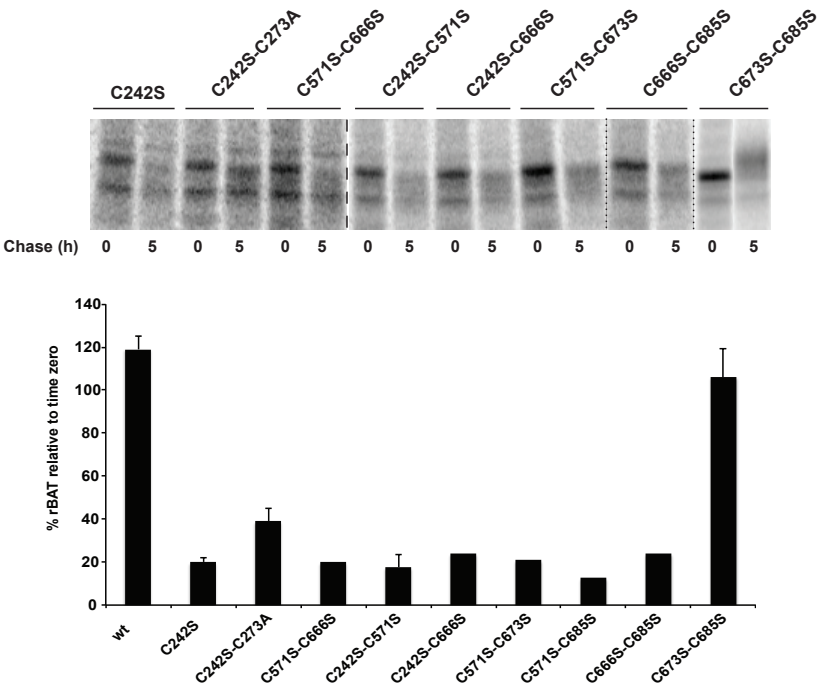

Figure 3.17. Stability of double cysteine rBAT mutants. HeLa cells were treated as in Figure 3.14. The results of a representative experiment are presented. The quantification measures the rBAT signal coprecipitated with the anti-$b^{0,+}$AT antibody at time 5 h relative to time zero. Dashed lines indicate different gels and dottted lines indicate that the intensity was linearly increased with ImageQuant. Data are mean ± S.E. of at least three independent experiments for each rBAT species, unless no error bars are depicted (2 experiments performed).

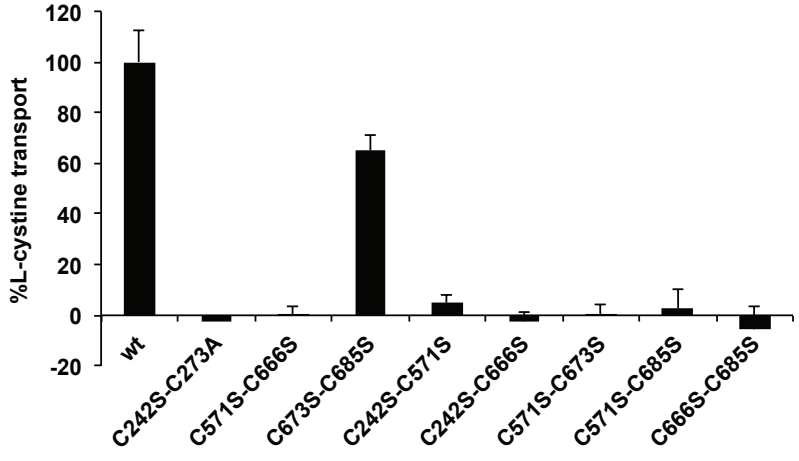

Figure 3.18. Transport activity of double cysteine rBAT mutants. Transport assays where performed as in Figure 3.15

well as cysteines C18 and C114. Pulse-chase and Endo H assays of these mutants were performed in order to study the mutants' stability and maturation. All three

mutants were degraded and showed no maturation (Figure 3.19A) and no significant transport activity (not shown).

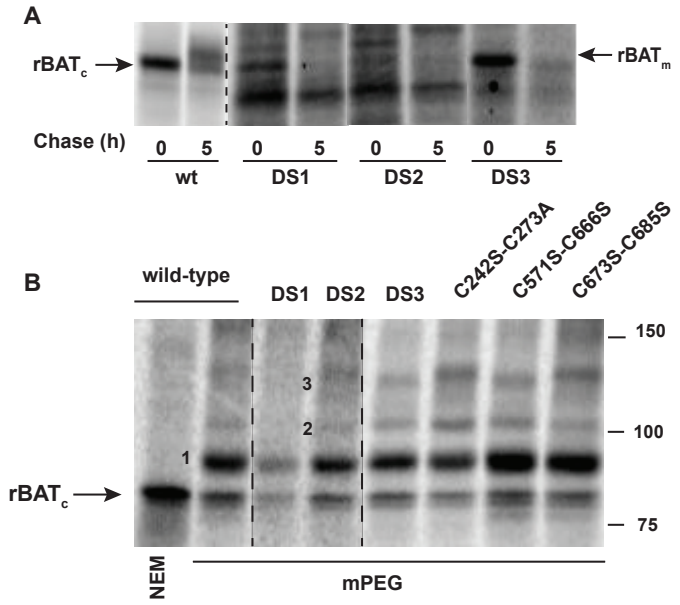

Figure 3.19. Stability and pegylation of rBAT disulfide mutants (DS) in the presence of $b^{0,+}AT$. A, Pulse-chase experiment with DS mutants. The analysis was performed as in Figure 3.14. The result of a representative experiment is presented. B, Pegylation of DS mutants. The experiment was performed as in Figure 3.12. A representative experiment is shown. rBAT$_c$, core-glycosylated rBAT, not pegylated. Dashed lines indicate that the intentsity of the lanes have been linearly increased by ImageQuant. Longer exposures did not show any di- or tri-pegylated species in DS1.

Next, we studied the pegylation pattern of these mutants in the presence of $b^{0,+}AT$. If the disulfide bond of the two cysteines presents in each mutant is formed, a band corresponding to one mPEG attached, corresponding to cysteine C18, should be observed. This was the case for all three mutants. Therefore, the three disulfide bonds can form independently from each other. However, it was observed that the only mutant that contained just one mPEG band was the mutant containing cysteines C242 and C273 (DS1). The mutants that contained cysteines C571 and C666 (DS2) or cysteines C673 and C685 (DS3) show as well bands corresponding to 2 and 3 mPEGs attached, similar to wild-type pegylation pattern (see also Figures 3.12 and 3.16). Between 1/5 and 1/3 of the pegylated rBAT in DS2 and DS3 mutants was found as di- and tri-pegylated species, similar to wild-type rBAT and thus without formation of the intramolecular disulfide (Figure 3.19). These results indicate that C242-C273, but not C571-C666 and C673-C685, is stably formed without the other two disulfides in the presence of $b^{0,+}AT$. Again this

supports that C242-C273 could be the first to form in rBAT.

DS2 and DS3 showed a similar pegylation pattern than wild-type rBAT but the band corresponding to 3 mPEGs attached presents a higher mobility in DS3 than that of DS2 and wild-type rBAT. Comparison with the pegylation pattern of wild-type rBAT and the double mutants (Figures 3.16 and 3.19) confirmed the 2 different mobilities of the tri-pegylated rBAT band. This suggests that, most likely that the C571-C666 is the last disulfide to be formed (see Discussion).

3.3 Oxidation of wild-type rBAT in the absence of $b^{0,+}AT$

Misfolded and unassembled secretory and membrane proteins are degraded *via* the endoplasmic reticulum-associated degradation (ERAD) pathway[83]. rBAT is degraded *via* the ERAD pathway in the absence of $b^{0,+}AT$[157]. It seemed that rBAT degradation was due to its unassembled state since the assembly with $b^{0,+}AT$ prevented rBAT degradation. This suggested that it was the unassembled state of rBAT *per se* that was recognized by the ERAD machinery. But another, non-exclusive possibility, is that unassembled rBAT is not folded. We adressed this question by comparing the pegylation of rBAT in the presence and absence of $b^{0,+}AT$.

If unassembled rBAT was to be fully oxidized a major band corresponding to two mPEGs attached should be expected, corresponding to cysteines C18 and also C114 (that would now be free as it cannot form the disulfide bond with $b^{0,+}AT$). While the major rBAT band had one mPEG attached when expressed in the presence of $b^{0,+}AT$ (Figure 3.20 lane 6), when rBAT was expressed alone, bands corresponding to one to four mPEGs attached (even five and six mPEGs attached were observed in some experiments) were present, being the major bands the ones corresponding to three and four mPEGs attached (Figure 3.20). This pattern did not change along a chase of 3 h. Longer chases were not performed because of rBAT degradation. This implied that, even if two of the pegylated cysteines were C18 and C114, at least one intramolecular bond was not present in unassembled rBAT. Similar experiments performed with stable MDCK cells[157,185] expressing much lower amounts of rBAT alone or rBAT together with $b^{0,+}AT$ gave similar results (not shown). For comparison wild-type rBAT and the double mutant C571S-C666S expressed with $b^{0,+}AT$ as well as $b^{0,+}AT$ alone are also

shown (Figure 3.20). Wild-type rBAT displays mainly 1, but also 2 and 3 mPEGs attached at time zero, but after 3 h of chase rBAT is post-translationally oxidized and a smear with one mPEG attached appears, corresponding to mature rBAT. Contrary, the double mutant C571S-C666S remains unchanged along the chase.

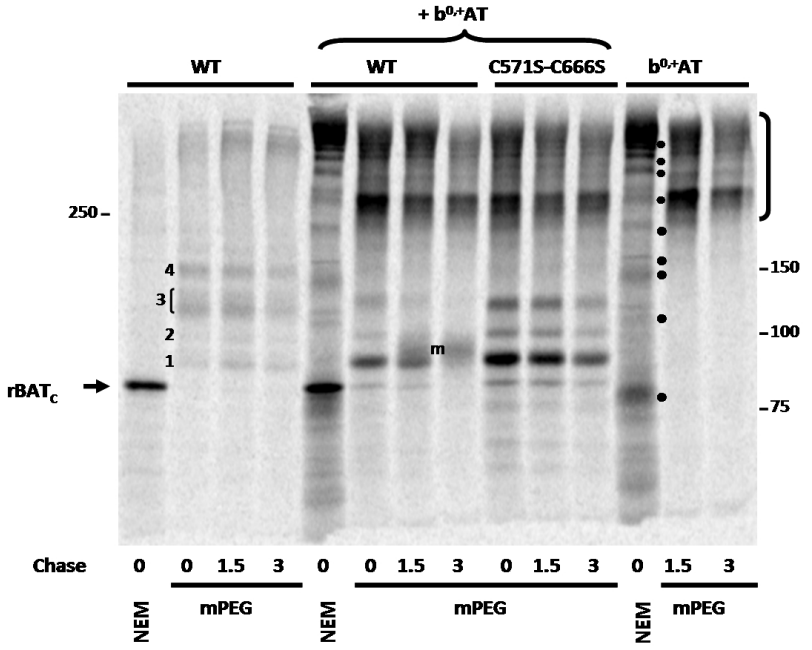

Figure 3.20. Oxidation of wild-type rBAT in the absence of $b^{0,+}AT$. HeLa cells were transfected with wild-type rBAT alone, $b^{0,+}AT$ alone, or wild-type or the C571S-C666S mutant together with $b^{0,+}AT$. The cells were labelled, and chased up to 3 h. The pegylation assay was carried out as in Figure 3.12. One representative experiment of three is shown. The letter **m** indicates mature glycosylated rBAT band with 1 mPEG attached. The circle • highlights bands that are not rBAT-specific, as they appear both in rBAT together with $b^{0,+}AT$ and in the $b^{0,+}AT$ alone samples. The lower of these bands is a non-covalent $b^{0,+}AT$ dimer. The bracket encompasses bands common to lanes 6-11 and 13-14 which, therefore, are not rBAT-specific. $rBAT_c$, core-glycosylated rBAT. This figure corresponds to Figure 7A of Rius et al.[248].

Therefore when expressed alone, rBAT remains unfolded along the chase, with at least one intramolecular disulfide not formed. In order to study if oxidative folding could resume if the time available for it was increased, we inhibited its degradation with the ER-mannosidase inhibitor dMNJ. This enzyme is essential for ERAD[249] and its inhibition avoids the degradation of unassembled rBAT[157] (Figure 3.5). We performed a pulse-chase in presence or absence of DMNJ. The inhibition of the degradation of rBAT by dMNJ did not change the pegylation pattern of unassembled rBAT in the absence of $b^{0,+}AT$ (Figure 3.21). This suggests that degradation and folding of unassembled rBAT are not competing mechansims and that unassembled rBAT is intrinsically unfolded. Therefore, unassembled

rBAT remains within the ER as an ensemble of different redox species, and it is unable to oxidize its ectodomain.

As rBAT alone is unfolded, and unfolded proteins tend to aggregate[5], we asked also the question whether unassembled rBAT was expressed mainly as a monomer or as disulfide-linked homodimers or aggregates. We compared pegylated and NEM-treated samples of unassembled rBAT under non-reducing and reducing conditions. We observed that between 2/3 and 3/4 of rBAT was found as monomeric species (Figure 3.22).

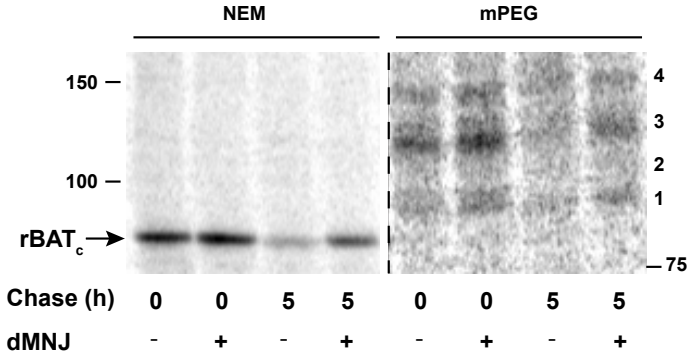

Figure 3.21. Pegylation of rBAT in the presence of the ERAD inhibitor dMNJ. HeLa cells were transfected only with wild-type rBAT. After 36 h the cells were labeled, chased for 5 h, and immediately pelleted and lysed in denaturing solution containing either 4 mM mPEG or 20 mM NEM. The protein was immunoprecipitated with the anti-$b^{0,+}$AT antibody, and the precipitates were run under reducing conditions. $rBAT_c$, rBAT core-glycosylated. dMNJ (1 mM) was present (+) or not (-) throughout the pulse-chase. Numbers on the right side indicate pegylated rBAT bands. One representative experiment of two is shown.

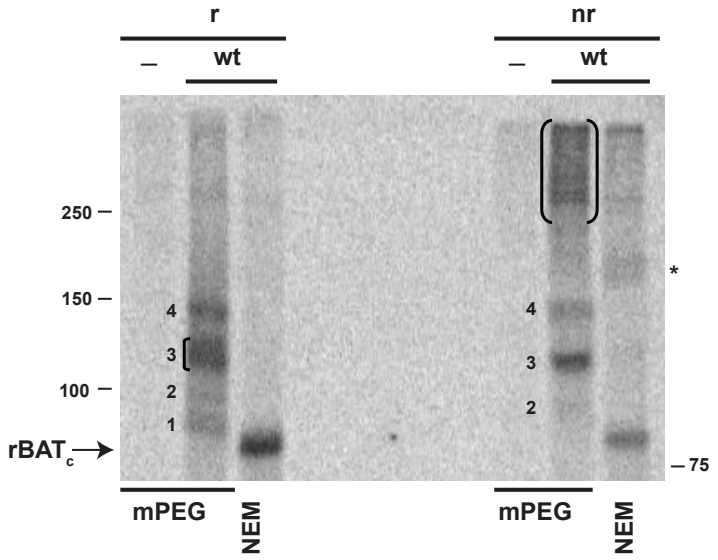

Figure 3.22. Pegylation of unassembled rBAT in reducing and non-reducing SDS-PAGE. HeLa cells were transfected with wild-type rBAT or with vector (-) alone. After 36 h the cells were labeled and immediately pelleted and lysed in denaturing solution containing either 4 mM mPEG or 20 mM NEM. After 30 min incubation at 30^{o}C, lysates were immunoprecipitated with the anti-rBAT antibody and the precipitates were run under reducing (r) or non-reducing (nr) conditions. One representative experiment from three is shown. The numbers (1 to 4) point to the rBAT-pegylated bands. The asterisk marks homodimeric rBAT. The disulfide-linked aggregated material observed in the mPEG-treated sample in non-reducing conditions is shown between brackets. rBAT$_c$: core-glycosylated rBAT.

3.4 Post-translational oxidative folding of rBAT in the presence of $b^{0,+}AT$

We wanted to study if the redox species observed when rBAT is expressed alone were able to fold when $b^{0,+}AT$ was expressed, i.e. if they could be *on-folding* pathway intermediates. If so, rBAT alone could be rescued after synthesis by the induction of $b^{0,+}AT$ expression. Therefore, $b^{0,+}AT$ was engineered into the pTRE-Tight vector, a plasmid that can be used to express a gene of interest in the Tet-Off system. HeLa cells expressing the Tet-Off advanced transactivator were transfected with rBAT-pcDNA3 and $b^{0,+}AT$-pTRE-Tight vector. The expression of $b^{0,+}AT$ was induced only in the absence of doxycycline in the medium. HeLa cells were transfected with rBAT-pcDNA3 and $b^{0,+}AT$-pTRE-Tight in presence of doxycycline. Cells were pulsed in the presence of doxycyline to avoid $b^{0,+}AT$ expression and chased in the presence of cold methionine and absence of doxycicline (inducing $b^{0,+}AT$ expression). Samples were immunoprecipitated with anti-$b^{0,+}AT$ antibody at different times in order to see if labeled rBAT could be

assembled with unlabeled newly synthesized $b^{0,+}AT$. Unfortunately, no conclusions could be taken from these experiments, as very few $b^{0,+}AT$ was produced. Other approaches should be tested in order to obtain a conclusive result, such as the use of *in vitro* transcription translation systems plus microsomes[250,251] (see Discussion).

In a different attempt, we tried to monitor the oxidative folding pathway of rBAT in the presence of $b^{0,+}AT$ by performing short pulses of 3 min, within the time needed to synthesize full length rBAT, followed by short chases of 1 and 10 min. We attempted to detect co-precipitated rBAT molecules that may have a different pegylation pattern to that of one mPEG attached and to see if this new pattern was similar to that of rBAT alone. The samples were then immunoprecipitated with $b^{0,+}AT$. Immediately after the pulse, rBAT was already disulfide-linked with $b^{0,+}AT$ (Figure 3.23 A) and the pegylation pattern at 1 and 10 minutes was similar to that at 5 h of chase. The heterodimer assembly takes place cotranslationally as disulfide linkage of rBAT with $b^{0,+}AT$ is a very fast event[157], this indicates that most likely a big part of the oxidative folding occurs cotranslationally.

Some proteins, as the gp160 of HIV-1[61] or the LDL receptor[54] have been described to accomplish their native oxidative state also in a post-translational way. We analysed if rBAT was capable of post-translational oxidation of its ectodomain in the presence of $b^{0,+}AT$ (Figure 3.23 B). We then studied if rBAT was able to oxidize its ectodomain and to associate with $b^{0,+}AT$ in a posttranslational manner. We performed the pulse in presence of DTT and the chase without the reducing agent. After the pulse, rBAT was completely reduced and was detected as an 8-pegylated band (see lane 5 in Figure 3.23 B) and, as expected, it was not assembled with $b^{0,+}AT$ (see lane 4 in Figure 3.23 B). After 1 h of chase with no reducing agent, rBAT was fully oxidized and assembled to $b^{0,+}AT$, showing the same pegylation pattern than when the pulse is performed with no DTT. The same was observed with a much shorter chase of 1 h (see lane 6 in Figure 3.23 B). Endo H analysis of the samples was also performed. rBAT with and without a DTT-pulse matured in a similar way, indicating that rBAT is able to oxidize its ectodomain in a post-translational way and mature. Therefore, a fully reduced unassembled rBAT can be an oxidative folding intermediate *in vivo*.

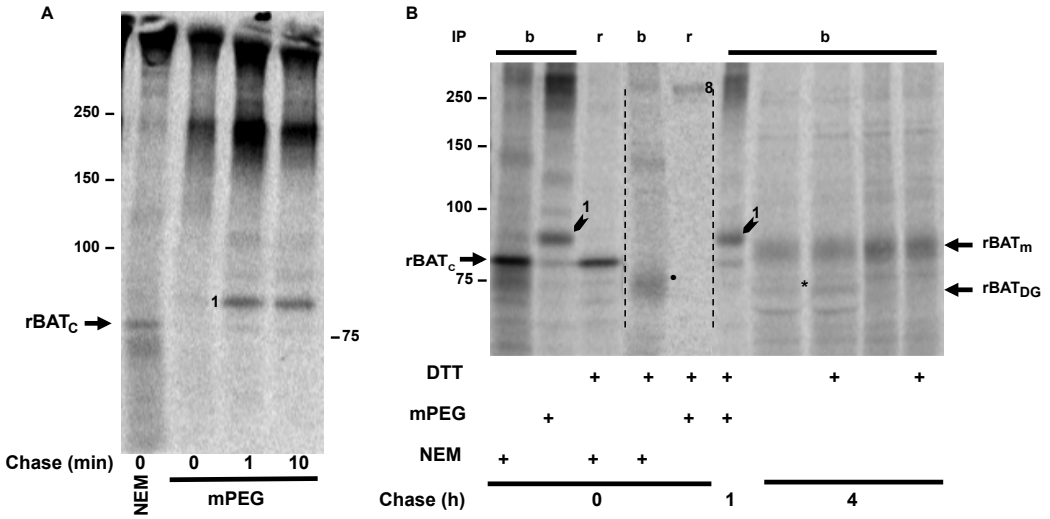

Figure 3.23. Post-translational oxidative folding of rBAT in the presence of $b^{0,+}AT$. A, HeLa cells were transfected with wild type rBAT and $b^{0,+}AT$. After 36 h the cells were labeled with 400 μCi/ml [35S]Met/Cys for 3 min and chased for the indicated times. Pegylation was performed as in Figure 3.12. Samples were immunoprecipitated with anti-$b^{0,+}AT$ antibody. Number 1 marks the band with 1 mPEG attached. One representative experiment from two is shown. B, HeLa cells were transfected with wild-type rBAT and $b^{0,+}AT$. After 36 h the cells were labeled in the presence or absence of 5 mM DTT (DTT +) and chased without DTT. Immediately after labeling or after 1 h of chase, the cells were pelleted and lysed in denaturing solution containing either 4 mM mPEG or 20 mM NEM. SAmples chased at 4 h were treated (lanes 7 and 8) or not treated (lanes 9 and 10) with Endo H. The samples were immunoprecipitated with the anti-$b^{0,+}AT$ (b) or the anti-rBAT (r) antibody, and run under reducing conditions. A representative experiment of three is shown. The intensity of lanes 4 and 5 was linearly increased with ImageQuant (dashed line). Numbers 1 and 8 mark the corresponding pegylated bands. Number 8 represents reduced and pegylated wild-type rBAT. The circle, • highlights dimeric $b^{0,+}AT$. The asterisk, $*$ marks $rBAT_{DG}$ (deglycosylated rBAT). $rBAT_m$, mature glycosylated rBAT; $rBAT_c$, core-glycosylated rBAT. Figures 3.23 A and B correspond to Supplementary Figure 3 and Figure 8 of Rius et al. [248].

3.5 Pegylation pattern of rBAT cysteine mutants in the absence of $b^{0,+}AT$

When expressed alone, wild-type rBAT presents bands corresponding to one to four mPEGs attached, the major bands corresponding to 3 and 4 mPEGs attached (see Section 3.3). We studied the number of free cysteines in rBAT cysteine mutants. Samples were pulsed for 15 min and incubated with 4 mM mPEG for 30 min (Figure 3.24). The pegylation observed in the mutants can be classified in 3 different patterns: C18S and C114S showed major bands corresponding to 1, 2 and 3 mPEGs attached (although the bands present a slightly different mobility in each mutant). Band 1 represented ∼50% of the total amount of pegylated

molecules. Mutants C571S to C685S show the same pegylation pattern, similar to wild-type, but the major bands correspond to 2 and 3 mPEGs attached. The fact that the same bands appear in different mutants (see Figure 3.24 lanes 7-10) implies that each particular band, despite containing an equal number of reduced cysteines, comprises, most likely, different reduced and oxidated cysteines. Finally, mutants C242S and C273A show a different pattern from the rest of the mutants (as when expressed with $b^{0,+}$AT). The major bands in these mutants are the ones corresponding to 4 and 5 mPEGs attached, indicating that in these mutants only one disulfide bond can be present (assuming pegylation of C18, C114 and C242 or C273). Other bands can also be observed but much less intense. Again, their pattern argues that unpairing of C242 and C273 seems particularly detrimental for rBAT folding.

We then studied the pegylation of the double mutants (Figure 3.25), that contain 6 cysteines. The double mutant C242S-C273A and those double mutants that contain cysteines C571 to C685 show a similar pattern to that of wild-type rBAT, being the more abundant species the ones corresponding to 1 and 3 mPEGs attached. The double mutants containing only one of the cysteines of domain B (C242 and C273) and one of the domain C and tail cysteines (C571, C666, C673 or C685) present a different pegylation pattern, with 5 and 6 mPEGs attached as the more abundant species. Once more, we observe that when one of the B domain cysteines are eliminated, rBAT seems to shift to a more unfolded conformation highlighting the importance of the B domain disulfide in rBAT folding.

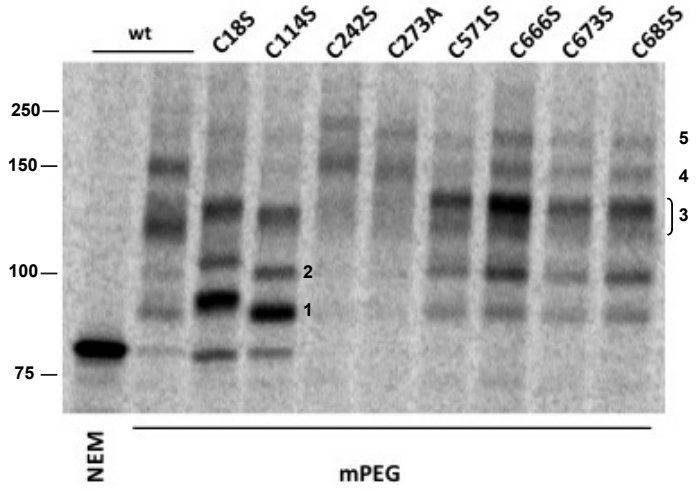

Figure 3.24. Pegylation pattern of single rBAT cysteine mutants in the absence of $b^{0,+}$AT. HeLa cells were transiently transfected with wilt-type or cysteine rBAT mutant and the pegylation was performed as in Figure 3.12. At least three independent experiments were performed. A representative experiment is shown. The numbers indicate the number of mPEGs attached. $rBAT_c$, core-glycosylated rBAT.

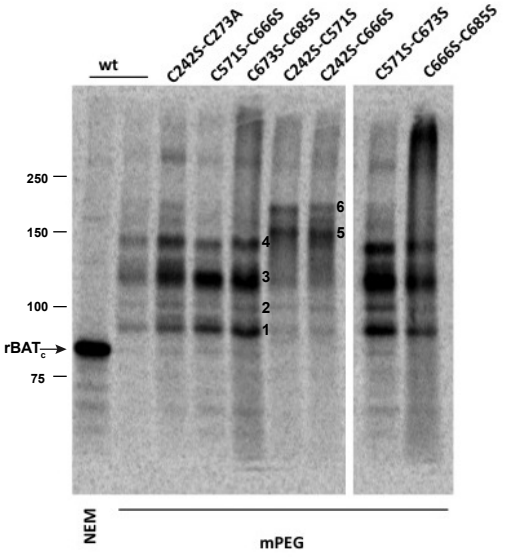

Figure 3.25. Pegylation pattern of double rBAT cysteine mutants in the absence of $b^{0,+}$AT. HeLa cells were transiently transfected with wilt-type or cysteine rBAT mutant and the pegylation was performed as in Figure 3.12. A representative experiment of 3 is shown. The numbers indicate the number of mPEGs attached. $rBAT_c$, core-glycosylated rBAT.

3.6 Role of N-glycans in the early biogenesis of rBAT

N-glycans have an important role in the correct folding of glycoproteins[62,69,233,235]. The N-glycan-dependent quality control of glycoprotein folding prevents endoplasmic reticulum to Golgi exit of folding intermediates, unrepairable misfolded glycoproteins and unassembled subunits of multimeric complexes[252].
Individual N-glycans present in a protein may play different roles in protein processing. Single N-glycans can play both a major role in promoting the correct folding[79] and in targeting misfolded glycoproteins for ER-associated degradation[80,81]. For instance, in cystic fibrosis membrane conductance regulator (CFTR)[82] a single N-glycan promotes folding (N900) while the N894 glycan supports degradation. Another example is the simian virus 5 hemagglutinin-neuraminidase protein where the third N-glycan is sufficient for achieving the correct folding of the protein[79]. Similar roles of the N-glycans have been described for the yeast carboxipeptidase Y[80,81,126] and the cell adhesion molecule CD 164[253] (see Introduction).

To study the role of N-glycans in the folding of rBAT we first find which of the N-glycan attachment consensus sites were used. Then, we analysed biogenesis and function of mutants that eliminate these N-glycans. The oligosaccharide chain can be attached to the asparagine of the consensus sites Asn-X(except Pro)-Thr/Ser. Human rBAT contains 6 consensus sites (Figure 3.26 A). None of them is completely conserved in rBAT orthologues (Figure 3.26 B). We generated mutants for each consensus site by changing the threonine or serine to alanine.

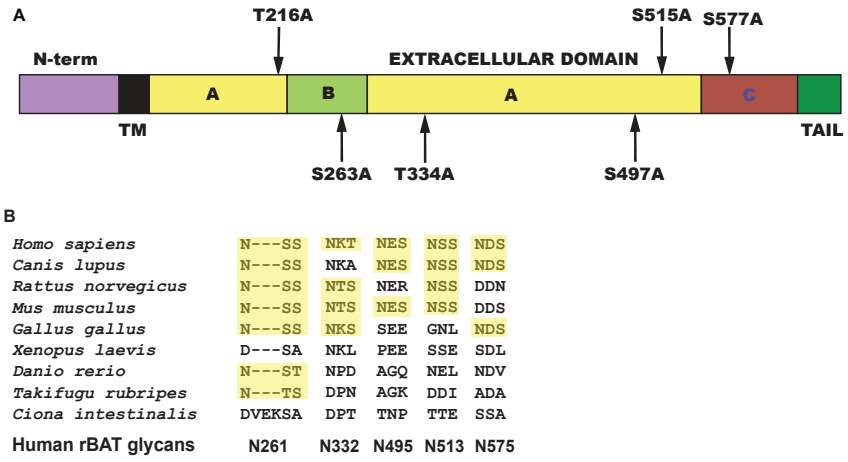

Figure 3.26. N-glycan consensus sites in rBAT. A, Scheme of human rBAT with the putative N-glycan positions and the introduced mutations. It is drawn to scale (top panel). A, B, and C, extracellular TIM barrel domain A, domain B, and domain C, respectively. B, Alignment of N-glycans in selected rBAT orthologues. The human rBAT N-glycans are indicated. Diferent species have diferent number of glycans in diferent positions. Conservation is marked in yellow.

3.6.1 Identification of the N-glycans of rBAT and their role in the biogenesis of the rBAT-$b^{0,+}$AT transporter

In order to know which of the putative N-glycosylation sites present in rBAT are glycosylated *in vivo*, we performed pulse experiments in transiently transfected HeLa cells. The mutants of those sites that are glycosylated in wild-type rBAT should show a smaller size than the wild-type rBAT. The mutants of an N-glycosylation site that is not used will have the same size as wild-type rBAT. As Figure 3.27 shows, all putative N-glycosylation sites are used except N214 (T216A mutant). An rBAT structural model of the extracellular domain of rBAT based on the known structure of its homologue 4F2hc places T216 as an internal residue near the putative active cleft[145]. This would explain the fact that this site is not used *in vivo*. Actually, the cystinuria mutant T216M has the same size as wild-type rBAT and leads to post-assembly degradation of rBAT[157]. The other sites are used *in vivo*, correlating with a surface position in the rBAT structural model[145]. The T216A mutant was not further studied.

In some proteins, single N-glycans have been described to be necessary[79,80] in directing substrate into the ERAD pathway. We did pulse-chase experiments of the N-glycan mutants in the absence of $b^{0,+}$AT. Transiently transfected HeLa cells were pulsed for 15 min and degradation was measured at 5 h of chase. The lysates

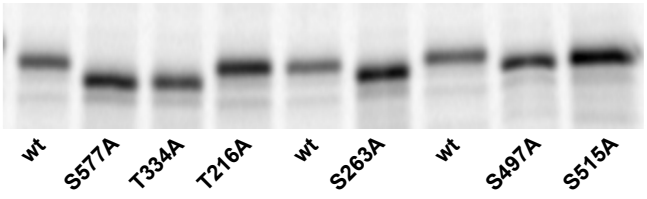

Figure 3.27. N-glycans of rBAT. HeLa cells transiently expressing wild-type rBAT or N-glycan mutants were starved for 30 min and labelled with [35S]Met/Cys for 15 min. Equivalent amounts of radioactivity incorporated into protein were immunoprecipitated with the anti-rBAT antibody. The precipitates were run under reducing conditions. A representative experiment is shown. At least n=2 experiments were performed for each mutant.

were immunoprecipitated with anti-rBAT antibody. In different parallel experiments were wild-type was always used as a control, no significant differences were found between the rate of degradation of the mutants compared to that of wild-type rBAT (Figure 3.28 and data not shown) suggesting that, in the presence of the other 4 N-glycans, no single N-glycan was required for the degradation of unassembled rBAT.

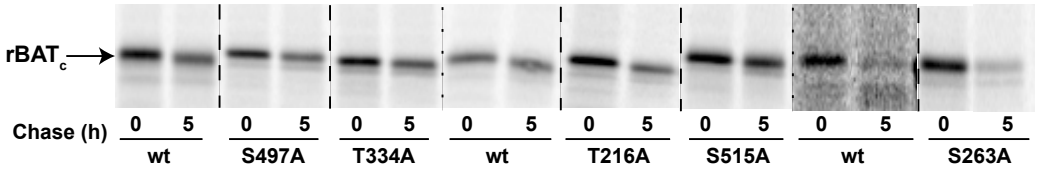

Figure 3.28. Degradation of N-glycan rBAT mutants. A pulse-chase experiment was performed as in Figure 3.13. rBAT$_c$, core-glycosylated rBAT. The dashed line indicates that irrelevant lanes were removed at these positions. The dotted lines separate different gels. A representative experiment of 2 is shown.

It has been shown that a single carboxipeptidase Y (CPY) N-glycan is a critical determinant for targeting CPY to ERAD[80,81](see section 3.6). When this N-glycan is eliminated, the protein is retained but not degraded, demonstrating that these mechanisms are separable. Specific signals embedded in glycoproteins can direct their degradation if they fail to fold. In order to study if any of the N-glycans present in rBAT played a similar role in misfolded rBAT we generated single site glycosylation mutants in M467K rBAT. This type I cystinuria rBAT mutant, as other TIM-barrel rBAT mutants, is directed for disposal after assembly with $b^{0,+}AT$[157]. We generated N-glycan mutants in the M467K background

and we analysed degradation by pulse-chase analysis. None of the double mutants M467K with N-glycans showed reduced degradation compared to the cystinuria mutant M467K (Figure 3.29). Moreover, no maturation was observed. These experiments were performed before our study of the Ng mutants (see Section 3.6.1). It is possible that in our initial setting 3.29, any role of an individual N-glycan in degradation might be masked by the presence of the other 4 N-glycans. Another possible approach would be to analyse the role of N-glycans in degradation by studying the Ng mutants in the M467K background.

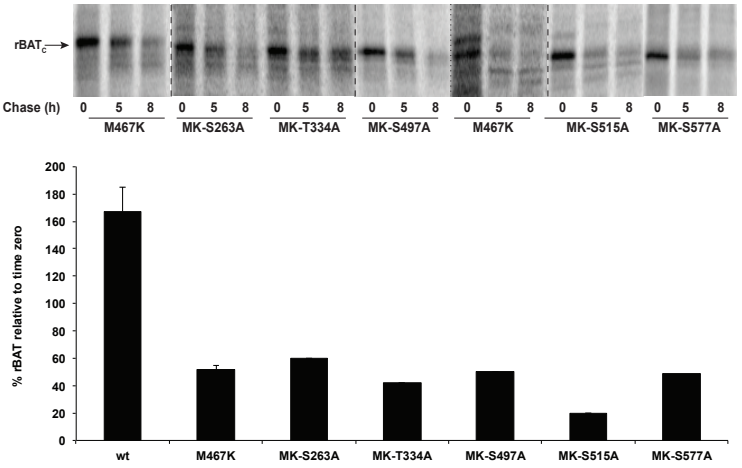

Figure 3.29. Stability of N-glycan M467K mutants. HeLa cells transiently expressing $b^{0,+}$AT together with rBAT mutants were labelled and chased for 5 h. Equivalent amounts of radioactivity incorporated into protein were immunoprecipitated with the anti-$b^{0,+}$AT antibody. The precipitates were run under reducing conditions. The results of representative experiments are presented. 2 independent experiments were performed with the double mutants, which gave very similar results. The quantification shows the mean valeu of the 2 experiments. rBAT$_c$, core-glycosylated rBAT. The dotted lines separate different gels. The dashed line indicates indicate lanes that have been linearly increased with ImageQuant.

The stability and maturation of N-glycan rBAT mutants in the presence of $b^{0,+}$AT was analysed in transiently transfected HeLa cells. The cells were labelled with [35S]Met/Cys for 30 min and chased for 5 h. Samples were immunoprecipitated with anti-$b^{0,+}$AT antibody. Co-immunoprecipitation of rBAT with anti-$b^{0,+}$AT indicates that all N-glycan mutants are able to assemble with $b^{0,+}$AT. The stability was measured by quantification of the total amount of rBAT (rBAT core-glycosilated and mature rBAT) at 5 h relative to the total amount of rBAT at 0 h of chase. No significant differences were found in the stability of rBAT N-glycan mutants expressed with $b^{0,+}$AT (Figure 3.30). The maturation of these mutants

was measured by Endo H analysis at 5 h of chase. All mutants showed a similar amount of Endo H sensitive rBAT (10-20 %) at 5 h of chase except for the S577A mutant, that displayed ∼50 % of immature rBAT suggesting an ER to Golgi traffic defect.

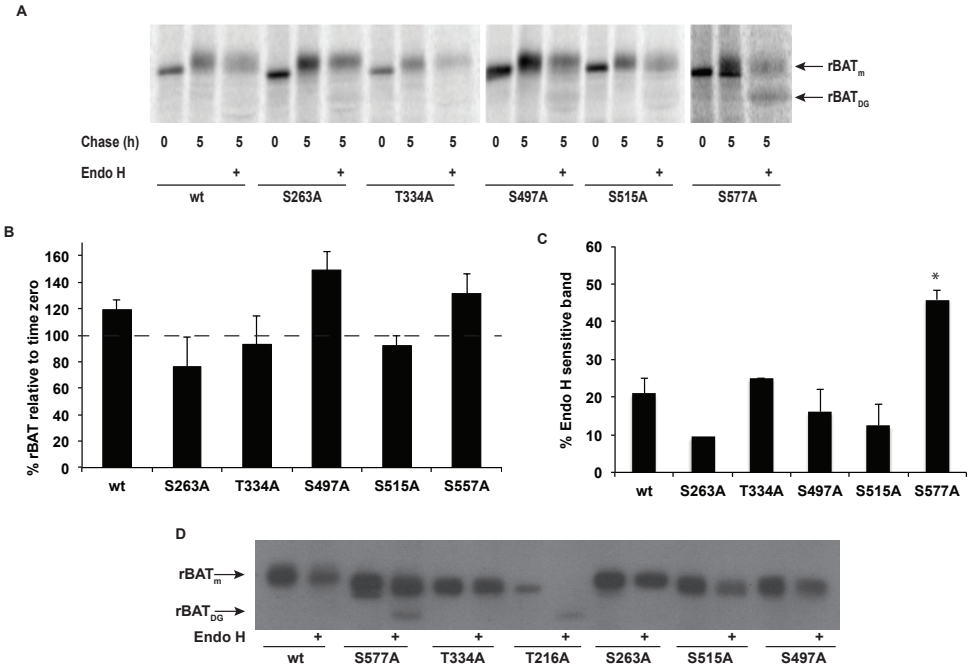

Figure 3.30. Stability and maturation of N-glycan rBAT mutants with $b^{0,+}$AT. A, A pulse-chase experiment was performed as in Figure 3.14. A representative experiment of at least 3 is presented. rBAT$_c$, core-glycosylated rBAT. B, Quantification of the rBAT signal co-precipitated with the anti-$b^{0,+}$AT antibody at time 5 h relative to time zero. Data are mean ± S.E. of at least three independent experiments for each rBAT species. C, Quantification of the percentage of Endo H sensitive band was performed as in Figure 3.14. Data are mean ± S.E. of at least three independent experiments for each rBAT species, unless no error bars are depicted (2 experiments were performed). The asterisk, ∗, indicates significant differences compared with wild type (unpaired Student's test). ∗, $p<0.005$. D, Total membranes of wild-type rBAT and N-glycan mutants were incubated with Endo H. Samples were loaded for SDS-PAGE and analysed by western blot with anti-rBAT antibody. Notice that, besides T216A, which does not mature, only in S577A some Endo H sensitive band is detected.

Western blot assays confirmed that all mutants (except for the T216A, the only putative N-glycan site not used) are able to mature (Figure 3.30 D) with the exception of mutant S577A, where a small fraction was Endo H sensitive. However, as for the cysteine mutants C673S and C685S (Figure 3.14), the amount of protein that has been able to arrive to the Golgi is higher than the amount of protein that is still retained in the ER. Again this likely reflects that the resident time of the protein in the post-ER compartments is much higher that the time spent by the

protein in the ER. Therefore, the delay in the ER-to-Golgi traffic is much better observed in the dynamic view of a pulse-chase.

To assure that the slower maturation of the mutant S577A was caused by the absence of the N575 N-glycan and not by the change to alanine, we generated the mutants N575D and N575Q. Pulse-chase assays confirmed that the maturation rate of these mutants was similar to S577A, concluding that it was most likely the absence of the N-glycan *per se* that caused the delay in rBAT maturation (Figure 3.31).

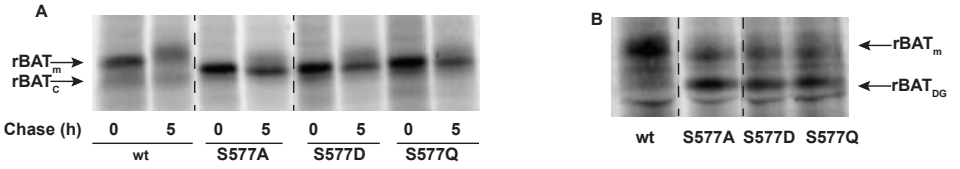

Figure 3.31. Maturation of N-glycan N575 rBAT mutants. A, A pulse-chase experiment was performed as in Figure 3.14. B, Endo H analysis at 5 h of chase. The results of a representative experiments are presented. rBAT$_c$, core-glycosylated rBAT; rBAT$_m$, mature rBAT. The intensity of lanes between dashed lines indicate that the intensity of the lanes have been linearly increased by ImageQuant.

We wanted also to analyse the importance of each N-glycan in the absence of the others. Therefore, we constructed mutants that carried only one of the 5 N-glycans of rBAT, (hereafter: Ng mutants) N261, (Ng261); N332, (Ng332); N495, (Ng495); N513, (Ng513); N575, (Ng575). We also generated a mutant without N-glycans (glycanless). Degradation, stability, maturation and functional assays were performed.

Preliminary degradation experiments (Figure 3.32) at 5 h of chase indicate that, in the absence of $b^{0,+}$AT, Ng332 mutant may be the only one that displays a similar degradation rate than wild-type rBAT, suggesting that it could be sufficient for degradation of unassembled rBAT. The degradation of the mutant Ng513 is similar to that of the mutant N-glycanless suggesting that this N-glycan has no role in rBAT degradation. The role of the rest of the mutants remains unclear; more experiments should be performed. However, these results indicate that rBAT degradation requires the presence of at least 1 N-glycan, as the N-glycanless mutant is more stable than wild-type rBAT.

We next analysed the stability and maturation of these mutants in presence of

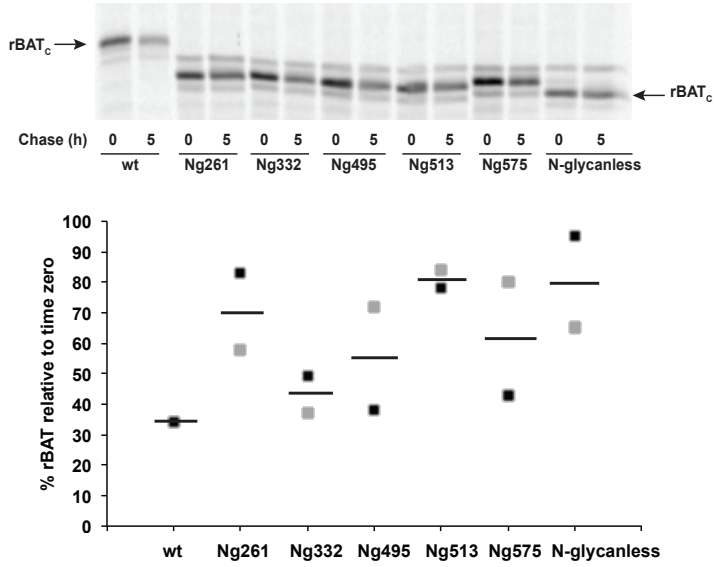

Figure 3.32. Degradation of Ng rBAT mutants. HeLa cells transiently expressing rBAT mutants were labelled and chased for 5 h. Equivalent amounts of radioactivity incorporated into protein were immunoprecipitated with the anti-rBAT antibody. The precipitates were run under reducing conditions. rBAT $_c$, core-glycosylated rBAT. Quantification of the rBAT signal coprecipitated with the anti-rBAT antibody at time 5 h relative to time zero. The quantification of 2 experiments is shown. Bars indicate the mean value.

$b^{0,+}$AT (Figures 3.33 and 3.34) at 5 h of chase. Only the N-glycanless mutant displayed a significant reduced stability, although the reduction was mild. We concluded that N-glycans do not greatly contribute to heterodimer stability in the cell.

In the Endo H assays it was difficult to quantify the deglucosylated and mature rBAT band in these mutants as they were positioned between two non-specific bands. However, the assays clearly show that the Ng575 mutant is the only one displaying a similar maturation to wild-type rBAT. The other mutants display an impaired maturation (Figure 3.34). Therefore, the N-glycan N575 seems to be necessary and sufficient for the maximal rate of ER-exit of the human cystinuria transporter. Other N-glycans, individually, can support a maturation rate at most similar and usually lower to the one of the S577A mutant.

The transport activity of Ng mutants was analysed with L-arginine transport assays (Figure 3.35). All mutants, including the N-glycanless, elicited transport activity, indicating that N-glycans are not absolutely essential neither for traffic to the plasma membrane nor for function. Anyway, the activity was clearly

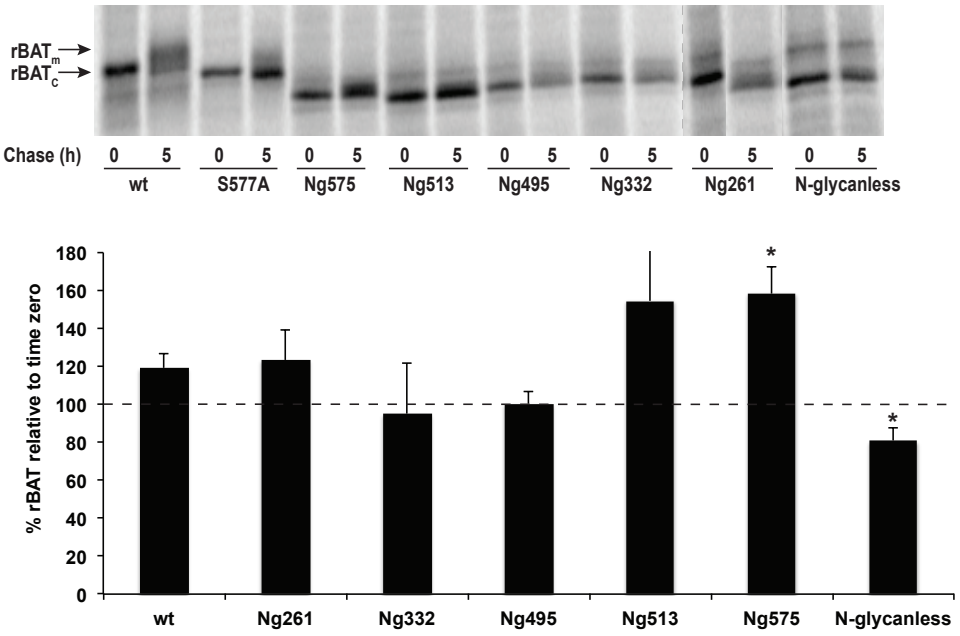

Figure 3.33. Stability of Ng rBAT mutants. HeLa cells transiently expressing $b^{0,+}$AT together with rBAT mutants were labelled and chased for 5 h. Equivalent amounts of radioactivity incorporated into protein were immunoprecipitated with the anti-$b^{0,+}$AT antibody. The precipitates were run under reducing conditions. The results of representative experiments are presented. Data are mean ± S.E. of at least three independent experiments for each rBAT species. rBAT$_c$, core-glycosylated rBAT. The dashed line separates different gels. Shown are significant differences compared with the wild-type (unpaired Student's t test). $*$, $p<0.05$.

reduced in the Ng and N-glycanless mutants. Further experiments are needed, included, quantification at the plasma membrane, to discern between trafficking and functional defects contributing to the decreased transport observed.

Altogether, the assays performed show that the N-glycans are not essential for the ER-exit neither the stability or function of the transporter. However, the N332 N-glycans does seem to play a role in degradation of rBAT and N575 is necessary for an efficient ER-exit of rBAT-$b^{0,+}$AT. We decided to further analyze the ER-exit of the transporter by studying the role of the N575 and other elements of the rBAT sequence.

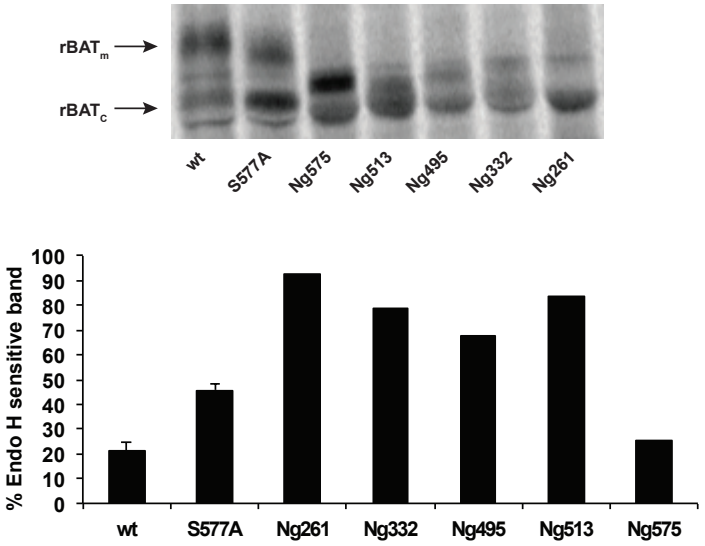

Figure 3.34. Endo H analysis of Ng rBAT mutants. HeLa cells transiently expressing $b^{0,+}$AT together with rBAT mutants were labelled and chased for 5 h. Samples were treated as in Figure 3.14. The quantification is the mean of 2 experiments. m, mature glycosylated rBAT; c, core glycosylated rBAT; rBAT $_{DG}$, deglycosylated rBAT. Quantification of the data was calculated as follows: Endo H sensitive rBAT=100 $\times$ $\frac{rBAT_{DG}}{rBAT_{DG}+rBAT_m}$.

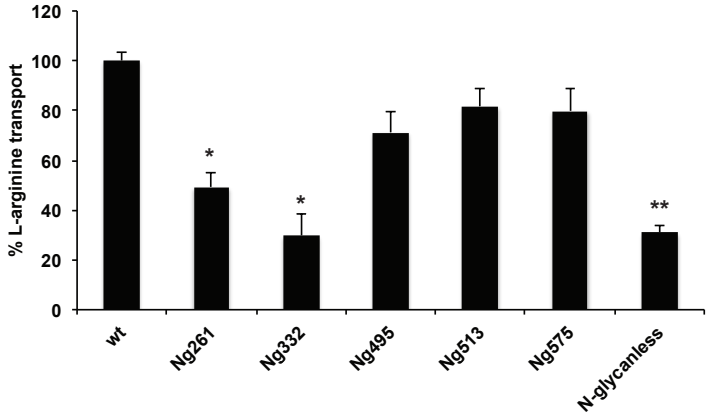

Figure 3.35. Transport activity of Ng rBAT mutants. HeLa cells were transfected with $b^{0,+}$AT and the wild-type or rBAT mutants, and after 36 h L-arginine transport was measured for 2 min (see Materials and methods). Data are the mean $\pm$ S.E. of at least 3 experiments for each mutant. Shown are significant differences compared to wild-type (unpaired Student's t test). $*$, $p<0.05$; $**$, $p<0.005$.

3.6.2 Pulse-chase imaging of the N-glycan mutant S577A

Wild-type human rBAT and the N-glycan mutant S577A were constructed into the SNAP-tag ® vector, a mammalian expression plasmid intended for the cloning and expression of SNAP-tag ® protein fusions in mammalian cells (see Materials and Methods). The SNAP-tag is a small protein based on human O_6-alkylguanine-DNA-alkyltransferase. SNAP-tag substrates are derivates of benzyl purines and benzyl pyrimidines. In the labelling reaction, the substituted benzyl group of the substrate is covalently attached to the SNAP-tag. The use of this system involves two steps: sub-cloning and expression of the protein of interest as a SNAP-tag fusion, and labeling of the fusion with the SNAP-tag with a cell-permeable functional group, allowing live-cell imaging of protein expression and localization. A cell-permeable non-fluorescent blocking agent (SNAP-Cell Block) allows time-resolved pulse-chase analysis of protein trafficking. First, we performed a pulse-chase experiment by labeling the cells with 35S-Methionine in the presence of $b^{0,+}$AT in order to confirm that the SNAP-tagged transporter was able to mature normally (Figure 3.36 A). The increase of 20 kDa is due to the SNAP protein. Then, pulse-chase imaging was performed by transiently transfecting HeLa cells with rBAT-SNAP26m and $b^{0,+}$AT. We can observe that at 3 h of chase the wild-type heterodimer already co-localizes in the plasma membrane (Figure 3.36 B), while the S577A mutant is still found in intracellular compartments. At 7 h the mutant was already localized in the plasma membrane. The microscopy confocal images confirm the results obtained in the pulse-chase assays.

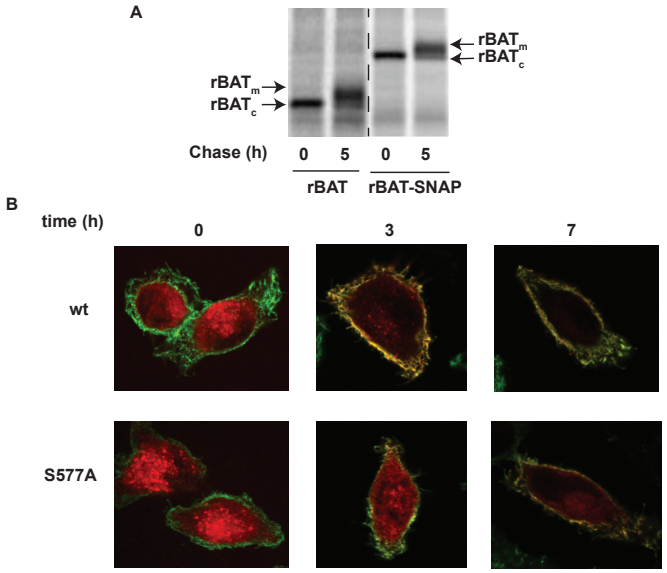

Figure 3.36. Pulse-chase of rBAT-SNAP and pulse-chase imaging of the N-glycan mutant S577A A, HeLa cells transiently expressing $b^{0,+}$AT together with rBAT and rBAT-SNAP were labelled and chased for 5 h. Equivalent amounts of radioactivity incorporated into protein were immunoprecipitated with the anti-$b^{0,+}$AT antibody. The precipitates were run under reducing conditions.Dashed lines indicate that the intensity of the lanes have been linearly increased by ImageQuant. B, Immunofluorescence of HeLa cells transiently expressing rBAT-SNAP26m and $b^{0,+}$AT. Cells were blocked with SNAP-Cell Block for 30 m, washed with DMEM medium for other 30 min, labeled with TMR for 15 min and washed again with DMEM medium for other 30 min. At different times cells were fixed and incubated also with anti-β-1 integrin to decorate the plasma membrane. A merge of a representative image for each time is presented. In red rBAT labeled with SNAP-Cell TMR-Star, a red fluorescent substrate that is based on tetramethylrhodamine and is suitable for standard rhodamine filter sets, in green β-1 integrin. Images from a representative experiment are shown. 3 independent experiments were performed.

3.7 ER-exit of the heterodimer in cells expressing a mutated form of ERGIC-53

ERGIC-53 is a mannose-specific membrane lectin that has been described to function as a cargo receptor for the transport of some soluble glycoproteins from the ER to the ERGIC (ER-Golgi intermediate compartment)[123,124]. One of the functions of ERGIC-53 is to capture transport-competent secretory glycoproteins in the ER and guide them through the COPII pathway to the ERGIC where dissociation occurs triggered by a pH-switch[124,125]. While the glycoproteins proceed through the secretory pathway, ERGIC-53 is recycled back to the ER. This capture mechanism is thought to accelerate the delivery of a number of glycoproteins

to post-ER compartments. ERGIC-53 has been described to be the cargo receptor for soluble glycoproteins such as cathepsin C[123], the blood coagulation factors V and VIII[128,254] and procathepsin Z[124,255]. For procathepsin Z, a folded surface-exposed β-hairpin loop, which is next to the critical N-linked glycan site, was required for efficient binding[126].

We wanted to analyse if the rBAT N-glycan N575 and the C-terminal disulfide bond played a similar role in the binding with ERGIC-53. As an initial step to study this we analysed if the mistargeting of ERGIC-53 interferred the ER exit of the heterodimer. We used the stably transformed HtTa-1 HeLa cell line (provided by Dr. H. Farhan, Biotechnology Institute, University of Konstanz) expressing in a tetracycline-inducible manner the KKAA mutant of ERGIC-53. This cytoplasmic tail mutant is unable to leave the ER because of the elimination of the ER exit determinant of ERGIC-53[256]. Since ERGIC-53 is a homo-oligomeric protein, overexpression of KKAA blocks the recycling of endogenous ERGIC-53 by mixed oligomer formation and thereby inactivate its transport receptor function. To minimize a possible upregulation of a compensatory mechanism for the lack of functional ERGIC-53, the mutant was expressed in the tet-controlled inducible system of Gossen and Bujard[257]. When expressed, the ERGIC-53 mutant is accumulated in the ER and retains the endogenous ERGIC-53 in this compartment, preventing its recycling[123]. We performed pulse-chase experiments, transiently transfecting HtTa-1 HeLa cells with rBAT and $b^{0,+}$AT, in presence and absence of tetracycline. Endo H analysis were also performed in order to analyse the ER-exit of the heterodimer (Figure 3.37). If ERGIC-53 had an important role in the ER-exit of the transporter we expected to see less or no maturation at all of the heterodimer. However no significant differences in the maturation and ER-exit of the heterodimer were observed when rBAT and $b^{0,+}$AT were synthesized in the presence of the ERGIC-53 mutant. Of course, this does not discard a role for ERGIC-53 in the biogenesis of rBAT-$b^{0,+}$AT. New experiments should be performed and other possible candidates may be tested (see Discussion).

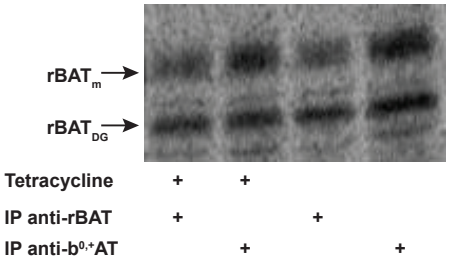

Figure 3.37. Maturation of wild-type rBAT in HtTa-1 cells expressing KKAA-ERGIC-53. Stably transformed HtTa-1 HeLa cell line transiently expressing rBAT and $b^{0,+}$AT were labelled and chased for 5 h. Equivalent amounts of radioactivity incorporated into protein were immunoprecipitated with the anti-$b^{0,+}$AT antibody. Endo H analysis was performed. The precipitates were run under reducing conditions. A representative experiment is shown.

3.8 Role of the N-glycan N575 and the cysteines C673 and C685 in the ER-exit of the heterodimer

The N-glycan mutant S577A and the cysteine mutants C673S and C685S present a qualitatively similar maturation defect. However, the double cysteine mutant C673S-C685S displays wild-type-like stability and maturation (Figures 3.14, 3.17 and 3.30). We wanted to test if there could be any kind of functional interaction between these elements concerning the maturation of the heterodimer. Double and triple mutants of the cysteines and the N-glycan were generated: S577A-C673S (N-C673S); S577A-C685S (N-C685S); S577A-C673S-C685S (N-C673S-C685S). A mutant that eliminates the C-terminal loop (Δ673-685) was also generated by mutating the C673 for a stop codon. Their stability and maturation was studied. Pulse-chase experiments were performed at 5 h of chase with wild-type and the single mutants as controls (Figure 3.38 mutant C685S not shown).

The Δ673-685 mutant is degraded (Figure 3.38 lanes 9 and 10). No significant differences in stability were found between the single and double mutants. The triple mutant N-C673S-C685S had a stability similar to both S577A and the double mutant C673S-C68S.

Maturation analysis of the mutants was performed by Endo H analysis at 5 h (Figure 3.39). As expected from the stability assays, the deletion mutant Δ673-685 showed no Endo H resistant band. The N-C673S-C685S showed a similar maturation than S577A ($\sim$ 50 % of Endo H sensitive band). The double mutants N-C673S and N-C685S showed a significatively slower maturation rate than the

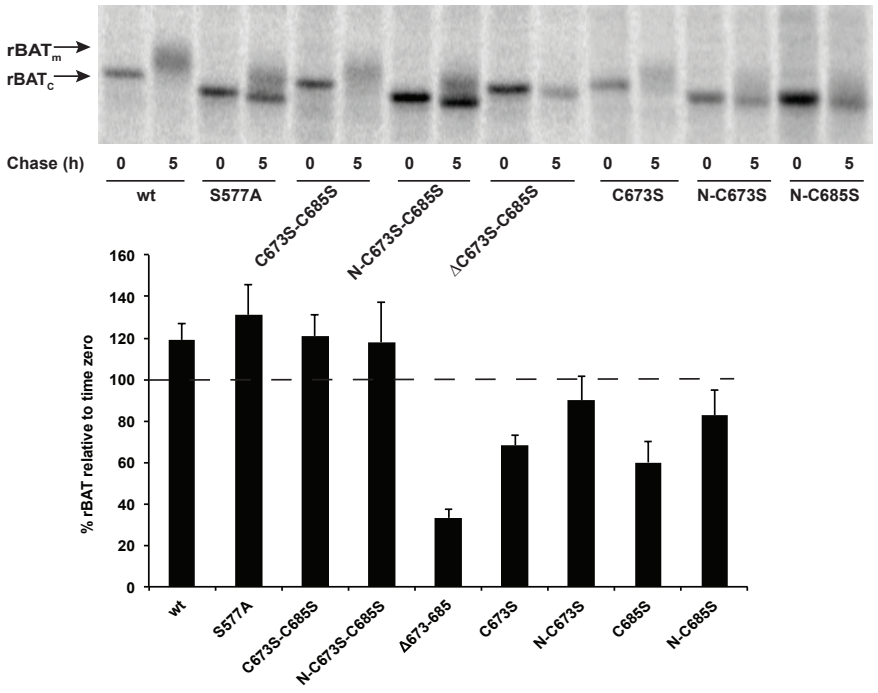

Figure 3.38. Stability of N575, C673S, C685S double mutants. Pulse-chase experiments were performed as in Figure 3.14. A representative experiment is presented. Data are mean ± S.E. of at least three independent experiments for each rBAT species. rBAT$_c$, core-glycosylated rBAT; rBAT$_m$,mature rBAT. The rBAT signal coprecipitated with the anti-b$^{0,+}$AT antibody at time 5 h was quantified relative to time zero.

single mutants ($\sim$ 70 % of Endo H sensitive band), different from their respective single mutants. All the results were compatible with additivity of the effect of C673S, C685S and S577A. Western blot and transport assays confirmed the results obtained with the pulse-chase experiments (Figure 3.40): all mutants, except for the Δ673-685, were able to mature. Transport experiments show that all of them were functional although to a less extent than wild-type rBAT.

Altogether, the results indicate that the mutant N-C673S-C685S shows a similar defect than the N-glycan mutant. However, it is surprising, given the other results, that the triple mutant shows a lower transport activity (see Discussion). The results obtained for the Δ673-685 mutant show that it is degraded and retained in the ER and therefore displays no transport. Given that the disulfide bond C673S-C685S mutant maturation was undistinguishable from the wild-type, this suggested that the C-terminal loop residues (674-684) of rBAT could play an important role in the biogenesis of the ER of the heterodimer. We decided to study this C-terminal loop.

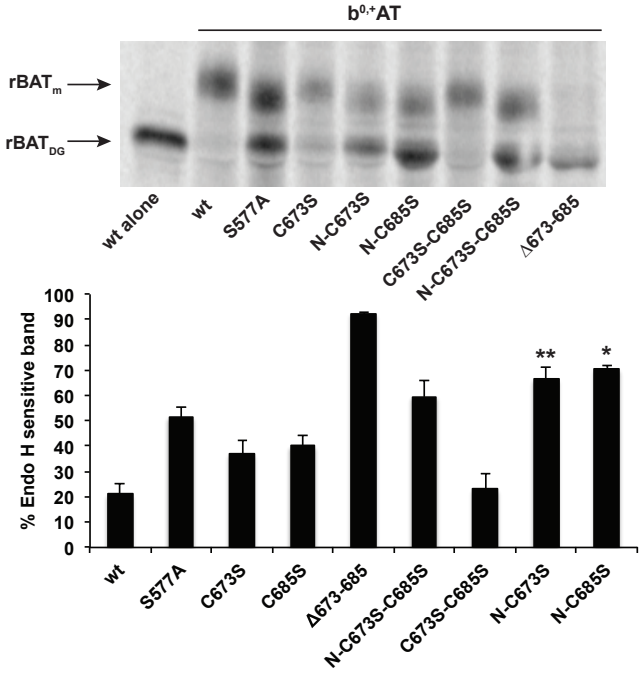

Figure 3.39. Endo H assay of N575, C673S, C685S and double and triple mutants. HeLa cells transiently expressing $b^{0,+}$AT together with rBAT mutants were labelled and chased for 5 h. Endo H analysis was performed as in (Figure 3.14). The asterisk indicates the significant difference between C673S and N-C673S and C685S with N-C685S (unpaired Student's t test). $*$, $p<0.05$; $**$, $p<0.005$.

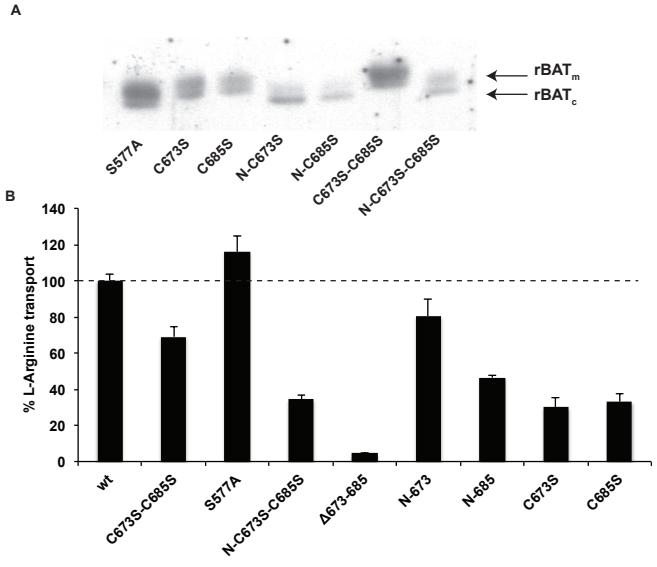

Figure 3.40. Western blot and transport of N575, C673S, C685S and double and triple mutants. A, Total membranes of transiently transfected HeLa cells were loaded for SDS-PAGE and analysed by western blot with anti-rBAT antibody. B, L-arginine transport assays were performed as in Figure 3.15.

3.9 Role of the C-terminal loop of rBAT in the biogenesis of the transporter

Alignment of rBAT orthologues of the loop residues present between cysteines C673 and C685 show that some of them are highly conserved (residues Y674, I 680, L681 and Y682) (Figure 3.41). We carried out an alanine scanning mutagenesis of the 11 residues that form the loop. Alanine scanning has been used to determine the contribution of single residues to the biogenesis and function of proteins. Alanine is the substitution residue of choice since it eliminates the side chain beyond the β carbon and yet does not alter the main-chain conformation (as can glycine or proline) nor does it impose extreme electrostatic or steric effects [258]. Each loop residue was mutated to alanine and their stability and maturation was studied. We also studied the cystinuria mutant L678P [220].

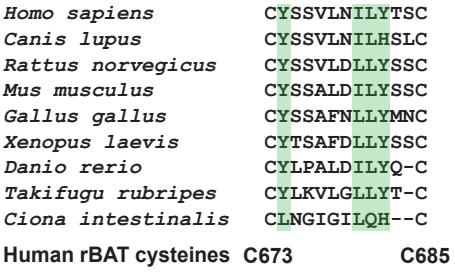

Figure 3.41. Alignment of the C-terminal loop in selected rBAT orthologues. The alignment of the C-terminal loop of rBAT was performed in selected rBAT orthologues with the program CLUSTAL. The more conserved residues are shown in green.

Stability of the loop mutants in the presence of $b^{0,+}$AT was measured with pulse-chase analysis. The loop mutants Y674A, L681A and Y682A presented more than 40% of degradation at 5h of chase; the rest of the mutants showed between 30% and no degradation at all (see Figure 3.42). The cystinuria mutant L678P showed a greatly reduced stability, much more than the L678A mutant.

Endo H analysis was also performed at 5 h of chase (Figure 3.43). These results, together with the previous stability results, prompted our initial classification of the C673-C685 loop mutants in 3 groups according to their ability to mature and their stability. Group 1, composed by the loop mutants S676A, V677A, I680A, T683A and S684A, showed a percentage of immature rBAT that range from 5 to 15%, which is similar to wild-type rBAT. In this group, only S676A presented almost 40% of the protein degraded at 5 h of chase. Group 2, formed by S675A, L678A and N679A, presented between 30 and 50% of Endo H sensitive band and

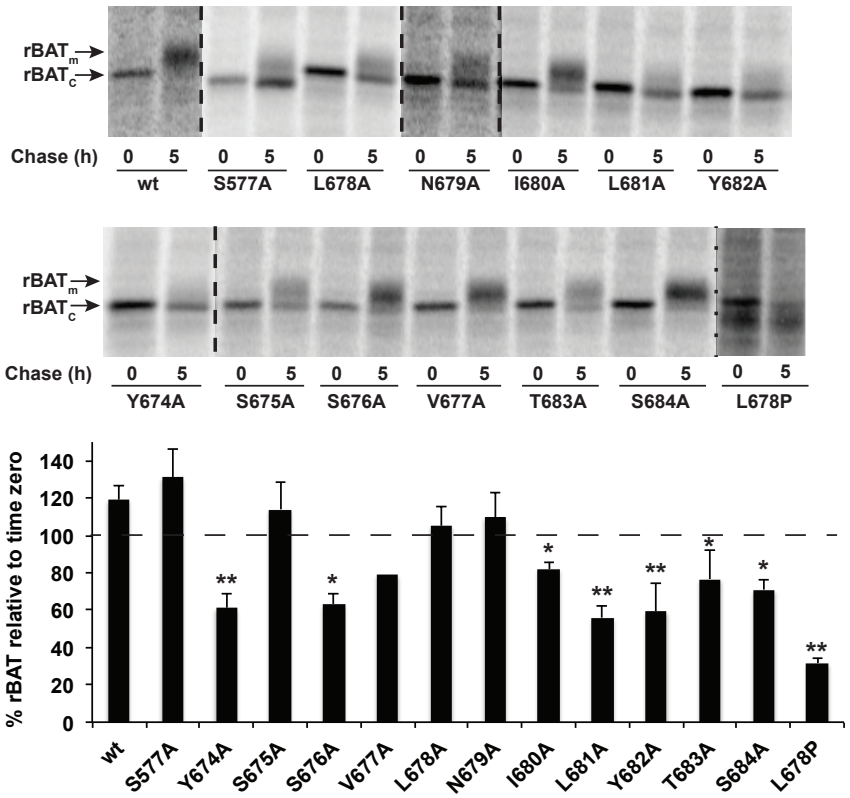

Figure 3.42. Stability of rBAT 673-685 loop mutants. Transiently transfected HeLa cells were processed as in Figure 3.14. Data are mean ± S.E. of at least three independent experiments for each rBAT species. rBAT$_c$, core-glycosylated rBAT; rBAT$_m$,mature rBAT. Dashed lines indicate that the intensity of the lanes have been linearly increased by ImageQuant. The dotted line indicates that the lanes correspond to a different gel. Shown are significant differences between wild-type and loop mutants (unpaired Student's t test). $*$, $p<0.05$; $**$, $p<0.005$.

no stability defects at 5h of chase (see above), similar to the properties of the N-glycan mutant S577A. Group 3 showed little maturation at 5h of chase (between 60 and 70% of Endo H sensitive band), and is composed by the loop mutants Y674A, L681A and Y682A. These mutants were clearly less stable than the wild-type (see above). The results for this last group residues, that are among the more conserved in the loop (Figure 3.41), may explain, at least in part, the results obtained when the whole loop is eliminated (Δ673-685 mutant, Figures 3.39 and 3.40).

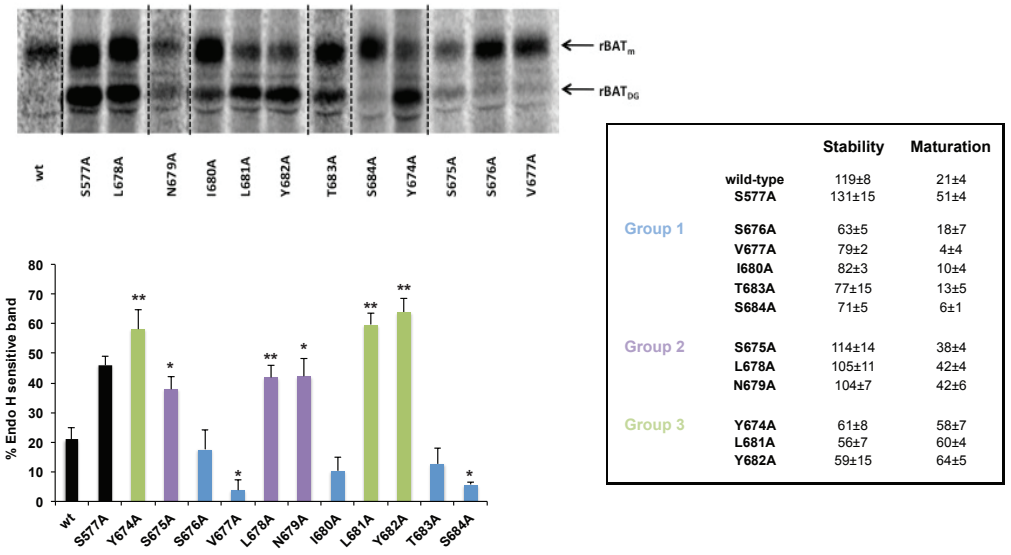

		Stability	Maturation
	wild-type	119±8	21±4
	S577A	131±15	51±4
Group 1	S676A	63±5	18±7
	V677A	79±2	4±4
	I680A	82±3	10±4
	T683A	77±15	13±5
	S684A	71±5	6±1
Group 2	S675A	114±14	38±4
	L678A	105±11	42±4
	N679A	104±7	42±6
Group 3	Y674A	61±8	58±7
	L681A	56±7	60±4
	Y682A	59±15	64±5

Figure 3.43. Maturation of rBAT 673-685 loop mutants. Endo H assays were performed as in Figure 3.14. rBAT$_{DG}$, deglycosylated rBAT; rBAT$_m$,mature rBAT. In blue group 1 members, group 2 mutants are depicted in purple and group 3 mutants in green. Shown are significant differences between double and single mutants (unpaired Student's t test). $*$, $p<0.05$; $**$, $p<0.005$.

3.9.1 Study of double mutants of the loop residues

Double loop mutants were generated of those residues that showed a maturation rate similar to the N-glycan mutant S577A (S675A, L678A, N679A), in order to study possible interactions between them. The stability, maturation and transport of the mutants were analysed. The double loop mutants displayed an important reduction of stability compared with the single mutants: ∼50% of rBAT was degraded in the double mutants at 5 h of chase while the single mutants displayed no degradation (Figure 3.44). Moreover, they were unable to mature. These results suggested that these synergistic defect on stability and maturation were due to their misfolding.

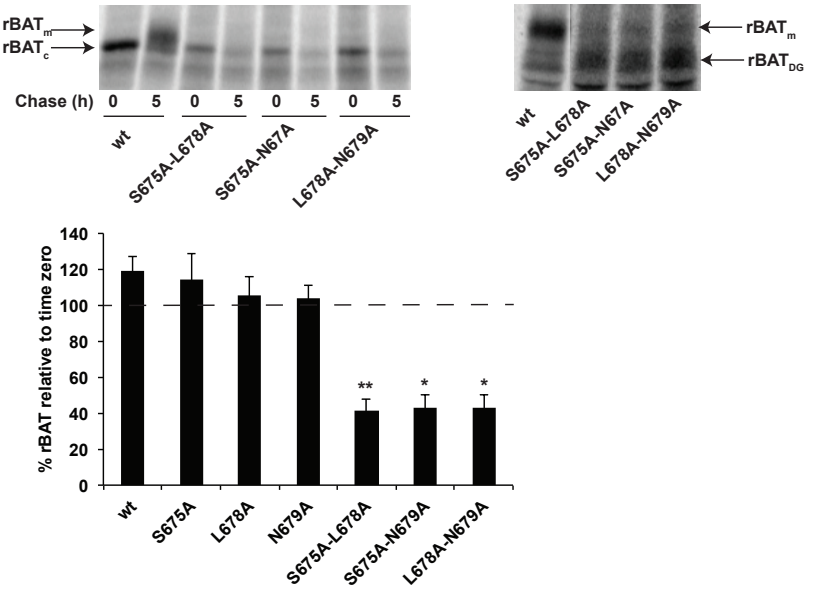

Figure 3.44. Stability and maturation of double loop mutants. Transiently transfected HeLa cells were treated as in Figure 3.14. Quantification of pulse-chase at 5 h of chase relative to time zero. Data are mean ± S.E. of at least three independent experiments for each rBAT species. rBAT$_c$, core-glycosylated rBAT; rBAT$_m$,mature rBAT. C, Endo H analysis at 5 h of chase.

3.9.2 Loop mutants in the C673S-C685S background

As explained in Section 3.2.2, the C673S-C685S mutant lacks the C-terminal disulfide, but behaves similar to wild-type in stability and maturation (Figures 3.17 and 3.18). However, the elimination of the C673-C685 loop (Δ673-685 mutant) abolishes maturation and function of the transporter (see Section 3.8 and Figures 3.38, 3.39 and 3.40). In order to study if there was an interplay between the C673-C685 disulfide and the residues within the loop, mutants from group 2 (S675A, L678A and N679A) and 3 (Y674A, L681A, Y682A) and the I680A mutant from group 1, that show a wild-type-like behaviour, as a control, were engineered into the C673S-C685S (CC) background by site-directed mutagenesis and studied by pulse-chase and western blot (Figure 3.45). If there is no interaction between the two elements (i.e; the disulfide and the loop residue) the effect in the double mutant should be additive[259,260]. Departure from additivity would suggest an interaction between the disulfide and the specific loop residue. Concerning stability, with the exception of Y674A, we observe more degradation in the double mutants. This synergistic effect was specifically striking in Group 2 mutants (S675A, L678A and N679A), suggesting that the presence of the disulfide masks stability effects

in the maturation of this 3 residues.

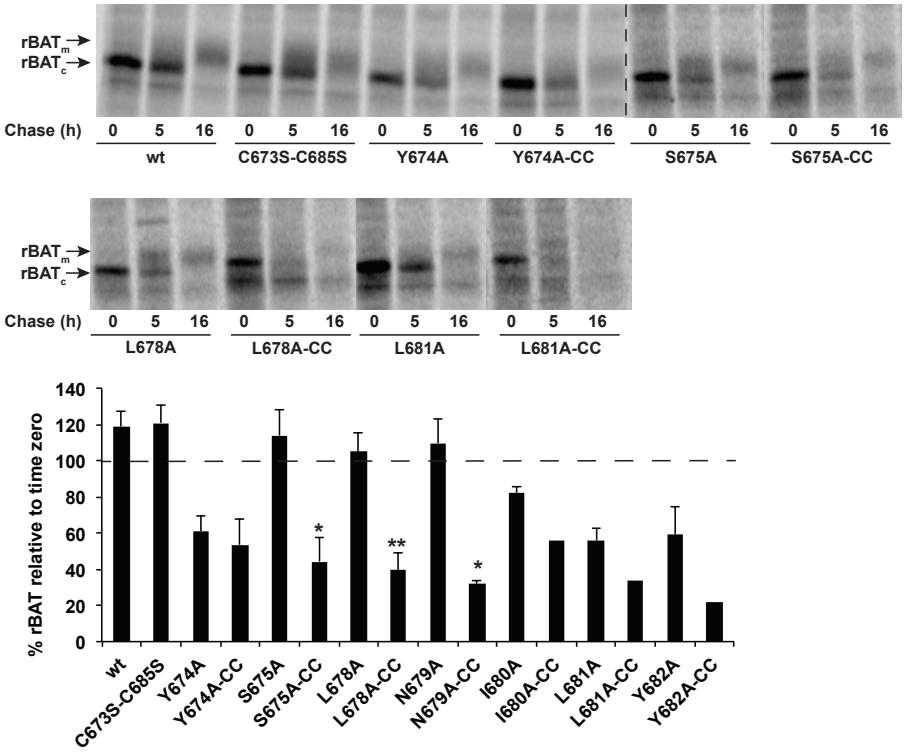

Figure 3.45. Stability of rBAT loop mutants in C673S-C685S background. Transiently transfected HeLa cells were treated as in Figure 3.14. A representative experiment is shown. Data are mean ± S.E. of at least three independent experiments for each rBAT species, unless no error bars are depicted were 2 experiments were performed. $rBAT_c$, core-glycosylated rBAT; $rBAT_m$, mature rBAT. Shown are significant differences between double mutants and their corresponding single loop mutant (unpaired Student's t test). $*$, $p<0.05$; $**$, $p<0.005$.

The higher degradation of these double mutants made difficult the study of their maturation. Therefore, Western Blots experiments were performed on a total membrane fraction (Figure 3.46 A, S675A and S675A-CC not shown). As expected, the I680A-CC group 1 mutant kept the wild-type behaviour, with no detectable immature band. Both group 2 and group 3 double mutants showed a great decrease in the maturation band compared to that of the single mutants. This synergistic effect suggests that, despite the disulfide bond is not essential *per se*, its absence seems to strongly potentiate the misfolding effects of several loop mutants. This argues that both the disulfide and these loop residues have an important role in the biogenesis of the heterodimer and explains the null phenotype of the Δloop mutant.

L-arginine transport of single and double loop mutants was performed (Figure 3.46 B). All group 1 mutants (except S676A) and the S675A mutant (group 2) showed wild-type-like transport. The rest of the single mutants showed a reduced transport activity, although to different extents. The Y682A-CC was the only mutant that showed a similar transport than the single mutant while the other mutants showed a transport decrease when expressed in the C673S-C685S background (see Discussion).

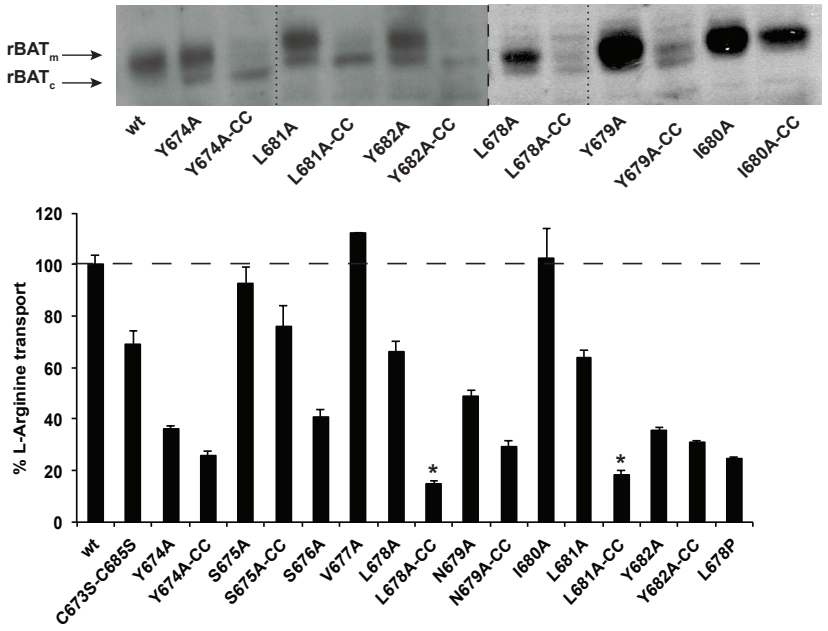

Figure 3.46. Maturation and L-arginine transport of rBAT loop mutants in C673S-C685S background. A, Total membranes of transiently transfected HeLa cells were loaded for SDS-PAGE and analysed by western blot with anti-rBAT antibody. rBAT$_c$, core-glycosylated rBAT; rBAT_m, mature rBAT. Dotted lines indicate that irrelevant lanes have been removed. Dashed lines indicate different gels. B, L-arginine transport in HeLa cells was performed as in Figure 3.15. Shown are significant differences between double mutants and their corresponding single loop mutant (unpaired Student's t test). $*$, $p<0.05$.

3.9.3 Group 2 mutants in the S577A background

Group 2 mutants (S675A, L678A and N679A) that show a maturation and stability similar to the N-glycan mutant S577A, were engineered into the S577A background by site-directed mutagenesis in order to study a possible interaction between these residues of the loop and the N-glycan. It was included also one mutant of the group 1 (I680A) as a control. We have began to analyse these mutants by pulse-chase and Endo-H assay (Figure **??** A). Regarding stability, the

N-I680A mutant matured as the S577A mutant, as expected. The double mutants displayed a lower stability, significantly different from the S577A mutant and from the single loop residues at 16 h. This synergistic effect observed suggests that these double mutations are causing a misfolding defect in rBAT.
The Endo H assays also show that the effect in the double mutants is less than additive (Figure **??**B) suggesting an interaction between the 2 elements. Transport assays with L-Arginine showed a decrease of the transport in the loop mutants in the S577A background, significantly different for the N-S675A and N-L678A compared to the single loop mutant (Figure 3.47).

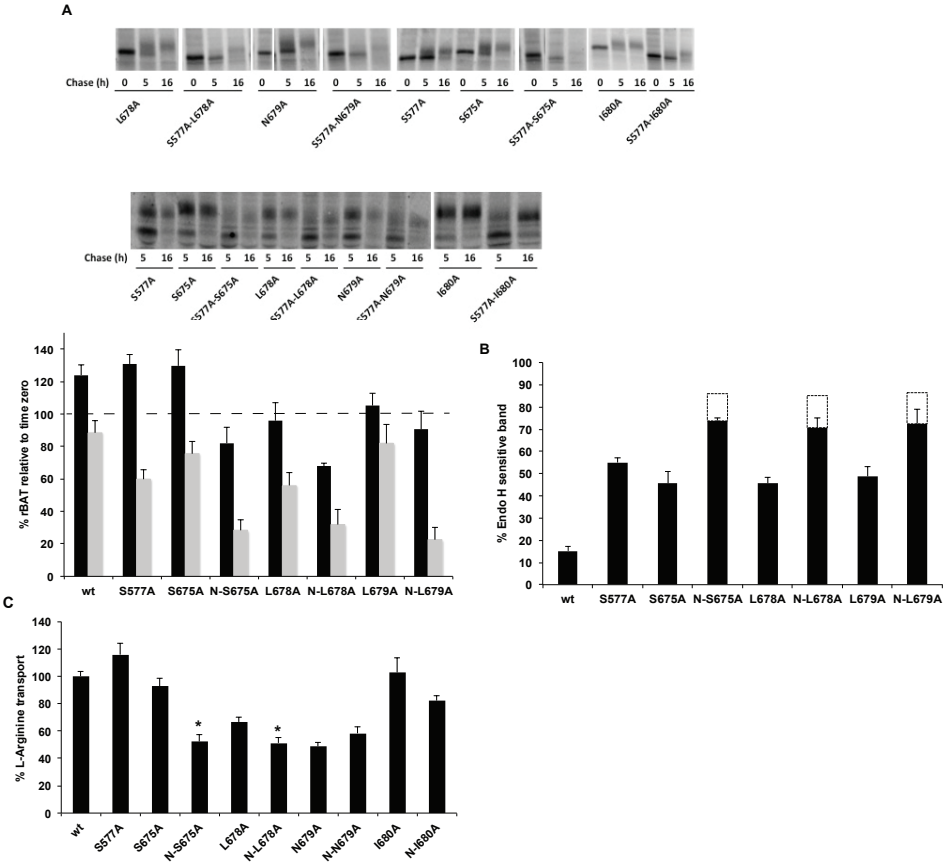

Figure 3.47. Maturation and L-arginine transport of group 2 mutants in the S577A background. A, Transiently transfected HeLa cells were treated as in Figure 3.14. Data are mean ± S.E. of at least three independent experiments for each rBAT species, unless no error bars are depicted were 2 experiments were performed. $rBAT_c$, core-glycosylated rBAT; $rBAT_m$,mature rBAT. B, Quantifications of Endo H sensitive band at 5 h of chase are shown. The dotted bars indicate the product of the effects of the two single mutants, the result expected for simple additivity. C, L-arginine transport in HeLa cells was performed as in 3.15. Shown are significant differences between double mutants and their correspondant single loop mutant (unpaired Student's t test). $*$, $p<0.05$.

Discussion

Knowledge of *in vivo* membrane protein folding is important to gain insight on the mechanisms of protein folding and misfolding, which are key issues in the study of misfolding diseases. Many of these diseases are caused by mutations in the membrane proteins. The aim of this thesis was to depict the different elements that play a role in the biogenesis of the cystinuria transporter rBAT-$b^{0,+}$AT. In order to study these elements we determined the role of the disulfide bonds and the N-glycans present in rBAT in the biogenesis of the heavy subunit rBAT and the heterodimer rBAT-$b^{0,+}$AT. Our initial results prompted also the analysis of the C-terminal tail of rBAT.

Here, we have found that the light subunit $b^{0,+}$AT is required for the folding of the heavy subunit rBAT. We have identified the disulfide bonds present in rBAT and their order of formation and we have described the oxidation state of rBAT in the absence of $b^{0,+}$AT. We have also identified the N-glycans present in rBAT and determined the role of the N-575 N-glycan in the ER-exit of rBAT-$b^{0,+}$AT, as well as the implication of some C-terminal loop residues in the folding and ER-exit of the transporter.

4.1 Oxidative folding of rBAT in the presence of $b^{0,+}$AT

The most direct form to find the disulfide bonds present in rBAT would be crystallization of the heavy subunit rBAT or the heterodimer. However, all attempts to overexpress the ectodomain of rBAT have failed, and its secondary and tertiary structures have, therefore, been predicted based on amino acid sequence similarity with 4F2hc (<30%) and with prokaryotic α-amylases (32%)[145,243,254,261–263].

Human rBAT contains eight cysteines. The first cysteine, C18, is cytosolic, and the rest of the cysteines, 114 to 685 are extracellular (Figure 3.7). Cysteine 114 is disulfide-linked with human $b^{0,+}$AT[141,242], cysteines 242 and 273 are localized in the domain B, cysteine 571 is in domain C, and cysteines 666, 673 and 685 are in the C-terminal tail of rBAT[145]. Cysteines 114 to 685 are conserved in all orthologues except for the cysteines localized in domain B (242 and 273) that are not conserved in two urochordate rBAT orthologues (Figure 3.8). This degree of conservation already suggested an important role in the biology of the transporter. The cristallization of the ectodomain of 4F2hc[145] suggested that cysteines 242

and 273 could be forming a disulfide bond, although there was no direct evidence. The number and identity of the disulfide bonds present between cysteines C571 to C685 was unknown, and the structural model did not offer any clue about this question.

We devised a strategy, using the alkylating agent mPEG (pegylation), to count free cysteines in rBAT, under denaturing conditions. In the absence of $b^{0,+}$AT the pegylation assays showed only 1 mPEG in rBAT. This mPEG was absent when C18 was mutated to serine, indicating that the ectodomain of rBAT was fully oxidised and, therefore, contained 3 disulfide bonds when $b^{0,+}$AT was present. Further pegylation, stability and maturation analysis performed in the presence of $b^{0,+}$AT with cysteine mutants of rBAT were required to map these 3 disulfides. Firstly, mPEG experiments with single cysteine mutants revealed the disulfide bond present in domain B (C242-C273). Stability, maturation and functional assays of these mutants uncovered the presence of another disulfide bond: C673-C685. Therefore, the remaining disulfide bond is formed by cysteines C571 and C666.

The first disulfide bond, formed by cysteines 242 and 273, is in the B-domain, a ∼90-residue-long globular insertion between the third β-strand (Aβ3) and the third α-helix (Aα3) of the TIM barrel A-domain. The presence of this disulfide bond was already suggested in the modelling of domain B with the *Bacillus cereus* α-1,6-glucosidase as a template[145]. Domain B is present in most α-amylases and forms the substrate-binding cleft together with the central domain A[264,265]. Some α-amylases have a disulfide in domain B, which might be important for enzyme stability[265]. The cysteine mutants of either of the two cysteines present in the domain B of rBAT (C242 and C273) as well as the double mutant C242S-C273A, are rapidly degraded, indicating a destabilizing effect (Figures 3.13 and 3.14). The pegylation pattern of this double cysteine mutant is similar to wild-type rBAT, suggesting that C242S-C273A does not influence the formation of the other two disulfides (Figure 3.16). However, the single mutants C242S and C273A and the double mutants combining C242S with C571S, C666S, and C673S, cause the prevalence of more reduced $b^{0,+}$AT - linked rBAT forms (Figures 3.12 and 3.16), indicating that having an impaired cysteine in the domain B affects the formation of the other two disulfide bonds. At first sight, this is surprising, because domain B and C are located at opposite sides of the central TIM barrel[145,264] (Figure 3.7), and thus the other two disulfides, C571-C666 and C673-C685, are located far

from the domain B disulfide. Moreover, cysteines 242 and 273 are at more than 300 amino acids from the C-terminal cysteines. The results suggest that the absence of the C242-C273 disulfide may cause misfolding of more C-terminal regions if C242 or C273 are unpaired. When cysteines C242 or C273 are unpaired, these cysteines may disturb the formation of the C-terminal disulfides. It is likely that the oxidation of rBAT after assembly with $b^{0,+}$AT is a co-translational event (see later). The mean translation rate is assumed to be 4-5 amino acids/sec in eukaryotes[51]. In this context, the results suggest that, if C242 or C273 are unpaired, Domain B is not stably folded at least 1 min after C273 is synthesized (when C571 is translated). Therefore, it is likely that the domain B disulfide could form first, initiating the intramolecular oxidation pathway, and preventing tin this way he C242 and C273 from interfering with other regions of the protein that may be still unfolded. Most likely when C571 appears in the lumen of the ER the domain B is already folded. Another possibility is that, when both C242 and C273 are present, their potential oxidation by attacking more C-terminal cysteines may be prevented by other mechanisms (for example, by chaperones binding). The pegylation pattern of the mutants C242S-C273A, C571S- C666S, and C673S-C685S is very similar (Figure 3.16), suggesting that any of the three disulfides could form independently of the others. To avoid non-native interactions between unpaired C242 or C273 with more C-terminal cysteines, the formation of this disulfide may initiate the intramolecular oxidation pathway. This is strongly supported by the experiments performed with mutants containing only of the natively paired cysteines, which show that C242-C273 is the only disulfide that is completely oxidized in the absence of the other two (Figure 3.19). This is not observed neither for C571-C666 nor C673-C685.

The disulfide bond formed by the cysteines 571 and 666 connects the domain C with the C-terminal tail that has no homology to known sequences. Cysteine 571 is in the β1 strand of domain C (Cβ1). Cβ1, Cβ2 and Cβ3 may form the mainly hydrophobic contacts between the C and the A domains (Aα6 to α8)[145]. The single and double mutants of the cysteines forming this disulfide bond are retained in the ER and rapidly degraded. This suggests that the connection between the N-terminal region of the C-domain and the tail is essential for biogenesis. The C571-C666 disulfide may stabilize and/or promote this connection (Figures 3.14 and 3.17).

The other disulfide bond, composed by cysteines 673 and 685 is localized in the

C-terminal tail and is the only one not essential *per se* for biogenesis (Figures 3.14 and 3.17). The double mutant shows a similar stability and maturation than wild-type rBAT, and displays a mild decrease in transport activity (Figure 3.17). The single mutants of this disulfide bond do show reduced stability, maturation and function compared with wild-type and the double mutant C673-C685, although to a less extent than the other cysteine mutants analysed, where no maturation and transport can be observed (Figures 3.13, 3.14 and 3.15). This suggests that it is the fact that one of the cysteines is unpaired that causes the defect. Perhaps this is due to interferences with C571 and C666. However, there are other possibilities: the Δ673-685 rBAT mutant showed no maturation and no transport activity indicating a key role of the 11-residue loop residues enclosed by the C673-C685 disulfide between the 2 cysteines in the biogenesis of the heterodimer. This loop could be stable in the context of the double mutant C673S-C685S, but not in the single mutants. Of course, both possibilities are not mutually exclusive (see below).

The pegylation pattern of mutants containing only the cysteines 571 and 666 or 673 and 685 (DS2 and DS3 mutants) is very similar to wild-type and double cysteine mutants (Figure 3.19), suggesting that, after the complete oxidation of C242-C273, the oxidation of C571-C666 and/or C673-C685 in wild-type rBAT is posttranslationally stabilized (Figure 3.20). Pegylation of the double mutants C571S-C673S and C666S-C685S is similar to the native disulfide mutants C571S-C666S and C673S-C685S, indicating that non-native disulfides bonds are present in C571S-C673S and C666S-C685S, most likely between the corresponding unpaired cysteines (Figure 3.16). The presence of non-native disulfides within the folding on-pathway of some disulfide-rich proteins has been already reported both *in vitro* and *in vivo* [54,55,266].

The pegylation experiments show that most probably the first disulfide to form in rBAT is the C242-C273, and suggested that the other disulfide bonds are formed post-translationally (see above), but does not help us to understand at first sight the order of formation of the other two. However, a careful analysis of the tri-pegylated band in wild-type and cysteine mutants could indicate the possible oxidation order for the C571-C666 and C673-C685 disulfides in the presence of $b^{0,+}$AT. The mobility of this band differs according to the mutant: observation of Figures 3.16 and 3.19 indicates that the slower band appears in wild-type, C242S-C273S, C673S-C685S, C666S-C685S, C666S-C673S and DS2; whereas the faster band appears in C571S-C666S, C571S-C673S, C571S-C685S and DS3. These re-

sults indicate that the slower band correlates with the absence of disulfides between C571 and C666, C673 or C685. In that way, wild-type rBAT present in the slow band 3 may contain the C242-C273 disulfide, the cysteine C571 reduced and pegylated, and a disulfide formed between two of the cysteines C666, C673 and C685, and the other one being reduced and pegylated. The other pegylated cysteine would be the cytoplasmatic cysteine C18. In the mono-pegylated band, most likely due to C18, three disulfide bonds are formed. The results point to C242-C273 forming first, and co-translationally; perhaps independently from $b^{0,+}$AT (see later). Our data is compatible with the post-translational formation of 2 disulfides between C571, 666, 673 and 685 but there could be different rBAT species containing either 2 native (band 1) or 2 non-native disulfides (band 3), or one native or non-native disulfide (Figure XXXX). Perhaps, $b^{0,+}$AT may act by shifting the equilibrium between band 1 and slow band 3 to the correct cysteine pairing of C571, then irreversibly stabilizing the oxidation of C571 to form the C571-C666 disulfide, that would be the last to form. The completion of this may occur post-translationally, as during the chase di and tri-pegylated bands dissapear giving raise to a band with 1 mPEG attached (see Figure 3.20). Therefore, $b^{0,+}$AT may act, after assembly with rBAT, as a platform for the folding of the heavy subunits stabilizing it. In this context, a recent study describes how the heavy subunit 4F2 stabilizes the light subunit LAT2 through the interaction of a large surface of the ectodomain of 4F2hc with the external face of LAT2[267]. In our case it seems like it is the heavy subunit that stabilizes the light subunit. In fact, $b^{0,+}$AT could also interact witha large region of the ectodomain of rBAT and it could help to keep the domain B away from domain C, avoiding disulfide bond formation between these 2 domains.

DS2 (mutant containing cysteines C571 and C666).

It was already known that, when expressed alone, rBAT is degraded via the ERAD pathway, and the heterodimerization blocks degradation of rBAT[157]. A potential mechanism would be the assembly with $b^{0,+}$AT could mask an exposed region in unassembled rBAT acting as a degradation determinant, similar to unassembled TCRα[136]. However, rBAT could be also recognized as an unfolded polypeptide. Actually, we found that, as unassembled rBAT does not complete the oxidative folding of its ectodomain (Figure3.20). rBAT pegylation shifted from mainly 3 and 4 mPEG bands in unassembled rBAT to the more intense one mPEG band in $b^{0,+}$AT-associated rBAT. As stated earlier in this section, unassembled rBAT was found as an ensemble of mPEG bands. The pegylated bands 1 to 4, and

even 5 and 6 but with a much less intensity, most likely reflected the presence of several unassembled rBAT redox species within the ER, which could be in equilibrium. The major bands with 3 and 4 mPEGs attached indicate that at least one intramolecular disulfide was not present (Figures 3.24 and 3.24). Different redox species in unassembled rBAT could represent the ensemble of *in vivo* redox intermediates detected in folding studies of disulfide-rich proteins in vitro [266]. However, we have not obtained experimental evidence in support of this, most likely because the initial oxidative folding of rBAT upon association $b^{0,+}$AT is too fast for our analysis.

The pegylation pattern of rBAT cysteine mutants in the absence of $b^{0,+}$AT was also analysed. The cysteine mutants C18S and C114S displayed a similar pegylation pattern with major bands corresponding to 1, 2 and 3 mPEGs attached, the band corresponding to one mPEG attached representing ∼50% of the pegylated molecules. It is surprising that both mutants have a similar pegylation pattern because, although both of them do not form intramolecular disulfides cysteines, one is located in the cytosol while the other is placed in the lumen. We have no clues as to why the absence of these cysteines despite its very different environments, display a similar pegylation pattern. It has to be considered, however, that the redox species might be very different between them (i.e the 3-PEG species, for instance, may contain different reduced species in both cases.

The mutants C242S and C273A display a different pattern with up to 4 and 5 mPEGs attached. This result indicates that in these mutants rBAT contains at most one disulfide bond and it is therefore likely to be more drastically misfolded folded than the other mutants. These results corroborate that when one of these cysteienes is unpaired rBAT is more unfolded, similar to what is observed also when rBAT is expressed together with $b^{0,+}$AT (Figure 3.19). The mutants C571S to C685S display a pegylation pattern with 2 and, specially 3 mPEGs attached. These mutants seem to show a more unfolded state compared to the single mutants of Domain B cysteines.The fact that the same bands appear in different mutants implies that the content of each band, containing homogeneous number of reduced cysteines, is likely to be heterogeneous concerning the identity of the reduced and oxidated cysteienes. It has been recently described for α and βTCR that less-hydrophobic TM segments of unassembled single-pass TM proteins can enter the ER lumen completely [268]. We have not explored the possibility with unassembled rBAT. Finally, a possible way to know the different oxidative species

present in each band would be to perform a mass-spectometry if enough material would be available.
The light subunit b$^{0,+}$AT could control posttranslationally the connectivity of the cysteines present in the C-domain and the C-terminal tail, irreversibly shifting the oxidative folding towards the native disulfides Cys-571-Cys-666 and Cys-673-Cys-685. In this way, the assembly with b$^{0,+}$AT may stabilize the interactions of the rBAT tail with the A-C interdomain interface and the C domain.

In vivo post-assembly folding of selected subunits in other heteromeric protein complexes have already been described[26–29]. The challenge is to dissect the different roles of each subunit in the assembly of the complex and in the folding of the other subunits. The folding of one subunit could be completely dependent of the other subunit, or could just facilitate its folding. This question has only been neatly solved for the Ig heavy chain C_H1 domain. C_H1 folding strictly depends on the association with the Ig light chain C_L domain[28]. Our results show that the redox state of rBAT in the absence of b$^{0,+}$AT does not change during the chase (Figure 3.20) and this results did not change when the degradation was delayed (Figure 3.21). This suggests that folding and degradation of unassembled rBAT are not competing events and that b$^{0,+}$AT assembly, besides providing more time for wild-type rBAT folding, may have a more active role in that process. Analogous to the CL-dependent folding of CH1[28], assembly with b$^{0,+}$AT might be mandatory for oxidation of the rBAT ectodomain. A direct proof for the hypothesis requires reconstitution of the assembly and folding reactions with the 2 purified subunits of the cystine transporter.

4.2 Role of the N-glycans in the biogenesis of rBAT-b$^{0,+}$AT

N-glycans have been described to play an important role in the folding and maturation of glycoproteins[64,65,269,270]. It has already been shown that individual N-glycans do not play equivalent roles in the processing of several glycoproteins, for instance the cystic fibrosis membrane conductance regulator, a channel protein involved in the pathology of the cystic fibrosis[82], human tyrosinase[271] and the simian virus 5 hemagglutinin-neuraminidase[79]. In rBAT orthologues, none of the N-glycans is completely conserved (see Section 3.6 and Figure 3.27). Of the 6 putative N-glycan consensus sites present in rBAT, all of them are used except for the N214 (Figure 3.27), the only one that was predicted to be located in an

internal position[145]. In fact, the cystinuria mutant T216M leads to post-assembly degradation of rBAT[157].

Our study of the N-glycans of rBAT indicate that they are not essential for the transporter (N-glycanless mutant is able to transport aminoacids, see Figure) although they are required for efficient degradation of unassembled rBAT, for ER-exit of the holotransporter and also for funtion and/or traffic beyond the Golgi complex. We have focused our effort on the role of the N-glycan N575 in the maturation of the transporter (see below).

The assays performed in N-glycan mutants show that they are not essential for the functionality of the transporter as the N-glycanless mutant induces transport activity. However, the transport is greatly reduced and this result can be due, at least in part, to the transitory transfection of rBAT and $b^{0,+}$AT that can cause different protein expression.

The unassembled glycanless mutant is much less degraded than wild-type rBAT indicating that N-glycans were required for the efficient degradation of unassembled rBAT. Whether this is due to an active role of N-glycans in degradation, or to aggregation of the glycanless mutant is not known. However, experiments with mutant containing only one N-glycan gave support to this hypothesis. As the N-glycanless mutant, the Ng515 mutant displays very little degradation, suggesting that this N-glycan does not have a relevant role in rBAT degradation. This degradation experiments also suggested a possible role in rBAT degradation of the N332 glycan (Figure 3.32). The mutant containing just this N-glycan is the only one that displayed a wild-type-like degradation behaviour, suggesting that this N-glycan is able to sustain degradation of rBAT for itself.

The unassembled Ng332 mutant (carrying only the N332 glycan) was degraded at a similar rate compared to the wild-type.

A similar role in degradation has already been described for the N894 glycan of the CFTR[82] and the simian virus 5 hemagglutinin-neuraminidase[79] and CPY[81].

When only this N-glycan was eliminated, no significant differences in rBAT degradation were observed (Figure 3.27). This can be explained because the presence of the other N-glycans may compensate the absence of N332, as has been already described for CPY N-glycans[81]. For the other N-glycans probably N515 does not play an important role in degradation as N515 seemed to be similar to the

N-glycanless mutant. It would be also interesting to study if N332 interacts with the ERAD machinery and the lectin chaperones CNX/CRT.

Several N-glycans of different proteins have already been described as important for the efficient intracellular transport. For instance, the N-terminal glycans of the yeast carboxipeptidase Y[126], the H,K-ATPaseβsubunit[272], tyrosinase[271]. The results obtained for the S577A mutant indicated that this N-glycan could be playing a similar role in the ER-exit of the heterodimer. When only this N-glycan is absent the maturation of the heterodimer is impaired, indicating a delay in the exit of the ER of the heterodimer (Figure 3.30). The same effect is observed for N575D and N575Q, strongly suggesting that it is the absence of the N-glycan and not the mutation to alanine that causes this defect in the maturation of the mutant (Figure 3.31). More important, when rBAT carried any of the 5 N-glycans individually, the transporter was able to mature, but the N575 glycan alone was the only one capable by its own to confer wild-type like maturation to rBAT-$b^{0,+}$AT. Moreover, when only this N-glycan is present, the heterodimer recovers a wild-type-like maturation (Figure 3.34).

We confirmed also the maturation deffect of the S577A mutant was by pulse-chase imaging. The technique had several experimental problems. Transitory transfection of rBAT and $b^{0,+}$AT gave little protein expression that made it sometimes hard to obtain good images. In order to avoid this problem stable transfection of wild-type rBAT and the mutant should have been performed, however, this was not done due to schedule issues. We also tried to quantify the amount of protein retained in the ER respect to that located in the membrane. However it was difficult to accomplish because TMR-star, with which the fusion protein was labelled, enters the cell in a permeable way obtaining at the earlier times of the pulse-chase a signal that is partially due to non-attached TMR. Athough the signal was higher than for samples transfected with pcDNA3, as every cell had a different expression it was difficult to ascertain how much of the signal was due to labeled rBAT-SNAP. Several washes were added after incubation with TMR but we were unable to erase this non-specific signal. Although we were not able to perform quantifications, qualitatively, the images confirm the results obtained with pulse-chase analysis. At 3h, wild-type rBAT already co-localizes with the membrane antibody while the N-glycan mutant S577A is still mainly localized in intracellular compartments, most probably ER (Figure **??**). Altogether, we concluded that the N575 N-glycan is the only N-glycan necessary and sufficient to

achieve the same maturation as wild-type rBAT. This impaired maturation observed for the N-glycan mutant S577A is similar to that observed for the cysteine mutants C673S and C685S (see below).

ERGIC-53 has been described to be the cargo receptor for other soluble glycoproteins as the blood coagulation factors V and VIII[128,254], cathepsin C[123] and cathepsin Z[255] [124]. The structure recognised for this last protein is a folded surface-exposed β-hairpin loop, which is next to the critical N-linked glycan site, was required for efficient binding[126]. We decided to study if the C-terminal loop of rBAT together with the N575 glycan could be playing a similar role. Endo H analysis performed in stably transformed cells expressing a mutant of ERGIC-53 that is retained in the ER were used to express the transporter. No differences in the maturation rate of the heterodimer compared to cells expressing a wild-type form of ERGIC-53 were observed, suggesting that ERGIC-53 does not participate in the ER exit of the transporter. However, only preliminary experiments were performed and other controls should be done, as transfecting this cells with cathepsin Z or trying to immunoprecipitate rBAT with ERGIC-53. It is also a possibility that the exit of the heterodimer is not only ERGIC-53-exit dependent and that the absence of it is replaced by other cargo receptors as Erv29p, Surf4 or Emp24p.

4.3 Role of the N-glycan N575, cysteines C673 and C685, and the C-terminal loop residue in the ER-exit of the heterodimer

Cysteine mutants C673S and C685S and the N-glycan S577A mutant presented a qualitatively similar maturation defect. This prompetd our hypothesis that these elements might be acting in a concerted manner as a maturation signal. In order to see if there was any functional interaction between them concerning the maturation pathway of the transporter we generated doble and triple mutants and we studied their stability, maturation and functionality. A mutant that eliminated the C-terminal tail of rBAT was also studied ($\triangle$673-685). The pulse-chase assays shows that the stability and maturation defect displayed in the N-C673S-C685S is not significantly different from that of S577A, indicating additivity in the mutant that lacks the N-glycan and the disulfide bond. The additivity in double mutants N-C673S, N-C685S indicate that the two elements act independently in the maturation of the heterodimer[260]. However it is difficult to discern if this results are

due to the interaction of the N-glycan with the cysteine or, on the contrary, that the impaired cysteine left is causing further misfolding, as for example, by interacting with either C571 or C666 and destabilizing this disulfide bond. In fact, the pegylation of cysteine mutants show that misfolding of the protein is sometimes bigger when one cysteine is impaired that when the both cysteines of the disulfide bond are eliminated. A possible way to study if this is taking place, would be to perform pegylation assays with these double mutants.

The $\triangle$673-685 mutant showed no maturation or transport and was degraded, indicating that the C-terminal loop of rBAT plays a key role in the maturation of the heterodimer. This loop has no homology to any known sequence. In order to understand the role of this loop we performed an alanine scanning of its 11 residues. The maturation studies revealed 3 different maturation phenotypes (Figure 3.43). Group 1 composed by the mutants S676A, V677A, I680A, T683A and S684A show a wild-type maturation behaviour suggesting that this residues do not play an important role in the stability of the loop. The second group formed by mutants S675A, L678A and N679A display between 30 and 50% of Endo H sensitive band, similar to the S577A N-glycan mutant and group 3 formed by mutants Y674A, L681A and Y682A present $>$ 60 % of Endo H sensitive band and show very little maturation. This last group explains, at least partially, the results obtained when the whole loop is removed and suggest that they have a key role in the maintainance of the loop structure. Accordingly, mutants Y674A, L681A and Y682A show the higher maturation rate but in the contrary mutants Y674A and Y682A display a low transport together with the S676A mutant. This is probably due to transitory transfection and more experiments should be performed to confirm the results.

In order to obtain more information of the interactions that take place in the C-terminal loop we studied the stability and maturation of group 2 and 3 loop mutants in the C-C background (Figures 3.45 and **??**). These assays show that the stability and maturation defect of the loop mutants S675A, L678A and N679A is strongly strenghtened in the C-C background. Despite that the C-terminal disulfide bond is not essential *per se*, its absence seems to strongly potentiate the misfolding effects of these loop mutants. This is probably due to the fact that when the disulfide bond is not present, this residues help to maintain the loop structure.

In another approach to gain insight in the loop interactions we generated double mutants of the N575 N-glycan and the group 2 residues. The decrease in stability indicates a synergistic effect in the double mutant suggesting that it is having an effect in the folding of the protein. The Endo H assays show that the double mutant tends to be less than additive indicating that these 2 elements (the N-glycan and the loop residue) interact in some way.

As it has no homology to any known sequence, the structure of the loop is unknown; however this study represents a first approach to understand which are the residues that play an important role in the biogenesis of the transporter.

4.4 A first approach to the biogenesis of rBAT-$b^{0,+}$AT

An ER exit signal at the cytoplasmic C terminus of $b^{0,+}$AT, active only after association with rBAT, has already been described[159]. This study together with the work accomplished in our group[157,248] forms a working model on how the biogenesis events in $b^{0,+}$AT and rBAT are coordinated in order to render a native complex: firstly, $b^{0,+}$AT folds within the ER and remains stable[157], then, fast, probably cotranslationally, the assembly of unfolded rBAT with $b^{0,+}$AT prevents its degradation and the oxidative folding of the ectodomain[248], that can also depend on the calnexin system[157]. Pegylation experiments show that this disulfide is not needed for oxidation of the intramolecular disulfides because the C114S mutant shows a similar pattern than wild-type rBAT as well as its transport activity (Figures 3.12 and 3.15). Therefore, non-covalent interactions between rBAT and $b^{0,+}$AT suffice for a functional complex. The fact that C114 is the first extracellular cysteine from rBAT and that it is far from the next one. This is reinforced by the very fast detection of the disulfide-linked heterodimer[157] (Figure 3.23A). Next the disulfide bond between C242 and C273 is most likely the first to form and probably cotranslationally in order to not disturb the formation of the rest of the disulfide bonds. This is strongly supported by the experiments performed with mutants containing one of the natively paired cysteines that shows that C242-C273 is completely oxidized in the absence of the other two disulfides (Figure 3.19). The assembly with $b^{0,+}$AT could also help to maintain the cysteines form the B domain far from the others. The correct pairing of the cysteines 571 to 685 would render the correct folding of the C-terminal loop. Once this structure is present and the $b^{0,+}$AT ER exit signal that is active only after association with rBAT is activated[159], the traffic of the complex to the plasma membrane is facilitated.

Future studies should address the detailed description of the oxidative and non-oxidative folding pathways of this heteromeric transporter and how end stages of rBAT ectodomain folding may be coupled with activation of the ER exit signal within $b^{0,+}$AT.

Conclusions

I. In the presence of $b^{0,+}$AT, rBAT contains 3 intramolecular disulfides: C242-C273, C571-C666 and C673-C685. They can form individually in the absence of any of the other two.

II. When expressed in the absence of $b^{0,+}$AT, rBAT remains unfolded with at least one intramolecular bond not formed. Therefore, $b^{0,+}$AT is required for the correct oxidation of the rBAT ectodomain.

III. The first formed disulfide bond is most likely C242-C273. The results suggest that the last oxidative step is the stable formation of the C571-C666 disulfide. This step may occur post-translationally only after assembly with $b^{0,+}$AT.

IV. The presence of an unpaired B domain cysteine causes oxidative misfolding and precludes the formation of at least one of the other two disulfides.

V. Disulfides C242-C273 and C571-C666 are essential for biogenesis as its absence causes retention in the ER and subsequent degradation of the heterodimer. The double mutant C673-C685 behaves as the wild-type protein, but the cysteine mutants C673S and C685S present reduced stability and maturation delay of the transporter.

VI. In the presence of $b^{0,+}$AT, rBAT is able to oxidize its ectodomain in a post-translational way and mature.

VII. rBAT contains 5 N-glycans: N261, N332, N495, N513 and N575. They are not essential neither for the ER-exit nor for stability or function of the transporter. The N332 N-glycan may suffice for ER-degradation of unassembled rBAT.

VIII. The N-glycan N575 is necessary and sufficient for maximal efficiency of ER-to-Golgi traffic of the human cystinuria transporter.

IX. The C-terminal loop of rBAT (673-685) plays a key role in the biogenesis and maturation of the heterodimer.

X. The results suggest that the C673-C685 disulfide helps to sabilize the conformation of the loop residues (674-684).

XI. The N-glycan N575 could interact funtionally or structurally with some C-terminal tail loop residues to form a luminal signal in rBAT-$b^{0,+}$AT required for ER-exit of the transporter. The formation of the C571-C666 may couple the last oxidative folding step with the formation of this signal.

Materials and Methods

5.1 Cell culture

All mammalian cell lines used are kept in incubators at 37°C in a humidifed atmosphere, containing 5 % CO_2. Cells are grown in culture dishes and are split regularly (2 times a week, when they reach 90-100 % confuency). They are detached from the culture dish by trypsinization and the resultant cell suspension is then reseeded. Passages are important in order to keep cells alive and growing under cultured conditions for extended periods of time.

5.1.1 Cell lines

HeLa (ATCC CCL-2)[273] was derived from a cervical carcinoma from a 31-year-old patient. This was the first aneuploid line derived from human tissue maintained in continuous cell culture. They are widely used for the study of proteins transiently transfected.

MDCK (ATCC CCL-34): The MDCK cell line are epithelial cells derived from a kidney of an apparently normal adult female cocker spaniel. They are a good epithelial cell model as they are able to polarize. 2 cell lines have been used:

- rBAT$b^{0,+}$AT-MDCK: MDCK cells that stably express rBAT and $b^{0,+}$AT.

- rBAT-MDCK: MDCK cells that stably express rBAT

Growing medium

HeLa cells: DMEM (Dulbecco's Modified Eagle Medium) medium from (Gibco #41966) containing 4,5 g of glucose, 2mM of L-glutamine and sodium pyruvate.

MDCK cells: DMEM medium from (Gibco #11885) containing 1 g/l of glucose and 2mM, L-glutamine and sodium pyruvate supplemented with:

- 400μg/ml of geneticin (G-418 sulfate, Gibco BRL) and 100μg/ml of higromicin (Roche) for rBAT-$b^{0,+}$AT-MDCK

- 100μg/ml of higromicin for rBAT-MDCK.

Both mediums are supplemented with:

- 10% Fetal Bovine Serum (FBS) from (Gibco #1270-106) that was previously heat inactivated 30 min at 56 °C.
- Penicillin-Streptomycin (100x) from (Gibco #5140-122) 100 U/ml.

5.1.2 Transitory transfection

Calcium phosphate

In this thesis transitory transfection was performed with calcium phosphate precipitation, in which calcium phosphate precipitates DNA and forms a complex that is thought to help the DNA enter the cell[274,275]. DNA precipitates are formed by mixing the DNA with a calcium and a phosphate solution. An important parameter for an efficient transfection is the pH of the phosphate solution. Usually different pH solutions between pH 6-7 are tested. Besides DNA of interest, a plasmid encoding the Green Fluorescent Protein (GFP) is transfected to monitor transfection effciency by FACS analysis. Cells are transfected at ∼40%. The amount of DNA and solutions vary according to the size of the cell plates (Table 5.1.2).

Table 5.2. Transfection rates for different cell plates.

	Cell culture plates		
	100 mm	60 mm	6-well
DNA mix	18 ug	7 μg	3,6 μg
GFP	2 μg	0,7 μg	0,4 μg
Milli Q H_2O	250 μl	80 μl	50 μl
$CaCl_2$	250 μl	80 μl	50 μl
Phosphate	500 μl	160 μl	100 μl

Solutions:

- Calcium solution: $CaCl_2$ 500 mM and BES 100 mM pH 6.95, filtered.
- Phosphate solution: NaCl 50 mM, Na_2HPO_4 0.75 mM and BES 50 mM. Aliquotes

that vary ∼0.02 in pH are tested in order to obtain an efficient transfection. Solutions are filtered.
- MilliQ filtered water

Before transfection fresh cell medium is added to the cell plates. First, the milliQ water is added to the DNA mix. Next, the $CaCl_2$ is added and the mix is shaked. Then, the phosphate solution is added drop by drop. Let rest the mixture for 15 min. After that, the solution is mixed again and is added to the cells drop by drop covering the whole plate. The cells are incubated with the mix overnight. The next morning cells are washed twice with PBS and fresh medium is added.

Lipofectamine LTX

In order to obtain a more constant percentage of transfection we performed Lipofectamine transfection for the pulse-chase imaging assays: Lipofectamine LTX Reagent with PLUS^{TM} Reagent (Invitrogen, # 15338-100). Transfection ws performed following the manufacturer's protocols.

5.1.3 Cell freezing and thawing

Material:

- Freezing solution: 90% FBS and 10% Dimethyl Sulphoxide (DMSO) from Sigma (#D2550)

Cryogenic storage of cell cultures is widely used to maintain reserves of cells. Cells are detached from the culture dish by trypsinization and pelleted. Freezing solution is added to the cell pellet, not exceeding $10x10^6$ cells/ml, and suspension is transferred to cold cryotubes which are rapidly transfered to the -70°C freezer before ultimately transferring cells to the liquid nitrogen container. For frozen cell recovery place the cryotube in warm water, agitating gently until completely thawed. Rapid thawing (60 to 90 seconds at 37°C) provides the best recovery for most cell cultures. Since DMSO may damage cells upon prolonged exposure, remove it as quickly as possible. Transfer the contents of the vial to a 15 ml centrifuge tube containing 10 ml of fresh medium and spin for 5 min at 100x g. Discard the supernatant containing the cryoprotective agent and resuspend the

cell pellet in fresh medium. Then transfer the cell suspension to a suitable culture vessel and incubate normally.

5.2 Pulse-chase assay

The analysis of the biogenesis of the tranpsorter was performed with the pulse-chase assay. The assay performed is based in the protocol described by A. Jansens and I. Braakman (Methods in Molecular Biology, vol 232. Protein Misfolding and Disease: Principles and Protocols). This assay allows the study of protein biogenesis in cells by labelling a population of cells for a small period of time and following its path through the cell. The steps of this assay are the following:

1. Radio-labelling of the cells with 35S-Methionine-Cysteine

2. Chase with cold L-methionine and L-cystine

3. Immunoprecipitation of proteins

4. Analysis by SDS-PAGE and autoradiography

Material:

Pulse-chase:

- Anti-radioactive paper BENCHGUARD (BG50 Bibby Sterlin)
- L-Methionine 50X (Sigma #M-5308)
- L-cysteine 100X (Fluka #30090)
- 20mM N-ethylmaleimide (NEM): stock 1M in ethanol at -20°C
- PBS 1X
- Protein inhibitors: Aprotinin 1U/ml, phenylmethylsulfonyl fluoride (PMSF) 1mM, Leupeptin 1 μM, Pepstatin A 1 μM
- Starving medium: DMEM (Gibco #21013-024) without L-glutamine, L-methionine and L-cystine supplemented with L-glutamine and 10% FBS dyalized (REF). This

serum does not contain amino acids.
- Pulse labelling: starving medium with 200 μCi/ml of 35S-Methionine-Cysteine. (RedivueTM PRO-MIX [S35] cell labelling mix AGQ0080 Amersham/Biosciences).
- Chase medium: DMEM (Gibco #41966) supplemented with 100 U/ml of penicillin y 100 μg/ml of streptomycin and 10% (v/v) of inactivated FBS, supplemented with 5mM of cold L-cysteine and L-methionine
- NET lysis buffer: TrisHCl 50mM pH 7.4, NaCl 150mM, 5mM EDTA, 0.5% IGEPAL with protease inhibitors: Aprotinin 1U/ml, PMSF 1mM, Leupeptin 1 μM and Pepstatin A 1 μM
- Scraper
- Ecolite(+)^{TM} Liquid Scintillation Cocktail (MP Biomedicals, #882475)

Immunoprecipitation and SDS-PAGE:

- Protein A sepharose 4B (Sigma #P-9424)
- Anti-bodies anti-rBAT and anti-$b^{0,+}$AT
- Borate buffer: 200 mM H_3BO_3, 50mM $Na_2B_4O_7$, 150 mM NaCl, 1% NP-40 and 0.1% ovalbumin, pH 8.3
- Hepes 40mM pH 8
- Dithiothreitol (DTT) 2M
- Coomassie solution
- Destaining solution: 30% methanol and 10% acetic acid in water
- Whatmann paper 3MM
- Storage pHospHor screen, Molecular Dynamic
- Escanner TypHoon 8600 (Molecular Dynamics Amersham/Biosciences)

Method:

Cells are transfected and seeded in 3.5 cm diameter plates at 60-70% confluence. The following day cells were incubated for 30 min in pre-warmed L-Methionine/L-Cystine free media containing 10% dialyzed FBS. Subsequently, cells are labeled for 15 (rBAT expressed alone) or 30 min (rBAT and $b^{0,+}$AT) with a mixture of [35S]methionine/cysteine (200 μCi/μl) and, after removal of the labeling media, incubated with pre-warmed media supplemented with 5 mM unlabeled L-methionine/ L-cysteine. At the indicated times, cells are washed twice with cold phosphate-buffered saline (PBS) and once with cold PBS containing 20 mM N-

ethylmaleimide (NEM) for 5 min. Cells were collected and lysed on a rotating wheel in 200 μl of NET buffer with the protease inhibitors aprotinin, leupeptin, PMSF, and pepstatin, and 20 mM NEM. After 30 min at 4°C, a post-nuclear supernatant is obtained by 10 min of 10000 g centrifugation at 4°C. Immunoprecipitations are performed from equivalent amounts of radioactivity incorporated into proteins, by adding an equal volume of immunoabsorbent borate buffer with the same protease inhibitors as the lysis buffer, and polyclonal antibodies to rBAT or $b^{0,+}$AT, in combination with protein A-Sepharose. Precipitates were washed four times with borate buffer and twice with HEPES,. Samples were run on SDS-PAGE under reducing (100mM DTT) or non-reducing conditions. Gels were stained for 30 min at RT with Coomassie brilliant blue to control for precipitating antibodies, then destained for another 30 in at RT, dried for 90 min at 80°C and put on an intensifying screen for quantification with a Phosphoimager Typhoon 8600 (Molecular Dynamics).

The relative intensities of the labeled bands are determined using phosphorimaging, as follows: each band is outlined by a rectangle (as tightly-fitting to the band as possible) and a rectangle of identical size is drawn in the closest area without any band in the lane. The relative positions of band and background rectangles are maintained within the experiment and among similar experiments. The value for each rectangle is calculated using the Local Average Background Correction of the ImageQuant software. The final value of the band is the difference between the value of the rectangle band and the value of the rectangle background. The data are plotted as intensity values of the fraction remaining obtained by dividing by the zero time value.

5.3 Pulse-chase imaging

In order to perform pulse-chase imaging assays, wild-type human rBAT and the N-glycan mutant S577A were constructed into the SNAP-tag ® vector. The SNAP-tag is a 20 kDa mutant of the human DNA repair protein O^6-alkylguanine- DNA alkyltransferase (hAGT) that reacts specifically and rapidly with benzylguanine (BG) and benzylchloropyrimidine (CP) derivatives leading to covalent labeling of the SNAP-tag with a synthetic probe. The ability to turn on the signal at will, together with the availability of a cell-permeable nonfluorescent blocking agent (SNAP-Cell Block) allows time-resolved pulse-chase analysis of protein trafficking

(Figure 5.48).

The plasmid encodes the SNAP-tag gene, which is expressed under control of the CMV promoter. The expression vector has an IRES (internal ribosome entry site) and a neomycin resistance gene downstream of SNAP-tag for the selection of stable transfectants. Codon usage of the gene is optimized for expression in mammalian cells. In our case, rBAT was cloned between AscI and NotI at the N-terminus of SNAP-tag. These assays were performed in collaboration with Dr. Francesc Tebar (Departament de Biologia Cellular, Immunologia i Neurociències, Institut d' Investigacions Biomèdiques Augustí Pi i Sunyer). Confocal images were acquired using a laser-scanning confocal spectral microscope (TCS SL; Leica) with the collaboration of the Unitat de Microscopia Confocal, Serveis Cientificotècnics, Facultat de Medicina, Universitat de Barcelona.

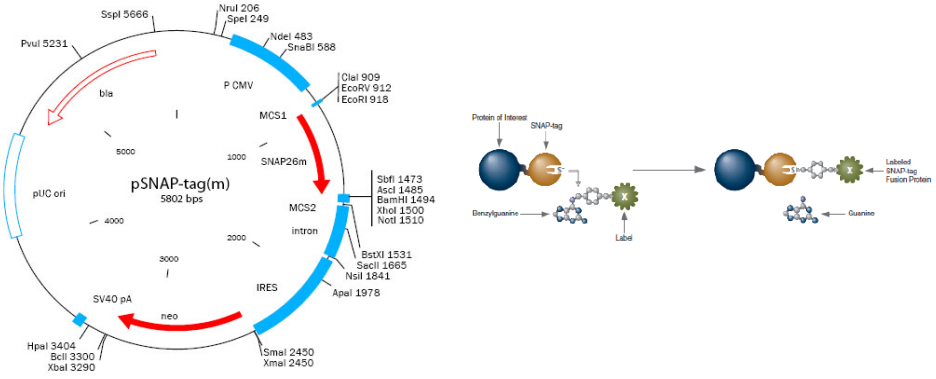

Figure 5.48. pSNAP-tag(m) vector map. A, pSNAP-tag(m) vector map. B, SNAP-tag reaction. TMR containing benzylguanine that interacts with the SNAP protein, labeling the protein of interest.

Materials:

- Paraformaldehyde (PFA) 4%
- Blocking solution: PBS 1X and 1 % BSA
- Washing solution: PBS 1X and 0,1 % BSA
- Permeabilization solution: PBS 1X, 0,1 % BSA and 0,1 % Triton X-100
- Primary antibody: β-1 integrin anti-rat and calnexin anti-mouse (both provided by Dr. Tebar)
- Secondary antibody: Alexa 488 and 647 anti-rat (provided by Dr. Tebar)
- MOWIOL Reagent
- SNAP-Cell TMR-Star 3 μM

- SNAP-Cell Block Bromothenylpteridine 10 μM

Method:

Cells were transfected with Lipofectamine LTX (see 5.1.2). The next day cells were seeded in 12 cm diameter cover slips. As pulse-chase assays, the experiment is performed 36 h after transfection. Cells are blocked with SNAP-Cell Block 2 μM (40 μl per cover slips) for 30 min at 37°C in a humidifed atmosphere, containing 5 % CO_2. Next, cover slips are washed 3 times with DMEM medium and a longer wash with DMEM medium of 30 min at 37°C in the cell incubator. Cells are then labelled with TMR 3 μM (40 μl per cover slips). Cover slips are then washed 3 times with DMEM medium and washed for another 1 h at 37°C in the cell incubator. At the desired times the coverslips are washed twice with PBS and fixed for 4 min with PFA 4 %. Cells are then washed again twice with PBS and once with the washing solution and incubated for 45 min at RT with the β-1 integrin antibody anti-rat (used as a plasma membrane marker). Cover slips are then washed twice with PBS and fixed for 14 min with PFA 4 % and subsequently washed twice again with PBS and once with the washing solution. Next, incubation with the secondary antibody Alexa 647 anti-rat for 30 min at RT. Finally, the cover slips are washed twice with PBS, rinsed with destilled water and mount with MOWIOL. After drying O/N, samples can be analysed by confocal microscope and are kept at rT in the dark.

In some experiments we also tried to use an intracellular primary antibody anti-calnexin. However, the TMR signal decreased for unknown reasons so we did not further continue with them.

Method:

After fixing for 14 min with PFA 4% cells are permeabilized for 5 min at RT with the permeabilization solution and blocked for other 5 min at RT. Next, cover slips are incubated with antibody calnexin anti-mouse for 45 min at RT and then washed once with the washing solution. Finally, cells are incubated for 30 min at RT with the secondary antibody Alexa 448 anti-mouse, washed twice with PBS, rinsed with water and mounted with MOWIOL.

5.4 Transport assay

The functional analysis of the transporter was performed by means of transport assays. In this experiment we measure the amount of radiolabelled amino acid that enters the cell after incubation with the transport medium. Cells were seeded in 24-well and the value obtained is the Mean ±SEM of the transport obtained for 4 wells. In this thesis transport assays were perfomed with L-cystine 40 μM or L-arginine 50 μM.

Material:

- MGA buffer (137 mM N-methyl-D-glucamine (Fluka, # 66930), 2,8 mM $CaCl_2 \cdot 2\ H_2O$, 1,2 mM $MgSO_2 \cdot 7\ H_2O$, 5,4 mM KCl, 10 mM HEPES, pH 7,4).
- Uptake solution (200 μl/well) with the desired concentration of cold amino acid plus 0,5 μCi/well of radioactive amino acid in 1x MGA at 37°C)
- Amino acid stocks
- Radioactive amino acids (L-[3H] amino acids at 1 mCi/mL purchased from Perkin-Elmer
- Stop solution (1x MGA at 4°C)
- Lysis solution (100 mM NaOH, 0,1 % SDS)
- Ecolite(+)^{TM} Liquid Scintillation Cocktail (MP Biomedicals, #882475)
- Scintillation vials with screw caps, 6 mL (ITISA, #SVC-06. 6 ml)

Method:

Cells are washed twice with of MGA 1x at 37°C. 200 μl of uptake solution at 37°C are added to each well for as long as the transport time we are assaying (2 min in this thesis). Aspirate solution and stop transport with stop solution at 4°C. Wash wells three times with stop solution. 250 μl of lysis solution are added into the wells, which are incubated at 37°C agitation until cell lysis. The lysate is homogenysed py pipetting and 100 μl are then transferred into scintillation vials with 3 ml of scintillation fluid and put to count (cpm). Protein concentration is measured with 15 μl duplicates. For the zero points cells are washed twice with of MGA 1x at 37°C. 200 μl of uptake solution at 37°C. Immediately after aspirate the uptake solution and add the stop solution at 4°C. Wash wells three times with stop solution. For the zero point wells, the transport is performed for each well

separately in order to minimize the basal transport.

Data analysis:

For L-cystine data were calculated as the difference between the uptake in each group minus the uptake in cells transfected with $b^{0,+}$AT alone, which is not different from the transport in vector-transfected cells.

L-arginine transport was quantitatively much less than L-cystine (as it is a less sensitive assay), so we performed a different data analysis to eluciate the functionality of the mutants. For eahc experiment we calculated the fold induction of the wild-type and the mutants over $b^{0,+}$AT and calculated the mean ± SEM. To normalize the data we substracted 1 to the mean values of the mutants and wild-type. Next, we divided the value of each mutant by the value of the wild-type. This result was multiplied by 100 (wild-type value was set to 100).

elicited a less sensitive transport, We calculated the fold induction of the mutant over $b^{0,+}$AT for every assay and calculated the mean ± SEM. To this value we substracted 1, that would be the value for the $b^{0,+}$AT transport. We divided this value with the wild-type value in order to correct for wild-type and finally it was shown as a percentage of tranport.

5.5 PEG-mal modification

In order to analyse the disulfide connectivity in rBAT we used mass-tagging of accessible sulfhydryl (-SH) groups with mPEG5000-maleimide (mPEG) (Figure 3.9). mPEG is a membrane-impermeant reagent that has been used to study the topology of some membrane proteins[244,245]. A molecule of mPEG attaches to a -SH group shifting the apparent molecular weight of the protein of interest by ∼5 kDa, which is easily detectable in SDS-PAGE.

Materials:

- TSD buffer 50 mM TrisHCl and 1% SDS
- TNN buffer 50 mM TrisHCl, 250 mM NaCl, 5 mMEDTA, 0.5% IGEPAL and

the protease inhibitors aprotinin, leupeptin, phenylmethylsulfonyl fluoride, and pepstatin
- Coomassie brilliant blue
- Destaining solution

Method:

A pulse or pulse-chase assay is performed with cells expressing rBAT or rBAT+ $b^{0,+}$AT labelling for 30 min with [35S]methionine/cysteine (200 μCi/μl). At the indicated times, cell dishes were washed three times with cold PBS, scraped and centrifugated for 5 min at 3000 g. The frozen pellet was resuspended with 100 ul of TSD buffer which contained 2 mg of PEG or 20 mM NEM. The samples were incubated for 30 min at 30°C. Lysates were centrifugated for 5 min at RT, supernatant was transferred. Immunoprecipitations were performed by adding one third of the volum sample and 12 volums of TNN buffer and polyclonal antibodies to rBAT or $b^{0,+}$AT, in combination with protein A-Sepharose. The immunoprecipitation was performed overnight at 4°C. Precipitates were washed three times with TNN buffer. Samples were run on SDS-PAGE under reducing (25mM DTT) or non-reducing conditions. Gels were stained with Coomassie brilliant blue to control for precipitating antibodies, dried and put on an intensifying screen for quantification with a Phosphoimager Typhoon 8600 (Molecular Dynamics).

mPEG modification with TCA

We also performed mPEG in presence of TCA that rapidly quenches putative artifactual thiol-disulfide exchange reactions. However, no differences were observed compared to modification without TCA. After the pulse-chase assay, cell dishes were washed three times in cold PBS and scraped with PBS 1mM EDTA. TCA was added to a final concentration of 10% and after mixing the sample was incubated for 30 min at 4°C. Samples were then centrifugated for 15 min at 4°C. The pellet was washed twice with cold acetone and dried for 30 min. Samples were sonicated with 150ul of TSD buffer containing 2mg of PEG-mal or 20mM NEM and incubated for 30 min at 30°C and centrifugated for 5 min at RT. Immunoprecipitations, electrophoresis and staining conditions were performed as described above.

5.6 DNA handling

5.7 cDNA constructs

rBAT and $b^{0,+}$AT pCDNA3.1 (Invitrogen) constructs were used. The pcDNA^{TM} vectors are designed for high-level, constitutive expression in a variety of mammalian cell lines. pCDNA3. 1 contains cytomegalovirus (CMV) enhancer-promoter for high-level expression, the ampicillin resistance gene and pUC origin for selection and maintenance in *E. coli*. The oligos used to generate the mutants are the following:

Table 5.3. Mutation oligonucleotides

Mutations	5'-3' sequence
Cysteine mutants	
C18S	GATGAGTATGAAGGGATCCCAGACAAACAACGGG
C114S	GCCCTCTCTCCAAAGTCCCTAGACTGGTGGCAGGAGGGG
C242S	CTGGCATGACTCTACCCATGAAAATGGC
C273A	GGCACTTTGACGAAGTGCGAAACCAAGCTTATTTTCATCAG
C571S	CCTCAACAGGGGCTGGTTTTCCCATTTGAGGAATGACAGCC
C666S	GCTTTCAGAGATAGATCCTTTGTTTCCAATCGAGC
C673S	CCAATCGAGCAAGCTATTCCAGTGTACTGAACATACTGTATACC
C685S	ATACCTCGTCTTAGGCACCTT
Δ673-685	CCAATCGAGCATGATATTCCAGTGTACTGAACATACTGTATACC
N-glycan mutants	
T216A	CATACCAAACCACGCGAGTGATAAACATATTTGG
S263A	GGAAACTCCGCTTGGCACTTTGACGAAGTGCG
T334A	CCAAGTAAATAAGGCCCAAATCCCGGACACGG
S497A	CCGCAAATCTCAATGAAGCCTATGATATTAATACCCTTCG
S515A	CAGTGGGACAATAGTGCAAATGCTGGTTTTTCTGAAGC
S577A	GCCATTTGAGGAATGACGCCCACTATGTTGTGTAC
N575D	GGGGCTGGTTTTGCCATTTGAGGGATGACAGCCACTATGTTGTG
N575Q	GGGGCTGGTTTTGCCATTTGAGGCAGGACAGCCACTATGTTGTG
Cystinuria mutants	
M467K	GGGAATCAGTATGTCAACGTGATGAACAAGCTTCTTTTCACACTCCC
L678P	CGAGCATGCTATTCCAGTGTACCGAACATACTGTATACCTCG

Mutations	5'-3' sequence
Loop mutants	
Y674A	CCAATCGAGCATGCGCTTCCAGTGTACTGAACATACTG
S675A	GCATGCTATGCCAGTGTACTGAACATACTGTATACCTCG
S676A	GCATGCTATTCCGCTGTACTGAACATACTGTATACCTCG
V677A	CGAGCATGCTATTCCAGTGCACTGAACATACTGTATACC
L678A	GCATGCTATTCCAGTGTAGCGAACATACTGTATACCTCG
N679A	GCATGCTATTCCAGTGTACTGGCCATACTGTATACCTCG
I680A	GCTATTCCAGTGTACTGAACGCACTGTATACCTCG
L681A	CCAGTGTACTGAACATAGCGTATACCTCGTGTTAGG
Y682A	CCAGTGTACTGAACATACTGGCTACCTCGTGTTAGGC
T683A	CCAGTGTACTGAACATACTGTATGCCTCGTGTTAGGCACC
S684A	CTGAACATACTGTATACCGCGTGTTAGGCACCTTTATGAAGAG
Double mutants	
S675A-L678A	GCATGCTATGCCAGTGTAGCGAACATACTGTATACCTCG
S675A-N679A	GCATGCTATGCCAGTGTACTGGCCATACTGTATACCTCG
L678A-N679A	GCATGCTATTCCAGTGTAGCGGCCATACTGTATACCTCG
C673S-Y674A	CCAATCGAGCAAGCGCTTCCAGTGTACTGAACATACTG
C673S-S675A	CCAATCGAGCAAGCTATGCCAGTGTACTGAACATACTG
L681A-C685S	CCAGTGTACTGAACATAGCGTATACCTCGTCTTAGG
Y682A-C685S	CCAGTGTACTGAACATACTGGCTACCTCGTCTTAGGC
Loop mutants	
Y674A	CCAATCGAGCATGCGCTTCCAGTGTACTGAACATACTG
S675A	GCATGCTATGCCAGTGTACTGAACATACTGTATACCTCG
S676A	GCATGCTATTCCGCTGTACTGAACATACTGTATACCTCG
V677A	CGAGCATGCTATTCCAGTGCACTGAACATACTGTATACC
L678A	GCATGCTATTCCAGTGTAGCGAACATACTGTATACCTCG
N679A	GCATGCTATTCCAGTGTACTGGCCATACTGTATACCTCG
I680A	GCTATTCCAGTGTACTGAACGCACTGTATACCTCG
L681A	CCAGTGTACTGAACATAGCGTATACCTCGTGTTAGG
Y682A	CCAGTGTACTGAACATACTGGCTACCTCGTGTTAGGC
T683A	CCAGTGTACTGAACATACTGTATGCCTCGTGTTAGGCACC
S684A	CTGAACATACTGTATACCGCGTGTTAGGCACCTTTATGAAGAG

5.7.1 Tet-off system

In the Tet-Off system, gene expression is turned on when tetracycline (Tc) or doxycycline (Dox) is removed from the culture medium by engineering the gene of interest into the pTRE-Tight vector (Figure . The TRE is located upstream of the minimal immediate early promoter of cytomegalovirus (PminCMV), which is silent in the absence of activation. tTA binds the TRE-and thereby activates transcription of Gene X-in the absence of Tc or Dox.

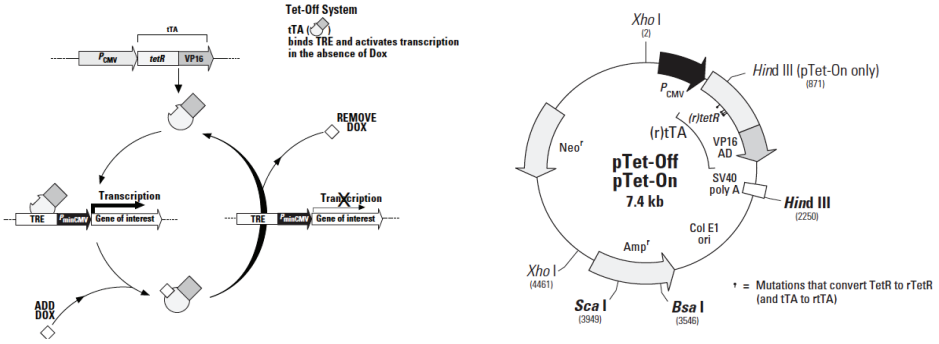

Figure 5.49. Schematic of gene regulation in the Tet-Off systems and the pTRE-Tight vector map.

HeLa cells expressing the Tet-Off advanced transactivator were transfected with rBAT-pcDNA3 and $b^{0,+}$AT-pTRE-Tight vector. The expression of $b^{0,+}$AT was induced only in the absence of doxycycline in the medium. HeLa cells were transfected with rBAT-pcDNA3 and $b^{0,+}$AT-pTRE-Tight in presence of doxycycline. Cells were pulsed in the presence of doxycyline to avoid $b^{0,+}$AT expression and chased in the presence of cold methionine and absence of doxycicline (inducing $b^{0,+}$AT expression).

5.7.2 PCR

Material:

- QuikChange Site-Directed Mutagenesis Kit (Stratagene, #200518-5)

PCR reaction mix:

	Volume (μl)
Reaction buffer (10X)	5
dNTP	1
Fw oligo (10 μM)	2
Rv oligo (10 μM)	2
template DNA (100 ng/μl)	2
H_2O	37
DNA polymerase	1

Method:

The procedure consists in a 16-cycle amplifcation from one strand of a plasmid template with primers containing the desired mutations. Primers contain roughly 45 bases and have melting temperatures above 75°C. The amplifcation reaction consists of an initial denaturing step of 1 min at 95°C followed by 16 cycles of a 30 s 95°C denaturing step, 1 min 50°C annealing step, and an extension step of 2 min for each kilobase of template plasmid. Subsequent incubation with 10 U of DpnI at 37°C for 1 h digests the original plasmid while leaving newly synthesized single stranded mutant plasmid intact for transformation into competent *E. coli* cells.

5.7.3 DNA electrophoresis

Material:

- TAE (40 mM Tris base, 20 mM acetic acid, 1 mM EDTA)
- SeaKem LE agarose (Lonza, #50004)
- 10x DNA loading buffer (1 % SDS, 50 % glycerol, 0. 05 % Bromophenol Blue)
- 1 Kb DNA ladder (Amersham, #15615-016)
- SYBR Safe DNA gel stain (Invitrogen, #SS33102)

Method:

DNA electrophoresis is performed using mini or wide submerged horizontal electrophoresis systems to separate DNA fragments by size. Gels are composed 1 % agarose melted in 1x TAE using a microwave oven, once agarose is melted and has cooled down 3,5 μl of SYBR is added to the mix. Gels are prepared in the mini or wide gel casters included in the gel units. DNA samples are mixed 10:1 with 10X loading buffer. Mini gels are typically run at 90 V for 1 h while wide gels are run at 130 V for 80 min. Gel bands for analytical purposes are visualized by UV light.

5.7.4 Plasmid purification

Nucleic acid purifcation from enzymatic reactions or gel electrophoresis were performed using the Gel Band Purifcation kit (GE Healthcare, #28-9034-71) following the manufacturer's protocols.

5.7.5 Restriction digest

Restriction digests for analytic purposes are typically carried out in 200 μl PCR tubes in 20 μL reactions containing 200 ng of plasmid and using the recommended buffers according to the enzyme supplier's protocol (New England Biolabs) for 3 h at 37°C. Restriction digests for cloning are typically performed in 1,5 mL microcentrifuge tubes using 1-2 μg of plasmid template in 50 μL reactions at 37°C overnight.

5.7.6 Dephosphorylation

Material:

- Alkaline Phosphatase, Calf Intestinal (CIP)(New England Biolabs, #M0290)

Method:

Dephosphorylation is performed on digested vector fragments to be used in the standard ligation procedure in order to avoid vector self-ligation. The reaction is performed in a 1,5 mL microcentrifuge tube using 1 μg of digested gel purifed vector, 2 μL of CIP, and 5 μL of the provided 10X NEB Buffer in a 50 μL reaction incubated for 1 h at 37°C.

5.7.7 Plasmid ligation

Material:

- T4 DNA Ligase (New England Biolabs, #M0202s)

Method:

The standard ligation is used for general cloning and plasmid constructions. The standard ligation uses gel purifed vector and insert fragments that had been previously digested to generate compatible cohesive ends. For all standard ligations vector fragments are dephosphorylated to avoid vector self-ligation. Ligations are performed in a reaction volume of 20 μL with 1 μL of T4 DNA Ligase, 2ml of 10X T4 DNA ligase buffer and, typically, a ratio insert:vector of 3/1 or 6/1 following the formula: $\frac{ngvector \times Kb\, insert}{Kb\, vector} \times \frac{insert}{vector}$ ratio= ng insert. The ligation reaction is incubated overnight at 16°C. Samples are heat-inactivated at 65°C for 10 min prior to transformation into competent *E. coli* cells.

5.7.8 Cell transformation

Material:

- XL Blue competent cells
- DNA of interest
- LB medium (1 % tryptone, 0,5 % yeast extract, 0,5 % NaCl, pH 7,5)
- LB plates containing the appropriate selection antibiotic (for preparing plates 1,5 % (w/v) of agar is added to the LB recipe described above)

Method:

Heat shock transformation of XL Blue competent cells is performed on ice. Competent cells are taken out from the -80°C freezer and are let to thaw on ice. 100 μl of thawed competent XL Blue are mixed with 50 ng of DNA and the mix stands on ice for 30 min. A 45 sec heat shock at 42°C is performed. After the heat shock cells stand on ice for 2 additional minutes. 900 μl of LB with no antibiotic are added to the cells, which are then incubated on rotation at 37°C for 1 h. After this time cells are seeded on a LB plate containing the suitable antibiotic and plates are incubated for around 12 h at 37°C inverted position.

5.7.9 Nucleic acid quantification

Nucleic acid concentration of 2 μL samples is directly quantifed with NanoDropND-1. 000 Spectrophotometer (Thermo Scientific).

5.7.10 Sequencing

Material:

- Big Dye 3. 1 (Invitrogen, #4337455)
Sequencing reaction mix:

	Volume (μl)
Reaction buffer (10X)	1
Sequence oligo (10 μM)	0,3
DNA from miniprep	2
H_2O	57
Big Dye	1

Method:

After PCR reaction is performed, 10 μL of bidistilled water are added to each tube. Samples are ready for precipitation and sequencing at the Genomic Unit of the UB Scientifc and Technical Services (PCB, Barcelona).

5.8 Protein analysis

5.8.1 Total membranes

Material:

- Homogenization buffer (25 mM Hepes, 4 mM EDTA, 250 mM sucrose with protease inhibitor mix, pH 7,4)
- Protease inhibitor mixture (1 mM phenylmethylsulfonyl fuoride, 1 U/ml aprotinin, 1 mM leupeptin and 1 mM pepstatin)
- 1,5 ml Microcentrifuge Polyallomer Tubes (Beckman, #357448)

Method:

Cells grown in 10 cm dishes are washed three times with 5 ml of ice-cold PBS and incubated for 5 m with 5 ml of ice-cold PBS with 20 mM NEM. 1 ml/plaque of homogenization buffer is added and cells are scraped and transferred into a 1,5 ml tube. Cell suspension is passed through a 25G needle 15 times and centrifuged at 5000 g for 5 min. The supernatant is transferred to microcentrifuge tubes and centrifuged at 150000 g for 90 m at 4°C in a TLA-55 rotor (Beckman Coulter). Membranes are resuspended in 100 μl of homogenization buffer.

5.8.2 Protein quantification

Purifed proteins are quantifed by colorimetry, using the BCA Protein Assay Kit (Pierce, #23225) and following the manufacturer's protocol. Quantification is normally performed in 96-well plates (Deltalab, #900011 and #900015).

Endo H assay

Material:

- Endo Hf kit (New England Biolabs, #P0703S)

Method:

Protein samples are treated with Glycoprotein Denaturing Buffer 10X (supplied with the enzymes) and incubated at 100 °C for 10 min. When the reaction has cooled down, G5 buffer 10X and 1 μl of Endo H is added and incubated at 37°C for 1 h.

SDS-PAGE

Sodium dodecyl sulfate polyacrylamide gel electrophoresis (SDS-PAGE) is used to separate protein samples by size. Proteins in the gel can be transferred to a PVDF membrane for Western blot analysis.

Material:

- Mini-PROTEAN 3 Electrophoresis System (Bio-Rad, #165-3301)
- 2-propanol
- Resolving gel solution (7,5 %, 10 % or 12 % w/v 29:1 acrylamide/bis-acrylamide mix (Laboratorios Conda, #8532), 0,375 M Tris·HCl pH 8,8, 0. 1 % SDS, 0,1 % APS, 0,04 % TEMED)
- Stacking gel solution (3,3 % w/v 29:1 acrylamide/bis-acrylamide mix, 0,125 M Tris·HCl pH 6,8, 0,1 % SDS, 0,1 % APS and 0,1 % TEMED)
- 3X protein loading buffer (150mM Tris-HCl pH 6,8, 30 % glycerol, 12 % w/v SDS)
- Samples are prepared with 100 mM DTT when needed
- 1X Running buffer (25mM Tris, 192mM glycine, 0,01 % w/v SDS)
- Prestained SDS-PAGE Standards (Bio-Rad, #161-0318)

Method:

Polyacrylamide gels are cast in the casting frame provided in the Mini-PROTEAN 3 system using 1,5 mm thick combs and spacers. Gels consist of a lower resolving layer comprised of approximately 3,5 ml of resolving gel and an upper layer of 1,5 ml of stacking gel. Right after the addition of TEMED, the resolving gel solution is poured on the cast. 1 ml of 2-propanol is overlaid on top of the resolving layer and removed once the resolving layer is polymerized. Stacking gel, after the incorporation of TEMED, is immediately poured over the resolving gel and the comb is placed on top. Protein samples are mixed with prepared with the protein loading buffer and heated to 95°C for 5 min. Gels are run in the running buffer at 25 mA/gel first (for the stacking gel) and 35 mA afterwards (resolving gel) for ∼90 min in the vertical electrophoresis system provided in the Mini-PROTEAN 3 system.

Protein immunoblot

Material:

- Immobilion-P Transfer membrane (PVDF)(Millipore, #IPVH00010)
- Mini Trans-Blot Electrophoretic Transfer Cell (Bio-Rad, #170-3930)

- Transfer buffer (25 mM Tris·HCl pH 8,3, 192 mM glycine, 20 % methanol)
- Blocking solution (5 % w/v non-fat dry milk in PBS)
- Incubation solution (1 % w/v non-fat dry milk in PBS, working dilution of antibody)
- Washing solution (0,01 % Triton X-100 in PBS)
- 23 cm x 28 cm Exposure Cassette (Molecular Dynamics)
- Amersham ECL^{TM} Western Blotting Detection Reagents (GE Healthcare, #RPN2109)
- Amersham Hyperflm ECL (18 x 24 cm)(GE Healthcare, #28-9068-37)
- Hyperprocessor^{TM} Automatic Film Processor (Amersham)
- Anti-bodies: anti-rBAT and anti-b$^{0,+}$AT diluted 1/1000
- Secondary anti-body: donkey anti-rabbit Jackson diluted 1/2 in glycerol. Diluted 1/25000 for incubation.

Method:

Mini-SDS-PAGE gels are transferred to polyvinylidene fuoride (PVDF) membranes using the Mini Trans-Blot Electrophoretic Transfer Cell at 250 mA for 1 h at 4°C in transfer buffer. Membranes are blocked with blocking solution for 1 h at RT on an orbital shaker. Membranes are then incubated with the appropriate primary antibody in incubation solution overnight at 4°C under rotation. After primary antibody incubation membranes are washed 3 times for 10 min with washing solution on the orbital shaker, and then incubated with an appropriate horseradish peroxidase (HRP) conjugated secondary antibody in incubation solution, for 45 min under rotation at room temperature. The membranes are again washed 3 times for 10 min in washing solution. Finally, membranes are placed on the exposure cassette in between two layers of plastic wrap. Antibody detection is then accomplished using the ECL^{TM} chemiluminescent system with exposure to X-ray film according to the manufacturer's instructions. Exposure times vary widely among different antibodies and protein samples, so different exposition times need to be tested every time. X-ray flms are developed in the automatic film processor.

5.9 Antibodies

Human antibody anti-b$^{0,+}$AT: polyclonal antibody against the MGDTGLRKRREDEKSIKS peptide (Research Genetics), that corresponds to the N-terminal 18

amino acids of the human protein of $b^{0,+}$AT. For Western Blot a 1/1000 dilution is used and 8 μl for immunoprecipitation.

Human antibody anti-rBAT: plyclonal antibody against the MAEDKSKRDSIEMSMKG peptide (Research Genetics), that corresponds to the N-terminal 17 amino acids of the human protein of rBAT. For Western Blot a 1/1000 dilution is used and 8 μl for immunoprecipitation.

Bibliography

[1] K. S. Hingorani and L. M. Gierasch. "Comparing protein folding in vitro and in vivo: foldability meets the fitness challenge." *Current Opinion in Structural Biology*, **2014**, 24, 81.

[2] E. T. Powers, R. I. Morimoto, A. Dillin, J. W. Kelly and W. E. Balch. "Biological and chemical approaches to diseases of proteostasis deficiency." *Annual Review of Biochemistry*, **2009**, 78, 959.

[3] D. N. Hebert and M. Molinari. "In and Out of the ER : Protein Folding , Quality Control , Degradation , and Related Human Diseases". *Physiological Review*, **2007**, 87, 1377.

[4] S. High. "Protein translocation at the membrane of the endoplasmic reticulum". *Progress in Biophysics and Molecular Biology*, **1995**, 63, 233.

[5] R. M. Vabulas, S. Raychaudhuri, M. Hayer-Hartl and F. U. Hartl. "Protein folding in the cytoplasm and the heat shock response." *Cold Spring Harbor Perspectives in Biology*, **2010**, 2, a004390.

[6] I. Braakman and D. N. Hebert. "Protein folding in the endoplasmic reticulum." *Cold Spring Harbor Perspectives in Biology*, **2013**, 5, a013201.

[7] F. U. Hartl and M. Hayer-Hartl. "Converging concepts of protein folding in vitro and in vivo." *Nature Structural & Molecular Biology*, **2009**, 16, 574.

[8] S. Blond-Elguindi, S. E. Cwirla, W. J. Dower, R. J. Lipshutz, S. R. Sprang, J. F. Sambrook and M. J. Gething. "Affinity panning of a library of peptides displayed on bacteriophages reveals the binding specificity of BiP." *Cell*, **1993**, 75, 717.

[9] S. Rüdiger, A. Buchberger and B. Bukau. "Interaction of Hsp70 chaperones with substrates." *Nature Structural Biology*, **1997**, 4, 342.

[10] K. E. Matlack, B. Misselwitz, K. Plath and T. a. Rapoport. "BiP acts as a molecular ratchet during posttranslational transport of prepro-alpha factor across the ER membrane." *Cell*, **1999**, 97, 553.

[11] C. Hammond and A. Helenius. "Folding of VSV G protein: Sequential interaction with BiP and calnexin." *Science*, **1994**, 266, 456.

[12] K. Sörgjerd, B. Ghafouri, B.-H. Jonsson, J. W. Kelly, S. Y. Blond and P. Hammarström. "Retention of misfolded mutant transthyretin by the chaperone BiP/GRP78 mitigates amyloidogenesis." *Journal of Molecular Biology*, **2006**, 356, 469.

[13] C. M. Farinha and M. D. Amaral. "Most F508del-CFTR Is Targeted to Degradation at an Early Folding Checkpoint and Independently of Calnexin." *Molecular and Cellular Biology*, **2005**, 25, 5242.

[14] S. Ishiguro, Y. Watanabe, N. Ito, H. Nonaka, N. Takeda, T. Sakai, H. Kanaya and K. Okada. "SHEPHERD is the Arabidopsis GRP94 responsible for the formation of functional CLAVATA proteins." *The EMBO Journal*, **2002**, 21, 898.

[15] S. Wanderling and B. Simen. "GRP94 is essential for mesoderm induction and muscle development because it regulates insulin-like growth factor secretion." *Molecular Biology of the Cell*, **2007**, 18, 3764.

[16] J. C. Maynard, T. Pham, T. Zheng, A. Jockheck-Clark, H. B. Rankin, C. B. Newgard, E. P. Spana and C. V. Nicchitta. "Gp93, the Drosophila GRP94 ortholog, is required for gut epithelial homeostasis and nutrient assimilation-coupled growth control." *Developmental Biology*, **2010**, 339, 295.

[17] S. N. Baviskar and M. S. Shields. "RNAi Silenced Dd-grp94 (Dictyostelium discoideum Glucose-Regulated Protein 94 kDa) Cell Lines in Dictyostelium Exhibit Marked Reduction in Growth Rate and Delay in Development." *Gene Expression*, **2011**, 15, 75.

[18] J. Melnick, J. Dul and Y. Argon. "Sequential interaction of the chaperones BiP and GRP94 with immunoglobulin chains in the endoplasmic reticulum." *Nature Letters*, **1994**, 370, 373.

[19] O. Ostrovsky, N. Ahmed and Y. Argon. "The chaperone activity of GRP94 toward insulin-like growth factor II is necessary for the stress response to serum deprivation." *Molecular Biology of the Cell*, **2009**, 20, 1855.

[20] O. Ostrovsky, D. Eletto, C. Makarewich, E. R. Barton and Y. Argon. "Glucose regulated protein 94 is required for muscle differentiation through its control of the autocrine production of insulin-like growth factors." *Biochimica et Biophysica Acta*, **2010**, 1803, 333.

[21] D. Eletto, D. Dersh and Y. Argon. "GRP94 in ER quality control and stress responses." *Seminars in Cell & Developmental Biology*, **2010**, 21, 479.

[22] J. C. Christianson, T. a. Shaler, R. E. Tyler and R. R. Kopito. "OS-9 and GRP94 deliver mutant alpha1-antitrypsin to the Hrd1-SEL1L ubiquitin ligase complex for ERAD." *Nature Cell Biology*, **2008**, 10, 272.

[23] P. J. Hogg. "Disulfide bonds as switches for protein function." *Trends in Biochemical Sciences*, **2003**, 28, 210.

[24] O. B. V. Oka and N. J. Bulleid. "Forming disulfides in the endoplasmic reticulum." *Biochimica et Biophysica Acta*, **2013**, 1833, 2425.

[25] W. Chen, J. Helenius, I. Braakman and A. Helenius. "Cotranslational folding and calnexin binding during glycoprotein synthesis." *Proceedings of the National Academy of Sciences of the United States of America*, **1995**, 92, 6229.

[26] D. C. Chapman and D. B. Williams. "ER quality control in the biogenesis of MHC class I molecules." *Seminars in Cell & Developmental Biology*, **2010**, 21, 512.

[27] W. B. Mitchell, J. Li, M. Murcia, N. Valentin, P. J. Newman, B. S. Coller, W. B. Mitchell, J. Li, M. Murcia, N. Valentin, P. J. Newman and B. S. Coller. "Mapping early conformational changes in αIIb and β 3 during biogenesis reveals a potential mechanism for αIIbβ 3 adopting its bent conformation." *Blood*, **2007**, 109, 3725.

[28] M. J. Feige, S. Groscurth and M. Marcinowski. "An unfolded CH1 domain controls the assembly and secretion of IgG antibodies." *Molecular Cell*, **2009**, 34, 569.

[29] M. V. Lith and A. M. Benham. "The DM alpha and DM beta Chain Cooperate in the Oxidation and Folding of HLA-beta." *The Journal of Immunology*, **2006**, 177, 5430.

[30] Y. Sakurai, I. Anzai and Y. Furukawa. "A primary role for disulfide formation in the productive folding of prokaryotic Cu,Zn-superoxide dismutase." *The Journal of Biological Chemistry*, **2014**, , .

[31] L. Ellgaard and L. W. Ruddock. "The human protein disulphide isomerase family: substrate interactions and functional properties." *EMBO Reports*, **2005**, 6, 28.

[32] M. M. Lyles and H. F. Gilbert. "Catalysis of the oxidative folding of ribonuclease A by protein disulfide isomerase: pre-steady-state kinetics and the utilization of the oxidizing equivalents of the isomerase." *Biochemistry*, **1991**, 30, 619.

[33] R. B. Freedman, A. D. Dunn and L. W. Ruddock. "Protein folding: a missing redox link in the endoplasmic reticulum." *Current Biology*, **1998**, 8, R468.

[34] J. Winter, P. Klappa, R. B. Freedman, H. Lilie and R. Rudolph. "Catalytic activity and chaperone function of human protein-disulfide isomerase are required for the efficient refolding of proinsulin." *The Journal of Biological Chemistry*, **2002**, 277, 310.

[35] R. Ushioda, J. Hoseki, K. Araki, G. Jansen, D. Y. Thomas and K. Nagata. "ERdj5 is required as a disulfide reductase for degradation of misfolded proteins in the ER." *Science*, **2008**, 321, 569.

[36] C. E. Jessop, T. J. Tavender, R. H. Watkins, J. E. Chambers and N. J. Bulleid. "Substrate specificity of the oxidoreductase ERp57 is determined primarily by its interaction with calnexin and calreticulin." *The Journal of Biological Chemistry*, **2009**, 284, 2194.

[37] H. Cai, C. C. Wang and C. L. Tsou. "Chaperone-like activity of protein disulfide isomerase in the refolding of a protein with no disulfide bonds." *The Journal of Biological Chemistry*, **1994**, 269, 24550.

[38] P. Kosuri, J. Alegre-Cebollada and J. Feng. "Protein folding drives disulfide formation". *Cell*, **2012**, 151, 794.

[39] T. J. Tavender, J. J. Springate and N. J. Bulleid. "Recycling of peroxiredoxin IV provides a novel pathway for disulphide formation in the endoplasmic reticulum." *The EMBO Journal*, **2010**, 29, 4185.

[40] L. A. Rutkevich and D. B. Williams. "Vitamin K epoxide reductase contributes to protein disulfide formation and redox homeostasis within the endoplasmic reticulum." *Molecular Biology of the Cell*, **2012**, 23, 2017.

[41] V. D. Nguyen, M. J. Saaranen, A.-R. Karala, A.-K. Lappi, L. Wang, I. B. Raykhel, H. I. Alanen, K. E. H. Salo, C.-C. Wang and L. W. Ruddock. "Two endoplasmic reticulum PDI peroxidases increase the efficiency of the use of peroxide during disulfide bond formation." *Journal of Molecular Biology*, **2011**, 406, 503.

[42] E. Zito, E. Melo, Y. Yang and A. S. Wahlander. "Oxidative protein folding by an endoplasmic reticulum localized peroxiredoxin". *Molecular Cell*, **2010**, 40, 787.

[43] A. R. Frand and C. A. Kaiser. "The ERO1 gene of yeast is required for oxidation of protein dithiols in the endoplasmic reticulum." *Molecular Cell*, **1998**, 1, 161.

[44] M. G. Pollard, K. J. Travers and J. S. Weissman. "Ero1p: a novel and ubiquitous protein with an essential role in oxidative protein folding in the endoplasmic reticulum." *Molecular Cell*, **1998**, 1, 171.

[45] A. Cabibbo. "ERO1-L, a human protein that favors disulfide bond formation in the endoplasmic reticulum." *Journal of Biological Chemistry*, **2000**, 275, 4827.

[46] M. Pagani, M. Fabbri, C. Benedetti, a. Fassio, S. Pilati, N. J. Bulleid, a. Cabibbo and R. Sitia. "Endoplasmic reticulum oxidoreductin 1-lbeta (ERO1-Lbeta), a human gene induced in the course of the unfolded protein response." *The Journal of Biological Chemistry*, **2000**, 275, 23685.

[47] B. P. Tu and J. S. Weissman. "The FAD- and O(2)-dependent reaction cycle of Ero1-mediated oxidative protein folding in the endoplasmic reticulum." *Molecular Cell*, **2002**, 10, 983.

[48] E. Gross, C. S. Sevier, N. Heldman, E. Vitu, M. Bentzur, C. A. Kaiser, C. Thorpe and D. Fass. "Generating disulfides enzymatically: reaction products and electron acceptors of the endoplasmic reticulum thiol oxidase Ero1p." *Proceedings of the National Academy of Sciences of the United States of America*, **2006**, 103, 299.

[49] M. J. Feige and L. M. L. Hendershot. "Disulfide bonds in ER protein folding and homeostasis." *Current Opinion in Cell Biology*, **2011**, 23, 167.

[50] T. Peters and L. K. Davidson. "The biosynthesis of rat serum albumin." *The journal of Biological Chemistry*, **1982**, 257, 8847.

[51] I. Braakman, H. Hoover-Litty, K. R. Wagner and A. Helenius. "Folding of influenza hemagglutinin in the endoplasmic reticulum." *The Journal of Cell Biology*, **1991**, 114, 401.

[52] L. Bergman and W. Kuehl. "Formation of an intrachain disulfide bond on nascent immunoglobulin light chains." *Journal of Biological Chemistry*, **1979**, 254, 8869.

[53] J. S. Weissman and P. S. Kim. "The pro region of BPTI facilitates folding." *Cell*, **1992**, 71, 841.

[54] A. Jansens, E. van Duijn and I. Braakman. "Coordinated nonvectorial folding in a newly synthesized multidomain protein." *Science (New York, N.Y.)*, **2002**, 298, 2401.

[55] X. Arias-Moreno, J. L. Arolas, F. X. Aviles, J. Sancho and S. Ventura. "Scrambled isomers as key intermediates in the oxidative folding of ligand binding module 5 of the low density lipoprotein receptor." *The Journal of Biological Chemistry*, **2008**, 283, 13627.

[56] U. Tatu, I. Braakman and a. Helenius. "Membrane glycoprotein folding, oligomerization and intracellular transport: effects of dithiothreitol in living cells." *The EMBO Journal*, **1993**, 12, 2151.

[57] I. Braakman, J. Helenius and a. Helenius. "Manipulating disulfide bond formation and protein folding in the endoplasmic reticulum." *The EMBO Journal*, **1992**, 11, 1717.

[58] A. de Silva, I. Braakman and A. Helenius. "Posttranslational folding of vesicular stomatitis virus G protein in the ER: involvement of noncovalent and covalent complexes." *The Journal of Cell Biology*, **1993**, 120, 647.

[59] S. Allen, Y. Hassan and B. N. J. "Intracellular folding of tissue-type plasminogen activator." *The Journal of Biological Chemistry*, **1995**, 270, 4797.

[60] P. Kim and P. Arvan. "Folding and assembly of newly synthesized thyroglobulin occurs in a pre-Golgi compartment." *Journal of Biological Chemistry*, **1991**, 266, 12412.

[61] A. Land, D. Zonneveld and I. Braakman. "Folding of HIV-1 envelope glycoprotein involves extensive isomerization of disulfide bonds and conformation-dependent leader peptide cleavage." *The FASEB Journal : official publication of the Federation of American Societies for Experimental Biology*, **2003**, 17, 1058.

[62] A. Helenius. "How N-linked Oligosaccharides Affect Glycoprotein Folding in the Endoplasmic Reticulum". *Molecular Biology of the Cell*, **1994**, 5, 253.

[63] E. S. Trombetta. "The contribution of N-glycans and their processing in the endoplasmic reticulum to glycoprotein biosynthesis." *Glycobiology*, **2003**, 13, 77R.

[64] B. Imperiali and K. W. Rickert. "Conformational implications of asparagine-linked glycosylation". *Proceedings of the National Academy of Sciences of the United States of America*, **1995**, 92, 97.

[65] B. Imperiali and S. E. O'Connor. "Effect of N-linked glycosylation on glycopeptide and glycoprotein structure." *Current Opinion in Chemical Biology*, **1999**, 3, 643.

[66] R. Kornfeld and S. Kornfeld. "Assembly of asparagine-linked oligosaccharides". *Annual Review of Biochemistry*, **1985**, 54, 631.

[67] J. J. Caramelo, O. A. Castro, G. de Prat-Gay and A. J. Parodi. "The endoplasmic reticulum glucosyltransferase recognizes nearly native glycoprotein folding intermediates." *The Journal of Biological Chemistry*, **2004**, 279, 46280.

[68] D. N. Hebert, B. Foellmer and A. Helenius. "Calnexin and calreticulin promote folding, delay oligomerization and suppress degradation of influenza hemagglutinin in microsomes." *The EMBO Journal*, **1996**, 15, 2961.

[69] A. Helenius and M. Aebi. "Roles of N-linked glycans in the endoplasmic reticulum." *Annual Review of Biochemistry*, **2004**, 73, 1019.

[70] D. N. Hebert, J. X. Zhang, W. Chen, B. Foellmer and a. Helenius. "The number and location of glycans on influenza hemagglutinin determine folding and association with calnexin and calreticulin." *The Journal of Cell Biology*, **1997**, 139, 613.

[71] R. Daniels, B. Kurowski, A. E. Johnson and D. N. Hebert. "N-linked glycans direct the cotranslational folding pathway of influenza hemagglutinin." *Molecular Cell*, **2003**, 11, 79.

[72] A. Vassilakos, M. F. Cohen-Doyle, P. A. Peterson, M. R. Jackson and D. B. Williams. "The molecular chaperone calnexin facilitates folding and assembly of class I histocompatibility molecules." *The EMBO Journal*, **1996**, 15, 1495.

[73] S. Rajagopalan, Y. Xu and M. B. Brenner. "Retention of unassembled components of integral membrane proteins by calnexin." *Science*, **1994**, 263, 387.

[74] A. N. Antoniou, S. Ford, M. Alphey, A. Osborne, T. Elliott and S. J. Powis. "The oxidoreductase ERp57 efficiently reduces partially folded in preference to fully folded MHC class I molecules." *The EMBO Journal*, **2002**, 21, 2655.

[75] J. A. Lindquist, G. J. Hämmerling and J. Trowsdale. "ER60/ERp57 forms disulfide-bonded intermediates with MHC class I heavy chain." *The FASEB Journal: official publication of the Federation of American Societies for Experimental Biology*, **2001**, 15, 1448.

[76] M. Molinari, C. Galli, V. Piccaluga, M. Pieren and P. Paganetti. "Sequential assistance of molecular chaperones and transient formation of covalent complexes during protein degradation from the ER." *The Journal of Cell Biology*, **2002**, 158, 247.

[77] M. Molinari and a. Helenius. "Glycoproteins form mixed disulphides with oxidoreductases during folding in living cells." *Nature*, **1999**, 402, 90.

[78] S. S. Vembar and J. L. Brodsky. "One step at a time: endoplasmic reticulum-associated degradation." *Nature Reviews. Molecular Cell Biology*, **2008**, 9, 944.

[79] D. Ng, S. Hiebert and R. Lamb. "Different Roles of Individual N-Linked Oligosaccharide Chains in Folding , Assembly , and Transport of the Simian Virus 5 Hemagglutinin-Neuraminidase". *Molecular and Cellular Biology*, **1990**, 10, 1989.

[80] E. Spear and D. T. W. Ng. "Single, context-specific glycans can target misfolded glycoproteins for ER-associated degradation." *The Journal of Cell Biology*, **2005**, 169, 73.

[81] Z. Kostova and D. H. Wolf. "Importance of carbohydrate positioning in the recognition of mutated CPY for ER-associated degradation." *Journal of Cell Science*, **2005**, 118, 1485.

[82] X.-B. Chang, A. Mengos, Y.-X. Hou, L. Cui, T. J. Jensen, A. Aleksandrov, J. R. Riordan and M. Gentzsch. "Role of N-linked oligosaccharides in the biosynthetic processing of the cystic fibrosis membrane conductance regulator." *Journal of Cell Science*, **2008**, 121, 2814.

[83] B. Meusser, C. Hirsch, E. Jarosch and T. Sommer. "ERAD: the long road to destruction." *Nature Cell Biology*, **2005**, 7, 766.

[84] N. Yagishita, K. Ohneda, T. Amano, S. Yamasaki, A. Sugiura, K. Tsuchimochi, H. Shin, K.-I. Kawahara, O. Ohneda, T. Ohta, S. Tanaka, M. Yamamoto, I. Maruyama, K. Nishioka, A. Fukamizu and T. Nakajima. "Essential role of synoviolin in embryogenesis." *The Journal of Biological Chemistry*, **2005**, 280, 7909.

[85] A. B. Francisco, R. Singh, S. Li, A. K. Vani, L. Yang, R. J. Munroe, G. Diaferia, M. Cardano, I. Biunno, L. Qi, J. C. Schimenti and Q. Long. "Deficiency of suppressor enhancer Lin12 1 like (SEL1L) in mice leads to systemic endoplasmic reticulum stress and embryonic lethality." *The Journal of Biological Chemistry*, **2010**, 285, 13694.

[86] Y. Eura, H. Yanamoto, Y. Arai, T. Okuda, T. Miyata and K. Kokame. "Derlin-1 deficiency is embryonic lethal, Derlin-3 deficiency appears normal, and Herp deficiency is intolerant to glucose load and ischemia in mice." *PloS One*, **2012**, 7, e34298.

[87] E. M. Quan, Y. Kamiya, D. Kamiya, V. Denic, J. Weibezahn, K. Kato and J. S. Weissman. "Defining the glycan destruction signal for endoplasmic reticulum-associated degradation." *Molecular Cell*, **2008**, 32, 870.

[88] S. Clerc, C. Hirsch, D. M. Oggier, P. Deprez, C. Jakob, T. Sommer and M. Aebi. "Htm1 protein generates the N-glycan signal for glycoprotein degradation in the endoplasmic reticulum." *The Journal of Cell Biology*, **2009**, 184, 159.

[89] C. M. Pickart. "Mechanisms underlying ubiquitination." *Annual Review of Biochemistry*, **2001**, 70, 503.

[90] C. Taxis, R. Hitt, S.-H. Park, P. M. Deak, Z. Kostova and D. H. Wolf. "Use of modular substrates demonstrates mechanistic diversity and reveals differences in chaperone requirement of ERAD." *The Journal of Biological Chemistry*, **2003**, 278, 35903.

[91] S. Vashist and D. T. W. Ng. "Misfolded proteins are sorted by a sequential checkpoint mechanism of ER quality control." *The Journal of Cell Biology*, **2004**, 165, 41.

[92] P. Carvalho, V. Goder and T. a. Rapoport. "Distinct ubiquitin-ligase complexes define convergent pathways for the degradation of ER proteins." *Cell*, **2006**, 126, 361.

[93] R. Bernasconi, C. Galli, V. Calanca, T. Nakajima and M. Molinari. "Stringent requirement for HRD1, SEL1L, and OS-9/XTP3-B for disposal of ERAD-LS substrates." *The Journal of Cell Biology*, **2010**, 188, 223.

[94] J. C. Christianson, J. a. Olzmann, T. a. Shaler, M. E. Sowa, E. J. Bennett, C. M. Richter, R. E. Tyler, E. J. Greenblatt, J. W. Harper and R. R. Kopito. "Defining human ERAD networks through an integrative mapping strategy." *Nature Cell Biology*, **2012**, 14, 93.

[95] R. Swanson, M. Locher and M. Hochstrasser. "A conserved ubiquitin ligase of the nuclear envelope/endoplasmic reticulum that functions in both ER-associated and Matalpha2 repressor degradation." *Genes & Development*, **2001**, 15, 2660.

[96] J. Bordallo, R. K. Plemper, a. Finger and D. H. Wolf. "Der3p/Hrd1p is required for endoplasmic reticulum-associated degradation of misfolded lumenal and integral membrane proteins." *Molecular Biology of the Cell*, **1998**, 9, 209.

[97] N. W. Bays, R. G. Gardner, L. P. Seelig, C. a. Joazeiro and R. Y. Hampton. "Hrd1p/Der3p is a membrane-anchored ubiquitin ligase required for ER-associated degradation." *Nature Cell Biology*, **2001**, 3, 24.

[98] A. Schulze, S. Standera, E. Buerger, M. Kikkert, S. van Voorden, E. Wiertz, F. Koning, P.-M. Kloetzel and M. Seeger. "The ubiquitin-domain protein HERP forms a complex with components of the endoplasmic reticulum associated degradation pathway." *Journal of Molecular Biology*, **2005**, 354, 1021.

[99] B. Mueller, E. J. Klemm, E. Spooner, J. H. Claessen and H. L. Ploegh. "SEL1L nucleates a protein complex required for dislocation of misfolded glycoproteins." *Proceedings of the National Academy of Sciences of the United States of America*, **2008**, 105, 12325.

[100] M. Burr and D. van den Boomen. "MHC class I molecules are preferentially ubiquitinated on endoplasmic reticulum luminal residues during HRD1 ubiquitin E3 ligase-mediated dislocation". *Proceedings of the National Academy of Sciences of the United States of America*, **2013**, 110, 14290.

[101] J. M. Younger, L. Chen, H.-Y. Ren, M. F. N. Rosser, E. L. Turnbull, C.-Y. Fan, C. Patterson and D. M. Cyr. "Sequential quality-control checkpoints triage misfolded cystic fibrosis transmembrane conductance regulator." *Cell*, **2006**, 126, 571.

[102] H. R. Stagg, M. Thomas, D. van den Boomen, E. J. H. J. Wiertz, H. a. Drabkin, R. M. Gemmill and P. J. Lehner. "The TRC8 E3 ligase ubiquitinates MHC class I molecules before dislocation from the ER." *The Journal of Cell Biology*, **2009**, 186, 685.

[103] M. Lerner and M. Corcoran. "The RBCC gene RFP2 (Leu5) encodes a novel transmembrane E3 ubiquitin ligase involved in ERAD". *Molecular Biology of the Cell*, **2007**, 18, 1670.

[104] J. P. Lu, Y. Wang, D. a. Sliter, M. M. P. Pearce and R. J. H. Wojcikiewicz. "RNF170 protein, an endoplasmic reticulum membrane ubiquitin ligase, mediates inositol 1,4,5-trisphosphate receptor ubiquitination and degradation." *The Journal of Biological Chemistry*, **2011**, 286, 24426.

[105] F. Tang, B. Wang, N. Li, Y. Wu, J. Jia, T. Suo, Q. Chen, Y.-J. Liu and J. Tang. "RNF185, a Novel Mitochondrial Ubiquitin E3 Ligase, Regulates Autophagy through Interaction with BNIP1". *PLoS ONE*, **2011**, 6, e24367.

[106] N. R. Salama, T. Yeung and R. W. Schekman. "The Sec13p complex and reconstitution of vesicle budding from the ER with purified cytosolic proteins." *The EMBO Journal*, **1993**, 12, 4073.

[107] C. Barlowe, L. Orci, T. Yeung, M. Hosobuchi, S. Hamamoto, N. Salama, M. F. Rexach, M. Ravazzola, M. Amherdt and R. Schekman. "COPII: a membrane coat formed by Sec proteins that drive vesicle budding from the endoplasmic reticulum." *Cell*, **1994**, 77, 895.

[108] J. S. Bonifacino and B. S. Glick. "The mechanisms of vesicle budding and fusion." *Cell*, **2004**, 116, 153.

[109] M. Kuehn, J. Herrmann and R. Schekman. "COPII-cargo interactions direct protein sorting into ER-derived transport vesicles." *Nature*, **1998**, 391, 187.

[110] M. Aridor, J. Weissman and S. Bannykh. "Cargo Selection by the COPII Budding Machinery during Export from the ER." *The Journal of Cell Biology*, **1998**, 141, 61.

[111] E. Mossessova, L. C. Bickford and J. Goldberg. "SNARE selectivity of the COPII coat." *Cell*, **2003**, 114, 483.

[112] E. A. Miller, T. H. Beilharz, P. N. Malkus, M. C. S. Lee, S. Hamamoto, L. Orci and R. Schekman. "Multiple Cargo Binding Sites on the COPII Subunit Sec24p Ensure Capture of Diverse Membrane Proteins into Transport Vesicles". *Cell*, **2014**, 114, 497.

[113] E. Miller, B. Antonny, S. Hamamoto and R. Schekman. "Cargo selection into COPII vesicles is driven by the Sec24p subunit." *The EMBO Journal*, **2002**, 21, 6105.

[114] M. W. Wendeler, J.-P. Paccaud and H.-P. Hauri. "Role of Sec24 isoforms in selective export of membrane proteins from the endoplasmic reticulum." *EMBO Reports*, **2007**, 8, 258.

[115] A. Schweizer, J. A. Fransen, T. Bächi, L. Ginsel and H. P. Hauri. "Identification, by a monoclonal antibody, of a 53-kD protein associated with a tubulo-vesicular compartment at the cis-side of the Golgi apparatus." *The Journal of Cell Biology*, **1988**, 107, 1643.

[116] I. Wada, D. Rindress, P. H. Cameron, W. J. Ou, J. J. Doherty, D. Louvard, A. W. Bell, D. Dignard, D. Y. Thomas and J. J. Bergeron. "SSR alpha and associated calnexin are major calcium binding proteins of the endoplasmic reticulum membrane." *The Journal of Biological Chemistry*, **1991**, 266, 19599.

[117] B. Singer-Krugersg, R. Frankll, F. Crausazs and H. Riezmans. "Partial purification and characterization of early and late endosomes from yeast." *The Journal of Biological Chemistry*, **1993**, 268, 14376.

[118] M. A. Stamnes, M. W. Craighead, M. H. Hoe, N. Lampen, S. Geromanos, P. Tempst and J. E. Rothman. "An integral membrane component of coatomer-coated transport vesicles defines a family of proteins involved in budding." *Proceedings of the National Academy of Sciences of the United States of America*, **1995**, 92, 8011.

[119] M. F. Rexach, M. Latterich and R. W. Schekman. "Characteristics of endoplasmic reticulum-derived transport vesicles." *The Journal of Cell Biology*, **1994**, 126, 1133.

[120] F. Schimmöller and B. Singer-Krüger. "The absence of Emp24p, a component of ER-derived COPII-coated vesicles, causes a defect in transport of selected proteins to the Golgi." *The EMBO Journal*, **1995**, 14, 1329.

[121] W. J. Belden and C. Barlowe. "Role of Erv29p in collecting soluble secretory proteins into ER-derived transport vesicles." *Science*, **2001**, 294, 1528.

[122] R. Schindler, C. Itin, M. Zerial, F. Lottspeich and H.-P. Hauri. "ERGIC-53, a membrane protein of the ER-Golgi intermediate compartment, carries an ER retention motif". *European Journal of Cell Biology*, **1993**, 61, 1.

[123] F. Vollenweider, F. Kappeler, C. Itin and H. P. Hauri. "Mistargeting of the lectin ERGIC-53 to the endoplasmic reticulum of HeLa cells impairs the secretion of a lysosomal enzyme." *The Journal of Cell Biology*, **1998**, 142, 377.

[124] C. Appenzeller, H. Andersson, F. Kappeler and H. P. Hauri. "The lectin ERGIC-53 is a cargo transport receptor for glycoproteins." *Nature Cell Biology*, **1999**, 1, 330.

[125] C. Appenzeller-Herzog, A.-C. Roche, O. Nufer and H.-P. Hauri. "pH-induced conversion of the transport lectin ERGIC-53 triggers glycoprotein release." *The Journal of Biological Chemistry*, **2004**, 279, 12943.

[126] C. Appenzeller-Herzog, B. Nyfeler, P. Burkhard, I. Santamaria, C. Lopez-otin and H.-p. Hauri. "Carbohydrate- and conformation-dependent cargo capture for ER-exit." *Molecular Biology of the Cell*, **2005**, 16, 1258.

[127] M. Moussalli, S. W. Pipe, H.-p. Hauri, W. C. Nichols, D. Ginsburg and R. J. Kaufman. "Mannose-dependent endoplasmic reticulum (ER)-Golgi intermediate compartment-53-mediated ER to Golgi trafficking of coagulation factors V and VIII." *The Journal of Biological Chemistry*, **1999**, 274, 32539.

[128] W. C. Nichols, U. Seligsohn, a. Zivelin, V. H. Terry, C. E. Hertel, M. a. Wheatley, M. J. Moussalli, H. P. Hauri, N. Ciavarella, R. J. Kaufman and D. Ginsburg. "Mutations in the ER-Golgi intermediate compartment protein ERGIC-53 cause combined deficiency of coagulation factors V and VIII." *Cell*, **1998**, 93, 61.

[129] O. Nufer, S. Mitrovic and H.-P. Hauri. "Profile-based data base scanning for animal L-type lectins and characterization of VIPL, a novel VIP36-like endoplasmic reticulum protein." *The Journal of Biological Chemistry*, **2003**, 278, 15886.

[130] Y. Kamiya, D. Kamiya, K. Yamamoto, B. Nyfeler, H.-P. Hauri and K. Kato. "Molecular basis of sugar recognition by the human L-type lectins ERGIC-53, VIPL, and VIP36." *The Journal of Biological Chemistry*, **2008**, 283, 1857.

[131] S. Otte and C. Barlowe. "Sorting signals can direct receptor-mediated export of soluble proteins into COPII vesicles." *Nature Cell Biology*, **2004**, 6, 1189.

[132] J. Dancourt and C. Barlowe. "Erv26p-Dependent Export of Alkaline Phosphatase from the ER Requires Lumenal Domain Recognition." *Traffic*, **2009**, 10, 1006.

[133] C. Bue, C. Bentivoglio and C. Barlowe. "Erv26p directs pro-alkaline phosphatase into endoplasmic reticulum-derived coat protein complex II transport vesicle." *Molecular Biology of the Cell*, **2006**, 17, 4780.

[134] M. Jonikas, S. Collins, V. Denic and E. Oh. "Comprehensive characterization of genes required for protein folding in the endoplasmic reticulum." *Science*, **2009**, 323, 1693.

[135] S. R. Caldwell, K. J. Hill and a. a. Cooper. "Degradation of endoplasmic reticulum (ER) quality control substrates requires transport between the ER and Golgi." *The Journal of Biological Chemistry*, **2001**, 276, 23296.

[136] J. S. Bonifacino, P. Cosson and R. D. Klausner. "Colocalized transmembrane determinants for ER degradation and subunit assembly explain the intracellular fate of TCR chains." *Cell*, **1990**, 63, 503.

[137] D. Ma, N. Zerangue, K. Raab-Graham, S. R. Fried, Y. N. Jan and L. Y. Jan. "Diverse trafficking patterns due to multiple traffic motifs in G protein-activated inwardly rectifying potassium channels from brain and heart." *Neuron*, **2002**, 33, 715.

[138] D. Jack, I. Paulsen and M. Saier. "The amino acid/polyamine/organocation (APC) superfamily of transporters specific for amino acids, polyamines and organocations". *Microbiology*, **2000**, 146, 1797.

[139] D. Wipf, U. Ludewig, M. Tegeder, D. Rentsch, W. Koch and W. B. Frommer. "Conservation of amino acid transporters in fungi, plants and animals." *Trends in Biochemical Sciences*, **2002**, 27, 139.

[140] S. Bröer and M. Palacín. "The role of amino acid transporters in inherited and acquired diseases." *The Biochemical Journal*, **2011**, 436, 193.

[141] J. Chillarón, R. Roca, A. Valencia, A. Zorzano and M. Palacín. "Heteromeric amino acid transporters: biochemistry, genetics, and physiology." *American journal of Physiology. Renal Physiology.*, **2001**, 281, F995.

[142] F. Verrey, C. Meier, G. Rossier and L. C. Kühn. "Glycoprotein-associated amino acid exchangers: broadening the range of transport specificity." *European Journal of Physiology*, **2000**, 440, 503.

[143] C. Wagner, F. Lang and S. Bröer. "Function and structure of heterodimeric amino acid transporters." *American Journal of Physiology. Cell Physiology*, **2001**, 281, 1077.

[144] M. Pineda, C. a. Wagner, A. Bröer, P. a. Stehberger, S. Kaltenbach, J. L. Gelpí, R. Martín Del Río, A. Zorzano, M. Palacín, F. Lang and S. Bröer. "Cystinuria-specific rBAT (R365W) mutation reveals two translocation pathways in the amino acid transporter rBAT-b0,+AT." *The Biochemical Journal*, **2004**, 377, 665.

[145] J. Fort, L. R. de la Ballina, H. E. Burghardt, C. Ferrer-Costa, J. Turnay, C. Ferrer-Orta, I. Usón, A. Zorzano, J. Fernández-Recio, M. Orozco, M. A. Lizarbe, I. Fita and M. Palacín. "The structure of human 4F2hc ectodomain provides a model for homodimerization and electrostatic interaction with plasma membrane." *The Journal of Biological Chemistry*, **2007**, 282, 31444.

[146] J. Bertran, A. Werner, M. L. Moore, G. Stange, D. Markovich, J. Biber, X. Testar, A. Zorzano, M. Palacín, H. Murer, X. Testar and A. Zorzano. "Expression cloning of a cDNA from rabbit kidney cortex that induces a single transport system for cystine and dibasic and neutral amino acids." *Proceedings of the National Academy of Sciences of the United States of America*, **1992**, 89, 5601.

[147] J. Bertran, S. Magagnin, A. Werner, D. Markovich, J. Biber, X. Testart, A. Zorzano, L. C. Kjhn, M. Palacín and H. Murer. "Stimulation of system y+-like amino acid transport by the heavy chain of human 4F2 surface antigen in Xenopus laevis oocytes." *Proceedings of the National Academy of Sciences*, **1992**, 89, 5606.

[148] S. S. Tate, N. Yan and S. Udenfriend. "Expression cloning of a Na(+)-independent neutral amino acid transporter from rat kidney." *Proceedings of the National Academy of Sciences of the United States of America*, **1992**, 89, 1.

[149] R. G. Wells, W. S. Lee, Y. Kanai, J. M. Leiden and M. A. Hediger. "The 4F2 antigen heavy chain induces uptake of neutral and dibasic amino acids in Xenopus oocytes." *The Journal of Biological Chemistry*, **1992**, 267, 15285.

[150] M. Gabrisko and S. Janecek. "Looking for the ancestry of the heavy-chain subunits of heteromeric amino acid transporters rBAT and 4F2hc within the GH13 alpha-amylase family." *The FEBS Journal*, **2009**, 276, 7265.

[151] M. Palacín and Y. Kanai. "The ancillary proteins of HATs: SLC3 family of amino acid transporters." *European Journal of Physiology*, **2004**, 447, 490.

[152] F. Verrey, E. I. Closs, C. a. Wagner, M. Palacín, H. Endou and Y. Kanai. "CATs and HATs: the SLC7 family of amino acid transporters." *European Journal of Physiology*, **2004**, 447, 532.

[153] Y. Kanai, M. G. Stelzner, W. S. Lee, R. G. Wells, D. Brown and M. A. Hediger. "Expression of mRNA (D2) encoding a protein involved in amino acid transport in S3 proximal tubule." *American journal of Physiology. Renal Physiology*, **1992**, 263, F1087.

[154] M. Furriols, J. Chillarón, C. Mora, A. Castello, J. Bertran, M. Campsq, X. Testar, S. Vilaro, A. Zorzano and M. Palacín. "rBAT, related to L-cystine transport, is localized to the microvilli of proximal straight tubules, and its expression is regulated in kidney by development." *The Journal of Biological Chemistry*, **1993**, 268, 27060.

[155] R. Pfeiffer, J. Loffing and G. Rossier. "Luminal heterodimeric amino acid transporter defective in cystinuria." *Molecular Biology of the Cell*, **1999**, 10, 4135.

[156] E. Fernández, M. Jiménez-Vidal, M. Calvo, A. Zorzano, F. Tebar, M. Palacín, J. Chillarón and A. Transporters. "The structural and functional units of heteromeric amino acid transporters. The heavy subunit rBAT dictates oligomerization of the heteromeric amino acid transporters." *The Journal of Biological Chemistry*, **2006**, 281, 26552.

[157] P. Bartoccioni, M. Rius, A. Zorzano, M. Palacín and J. Chillarón. "Distinct classes of trafficking rBAT mutants cause the type I cystinuria phenotype." *Human Molecular Genetics*, **2008**, 17, 1845.

[158] C. Bauch and F. Verrey. "Apical heterodimeric cystine and cationic amino acid transporter expressed in MDCK cells." *American Journal of Physiology. Renal physiology*, **2002**, 283, 181.

[159] S. Sakamoto, A. Chairoungdua, S. Nagamori, P. Wiriyasermkul, K. Promchan, H. Tanaka, T. Kimura, T. Ueda, M. Fujimura, Y. Shigeta, Y. Naya, K. Akakura, H. Ito, H. Endou, T. Ichikawa and Y. Kanai. "A novel role of the C-terminus of b 0,+AT in the ER-Golgi trafficking of the rBAT-b 0,+AT heterodimeric amino acid transporter." *The Biochemical Journal*, **2009**, 417, 441.

[160] E. Fernández, M. Carrascal, F. Rousaud, J. Abián, A. Zorzano, M. Palacín and J. Chillarón. "rBAT-b(0,+)AT heterodimer is the main apical reabsorption system for cystine in the kidney." *American Journal of Physiology. Renal Physiology*, **2002**, 283, F540.

[161] C. C. Feral, N. Nishiya, C. a. Fenczik, H. Stuhlmann, M. Slepak and M. H. Ginsberg. "CD98hc (SLC3A2) mediates integrin signaling." *Proceedings of the National Academy of Sciences of the United States of America*, **2005**, 102, 355.

[162] S. Ohgimoto, N. Tabata and S. Suga. "Molecular Characterization of Fusion Regulatory Protein-1 (FRP-1) That Induces Multinucleated Giant Cell Formation of Monocytes and HIV gpl60-Mediated Cell Fusion." *The Journal of Immunology*, **1995**, 1, 3585.

[163] A. Takesono, J. Moger, S. Farooq, E. Cartwright, I. B. Dawid, S. W. Wilson and T. Kudoh. "Solute carrier family 3 member 2 (Slc3a2) controls yolk syncytial layer (YSL) formation by regulating microtubule networks in the zebrafish embryo." *Proceedings of the National Academy of Sciences*, **2012**, 109, 3371.

[164] J. Cantor, C. D. Browne, R. Ruppert, C. C. Féral, R. Fässler, R. C. Rickert and M. H. Ginsberg. "CD98hc facilitates B cell proliferation and adaptive humoral immunity." *Nature Immunology*, **2009**, 10, 412.

[165] P. Fogelstrand, C. C. Féral, R. Zargham and M. H. Ginsberg. "Dependence of proliferative vascular smooth muscle cells on CD98hc (4F2hc, SLC3A2)." *The Journal of Experimental Medicine*, **2009**, 206, 2397.

[166] B. C. Fuchs and B. P. Bode. "Amino acid transporters ASCT2 and LAT1 in cancer: partners in crime?" *Seminars in Cancer Biology*, **2005**, 15, 254.

[167] M. Ichinoe, T. Mikami, T. Yoshida, I. Igawa, T. Tsuruta, N. Nakada, N. Anzai, Y. Suzuki, H. Endou and I. Okayasu. "High expression of L-type amino-acid transporter 1 (LAT1) in gastric carcinomas: comparison with non-cancerous lesions." *Pathology International*, **2011**, 61, 281.

[168] K. Kaira, N. Oriuchi, H. Imai, K. Shimizu, N. Yanagitani, N. Sunaga, T. Hisada, T. Ishizuka, Y. Kanai, H. Endou, T. Nakajima and M. Mori. "L-type amino acid transporter 1 (LAT1) is frequently expressed in thymic carcinomas but is absent in thymomas." *Journal of Surgical Oncology*, **2009**, 99, 433.

[169] K. Kaira, N. Oriuchi, H. Imai, K. Shimizu, N. Yanagitani, N. Sunaga, T. Hisada, O. Kawashima, Y. Kamide, T. Ishizuka, Y. Kanai, T. Nakajima and M. Mori. "CD98 expression is associated with poor prognosis in resected non-small-cell lung cancer with lymph node metastases." *Annals of Surgical Oncology*, **2009**, 16, 3473.

[170] K. Kaira, N. Oriuchi, K. Shimizu, T. Ishikita, T. Higuchi, H. Imai, N. Yanagitani, N. Sunaga, T. Hisada, T. Ishizuka, Y. Kanai, H. Endou, T. Nakajima, K. Endo and M. Mori. "Correlation of angiogenesis with 18F-FMT and 18F-FDG uptake in non-small cell lung cancer." *Cancer Science*, **2009**, 100, 753.

[171] K. Kaira, N. Oriuchi, H. Imai, K. Shimizu, N. Yanagitani, N. Sunaga, T. Hisada, S. Tanaka, T. Ishizuka, Y. Kanai, H. Endou, T. Nakajima and M. Mori. "L-type amino acid transporter 1 and CD98 expression in primary and metastatic sites of human neoplasms." *Cancer Science*, **2008**, 99, 2380.

[172] K. Kaira, N. Oriuchi, T. Takahashi, K. Nakagawa, Y. Ohde, T. Okumura, H. Murakami, T. Shukuya, H. Kenmotsu, T. Naito, Y. Kanai, M. Endo,

H. Kondo, T. Nakajima and N. Yamamoto. "L-type amino acid transporter 1 (LAT1) expression in malignant pleural mesothelioma." *Anticancer Research*, **2011**, 31, 4075.

[173] J. H. Yoon, I. J. Kim, H. Kim, H.-J. Kim, M. J. Jeong, S. G. Ahn, S. a. Kim, C. H. Lee, B. K. Choi, J.-K. Kim, K. Y. Jung, S. Lee, Y. Kanai, H. Endou and D. K. Kim. "Amino acid transport system L is differently expressed in human normal oral keratinocytes and human oral cancer cells." *Cancer Letters*, **2005**, 222, 237.

[174] E. Gasol, M. Jiménez-Vidal, J. Chillarón, A. Zorzano and M. Palacín. "Membrane topology of system xc- light subunit reveals a re-entrant loop with substrate-restricted accessibility." *The Journal of Biological Chemistry*, **2004**, 279, 31228.

[175] M. Pineda, E. Fernández, D. Torrents, R. Estévez, C. López, M. Camps, J. Lloberas, A. Zorzano and M. Palacín. "Identification of a membrane protein, LAT-2, that Co-expresses with 4F2 heavy chain, an L-type amino acid transport activity with broad specificity for small and large zwitterionic amino acids." *The Journal of Biological Chemistry*, **1999**, 274, 19738.

[176] D. P. Rajan, W. Huang, R. Kekuda, R. L. George, J. Wang, S. J. Conway, L. D. Devoe, F. H. Leibach, P. D. Prasad and V. Ganapathy. "Differential influence of the 4F2 heavy chain and the protein related to b(0,+) amino acid transport on substrate affinity of the heteromeric b(0,+) amino acid transporter." *The Journal of Biological Chemistry*, **2000**, 275, 14331.

[177] G. Rossier, C. Meier, C. Bauch, V. Summa, B. Sordat, F. Verrey and L. C. Kuhn. "LAT2, a New Basolateral 4F2hc/CD98-associated Amino Acid Transporter of Kidney and Intestine." *Journal of Biological Chemistry*, **1999**, 274, 34948.

[178] H. Segawa. "Identification and functional characterization of a Na+-independent neutral amino acid transporter with broad substrate selectivity." *The Journal of Biological Chemistry*, **1999**, 274, 19745.

[179] Y. Fukasawa. "Identification and characterization of a Na+-independent neutral amino acid transporter that associates with the 4F2 heavy chain and exhibits substrate selectivity for small neutral D- and L-amino acids." *The Journal of Biological Chemistry*, **2000**, 275, 9690.

[180] A. Chairoungdua, H. Segawa, J. Y. Kim, K. I. Miyamoto, H. Haga, Y. Fukui, K. Mizoguchi, H. Ito, E. Takeda, H. Endou and Y. Kanai. "Identification of an amino acid transporter associated with the cystinuria-related type II membrane glycoprotein." *The Journal of Biological Chemistry*, **1999**, 274, 28845.

[181] L. Feliubadaló, M. Font, J. Purroy, F. Rousaud, X. Estivill, V. Nunes, E. Golomb, M. Centola, I. Aksentijevich, Y. Kreiss, B. Goldman, M. Pras, D. L. Kastner, E. Pras, P. Gasparini, L. Bisceglia, E. Beccia, M. Gallucci, L. de Sanctis, A. Ponzone, G. F. Rizzoni, L. Zelante, M. T. Bassi, a. L. George, M. Manzoni, A. De Grandi, M. Riboni, J. K. Endsley, A. Ballabio, G. Borsani, N. Reig, E. Fernández, R. Estévez, M. Pineda, D. Torrents, M. Camps, J. Lloberas, A. Zorzano and M. Palacín. "Non-type I cystinuria caused by mutations in SLC7A9, encoding a subunit (bo,+AT) of rBAT." *Nature Genetics*, **1999**, 23, 52.

[182] Y. Kanai, Y. Fukasawa, S. H. Cha, H. Segawa, A. Chairoungdua, D. K. Kim, H. Matsuo, J. Y. Kim, K. Miyamoto, E. Takeda and H. Endou. "Transport properties of a system y+L neutral and basic amino acid transporter. Insights into the mechanisms of substrate recognition." *The Journal of Biological Chemistry*, **2000**, 275, 20787.

[183] D. Torrents. "Identification and Characterization of a Membrane Protein (y+L Amino Acid Transporter-1) That Associates with 4F2hc to Encode the Amino Acid Transport Activity y+L." *Journal of Biological Chemistry*, **1998**, 273, 32437.

[184] R. Pfeiffer, G. Rossier, B. Spindler, C. Meier, L. Kühn and F. Verrey. "Amino acid transport of y+L-type by heterodimers of 4F2hc/CD98 and members of the glycoprotein-associated amino acid transporter family." *The EMBO Journal*, **1999**, 18, 49.

[185] N. Reig, J. Chillarón, P. Bartoccioni, E. Fernández, A. Bendahan, A. Zorzano, B. Kanner, M. Palacín and J. Bertran. "The light subunit of system b(o,+) is fully functional in the absence of the heavy subunit." *The EMBO Journal*, **2002**, 21, 4906.

[186] G. Pujadas and J. Palau. "Evolution of alpha-amylases: architectural features and key residues in the stabilization of the (beta/alpha)(8) scaffold." *Molecular Biology and Evolution*, **2001**, 18, 38.

[187] J. Chillarón, M. Font-Llitjós, J. Fort, A. Zorzano, D. S. Goldfarb, V. Nunes and M. Palacín. "Pathophysiology and treatment of cystinuria." *Nature Reviews. Nephrology*, **2010**, 6, 424.

[188] Y. Fang, H. Jayaram, T. Shane, L. Kolmakova-Partensky, F. Wu, C. Williams, Y. Xiong and C. Miller. "Structure of a prokaryotic virtual proton pump at 3.2 A resolution." *Nature Letters*, **2009**, 460, 1040.

[189] X. Gao, F. Lu, L. Zhou, S. Dang, L. Sun, X. Li, J. Wang and Y. Shi. "Structure and mechanism of an amino acid antiporter." *Science*, **2009**, 324, 1565.

[190] X. Gao, L. Zhou, X. Jiao, F. Lu, C. Yan, X. Zeng, J. Wang and Y. Shi. "Mechanism of substrate recognition and transport by an amino acid antiporter." *Nature*, **2010**, 463, 828.

[191] L. Kowalczyk, M. Ratera, A. Paladino, P. Bartoccioni, E. Errasti-murugarren, E. Valencia, G. Portella, S. Bial, A. Zorzano, I. Fita, M. Orozco, X. Carpena, J. L. Vázquez-Ibar and M. Palacín. "Molecular basis of substrate-induced permeation by an amino acid antiporter." *Proceedings of the National Academy of Sciences of the United States of America*, **2011**, 108, 3935.

[192] P. Shaffer and A. Goehring. "Structure and mechanism of a Na+independent amino acid transporter." *Science*, **2009**, 325, 1010.

[193] D. Ma, P. Lu, C. Yan, C. Fan, P. Yin, J. Wang and Y. Shi. "Structure and mechanism of a glutamate-GABA antiporter." *Nature*, **2012**, 483, 632.

[194] P. Bartoccioni, C. Del Rio, M. Ratera, L. Kowalczyk, J. M. Baldwin, A. Zorzano, M. Quick, S. a. Baldwin, J. L. Vázquez-Ibar and M. Palacín. "Role of transmembrane domain 8 in substrate selectivity and translocation of SteT, a member of the L-amino acid transporter (LAT) family." *The Journal of Biological Chemistry*, **2010**, 285, 28764.

[195] M. Palacín, P. Goodyer, V. Nunes and P. Gasparini. *Metabolic and molecular bases of inherited diseases.* McGraw-Hill, New York, **2001**.

[196] S. Segal and S. O. Thier. *The metabolic and molecular bases of inherited disease.* McGraw-Hill, New York, **1995**.

[197] M. Palacín, G. Borsani and G. Sebastio. "The molecular bases of cystinuria and lysinuric protein intolerance." *Current Opinion in Genetics & Development*, **2001**, 11, 328.

[198] S. Thier, F. Maurice, S. Segal and L. Rosenberg. "Cystinuria: in vitro demonstration of an intestinal transport defect." *Science*, **1964**, 143, 482. Cited By (since 1996)13.

[199] S. O. Thier, S. Segal, M. Fox, a. Blair and L. E. Rosenberg. "Cystinuria: defective intestinal transport of dibasic amino acids and cystine." *The Journal of Clinical Investigation*, **1965**, 44, 442.

[200] L. E. Rosenberg, J. L. Durant and J. M. Holland. "Intestinal absorption and renal extraction of cystine and cysteine in cystinuria." *New England Journal of Medicine*, **1965**, 273, 1239. PMID: 5841926.

[201] H. Daniel. "Molecular and integrative physiology of intestinal peptide transport." *Annual Review of Physiology*, **2004**, 66, 361.

[202] L. D. Strologo. "Comparison between SLC3A1 and SLC7A9 cystinuria patients and carriers: a need for a new classification." *Journal of the American Society of Nephrology*, **2002**, 13, 2547.

[203] P. Goodyer, I. Saadi, P. Ong, G. Elkas and R. Rozen. "Cystinuria subtype and the risk of nephrolithiasis." *Kidney International*, **1998**, 54, 56.

[204] D. S. Milliner and M. E. Murphy. "Urolithiasis in pediatric patients." *Mayo Clinic Proceedings*, **1993**, 68, 241.

[205] X. Martin, M. Salas, M. Labeeuw, N. Pozet, A. Gelet and J. M. Dubernard. "Cystine stones: the impact of new treatment." *British Journal of Urology*, **1991**, 68, 234.

[206] P. Jaeger, L. Portmann, A. Saunders, L. E. Rosenberg and S. O. Thier. "Anticystinuric effects of glutamine and of dietary sodium restriction". *New England Journal of Medicine*, **1986**, 315, 1120.

[207] D. S. Goldfarb, F. L. Coe and J. R. Asplin. "Urinary cystine excretion and capacity in patients with cystinuria." *Kidney International*, **2006**, 69, 1041.

[208] L. M. Rodriguez, F. Santos, S. Malaga and V. Martinez. "Effect of a low sodium diet on urinary elimination of cystine in cystinuric children". *Nephron*, **1995**, 71, 416.

[209] J. S. Rodman, P. Blackburn, J. J. Williams, A. Brown, M. A. Pospischil and C. M. Peterson. "The effect of dietary protein on cystine excretion in patients with cystinuria". *Clinical Nephrology*, **1984**, 22, 273.

[210] C. Dent and M. Friedman. "Treatment of cystinuria." *British Medical Journal*, **1965**, 1, 403.

[211] E. Fjellstedt, T. Denneberg, J.-O. Jeppsson and H.-G. Tiselius. "A comparison of the effects of potassium citrate and sodium bicarbonate in the alkalinization of urine in homozygous cystinuria". *Urological Research*, **2001**, 29, 295.

[212] S. P. Sterrett, K. L. Penniston, J. S. Wolf and S. Y. Nakada. "Acetazolamide is an effective adjunct for urinary alkalization in patients with uric acid and cystine stone formation recalcitrant to potassium citrate." *Urology*, **2008**, 72, 278.

[213] M. Lotz and F. C. Bartter. "Stone dissolution with D-penicillamine in cystinuria." *British Medical Journal*, **1965**, 2, 1408.

[214] G. M. Preminger, H.-G. Tiselius, D. G. Assimos, P. Alken, a. Colin Buck, M. Gallucci, T. Knoll, J. E. Lingeman, S. Y. Nakada, M. S. Pearle, K. Sarica, C. Türk and J. S. Wolf. "2007 Guideline for the Management of Ureteral Calculi." *European Urology*, **2007**, 52, 1610.

[215] D. M. Rudnick, P. M. Bennett and S. P. Dretler. "Retrograde renoscopic fragmentation of moderate-size (1.5-3.0-cm) renal cystine stones." *Journal of Endourology*, **1999**, 13, 483.

[216] L. E. Rosenberg, S. Downing, J. L. Durant and S. Segal. "Cystinuria: biochemical evidence for three genetically distinct diseases." *The Journal of Clinical Investigation*, **1966**, 45, 365.

[217] M. Font-Llitjós, M. Jiménez-Vidal, L. Bisceglia, M. Di Perna, L. de Sanctis, F. Rousaud, L. Zelante, M. Palacín and V. Nunes. "New insights into cystinuria: 40 new mutations, genotype-phenotype correlation, and digenic inheritance causing partial phenotype." *Journal of Medical Genetics*, **2005**, 42, 58.

[218] P. R. Goodyer, C. Clow, T. Reade and C. Girardin. "Prospective analysis and classification of patients with cystinuria identified in a newborn screening program". *Journal of Pediatrics*, **1993**, 122, 568.

[219] E. Pras, N. Arber, I. Aksentijevich and G. Katz. "Localization of a gene causing cystinuria to chromosome 2p." *Nature Genetics*, **1994**, 6, 415.

[220] M. Calonge, P. Gasparini, J. Chillarón, M. Chillón, M. Gallucci, F. Rousaud, L. Zelante, X. Testar, B. Dallapiccola, F. Di Silverio and Others. "Cystinuria caused by mutations in rBAT, a gene involved in the transport of cystine." *Nature Genetics*, **1994**, 6, 420.

[221] M. J. Calonge, V. Volpini, L. Bisceglia, F. Rousaud, L. de Sanctis, E. Beccia, L. Zelante, X. Testar, a. Zorzano and X. Estivill. "Genetic heterogeneity in cystinuria: the SLC3A1 gene is linked to type I but not to type III cystinuria." *Proceedings of the National Academy of Sciences of the United States of America*, **1995**, 92, 9667.

[222] R. Wartenfeld, E. Golomb, G. Katz, S. J. Bale, B. Goldman, M. Pras, D. L. Kastner and E. Pras. "Molecular analysis of cystinuria in Libyan Jews: exclusion of the SLC3A1 gene and mapping of a new locus on 19q." *American Journal of Human Genetics*, **1997**, 60, 617.

[223] L. Bisceglia and M. Calonge. "Localization, by linkage analysis, of the cystinuria type III gene to chromosome 19q13.1." *American Journal of Human Genetics*, **1997**, 60, 611.

[224] J. Chillarón, R. Estévez, I. Samarzija, S. Waldegger, X. Testar, F. Lang, A. Zorzano, A. Busch, M. Palacín, D. Silverio and M. Palacõ. "An intracellular trafficking defect in type I cystinuria rBAT mutants M467T and M467K." *The Journal of Biological Chemistry*, **1997**, 272, 9543.

[225] Y. Shigeta, Y. Kanai, a. Chairoungdua, N. Ahmed, S. Sakamoto, H. Matsuo, D. K. Kim, M. Fujimura, N. Anzai, K. Mizoguchi, T. Ueda, K. Akakura, T. Ichikawa, H. Ito and H. Endou. "A novel missense mutation of SLC7A9 frequent in Japanese cystinuria cases affecting the C-terminus of the transporter." *Kidney International*, **2006**, 69, 1198.

[226] L. Bisceglia, L. Fischetti, P. D. Bonis, O. Palumbo, B. Augello, P. Stanziale, M. Carella and L. Zelante. "Large rearrangements detected by MLPA, point mutations, and survey of the frequency of mutations within the SLC3A1 and SLC7A9 genes in a cohort of 172 cystinuric Italian patients". *Molecular Genetics and Metabolism*, **2010**, 99, 42.

[227] L. Harnevik, E. Fjellstedt, A. Molbaek, T. Denneberg and P. Söderkvist. "Mutation analysis of SLC7A9 in cystinuria patients in Sweden." *Genetic Testing*, **2003**, 7, 13.

[228] S. P. DiBartola, D. J. Chew and M. L. Horton. "Cystinuria in a cat." *Journal of the American Veterinary Medical Association*, **1991**, 198, 102.

[229] P. S. Henthorn, J. Liu, T. Gidalevich, J. Fang, M. Casal, D. Patterson and U. Giger. "Canine cystinuria: polymorphism in the canine SLC3A1 gene and identification of a nonsense mutation in cystinuric Newfoundland dogs". *Human Genetics*, **2000**, 107, 295.

[230] K. C. Bovee, M. Bush, J. Dietz, P. Jezyk and S. Segal. "Cystinuria in the maned wolf of South America". *Science*, **1981**, 212, 919.

[231] T. Peters, C. Thaete, S. Wolf, a. Popp, R. Sedlmeier, J. Grosse, M. C. Nehls, a. Russ and V. Schlueter. "A mouse model for cystinuria type I." *Human Molecular Genetics*, **2003**, 12, 2109.

[232] L. Feliubadaló, M. L. Arbonés, S. Mañas, J. Chillarón, J. Visa, M. Rodés, F. Rousaud, A. Zorzano, M. Palacín and V. Nunes. "Slc7a9-deficient mice develop cystinuria non-I and cystine urolithiasis." *Human Molecular Genetics*, **2003**, 12, 2097.

[233] M. Molinari. "N-glycan structure dictates extension of protein folding or onset of disposal." *Nature Chemical Biology*, **2007**, 3, 313.

[234] A. A. McCracken and J. L. Brodsky. "Recognition and delivery of ERAD substrates to the proteasome and alternative paths for cell survival." *Current Topics in Microbiology and Immunology*, **2005**, 300, 17.

[235] A. Parodi. "Protein glucosylation and its role in protein folding." *Annual Review of Biochemistry*, **2000**, 69, 69.

[236] M. Guillén, D. Corella, M. L. Cabello, J. I. González, a. Sabater, J. F. Chaves and J. Hernández-Yago. "Identification of novel SLC3A1 gene mutations in Spanish cystinuria families and association with clinical phenotypes." *Clinical Genetics*, **2005**, 67, 240.

[237] R. R. Kopito. "Biosynthesis and degradation of CFTR." *Physiological Reviews*, **1999**, 79, S167.

[238] H. K. Jensen, H. Holst, L. G. Jensen, M. M. Jø rgensen, P. H. Andreasen, T. G. Jensen, B. S. Andresen, F. Heath, P. S. Hansen, S. Neve, K. Kristiansen, O. Faergeman, S. Kø lvraa, L. Bolund and N. Gregersen. "A common W556S mutation in the LDL receptor gene of Danish patients with familial hypercholesterolemia encodes a transport-defective protein." *Atherosclerosis*, **1997**, 131, 67.

[239] R. Halaban, S. Svedine, E. Cheng, Y. Smicun, R. Aron and D. N. Hebert. "Endoplasmic reticulum retention is a common defect associated with tyrosinase-negative albinism." *Proceedings of the National Academy of Sciences of the United States of America*, **2000**, 97, 5889.

[240] M. Aridor and L. Hannan. "Traffic jam: a compendium of human diseases that affect intracellular transport processes." *Traffic*, **2000**, 1, 836.

[241] M. Aridor and L. a. Hannan. "Traffic jams II: an update of diseases of intracellular transport." *Traffic*, **2002**, 3, 781.

[242] A. B. Deora. "Progressive C-terminal Deletions of the Renal Cystine Transporter, NBAT, Reveal a Novel Bimodal Pattern of Functional Expression." *The Journal of Biological Chemistry*, **1998**, 273, 32980.

[243] K. Watanabe, Y. Hata, H. Kizaki, Y. Katsube and Y. Suzuki. "The refined crystal structure of Bacillus cereus oligo-1,6-glucosidase at 2.0 A resolution: structural characterization of proline-substitution sites for protein thermostabilization." *Journal of Molecular Biology*, **1997**, 269, 142.

[244] Z.-Y. Guo, C. C. Y. Chang, X. Lu, J. Chen, B.-l. Li and T.-y. Chang. "The disulfide linkage and the free sulfhydryl accessibility of acyl-coenzyme A: cholesterol acyltransferase 1 as studied by using mPEG 5000-maleimide." *Biochemistry*, **2005**, 44, 6537.

[245] J. Lu and C. Deutsch. "Pegylation: a method for assessing topological accessibilities in Kv1.3." *Biochemistry*, **2001**, 40, 13288.

[246] J. Bardwell. "Thiol modifications in a snapshot." *Nature Biotechnology*, **2005**, 23, 42.

[247] A. Delaunay, A. D. Isnard and M. B. Toledano. "H2O2 sensing through oxidation of the Yap1 transcription factor." *The EMBO Journal*, **2000**, 19, 5157.

[248] M. Rius and J. Chillarón. "Carrier subunit of plasma membrane transporter is required for oxidative folding of its helper subunit." *The Journal of Biological Chemistry*, **2012**, 287, 18190.

[249] K. Kanehara, S. Kawaguchi and D. T. W. Ng. "The EDEM and Yos9p families of lectin-like ERAD factors." *Seminars in Cell & Developmental Biology*, **2007**, 18, 743.

[250] T. Marquardt, D. N. Hebert and a. Helenius. "Post-translational folding of influenza hemagglutinin in isolated endoplasmic reticulum-derived microsomes." *The Journal of Biological Chemistry*, **1993**, 268, 19618.

[251] P. Deprez, M. Gautschi and A. Helenius. "More than one glycan is needed for ER glucosidase II to allow entry of glycoproteins into the calnexin/calreticulin cycle." *Molecular Cell*, **2005**, 19, 183.

[252] J. J. Caramelo and A. Parodi. "How sugars convey information on protein conformation in the endoplasmic reticulum." *Seminars in Cell & Developmental Biology*, **2007**, 18, 732.

[253] B. Potter, G. Ihrke and J. Bruns. "Specific N-glycans direct apical delivery of transmembrane, but not soluble or glycosylphosphatidylinositol-anchored forms of endolyn in Madin-Darby Canine Kidney cells." *Molecular Biology of the Cell*, **2004**, 15, 1407.

[254] D. Zhang, N. Li, S.-M. Lok, L.-H. Zhang and K. Swaminathan. "Isomaltulose synthase (PalI) of Klebsiella sp. LX3. Crystal structure and implication of mechanism." *The Journal of Biological Chemistry*, **2003**, 278, 35428.

[255] B. Nyfeler, S. W. Michnick and H.-P. Hauri. "Capturing protein interactions in the secretory pathway of living cells." *Proceedings of the National Academy of Sciences of the United States of America*, **2005**, 102, 6350.

[256] F. Kappeler, D. R. Klopfenstein, M. Foguet, J. P. Paccaud and H.-P. Hauri. "The recycling of ERGIC-53 in the early secretory pathway." *The Journal of Biological Chemistry*, **1997**, 272, 31801.

[257] M. Gossen and H. Bujard. "Tight control of gene expression in mammalian cells by tetracycline-responsive promoters." *Proceedings of the National Academy of Sciences of the United States of America*, **1992**, 89, 5547.

[258] B. C. Cunningham and J. A. Wells. "High-resolution epitope mapping of hGH-receptor interactions by alanine-scanning mutagenesis." *Science*, **1989**, 244, 1081.

[259] A. S. Mildvan, D. J. Weber and A. Kuliopulos. "Quantitative interpretations of double mutations of enzymes." *Archives of Biochemistry and Biophysics*, **1992**, 294, 327.

[260] A. S. Mildvan. "Inverse thinking about double mutants of enzymes." *Biochemistry*, **2004**, 43, 10.

[261] S. Ravaud, X. Robert, H. Watzlawick, R. Haser, R. Mattes and N. Aghajari. "Structural determinants of product specificity of sucrose isomerases." *FEBS Letters*, **2009**, 583, 1964.

[262] H. Hondoh, W. Saburi, H. Mori, M. Okuyama, T. Nakada, Y. Matsuura and A. Kimura. "Substrate recognition mechanism of alpha-1,6-glucosidic linkage hydrolyzing enzyme, dextran glucosidase from Streptococcus mutans." *Journal of Molecular Biology*, **2008**, 378, 913.

[263] T. Shirai, V. S. Hung, K. Morinaka, T. Kobayashi and S. Ito. "Crystal structure of GH13 alpha-glucosidase GSJ from one of the deepest sea bacteria." *Proteins*, **2008**, 73, 126.

[264] J. Fitter. "Structural and dynamical features contributing to thermostability in alpha-amylases." *Cellular and Molecular Life Sciences*, **2005**, 62, 1925.

[265] S. Janecek, B. Svensson and B. Henrissat. "Domain evolution in the alpha-amylase family." *Journal of Molecular Evolution*, **1997**, 45, 322.

[266] J.-Y. Chang. "Diverse pathways of oxidative folding of disulfide proteins: underlying causes and folding models." *Biochemistry*, **2011**, 50, 3414.

[267] A. Rosell, M. Meury, E. Alvarez-Marimon, M. Costa, L. Perez-Cano, A. Zorzano, J. Fernandez-Recio, M. Palacín and D. Fotiadis. "Structural bases for the interaction and stabilization of the human amino acid transporter LAT2 with its ancillary protein 4F2hc." *Proceedings of the National Academy of Sciences*, **2014**, 111, 2966.

[268] M. J. Feige and L. M. Hendershot. "Quality control of integral membrane proteins by assembly-dependent membrane integration." *Molecular Cell*, **2013**, 51, 297.

[269] N. Mitra, S. Sinha, T. N. C. Ramya and A. Surolia. "N-linked oligosaccharides as outfitters for glycoprotein folding, form and function." *Trends in Biochemical Sciences*, **2006**, 31, 156.

[270] S. R. Hanson, E. K. Culyba, T.-l. Hsu, C.-h. Wong, J. W. Kelly and E. T. Powers. "The core trisaccharide of an N-linked glycoprotein intrinsically accelerates folding and enhances stability." *Proceedings of the National Academy of Sciences of the United States of America*, **2009**, 106, 3131.

[271] D. Cioaca, S. Ghenea, L. N. Spiridon, M. Marin, A. J. Petrescu and S. M. Petrescu. "C-terminus glycans with critical functional role in the maturation of secretory glycoproteins." *PloS One*, **2011**, 6, e19979.

[272] O. Vagin, S. Turdikulova and G. Sachs. "The H,K-ATPase beta subunit as a model to study the role of N-glycosylation in membrane trafficking and apical sorting." *The Journal of Biological Chemistry*, **2004**, 279, 39026.

[273] D. Dubbs and W. Scherer. "Variants of Japanese encephalitis virus cytopathic for L mouse fibroblasts and lass human epithelial cells." *Japanese Journal of Medical Science & Biology*, **1969**, 22, 253.

[274] J. Sambrook, E. F. E. F. Fritsch, T. Maniatis and C. S. H. Laboratory. *Molecular cloning : a laboratory manual*. New York : Cold Spring Harbor Laboratory Press, 2nd ed edition, **1989**.

[275] M. Wigler, R. Sweet, G. Sim, B. Wold and A. Pellicer. "Transformation of mammalian cells with genes from procaryotes and eucaryotes." *Cell*, **1979**, 16, .

Summary in spanish

7.1 Introducción

Las células de mamífero expresan más de 10000 proteínas distintas que son sintetizadas en los ribosomas como cadenas de aminoácidos. Para ejercer su función, estas cadenas deben adquirir su plegamiento nativo. Cómo esto ocurre y cómo las células mantiene la integridad conformacional del proteoma es uno de los problemas fundamentales en biología.

El control de calidad de proteínas y el mantenimiento de la homeostasis del proteoma es crucial para el buen funcionamiento celular y del organismo. Para mantener esta homeostasis es imprescindible el papel de varios cientos de proteinas[2], incluyendo chaperonas y reguladores de chaperonas que asisten en el plegamiento *de novo*, en ciclos de plegamiento de proteinas mal plegadas y en el sistema de ubiquitinación y degradación por el proteasoma, que median la eliminación de proteinas irreversiblemente mal plegadas y de agregados de proteinas.

7.1.1 Plegamiento en el retículo endoplasmático

El retículo endoplasmático (RE) confiere un compartimento intracelular distinto del citosol donde se llevan a cabo las modificaciones post-traduccionales y es donde se lleva a cabo el control de calidad de proteínas, permitiendo la salida del RE sólo cuando las proteínas se encuentran plegadas y modificadas correctamente. Varias moléculas incluyendo lectinas, proteínas disulfuro isomerasas y chaperonas moleculares tienen un papel el control de calidad en el RE. Todavía se conoce poco sobre qué chaperonas necesita cada proteína y en qué momento intervienen cada una de ellas durante el plegamiento. Es más, se sabe muy poco sobre cómo son las vías de plegamiento de proteínas en la célula en comparación con nuestro conocimiento *in vitro*.

7.1.2 Papel de los N-glicanos en la degradación y plegamiento en el RE

La presencia de N-glicanos en proteínas favorece el plegamiento y el tráfico intracelular[62,63]. Los N-glicanos son estructuras altamente flexibles e hidrofílicas que enmascaran zonas hidrofóbicas de proteínas, lo que tiene un efecto impor-

tante en el proceso de plegamiento y estabilización de proteínas[64,65]. Muchas glicoproteínas necesariamente requieren de la interacción con el sistema de lectinas CNX/CRT para plegarse correctamente. CNX y CRT son dos lectinas presentes en el ER que unen específicamente a N-glicanos monoglucosilados de estructura Glc1Man7-9GlcNAc2[62,69]. Después de la transferencia en el RE, comienza el procesamiento del oligosacárido transferido. La glucosidasa I elimina el residuo de glucosa más externo y la glucosidasa II (GII) los dos residuos remanentes. Los N-glicanos monoglucosilados pueden producirse por deglucosilación parcial de Glc3Man9GlcNAc2 o por reglucosilación de los glicanos libres de glucosas por acción de la UDP-Glc: glicoproteína glucosiltransferasa (UGGT). Los glicanos monoglucosilados formados por cualquiera de los dos caminos tienen una existencia transitoria *in vivo,* ya que las glucosas son eliminadas por la GII. UGGT[67,235] transfiere residuos de glucosa únicamente a oligosacáridos unidos a proteínas no plegadas correctamente. Esta enzima se comporta, por lo tanto, como sensor de la conformación de glicoproteínas. Durante este tiempo las proteínas se ensamblan en complejos oligoméricos y forman puentes disulfuros. La formación de puentes disulfuro en el RE es catalizada por la familia de ditiol-disulfuro oxidoreductasas (PDI)[31]. Erp57, un miembro de la familia de PDI (protein-disulfide isomerase) en asociación con calnexina y calreticulina interacciona con las glicoproteínas, actuando como oxidorreductasa tiol-disulfuro, y promoviendo la formación de puentes disulfuros sólo de las proteínas monoglucosiladas. La interacción de los N-glicanos monoglucosilados con CNX/CRT facilita el plegamiento correcto de las glicoproteínas al prevenir la agregación y suprimir la formación de puentes disulfuro no nativos[68,72]. Una vez correctamente plegada, la glicoproteína sale del ciclo y continúa su tránsito por la vía secretora.

Existen un gran número de patologías relacionadas con conformaciones anómalas de plegamiento como la fibrosis cística, la retinitis pigmentosa, el Alzheimer, etc.[240,241]. Todas estas patologías derivan de una alteración conformacional de la proteína implicada.

En esta tésis se ha querido profundizar en la biogénesis de proteínas de membrana: plegamiento, ensamblaje y salida del RE (maduración). Nuestro modelo de estudio ha sido el transportador humano rBAT-$b^{0,+}$AT perteneciente a la familia de transportadores heteroméricos de aminoácidos y cuya ausencia causa cistinuria.

7.1.3 Transportadores heteroméricos de aminoácidos

La familia de transportadores heteroméricos de aminoácidos (HAT) pertenece a una de las 5 superfamilias de transportadores descritas, llamada APC (Amino acid, Polyamine and Organic Cation transporter) que incluye transportadores de levadura, plantas y animales[138,139]. La familia de transportadores heteroméricos HAT es la única que presenta una unidad funcional constituida por al menos una subunidad pesada (HSHAT) y una subunidad ligera (LSHAT) siendo ésta última la que confiere la especificidad de sustrato y actividad de transporte, unidas por un puente disulfuro conservado en todos los miembros de la familia[141–143] (ver Tabla 1.1).

El transportador rBAT-$b^{0,+}$AT constituye el sistema $b^{0,+}$-like. La unidad funcional es el heterodímero. rBAT es la subunidad pesada y $b^{0,+}$AT es la ligera. Se expresa en membranas apicales de células epiteliales del intestino delgado y del túbulo proximal de riñon. Fisiologicamente, $b^{0,+}$-like es el responsable del influjo de cistina y aminoácidos dibásicos con alta afinidad y eflujo de aminoácidos neutros, independiente de sodio. Mutaciones en rBAT o $b^{0,+}$AT causan cistinuria. El transporte defectuoso de cistina provoca su precipitación y la formación de cálculos en el tracto urinario.

7.2 Objetivos

El objetivo general de esta tésis es el de describir los mecanismos de la biogénesis del transportador de cistinuria rBAT-$b^{0,+}$AT, como modelo para el estudio de proteínas de membrana.

Los puentes disulfuro y los N-glicans son cruciales para el correcto plegamiento, ensamblaje y tráfico de proteíns. Por eso, los objetivos de este estudio son:

I. Identificar los puentes disulfuro intramoleculares y el de describir el plegamiento oxidativo de rBAT-$b^{0,+}$AT.

II. Describir el papel de los puentes disulfuro en la biogénesis del transportador.

III. Dilucidar si la subunidad ligera $b^{0,+}$AT es o no requerida para el plegamiento de rBAT.

IV. Identificar la posición de los N-glicanos de rBAT y describir su papel en la biogénesis y funcionalidad del transportador.

Como consecuencia de los resultados obtenidos en los objetivos anteriores, un objetivo final fue el de:

V. Analizar el papel de la cola C-terminal de rBAT (674-684) en el plegamiento y la salida del RE del transportador.

7.3 Resultados

7.3.1 Antecedentes

Estudios previos en nuestro grupo analizaron la biogénesis de rBAT salvaje en presencia y ausencia de $b^{0,+}$AT, asi como la biogénesis de algunos mutantes de cistinuria en células MDCK y HeLa[157]. En ausencia de $b^{0,+}$AT, rBAT se degrada rápidamente mientras que $b^{0,+}$AT se mantiene estable. Se estudiaron también algunos de los factores involucrados en la degradación de rBAT. La adición de los inhibidores del proteasoma MG132 y lactacistina retrasaban la degradación de rBAT. El inhibidor de manosidasas del ER deoxymanojirimicina (dMNJ) tuvo el mismo efecto, indicando que la degradación de rBAT está mediada, al menos en parte, por la vía ERAD (ER-Associated Degradation)[233,234]. Se analizó también si rBAT es un sustrato del ciclo CNX/CRT. La adición de castanospermina aceleró la degradación de rBAT sugiriendo que la interacción con el sistema de chaperonas de la calnexina retrasa la degradación de rBAT[157]. Antes de ser degradada, rBAT tiene una fase lag de $\sim$ 2 h en células HeLa en la que podría ser retenida por chaperonas en espera de unirse con la subunidad ligera $b^{0,+}$AT. De hecho, el ensamblaje de rBAT con $b^{0,+}$AT impide la degradación de la subunidad pesada. El heterodimero puede entonces salir del RE y llegar al Golgi donde adquiere una N-glicosilación compleja. También se estudiaron algunos mutantes de cistinuria. Todas las mutaciones de rBAT que causan cistinuria de tipo I se localizan en el dominio extracelular, excepto las mutaciones L89P y I105R[236]. El estudio analizó los mutantes de cistinuria de tipo I L89P, T216M, R365W, M467K y M467T en ausencia y presencia de $b^{0,+}$AT. El estudio de la biogénesis de los mutantes de TIM barrel que causan cistinuria de tipo I muestra que estos mutantes no tienen actividad de transporte[157]. Ninguno de ellos adquirió N-glicosilación compleja, indicando localización en el RE. Estos mutantes eran capaces de unirse a $b^{0,+}$AT pero eran posteriormente degradados, lo que sugiere que estas mutaciones causan un mal plegamiento del dominio extracelular de rBAT.

Varias enfermedades en humanos son causadas por mutaciones que inducen un mal plegamiento de las proteinas como la fibrosis cística[237], la hicercolesterolemia familiar[238], la cistinuria[157] y muchas más[240,241]. Nuestro estudio y otros sugieren que el conocimiento del plegamiento *in vivo* es importante para dilucidar mejor los mecanismos del plegamiento de proteínas y los factores que provocan un mal plegamiento ya que son elementos clave en el estudio de enfermedades de plegamiento.

La formación de los puentes disulfuro y la presencia de N-glicanos tienen un papel importante en el plegamiento de proteinas[235]. De hecho, este plegamiento puede ser monitorizado *in vivo* siguiento la oxidación de los puentes disulfuro[56,57]. Con el propósito de analizar la biogénesis del transportador rBAT-$b^{0,+}$AT humano y los elementos involucrados en el plegamiento de rBAT, estudiamos el papel de los residuos de cisteína y de los N-glicanos presentes en rBAT.

7.3.2 Papel de los residuos de cisteína de rBAT en presencia/ausencia de $b^{0,+}$AT

rBAT humano contiene 8 cisteínas. La primera, la cisteína 18, es citosólica. El resto son extracelulares. La cisteína 114 forma un puente disulfuro con $b^{0,+}$AT[141,242], las cisteínas 242 y 273 se encuentran en el dominio B, la cisteína 571 está en el dominio C y, finalmente, las cisteínas 666, 673 y 685 se localizan en la cola C-terminal de rBAT[145]. La cisteína 685 es el residuo C-terminal. Las cisteínas 114 a 685 estan conservadas en todos los ortólogos excepto las cisteínas 242 y 273 que son residuos de serina en 2 urocordados.

La estructura de rBAT no ha sido resuelta y, por tanto, se desconocen los puentes disulfuros que contiene. Con el objetivo de describir los puentes disulfuro presentes en rBAT, estudiamos las cisteínas libres presentes en r BAT salvaje y en los mutantes de cisteína en presencia y ausencia de $b^{0,+}$AT. El mPEG5000-maleimida (mPEG) se une a los grupos sulfidrilos (-SH) accesibles en una proteína. La unión de una molécula de mPEG produce un incremento del peso de la proteína de $\sim$5 kDa, fácilmente detectable en un gel SDS-PAGE. De esta manera, aparecerán bandas de distintos tamaños según el número de moléculas de mPEG unidas.

Cuando hubimos confirmado que las 8 cisteínas de rBAT eran accesibles a mPEG (Figura 3.11) empezamos a analizar mutantes de cisteína de rBAT. Para generar mutantes de cisteína se reemplazaron las cisteínas por serinas, excepto en el caso de la C273, que fue reemplazada por alanina. Se expresaron los mutantes y rBAT salvaje en presencia de $b^{0,+}$AT en células HeLa. Las células se marcaron radioactivamente con 35S]Met/Cis, las muestras se incubaron con mPEG en condiciones desnaturalizantes y se inmunoprecipitaron con un anticuerpo anti-$b^{0,+}$AT. La co-inmunoprecipitación con anti-$b^{0,+}$AT indica que todos los mutantes de cisteína pueden ensamblarse con $b^{0,+}$AT. Los resultados eran consistentes con la presencia de 3 puentes disulfuros intramoleculares en el ectodominio de rBAT en presencia de $b^{0,+}$AT. No así en ausencia de $b^{0,+}$AT (ver más adelante) lo que mostró que $b^{0,+}$AT es necesario para el plegamiento oxidativo de rBAT. El hecho de que los mutantes C242S y C273A presentaran un patrón similar entre ellos y distinto al resto de los mutantes de cisteína suggiere que estas 2 cisteínas podrían formar un puente disulfuro (Figura 3.12). Sin embargo estos resultados no esclarecían qué puentes disulfuro se encuentran entre las cisteínas C571 a C685.

Con este propósito estudiamos la biogénesis de los mutantes de cisteína. Se llevaron a cabo experimentos de pulso y caza para analizar la estabilidad y la maduración de estos mutantes en presencia y ausencia de $b^{0,+}$AT. Para estudiar la degradación de los mutantes de cisteína, se ayunaron las células HeLa transfectadas durante 30 min y se marcaron con [35]Met/Cis durante 15 min. Se cuantificó la degradación después de 5 h de caza (Figura 3.13).

Seguidamente realizamos ensayos de transporte de L-cistina en células HeLa en los mutantes de cisteína (Figura 3.15). Tal y como esperábamos, los mutantes que no presentaban banda madura en los experimentos de pulso y caza no mostraron actividad de transporte. Los mutantes C18S y C114S presentaron un transporte similar al de rBAT salvaje. Los mutantes C673S y C685S son funcionales pero presentaron menos transporte que rBAT salvaje.

Los análisis con mPEG muestran que los mutantes C242S y C273A presentan un patrón similar entre ellos y distinto del resto de mutantes . Los experimentos de pulso y caza indican que las cisteínas C673 y C685 sufren una maduración más lenta, mientras que los otros mutantes son retenidos en el RE. Estos resultados indican que los puentes disulfuros presentes en rBAT son: C242-C273, C571-C666 y C673-C685. Seguidamente, se generaron dobles mutantes de cisteína con tal de

estudiar más profundamente el papel de los puentes disulfuro en rBAT.

Análisis de los dobles mutantes de cisteína

Se generaron doubles mutantes con las cisteínas que forman los probables puentes disulfuro y también dobles mutantes con distintas combinaciones. Los experimentos mostraron que aquellos mutantes que contienen una cisteína del dominio B desapareada muestran un patrón de hasta 4 y 5 mPEGs unidos, lo que indica que no están formando ningún puente disulfuro, mientras que el resto de los mutantes, incluido el mutante C242S-C273A, tienen principalmente solo 1 mPEG unido (Figura 3.16). El hecho de que el mutante C242S-C273A no presente este patrón con hasta 4 mPEGs unidos indica que lo que provoca el mal plegamiento de la proteína no es la ausencia del puente disulfuro sino que una cisteína esté desapareada. De hecho, esto ya es visible en el estudio de mutantes simples de cisteína.

Seguidamente se estudió la biogenesis de estos mutantes mediante análisis de pulso y caza a 5 h. Los dobles mutantes que combinan las cisteínas C242 a C666 con C242 a C685 muestran un importante reducción en la señal de rBAT co-precipitado con anti-$b^{0,+}$AT (Figura 3.17). Los mutantes eran retenidos en el RE y no presentaban banda madura en los ensayos de Endo H. Estos mutantes también eran degradados de manera similar a los mutantes simples de las cisteínsa C242 a C666. Es interesante resaltar que el doble mutante C673S-C685S era el único que presentaba una maduración como la de rBAT salvaje. En cambio, como se ha mostrado anteriormente, los mutantes simples de estas cisteínas son parcialmente degradados y una maduración más lenta (Figura 3.14). Estos resultados refuerzan la hipótesis de que estas 2 cisteínas estan formando un puente disulfuro. Los análisis de transporte de L-cistina reforzaron los resultados obtenidos en los experimentos de estabilidad y maduración (Figura 3.18). Los dobles mutantes que no mostraban maduración tampoco presentaron transporte de cistina. El doble mutante C673S-C685S presenta más transporte que los mutantes simples de estas cisteínas (Figura 3.15).

El próximo paso fue estudiar la pegilación y la biogénesis de mutantes que contenían solo un puente disulfuro nativo (C242-C273, DS1; C571-C666, DS2; C673-C685, DS3) así como las cisteínas C18 y C114. Se realizaron análisis de pulso y caza y Endo H. Los 3 mutantes son degradados, no maduran (Figura 3.19A) ni presentan transporte de L-cistina. Los estudios de pegilación de estos mutantes en presencia de $b^{0,+}$AT muestran que todos ellos pueden formar el puente disulfuro lo

que indica que los 3 puentes disulfuro pueden formarse independientemente el uno del otro. De todas maneras, el mutante DS1 es el único que presenta únicament la banda con sólo 1 mPEG. Los otros dos mutantes presentan también bandas minoritarias correspondientes a 2 y 3 mPEG unidos. Estos resultados indican que C242-C273, contrariamente a C571-C666 y C673-C685, es capaz de formarse de manera estable en ausencia de los otros dos puentes disulfuro. Esto también refuerza la idea de que C242-C273 es el primer puente disulfuro en formarse. Los mutantes DS2 y DS3 muestran un patrón similar al de rBAT salvaje, pero la banda correspondiente a 3 mPEGs unidos presenta una mayor movilidad en DS3 que en DS2 y rBAT salvaje. Comparaciones con el patrón de pegilación con los demás mutantes dobles (Figuras 3.16 and 3.19) confirman las 2 mobilidades de la banda de 3 mPEGs unidos, sugieren que, muy probablemente, C571-C666 es el último puente disulfuro en formarse (ver Discusión).

7.3.3 Oxidación de rBAT salvaje en ausencia de $b^{0,+}$AT

rBAT se degrada por la vía ERAD en ausencia de $b^{0,+}$AT[157]. El estudio sugería que es el hecho de no estar asociado con $b^{0,+}$AT lo que hace que rBAT sea reconocida por la maquinaria ERAD, pero otra posibilidad no excluyente es que rBAT sola no se encuentra plegada. Estudiamos esta posibilidad a través del análisis del patrón de pegilación de rBAT en presencia y ausencia de $b^{0,+}$AT.

Si rBAT expresada en ausencia de $b^{0,+}$AT se encontrara completamente oxidada presentaría una banda correspondiente a 2 mPEGs unidos correspondientes a las cisteínas C18 y C114 (ya que ahora no estaría formando el puente disulfuro con $b^{0,+}$AT). Cuando rBAT se expresa en ausencia de $b^{0,+}$AT presenta bandas que corresponden entre 1 y 4 mPEGs (Figura 3.20). Este patrón se mantuvo inalterado durante una caza de 3 h. Este resultado implica que aún siendo 2 de las cisteínas libres C18 y C114, almenos 1 puente disulfuro intramolecular no está presente en rBAT expresado en ausencia de $b^{0,+}$AT. Se realizó un experimento de pulso y caza con rBAT salvaje y el doble mutante C571S-C666S expresados con $b^{0,+}$AT (Figura 3.20). rBAT salvaje presenta principalmente bandas correspondientes a 1, 2 y 3 mPEGs unidos a tiempo 0, pero después de 3 h de caza rBAT se oxida post-traduccionalmente y aparece un aumento del tamaño de la banda correspondiente a 1 mPEG unido debido a la maduración del heterodímero. En cambio, el doble mutante C571S-C666S permanece invariable.

Por tant, cuando rBAT se expresa en ausencia de $b^{0,+}$AT permanece desplegada durante la caza con almenos 1 puente disulfuro intramolecular no formado. Se realizaron experimentos de pulso y caza en presencia del inhibidor de manosidasas del RE dMNJ para estudiar si dando más tiempo a rBAT antes de su degradación era capaz de plegarse correctamente. A pesar de bloquear la degradación de rBAT, el patrón de pegylación no cambio en ausencia de $b^{0,+}$AT (Figura 3.21). Esto sugiere que en ausencia de $b^{0,+}$AT rBATse encuentra intrínsicamente desplegado. Por tanto, rBAT permanece com un conjunto de distintas poblaciones redox y no es capaz de oxidar su ectodominio.

Como rBAT sola se mantiene desplegada y las proteínas desplegadas tienen tendencia a agregarse[5], quisimos ver si en estas condiciones rBAT se expresa priniciplamente como un monómero o como homodímeros unidos mediante puentes disulfuro o agregados. Comparamos muestras de rBAT sola pegiladas con otras tratadas con NEM en condiciones reductoras y no reductoras. Observamos que entre 2/3 y 3/4 de rBAT se encuentra en forma monomérica (Figura 3.22).

7.3.4 Plegamiento post-traduccional de rBAT en presencia de $b^{0,+}$AT

Con el fin de estudiar si las especies redox que se observan en rBAT sola son capaces de plegarse después de expresar $b^{0,+}$AT, se clonó $b^{0,+}$AT en el plásmido pTRE-Tight donde se puede expresar el gen de interés en un sistema Tet-off. No se pudieron sacar conclusiones de estos experimentos ya que se expresaban cantidades muy pequeñas de $b^{0,+}$AT. Llevamos a cabo otro intento llevando a cabo experimentos de pulso y caza con un pulso corto de 3 min seguido de tiempos de caza de 1 y 10 min. Inmediatamente después del pulso rBAT ya está unido a $b^{0,+}$AT (Figura 3.23 A) y el patrón de pegilación a 1 y 10 min de caza era el mismo que a 5 h de caza. El ensamblaje del heterodímero se da co-traduccionalmente ya que la unión con puente disulfuro con $b^{0,+}$AT es un evento muy rápido[157], lo que indica que muy probablemente una gran parte del plegamiento oxidativo ocurre co-traduccionalmente.

Algunas proteínas son capaces de completar su plegamiento oxidativo nativo de manera post-traduccional[54,61]. Analizamos si rBAT era también capaz de lograrlo en presencia de $b^{0,+}$AT (Figura 3.23 B). Se realizó un pulse en presencia de DTT que se retiró durante la caza. Después del pulso rBAT estaba completamente reducida (ver carril 5 en Figura 3.23 B) y no se encontraba unida a $b^{0,+}$AT (ver

carril 4 en Figura 3.23 B). Después de 1 h de caza rBAT está completamente oxidada y unida a $b^{0,+}$AT y presenta el mismo patrón de pegilación que en un pulso sin presencia de DTT. Ensayos con Endo H muestran que también es capaz de madurar normalmente. Por tanto, rBAT completamente reducido puede ser un intermediario del plegamiento *in vivo*.

7.3.5 Unión de mPEG de los mutantes de cisteína de rBAT en ausencia de $b^{0,+}$AT

Se obtuvieron 3 patrones distintos de pegilación: C18S y C114S muestran principalmente bandas correspondientes a 1, 2 y 3 mPEGs unidos. Los mutantes C571 a C685 presentaron el mismo patrón, similar al de rBAT salvaje pero con bandas correspondientes principalmente a 2 y 3 mPEGs unidos. Finalmente, los mutantes C242S y C273A muestran un patrón distinto con bandas mayoritarias correspondientes a 4 y 5 mPEGs, lo que indica que en estos mutantes sólo un puente disulfuro está presente. Este patrón confirma que el hecho de que una de las cisteínas del dominio B esté desapareada es perjudicial para el plegamiento de rBAT.

Experimentos similares en los dobles mutantes de cisteína indican que los dobles mutantes que contienen una cisteína del dominio B y otra del dominio C o de la cola C-terminal presentan un patrón distinto con hasta 5 y 6 mPEGs unidos. Estos resultados también muestran que cuando una cisteína del dominio B esta desapareada rBAT se encuentra más desplegado recalcando la importancia de este dominio en el plegamiento de rBAT.

7.3.6 Papel de los N-glicanos en la biogénesis de rBAT

Los N-glicanos ejercen un papel importante en el correcto plegamiento de las glicoproteínas[62,69,233,235]. Los N-glicanos presentes en proteínas pueden tener roles distintos en la biogénesis de una proteína, como facilitar el plegamiento[79], o dirigir glicoproteínas mal plegadas para su degradación[80,81].

Primero, determinamos qué lugares consenso de N-glicanos eran usados en rBAT. Los N-glicanos pueden unirse a la asparagina de los lugares consenso Asn-X(excepto Pro)-Thr/Ser. rBAT humano contiene 6 lugares consenso (Figura 3.26 A). Ninguno de ellos se encuentra completamente conservado en los ortólogos de rBAT (Figura 3.26 B). El pulso con marcaje radioactivo con rBAT muestra que rBAT contiene

5 N-glicanos: N261, N332, N495, N513 and N575 (Figura 3.27). Seguidamente, analizamos la biogénesis y funcionalidad de estos mutantes.

Se estudió la estabilidad y la maduración de los mutantes de N-glicanos de rBAT en presencia de $b^{0,+}$AT en células HeLa transfectadas transitoriamente. Las células fueron marcadas radioactivamente con [35S]Met/Cis durante 30 min y una caza de 5 h. Las muestras se inmunoprecipitaron con el anticuerpo anti-$b^{0,+}$AT. No se observaron diferencias significativas en la estabilidad de estos mutantes en presencia de $b^{0,+}$AT (Figura 3.30). Se analizó también la maduración de estos mutantes con análisis de Endo H a 5 h de caza. Todos los mutantes mostraron una maduración similar a la de rBAT salvaje (10-20 %) excepto el mutante S577A que a 5 h presenta ∼50 % de banda inmadura indicando un efecto sobre la salida del RE. El análisis de los mutantes N575D y N575Q confirma que el defecto de plegamiento se debe a la ausencia del N-glicano y no al cambio por alanina (Figura 3.31).

Seguidamente, se analizó la importancia de cada N-glicano en ausencia de todos los demás. Se generaron mutantes que contenían un N-glicano cada uno, mutantes Ng: N261, (Ng261); N332, (Ng332); N495, (Ng495); N513, (Ng513); N575, (Ng575). También se generó un mutante que no contenía ningún N-glicano. Se estudió su degradación, estabilidad maduración y funcionalidad.

Los análisis preliminares de degradación (Figura 3.32) a 5 h de caza indican que, en ausencia de $b^{0,+}$AT, el mutante Ng332 es el único que presenta una degradación similar a rBAT salvaje, lo que sugiere que este N-glicano podría ser suficiente para la degradación de rBAT expresado en ebsencia de $b^{0,+}$AT. La degradación del mutante Ng513 es similar a la del mutante deficiente en N-glicanos, lo que sugiere que este N-glicano no ejerce ningún papel en la degradación de rBAT.

Los análisis de estabilidad y maduración de estos mutantes en presencia de $b^{0,+}$AT (Figuras 3.33 y 3.34). Los resultados indican que los N-glicanos no tienen un papel importante en la estabilidad del heterodímero.

Los experimentos con Endo H muestran que el mutante Ng575 es el único que presenta una maduración similar a la de rBAT salvaje (Figura 3.34). Por tanto el N-glicano N575 es necesario y suficiente para obtener la tasa máxima de maduración del transportador. Por otra parte los ensayos de transporte con L-arginina

muestran que todos los mutantes, incluido el mutante deficiente en N-glicanos, presentan transporte. Por tanto, los N-glicanos no son esenciales ni para la biogénesis ni para la función del transportador.

7.3.7 Papel del N-glicano N575 y las cisteínas C673 y C685 en la sálida del RE del heterodímero

Los mutantes S577A, C673S y C685S presenta un defecto de maduración cualitativamente similar. En cambio, el doble mutante C673S-C685S muestra una estabilidad y maduración similar a rBAT salvaje (Figuras 3.14, 3.17 y 3.30). Quisimos estudiar si podría haber alguna interacción entre estos elementos en la maduración del heterodímero. Se generaron dobles y triples mutantes: S577A-C673S (N-C673S); S577A-C685S (N-C685S); S577A-C673S-C685S (N-C673S-C685S) así como un mutante que elimina la cola C-terminal de rBAT (Δ673-685). Se analizó la estabilidad y la maduración mediante análisis de pulso y caza.

El mutante N-C673S-C685S presenta un defecto similar al del mutante S577A. No hallamos evidencias de interacciones entre C673 y/o C685, y el N-glicano N575. Sin embargo, el mutante Δ673-685 era degradado y retenido en el RE. Dado que el mutante C673S-C685S madura de manera similar a rBAT salvaje, esto sugiere que los residuos de la cola C-terminal de rBAT (674-684) podrían tener un papel importante en la biogénesis del heterodímero. Decidimos estudiar esta cola C-terminal.

7.3.8 Papel de la cola C-terminal de rBAT en la biogénesis del transportador

Algunos residuos de la cola C-terminal de rBAT se encuentran muy conservados entre los ortólogos de rBAT (residuos Y674, I 680, L681 y Y682) (Figura 3.41). Se mutó cada residuo a alanina (*alanine scanning analysis*) y se estudió la estabilidad y la maduración de estos mutantes.

Los experimentos muestran que los mutantes Y674A, L681A y Y682A presentan más del 40 % de degradación a 5 h de caza; el resto de los mutantes mostraba entre 30 % y ninguna degradación (Figura 3.42). Los análisis de Endo H y estabilidad

dieron pie a la clasificación de los mutantes en 3 grupos distintos. Los mutantes del grupo 1 (S676A, V677A, I680A, T683A y S684A) presentan una maduración similar a la de rBAT salvaje, en este grupo solo el mutante S676A presenta casi un 40% de degradación . El grupo 2, compuesto por los mutantes S675A, L678A y N679A, presentan entre un 30 y 50 % de banda sensible a Endo H, similar al mutante S577A y su estabilidad es similar a la de rBAT salvaje estaba claramente reducida. El grupo 3, formado por los mutantes Y674A, L681A y Y682A, presentaban una casi nula maduración. Estos resultados. Estos resultados pueden explicar al menos en parte, los resultados obtenidos en el mutante Δ673-685 (Figuras 3.39 y 3.40).

7.3.9 Estudio de dobles mutantes de la cola C-terminal de rBAT

Se generaron dobles mutantes de los residuos del grupo 2, con el fin de estudiar posibles interacciones entre ellos. Se estudió la estabilidad, maduración y transporte de estos mutantes. Estos mutantes presentaron una importante reducción de la estabilidad en comparación con los mutantes simples y eran retenidos en el RE. Sugiriendo un efecto sinérgico sobre el plegamiento del heterodímero.

7.3.10 Mutantes de la cola C-terminal de rBAT en el *background* C673S-C685S

Como se ha explicado anteriormente el mutante C673S-C685S madura de manera similar a rBAT salvaje (Figuras 3.17 y 3.18). Se estudió si los residuos del grupo 2 y 3 de la cola C-terminal de rBAT interaccionaban con las cisteínas del puente disulfuro. Los estudios de estabilidad mostraron que estos dobles mutantes sufren una mayor degradación que los mutantes simples. Esta sinergia, especialmente en los residuos del grupo 2, sugiere que la presencia del puente disulfuro enmascara los efectos desestabilizadores de mutaciones en estos 3 residuos.

7.3.11 Mutantes del grupo 2 en el *background* S577A

Se estudió la estabilidad y maduración de los dobles mutantes del grupo 2 junto con el mutante de N-glicano S577A para analizar la posible interacción entre los dos elementos. Estos dobles mutantes presentan un efecto sinérgico en la estabilidad del heterodímero (Figura **??** A) y, parece que también, un efecto menor al de la aditividad sobre la maduración (Figura **??**). Esto sugiere que existe interacción

funcional y/o estructural entre estos dos residuos y el N-glicano N575. Probablemente, esta interacción es necesaria para el plegamiento correcto, y además podría ser importante para la formación de una señal conformacional de salida del RE del heterodímero localizado en el lumen del RE.

7.4 Discussión

El estudio de los mutantes de cisteína muestra el distinto papel que juega cada puente disulfuro en la biogénesis del transportador. Los mutantes de las cisteínas del dominio B así como el doble mutante de estas cisteínas son rápidamente degradados, indicando su efecto desestabilizador (Figuras 3.13 and 3.14). Además, como en los mutantes C242S y C273A, los dobles mutantes que combinan una cisteína del dominio B con cisteínas de C571 a C673 presentan formas más desplegadas de rBAT (Figuras 3.12 and 3.16), indicando que una cisteína del dominio B desapareada afecta a la formación de los demás puentes disulfuro. Esto resulta sorprendente ya que el dominio B y el C se encuentran en lados opuestos del TIM *barrel* central[145,264] (Figure 3.7) y por tanto muy alejados. Los resultados sugieren que si C242 y C273 estan desapareadas, el dominio B no está establemente plegado. Es probable que el puente disulfuro del dominio B se forme primero para evitar la interacción de estas cisteínas con las siguientes. El hecho de que sea el único que se oxida completamente en ausencia de los otros dos puentes disulfuro refuerza esta hipótesis (Figure 3.19).
La estabilización de los otros 2 puentes disulfuro podría darse post-traducccionalmente ya que durante la caza las bandas di y tri-pegiladas desaparecen para formar la banda correspondiente a 1 mPEG unido (Figura 3.20). Un estudio reciente describe como la subunidad pesada 4F2 estabiliza la subunidad ligera LAT2 a través de la interacción de una amplia región del ectodominio de 4F2 con cara externa de LAT2[267]. En nuestro caso parece que es la subunidad pesada la que estabiliza la subunidad ligera. $b^{0,+}$AT podría también con el ectodominio de rBAT manteniendo el dominio B alejado del dominio C evitando así la formación de puentes disulfuro entre los 2 dominios. La estabilización de estos puentes disulfuro puede ser inducida por $b^{0,+}$AT, el cual es necesario para el plegamiento de rBAT.

El análisis de los N-glicanos de rBAT muestra que ninguno de ellos es esencial para el transportador aunque son necesarios para una degradación eficiente (N-glicano 332) para la salida del RE (el N-glicano N575) que es necesario y suficiente para una maduración similar a la de rBAT salvaje; y para ser plenamente funcional, ya

que los mutantes presentan un transporte menor.

El mutante Δ673-685 es retenido en el RE y posteriormente degradado, lo que muestra la importancia de la cola C-terminal de rBAT en la biogénesis del transportador. El estudio de los mutantes simples así como los mutantes dobles de esta región muestran que la mutación de algunos residuos provoca la desestabilización del heterodímero y una elevada disminución de la maduración, lo que explica, almenos en parte el fenotipo observado en Δ673-685. También sugieren que el puente disulfuro C673-C685 no es esencial para la biogénesis, pero facilita la maduración del transportador mediante la estabilización de algunos residuos del loop 673-685. Algunos de estos residuos también interaccionan con el N-glicano S575. Es posible que estos elementos constituyan una señal luminal y conformacional de salida del RE del heterodímero. Esta señal podría ser reconocida inicialmente para después facilitar el papel de otra señal de salida, esta vez situada en el extremo C-terminal citosólico de $b^{0,+}AT$[159]

7.5 Conclusiones

I. En presencia de $b^{0,+}AT$, rBAT contiene 3 puentes disulfuro intramoleculares: C242-C273, C571-C666 y C673-C685. Pueden formarse individualmente en la ausencia de los otros dos.

II. Cuando se expresa en presencia de $b^{0,+}AT$, rBAT permance desplegada con al menos un puente disulfuro intramolecular no formado. Por tanto, $b^{0,+}AT$ es requerido para el plegamiento oxidativo del ectodominio de rBAT.

III. El primer puente disulfuro en formarse es, muy probablemente, C242-C273. Estos resultados sugieren que el puente disulfuro C571-C666 es el último en formarse establemente. Este paso puede ocurrir post-traduccionalmente después de la unión con $b^{0,+}AT$.

IV. La presencia de una cisteína desapareada en el dominio B causa un mal plegamiento en rBAT y evita la formación de al menos uno de los otros dos puentes disulfuro.

V. Los puentes disulfuro C242-C273 y C571-C666 son esenciales para la biogénesis y su ausencia causa la retención en el RE y la subsecuente degradación del heterodímero. El doble mutante C673-C685 se comporta como rBAT salvaje pero los mutantes de cisteína C673S y C685S presenta una menos estabilidad

y un defecto en la maduración del transportador.

VI. En presencia de $b^{0,+}$AT, rBAT es capaz de oxidar su ectodominio de manera post-traduccional y madurar.

VII. rBAT contiene 5 N-glicanos: N261, N332, N495, N513 y N575. No son esenciales ni para la salida del RE ni para la estabilidad o la funcionalidad del transportador. El N-glicano N332 puede ser suficiente para la degradación de rBAT solo.

VIII. El N-glicano N575 es necesario y suficiente para la máxima eficiencia del tráfico del RE a Golgi del transportador.

IX. La cola C-terminal de rBAT (673-685) juega un papel clave en la biogénesis y maduración del heterodímero.

X. Los resultados sugieren que el puente disulfuro C673-C685 ayuda a estabilizar la conformación de los residuos de la cola C-terminal (674-684).

XI. El N-glicano N575 podría interaccionar funcional o estructuralmente con algunos residuos de la cola C-terminal para formar una señal luminal en rBAT-$b^{0,+}$AT requerida para la salida del RE del transportador. La formación del puente disulfuro C571-C666 puede acoplar la última etapa del plegamiento oxidativo formando esta señal.

Appendix I

- M. Rius and J. Chillarón.
  "Carrier subunit of plasma membrane transporter is required for oxidative folding of its helper subunit", *The Journal of Biological Chemistry*, **2012**, 287, 18190.

All the results of this publication are contained within this thesis. M. Rius has performed all the experiments and contributed to their design and to the writing of the manuscript.

THE JOURNAL OF BIOLOGICAL CHEMISTRY VOL. 287, NO. 22, pp. 18190–18200, May 25, 2012

Carrier Subunit of Plasma Membrane Transporter Is Required for Oxidative Folding of Its Helper Subunit*[S]

Received for publication, November 9, 2011, and in revised form, April 5, 2012 Published, JBC Papers in Press, April 9, 2012, DOI 10.1074/jbc.M111.321943

Mònica Rius, and Josep Chillarón[1]

From the Department of Physiology and Immunology, Faculty of Biology, University of Barcelona, E-08028 Barcelona, Spain

Background: Misfolding of the rBAT subunit of a cystine transporter causes type I cystinuria.
Results: rBAT contains three native intramolecular disulfides (two essential) *in vivo* only when the carrier subunit $b^{0,+}$AT is present.
Conclusion: $b^{0,+}$AT controls both degradation and folding of rBAT.
Significance: Learning how subunit folding and assembly of membrane protein complexes is coordinated is essential to understand protein biogenesis *in vivo*.

We study the amino acid transport system $b^{0,+}$ as a model for folding, assembly, and early traffic of membrane protein complexes. System $b^{0,+}$ is made of two disulfide-linked membrane subunits: the carrier, $b^{0,+}$ amino acid transporter ($b^{0,+}$AT), a polytopic protein, and the helper, related to $b^{0,+}$ amino acid transporter (rBAT), a type II glycoprotein. rBAT ectodomain mutants display folding/trafficking defects that lead to type I cystinuria. Here we show that, in the presence of $b^{0,+}$AT, three disulfides were formed in the rBAT ectodomain. Disulfides Cys-242-Cys-273 and Cys-571-Cys-666 were essential for biogenesis. Cys-673-Cys-685 was dispensable, but the single mutants C673S, and C685S showed compromised stability and trafficking. Cys-242-Cys-273 likely was the first disulfide to form, and unpaired Cys-242 or Cys-273 disrupted oxidative folding. Strikingly, unassembled rBAT was found as an ensemble of different redox species, mainly monomeric. The ensemble did not change upon inhibition of rBAT degradation. Overall, these results indicated a $b^{0,+}$AT-dependent oxidative folding of the rBAT ectodomain, with the initial and probably cotranslational formation of Cys-242-Cys-273, followed by the oxidation of Cys-571-Cys-666 and Cys-673-Cys-685, that was completed posttranslationally.

Around 30% of ORFs in a genome are predicted to encode integral membrane proteins. Recently, the crystal structure of many membrane proteins has prompted detailed mechanistic hypothesis on the structure-function of several membrane protein families (1–3). In contrast, another central question in membrane protein biology, namely biogenesis (*e.g.* synthesis, membrane insertion, folding, oligomerization, and trafficking), still lags behind structure-function studies (4).

Despite many important contributions to the biogenesis field, there is increasing recognition of a need for more research in this area, both to use new and varied protein models and to develop better experimental methods (4–6). Many key results have been obtained with viral (7), monomeric (5, 8), and oligomeric proteins composed of identical or closely related subunits (9, 10). An underrepresented class is the hetero-oligomeric membrane proteins with subunits showing a wide range of different topologies and structures (11–13). These proteins provide a unique opportunity to analyze how the steps of biogenesis in each subunit are coordinated to attain the native functional complex.

The heteromeric amino acid transporters (HATs)[2] are composed of two disulfide-linked polypeptides. The heavy subunits are type II membrane glycoproteins and the light subunits are 12-transmembrane domain unglycosylated proteins. The heterodimer is the functionally relevant unit (14, 15). The physiological role of HATs is highlighted by their involvement in cancer, immune function, and several human inherited diseases such as cystinuria and lysinuric protein intolerance (16–18). Nine mammalian heteromeric amino acid transporter light subunits are known, and each one mediates a different amino acid transport activity (15). The structure of a prokaryotic homologue of the heteromeric amino acid transporter light subunits has been solved, and the transport mechanism is now under close experimental scrutiny (2, 19). The heteromeric amino acid transporter heavy subunit is a helper protein required for trafficking to the plasma membrane (14, 15). The two mammalian heteromeric amino acid transporter heavy subunits are 4F2hc and rBAT. The ectodomain of 4F2hc consists of a $(\beta/\alpha)_8$ TIM-barrel domain A and an antiparallel eight-stranded β-sheet domain C, similar to α-glucosidases, but 4F2hc shows no glucosidase activity, as predicted (20). A working model of the rBAT ectodomain has been reported (20). rBAT differs from 4F2hc in the presence of the α-glucosidase B-domain between Aβ2 and Aα3 of the TIM barrel and an ~30 residue C-terminal tail without any noticeable homology.

System $b^{0,+}$ is formed by rBAT and the heteromeric amino acid transporter light subunit $b^{0,+}$AT. It exchanges extracellu-

* This study was supported by Spanish Ministerio de Ciencia e Innovación Grants BFU2006-06788/BMC and BFU2009-07215/BMC (to J. C.).
[S] This article contains supplemental Figs. 1–3.
[1] To whom correspondence should be addressed: Department of Physiology and Immunology, Faculty of Biology, University of Barcelona, Av. Diagonal, 643, E-08028, Barcelona, Spain. Tel.: 34-934039385; Fax: 34-934110358; E-mail: jchillaron@ub.edu.

[2] The abbreviations used are: HAT, heteromeric amino acid transporter; rBAT, related to $b^{0,+}$ amino acid transporter; ER, endoplasmic reticulum; NEM, *N*-ethylmaleimide; DS, disulfide mutant; ERAD, endoplasmic reticulum-associated degradation; dMNJ, 1-deoxymannojirimycin.

lar cystine and dibasic amino acids for intracellular neutral amino acids at the apical membrane of the epithelial cells of the kidney and small intestine (21, 22). Each subunit depends on the other for traffic to the plasma membrane. Without $b^{0,+}$AT, rBAT is translocated into the endoplasmic reticulum (ER), *N*-glycosylated, and rapidly degraded, whereas without rBAT, $b^{0,+}$AT remains stable within the ER, most likely already folded (23–25). Mutations in either rBAT or $b^{0,+}$AT decrease functional system $b^{0,+}$ at the plasma membrane, leading to the formation of cystine stones in the kidney, the hallmark of cystinuria (OMIM 220100). Most mutations in $b^{0,+}$AT cause the partially dominant non-type I cystinuria phenotype, whereas most rBAT mutations cause the recessive type I cystinuria phenotype (26). We have shown that mutations in the rBAT ectodomain lead to folding/trafficking defects underlying type I cystinuria (27).

Here, we report insight into the biogenesis of system $b^{0,+}$, focusing on the folding of the helper subunit. The intramolecular disulfide connectivity of rBAT and the importance and diverse roles of these disulfides in the biogenesis of the heterodimer are uncovered. Finally, we show that, within the cell, oxidative folding of the helper subunit rBAT does not proceed in the absence of the catalytic subunit $b^{0,+}$AT.

EXPERIMENTAL PROCEDURES

Reagents and Antibodies—Reagents were purchased from Sigma unless otherwise indicated. Pro-mix L-[^{35}S] *in vitro* cell labeling mix (L-[^{35}S]methionine and L-[^{35}S]cysteine) was purchased from PerkinElmer Life Sciences. DMEM media without L-methionine and L-cystine and dialyzed FBS were from Invitrogen. Antibodies against the N termini of human $b^{0,+}$AT and rBAT are described elsewhere (22, 28).

cDNA Constructs—The vectors for mammalian cell expression of human rBAT and $b^{0,+}$AT were as described elsewhere (28). The human rBAT mutants were obtained by site-directed mutagenesis (QuikChange, Stratagene) of pCDNA3-rBAT using the following mutagenic oligonucleotides (only sense oligonucleotides are shown): C18S, 5′-GAT GAG TAT GAA GGG ATC CCA GAC AAA CAA CGG G-3′; C114S, 5′-GCC CTC TCT CCA AAG TCC CTA GAC TGG TGG CAG GAG GGG-3′; C242S, 5′-CTG GCA TGA CTC TAC CCA TGA AAA TGG C-3′; C273A, 5′-GGC ACT TTG ACG AAG TGC GAA ACC AAG CTT ATT TTC ATC AG-3′; C571S, 5′-CCT CAA CAG GGG CTG GTT TTC CCA TTT GAG GAA TGA CAG CC-3′; C666S, 5′-GCT TTC AGA GAT AGA TCC TTT GTT TCC AAT CGA GC-3′; C673S, 5′-CCA ATC GAG CAA GCT ATT CCA GTG TAC TGA ACA TAC TGT ATA CC-3′; and C685S, 5′-ATA CCT CGT CTT AGG CAC CTT-3′.

All mutations were confirmed by DNA sequencing using the BigDye Terminator v3.1 cycle sequencing kit (Applied Biosystems).

Cell Culture and Transfection—HeLa and Madin Darby canine kidney IIJ cells were grown in Dulbecco's modified Eagle's medium (Invitrogen) supplemented with 10% fetal calf serum (heat-inactivated), 100 units/ml penicillin (Invitrogen), and 0.1 mg/ml streptomycin (Invitrogen) at 37 °C in a humidified atmosphere containing 5% CO_2. Stably transfected Madin Darby canine kidney-derived cell lines were described elsewhere (25). Calcium phosphate transient transfection of HeLa cells was performed as described (28). The efficiency of transfection was above 70% in all experiments. For transient transfections, 10-cm diameter plates were incubated with a mixture of DNA containing 2 μg of pEGFP (green fluorescence protein, Clontech), 6 μg of pCDNA3-rBAT (wild-type or the different mutants), and 12 μg of pCDNA3-$b^{0,+}$AT as described (27, 28). These conditions allow most, if not all, of the expressed rBAT to bind to $b^{0,+}$AT (27). When rBAT or $b^{0,+}$AT were transfected alone, 12 or 6 μg of pCDNA3 was added, respectively.

Transport Measurements—Influx experiments of 40 μM L-[^{35}S]cystine (Perkin Elmer) were performed in transfected HeLa cells as described (28).

Endoglycosidase H Assay—The enzyme was obtained from New England Biolabs and used following the protocol of the manufacturer.

Pulse-chase and Immunoprecipitation Protocols—Cells were transfected at 40–50% confluence and seeded the next day in 3.5-cm diameter plates at 60–70% confluence. 36 h after transfection, the cells were incubated for 30 min in prewarmed L-methionine/L-cystine-free media containing 10% dialyzed FBS. Subsequently, cells were labeled with a mixture of [^{35}S]methionine/cysteine (200 μCi/ml) for 30 min (if not otherwise indicated). When indicated, 5 mM DTT was included only during the labeling time. After removal of the labeling media, the cells were incubated with prewarmed media supplemented with 5 mM unlabeled L-methionine/L-cysteine. At this step, two different protocols were used: one for pegylation experiments (see last section) and one for the rest of the experiments. The last one is used in (27) and is detailed here. At the indicated chase times (or just after the pulse), cells were washed twice in cold PBS and once for 5 min in cold PBS containing 20 mM *N*-ethylmaleimide. Cells were collected and lysed on a rotating wheel in 0.2 ml of NET buffer (150 mM NaCl, 5 mM EDTA, 50 mM Tris (pH 7.4), 0.5% IGEPAL CA-630) with the protease inhibitors aprotinin, leupeptin, phenylmethylsulfonyl fluoride, and pepstatin, and with 20 mM NEM. After 30 min at 4 °C, a postnuclear supernatant was obtained by 10-min centrifugation at 10,000 × *g* at 4 °C. Where indicated, 1 mM 1-deoxymannojirimycin (dMNJ) (Calbiochem) was included from the beginning of the starving period to the end of the chase.

Immunoprecipitations were performed from equivalent amounts of radioactivity incorporated into proteins by adding an equal volume of immunoabsorbent buffer (200 mM H_3BO_3, 50 mM $Na_2B_4O_7$, 150 mM NaCl, 1% IGEPAL CA-630, and 0.1% ovalbumin (pH 8.3)) with the same protease inhibitors as the lysis buffer, and polyclonal antibodies to rBAT or $b^{0,+}$AT, in combination with protein A-Sepharose. Precipitates were washed four times in borate-NaCl buffer (0.5% IGEPAL CA-630, 0.3 M NaCl, 25 mM $Na_2B_4O_7$ and 0.1 M H_3BO_4, pH 8.3) and twice in 40 mM HEPES (pH 8). Samples were run on SDS-PAGE under reducing (100 mM DTT) conditions. Gels were stained with Coomassie Brilliant Blue to control for precipitating antibodies, dried, and placed on an intensifying screen for quantification with a Phosphoimager Typhoon 8600 (Molecular Dynamics).

Data Analysis—The relative intensities of the labeled bands were determined using phosphorimaging as follows: each band

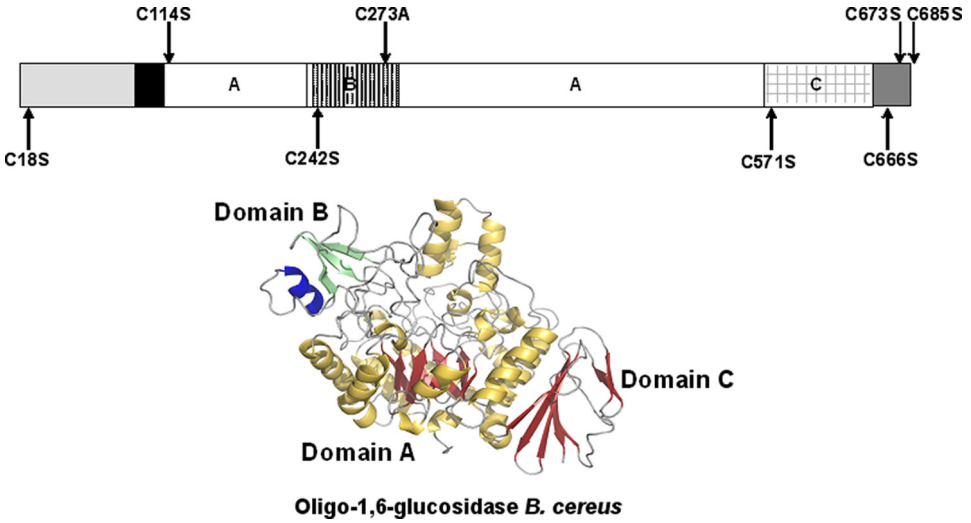

FIGURE 1. **Cysteine residues in human rBAT.** A scheme of human rBAT with the cysteine positions and the corresponding mutations is drawn to scale (*top panel*). *A*, *B*, and *C*, extracellular TIM barrel domain A, domain B, and domain C, respectively. The N-terminal cytoplasmic segment is *pale gray*, the transmembrane domain is *black*, and the C-terminal tail is *dark gray*. The crystal structure of oligo-1,6-glucosidase from *Bacillus cereus* (PDB code 1UOK) (47) is shown to observe the opposite position of domain B relative to domain C.

was outlined by a rectangle (as tightly fitting to the band as possible), and a rectangle of identical size was drawn in the closest area without any band in the lane. The relative positions of band and background rectangles were maintained within the experiment and in similar experiments. The value for each rectangle was calculated using the local average background correction of the ImageQuant software. The final value of the band was the difference between the value of the rectangle band and the value of the rectangle background. The data were plotted as intensity values of the fraction remaining obtained by dividing by the value at time zero.

$mPEG_{5000}$-maleimide (mPEG) modification—Several pegylation conditions (*e.g.* varying time and temperature of incubation and mPEG concentration) were assayed for wild-type rBAT in the absence or presence of $b^{0,+}AT$. The chosen conditions allowed for maximal pegylation. Additionally, lysis of the cells in trichloroacetic acid immediately after scraping and prior to mPEG modification did not result in significantly different rBAT pegylation.

Pulse and chase were performed as stated above. At the indicated times, cells were washed three times in cold PBS, scraped, and collected for 5 min at 3000 × *g* at 4 °C. The cell pellet was frozen at −20 °C for at least 1 h. The frozen pellet was lysed in 100 μl of TSD buffer (50 mM Tris HCl (pH 7.5), 1% SDS) (29) with 4 mM mPEG (NOF Corp., Japan) or 20 mM NEM, incubated for 30 min at 30 °C, and centrifuged for 5 min at 17,000 × *g* at room temperature. For immunoprecipitations, one-third of the supernatant together with 12 volumes of TNN buffer (50 mM Tris HCl 7.5, 250 mM NaCl, 5 mM EDTA, 0.5% IGEPAL CA-630) (29) with the protease inhibitors aprotinin, leupeptin, phenylmethylsulfonyl fluoride, and pepstatin, was incubated overnight at 4 °C with polyclonal antibodies to rBAT or $b^{0,+}AT$ in combination with protein A-Sepharose. Precipitates were washed three times in TNN buffer. Samples were run on SDS-PAGE under reducing (25 mM DTT) or non-reducing conditions. Gels were stained with Coomassie Brilliant Blue to control for precipitating antibodies, dried, and placed on an intensifying screen for quantification with a Phosphoimager Typhoon 8600 (Molecular Dynamics).

RESULTS

Our aim was to study early biogenesis of the rBAT-$b^{0,+}AT$ heterodimer. We used transiently transfected HeLa cells, a valid model for the functional expression of system $b^{0,+}$ (25, 27). Protein folding *in vivo* can be monitored by following the oxidation of disulfide bonds (7, 30). Human rBAT has eight cysteines (Fig. 1). Cys-18 is cytosolic. Cys-114 to Cys-685 are extracellular. Cys-114 is disulfide-linked with human $b^{0,+}AT$ (31, 32), Cys-242 and Cys-273 are localized to domain B, Cys-571 is in domain C, and Cys-666 to Cys-685 are in the C-terminal tail (20). Cys-685 is the C-terminal residue. Cys-114 to Cys-685 are conserved in all vertebrate orthologues. Cys-242 and Cys-273 are not conserved in the two annotated urochordate rBAT orthologues.

Disulfide Connectivity of rBAT in the Presence of $b^{0,+}AT$—In the proposed structural model of the rBAT ectodomain, Cys-242 and Cys-273 are at a distance compatible with a disulfide (20), but the intramolecular disulfide connectivity of rBAT is unknown. We used mass tagging under denaturing conditions with the cysteine-specific pegylation reagent $mPEG_{5000}$-maleimide (mPEG; M_r, 5 kDa) (9, 33) to count the number of reduced cysteines in rBAT. Each mPEG attached should produce an increase in the rBAT molecular mass, easily detectable in SDS-PAGE, although not completely predictable because SDS does not bind mPEG.

First, we made sure that the eight cysteines were accessible to mPEG. rBAT was synthesized in HeLa cells in the presence of [^{35}S]Met/Cys and the reducing agent DTT (supplemental Fig. 1, *lanes 1–9*). In these conditions, rBAT (which remains core-glycosylated because of its presence in the ER (27)) is reduced because of the more reducing conditions in the ER lumen (7, 30). The cells were lysed in denaturing solution containing mPEG without or with increasing concentrations of the alkylating agent NEM (M_r, 0.125 kDa). rBAT was immunoprecipitated

with a specific antibody against the N terminus (27), and the precipitates ran in reducing SDS-PAGE. As expected, an eight-step ladder was detected for wild-type rBAT (supplemental Fig. 1, *lanes 2–9*), confirming that under these experimental conditions all rBAT cysteines are accessible to mPEG.

To analyze the disulfide connectivity of rBAT, single Cys/Ser rBAT mutants (C18S to C242S, and C571S to C685S) were constructed. Cys-273 was changed to Ala (C273A) because mutation to Ser generated a new and used *N*-glycosylation acceptor site (data not shown). All cysteine mutants in this study did associate via a disulfide link with $b^{0,+}AT$ (data not shown and Fig. 2), with the expected exception of C114S. The mutants and the wild type, together with $b^{0,+}AT$, were expressed in HeLa cells, labeled with [^{35}S]Met/Cys, pegylated under denaturing conditions, and immunoprecipitated with a specific antibody against $b^{0,+}AT$ or, for the C114S mutant, against rBAT. As a control, parallel samples were alkylated with NEM. The precipitates were run in reducing SDS-PAGE, and the pegylation pattern was examined. We assumed that cysteines in wild-type rBAT assembled with $b^{0,+}AT$ were oxidized in the form of inter- (with $b^{0,+}AT$) or intramolecular disulfides. As a starting point, our null hypothesis was that the rBAT ectodomain was fully oxidized in the presence of $b^{0,+}AT$ and that single cysteine mutants of intramolecular disulfides disturbed only the oxidation of its partner cysteine residue. As Cys-18 is cytosolic and Cys-114 is disulfide-linked with $b^{0,+}AT$, we expected only one mPEG bound to wild-type rBAT. Single mutants should be modified with two mPEGs (to Cys-18 and to the now unpaired cysteine), with the exceptions of C18S (expected to be unmodified) and C114S (expected to be like the wild type). The results were partially consistent with the initial hypothesis (Fig. 2*A*). Mostly, there was no mPEG attached on C18S, one mPEG on the wild type and C114S, and two mPEGs on C571S to C685S. In contrast, the major C242S and C273A bands had three and four mPEGs attached (Fig. 2*A*, *lanes 4–5*), with similar pegylation in both mutants. The simplest interpretation of the data is as follows: 1) if present, Cys-18 is reduced and pegylated; 2) the ectodomain of the wild type, C18S, and C114S rBAT contains three intramolecular disulfide bonds; 3) Cys-571 to Cys-685 form two disulfides among them and, when one of these cysteines is unpaired, this does not appear to affect the other disulfides; and 4) Cys-242 and Cys-273 are disulfide-linked, and unpairing of any of them precludes formation of at least one of the other two disulfides, *e.g.* the pegylated cysteines in C242S band 3 might be Cys-18, Cys-273, and any Cys from Cys-571 to Cys-685. The proposed structural model of rBAT (20) and the fact that Cys-242 and Cys-273 are the only cysteines not absolutely conserved in the ectodomain also support the Cys-242-Cys-273 disulfide.

Next, we performed pegylation experiments with double cysteine rBAT mutants (Fig. 2*B*). C242S-C571S and C242S-C666S (and C242S-C673S, not shown) showed a major band with four attached mPEGs (Fig. 2*B*, *second gel*, *lanes 6–7*). As Cys-18 is pegylated and Cys-114 is linked to $b^{0,+}AT$, the remaining three pegylated cysteines indicated that there were no intramolecular disulfides in these mutants. Strikingly, the more abundant species in C242S-C273A had only one mPEG attached, as in wild-type rBAT. This indicated that it was not the absence of the

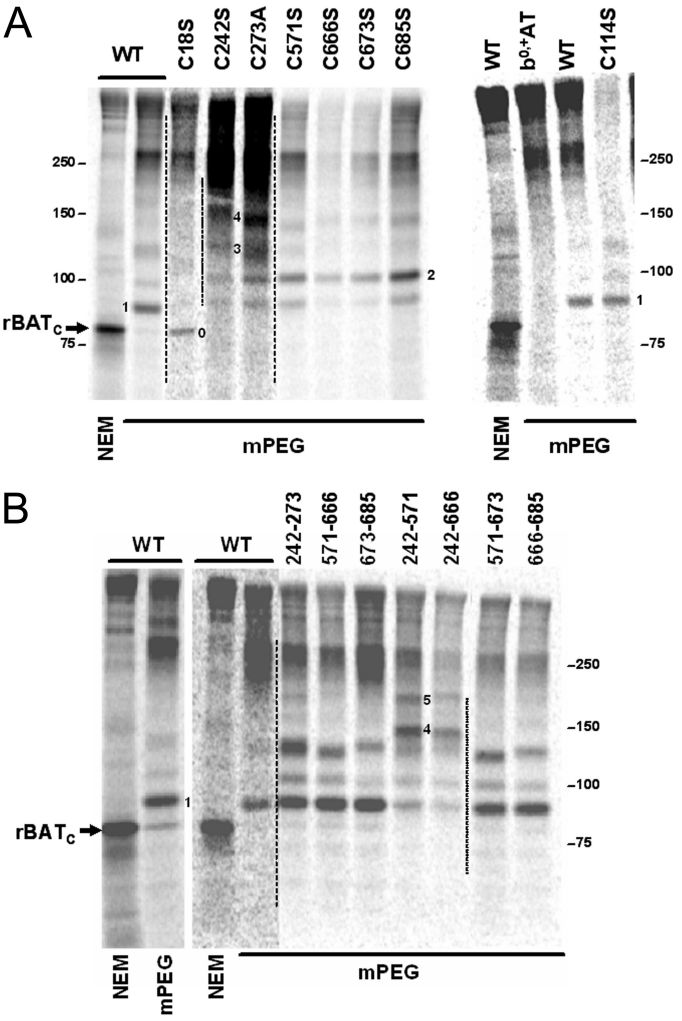

FIGURE 2. **Pegylation of cysteine rBAT mutants.** HeLa cells were transfected with WT or mutant (CXS/A) rBAT together with $b^{0,+}AT$ or $b^{0,+}AT$ alone. After 36 h the cells were labeled, pelleted immediately, and lysed in denaturing solution with either 4 mM mPEG or 20 mM NEM (for clarity, only WT with NEM is shown. The results for the mutants were the same). After incubation for 30 min at 30 °C, the lysates were immunoprecipitated with the anti-$b^{0,+}AT$ antibody, and the precipitates were run under reducing conditions. C114S was immunoprecipitated with the anti-rBAT antibody. Numbers *0* to *5* highlight the more intense rBAT bands detected in each lane. *rBAT$_C$*, core-glycosylated rBAT (after the pulse, only this rBAT form is detected (27)). *A*, analysis of single mutants. *Dashed lines* indicate that the Gray/Color Adjust tool of the View mode of the ImageQuant software (see "Experimental Procedures") was used to linearly increase the intensity of *lanes 3* to *5*. Irrelevant lanes were removed between *lanes 3* and *4* (*dotted line*). At least three independent experiments were performed with wild-type rBAT, the rBAT mutants, and $b^{0,+}AT$ alone. *B*, analysis of double mutants. The first gel (two lanes), from a different experiment, is shown to more clearly see the wild-type pegylation. This is also observed in the second gel. However, here the intensity of wild type *lanes 1* and *2* was linearly increased with ImageQuant (*dashed line*) as in *A*. Irrelevant lanes were removed between *lanes 7* and *8* of the second gel (*dotted line*). Numbers *4* and *5* highlight bands in C242S-C571S and C242S-C666S with four and five mPEGs attached. Number *1* marks the more intense rBAT band detected in all the other mPEG-treated samples. A representative experiment is shown from at least three for the wild type and each rBAT mutant.

Cys-242-Cys-273 disulfide *per se* but the presence of unpaired Cys-242 or Cys-273 that was responsible for the impaired oxidation of the ectodomain. C571S-C666S, C673S-C685S, C571S-C673S, and C666S-C685S also displayed a pattern with mainly one mPEG attached, like wild type rBAT (Fig. 2*B*). Assuming the formation of the B-domain Cys-242-Cys-273 disulfide, this implied the presence of non-native disulfides

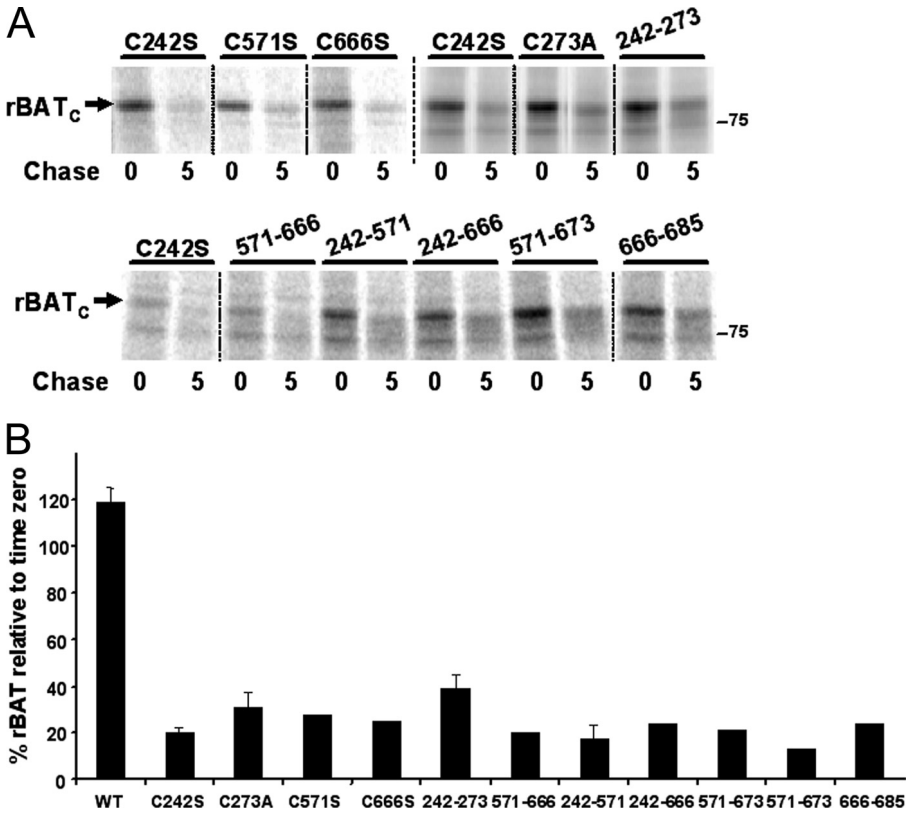

FIGURE 3. **Degradation of cysteine rBAT mutants.** *A*, HeLa cells transiently expressing $b^{0,+}$AT together with rBAT mutants were labeled and chased for 5 h. Equivalent amounts of radioactivity incorporated into protein were immunoprecipitated with the anti-$b^{0,+}$AT antibody. The precipitates were run under reducing conditions. The results of representative experiments are presented (top first gel, *lanes 1–6*; top second gel, *lanes 7–12*; bottom gel; *lanes 1–12*). *rBAT$_C$*, core-glycosylated rBAT. The *dashed line* separates the top two gels. The *dotted line* indicates that irrelevant lanes were removed at these positions. *B*, quantification of the rBAT signal coprecipitated with the anti-$b^{0,+}$AT antibody at time 5 h relative to time zero. The wild-type value, obtained from other experiments (see Fig. 4 and Ref. 27), is shown for comparison. Data are mean ± S.E. of at least three independent experiments for each rBAT species, unless no error bars are depicted. In these cases, the value plotted is the highest from two independent experiments for each mutant. For C242S-C673S and C666S-C673S, the values were 25 and 14%, respectively, in a single experiment.

between the C-domain and the terminal tail in these mutants. For instance, the band with one mPEG attached in C571S-C666S should contain the Cys-673-Cys-685 disulfide. Within the one-mPEG band in C571S-C673S, the Cys-666-Cys-685 disulfide should be present. It is highly unlikely that both Cys-673-Cys-685 and Cys-666-Cys-685 are present in the native population of rBAT molecules.

Role of Cysteine Residues in Transporter Biogenesis—We have reported the maturation kinetics and amino acid transport function of wild-type rBAT-$b^{0,+}$AT and shown that several rBAT ectodomain cystinuria mutants completely preclude maturation, leading to fast degradation in HeLa cells (27). We did similar pulse-chase experiments in the presence of $b^{0,+}$AT to dissect the role of cysteines and disulfides of rBAT in the biogenesis of the rBAT-$b^{0,+}$AT heterodimer. We monitored in-cell stability and maturation of N-glycosylation (as a measure of ER-to-Golgi traffic) of rBAT. The results also revealed Cys-571 to Cys-685 disulfide connectivity (see below). We observed a strong decrease in the rBAT signal coprecipitated with the anti-$b^{0,+}$AT antibody at 5 h of chase in C242S to C666S single mutants (Fig. 3). The mutants were retained in the ER, as no endoglycosidase H-resistant bands were detected (data not shown). The same happened with double mutants combining C242S to C666S with C242S to C685S, although C242S-C273A disposal was slower (Fig. 3). Therefore, the stability of all these mutants was highly compromised, similar to rBAT type I cystinuria mutants (27). In contrast, C18S, C114S, and wild-type rBAT were not degraded and matured similarly (Fig. 4). This is consistent with the non-conservation of Cys-18, and confirmed that the intermolecular disulfide between rBAT and $b^{0,+}$AT is not essential (31, 32).

The cysteine mutants within the C-terminal tail had a distinct effect on rBAT-$b^{0,+}$AT biogenesis (Fig. 4). C673S-C685S was the only mutant with wild type-like behavior in stability and maturation. In contrast, C673S and C685S had similar defects. Both were capable of maturation, but to a limited extent, compared with the wild type, and their stability was also compromised, although much less than rBAT mutants containing Cys-242 to Cys-666. These results, combined with the pegylation experiments showing oxidation of all the ectodomain cysteines and the presence of the Cys-242-Cys-273 disulfide, indicated that the three intramolecular disulfides of rBAT in the presence of $b^{0,+}$AT were Cys-242-Cys-273, Cys-571-Cys-666, and Cys-673-Cys-685. Absence of the first two disulfides dramatically reduced stability, leading to ER retention and degradation. The C-terminal disulfide Cys-673-Cys-685 was not required for biogenesis of the transporter, but the C673S and C685S single mutants displayed reduced stability and maturation. Unpaired Cys-673 or Cys-685 could impair a local fold-

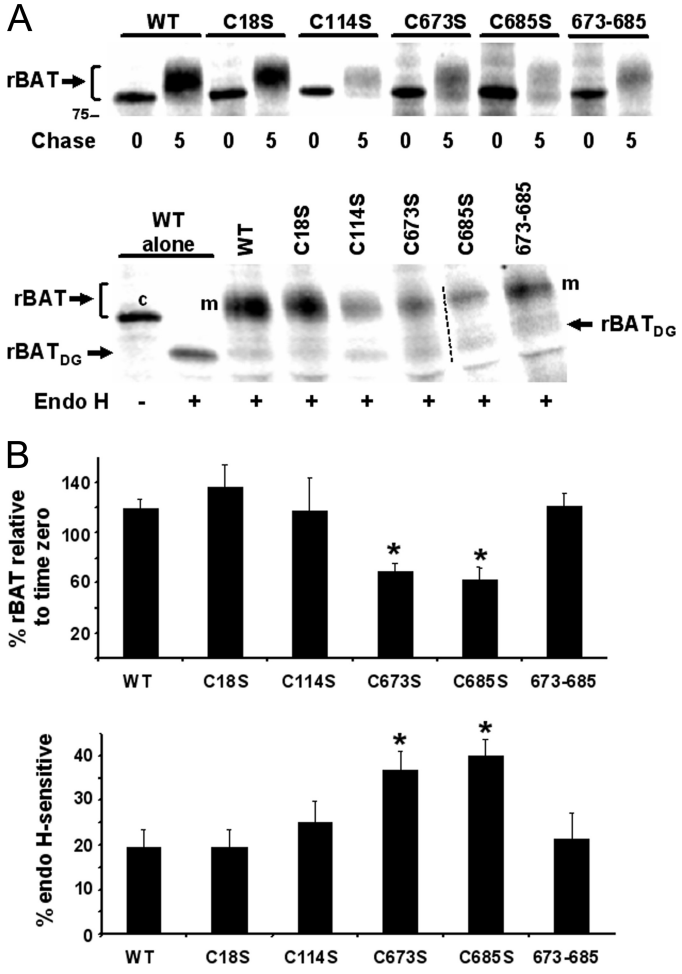

FIGURE 4. **Stability and maturation of cysteine rBAT mutants.** *A*, the procedures were as in Fig. 3*A*, except that the anti-rBAT antibody was used for C114S rBAT and for rBAT in the absence of $b^{0,+}$AT. At 5 h, chase parallel samples were treated with endoglycosidase H (*Endo H*). The result of a representative experiment is presented. The first two lanes of the bottom gel show the complete endoglycosidase H sensitivity of rBAT when expressed in the absence of $b^{0,+}$AT. The two gels were processed simultaneously. In the bottom gel, the intensity of the last two lanes was linearly increased with ImageQuant (*dashed line*). *rBAT*, core- and mature-glycosylated rBAT; *m*, mature glycosylated rBAT; *c*, core glycosylated rBAT; *rBAT$_{DG}$*, deglycosylated rBAT. *B*, *top panel*, the quantification of the rBAT signal coprecipitated with the anti-$b^{0,+}$AT antibody at time 5 h relative to time zero is shown. The core-glycosylated band and the mature glycosylated rBAT smears from the lanes without endoglycosidase H were quantified together. *Bottom*, deglycosylated and mature rBAT bands from the endoglycosidase H-treated 5 h chase lanes were quantified. Data were calculated as follows: % endo H-sensitive rBAT = 100 × [rBAT$_{DG}$/(rBAT$_{DG}$ + rBAT$_m$)]. Both in the top and bottom graphs, data are mean ± S.E. of at least five experiments for each rBAT species, with the exception of C18S ($n = 4$). Shown are significant differences compared with the wild type (unpaired Student's *t* test). *, $p < 0.005$ for the top graph; and *, $p < 0.05$ for the bottom graph.

ing element, which, however, was maintained when both cysteines were replaced by serine.

Next, we measured L-cystine transport in HeLa cells expressing wild type and cysteine rBAT mutants with $b^{0,+}$AT (Fig. 5). The data were comparable between groups because of the similar transfection efficiency (27). All mutants that did not mature were unstable (see Fig. 3) and failed to elicit significant cystine transport. C18S and C114S had very similar transport activity compared with the wild type. C673S-C685S, C673S, and C685S were functional. The double mutant induced higher transport activity than the single ones, as expected from the previous results (see Fig. 4). Overall, this functional assay supported our previous conclusions, which help to explain how the cystinuria mutations C666W, C673R, and C673W (34–36) may cause the disease.

Oxidation of Single Intramolecular rBAT Disulfides in the Presence of $b^{0,+}$AT—Wild-type rBAT and the double mutants containing C571S to C685S had mainly one mPEG attached in the presence of $b^{0,+}$AT. Minor bands with two and three mPEGs attached were also detected (Fig. 2, and see also below, Figs. 6, 7*A*, and 8). Three rBAT disulfide mutants (DS) were constructed containing just one of the natively paired cysteines (Cys-242-Cys-273, DS1; Cys-571-Cys-666, DS2; Cys-673-Cys-685, DS3), and also Cys-18 and Cys-114. The DS mutants expressed with $b^{0,+}$AT were retained in the ER, displayed a greatly compromised stability, and did not induce any transport activity (data not shown). Next, pegylation of these mutants was tested (Fig. 6). More than a third of DS2 and DS3 rBAT molecules did not form the intramolecular disulfide (bands with two and three mPEGs attached). In contrast, DS1 showed mainly the band with one mPEG (less than 5% in bands 2 and 3) (Fig. 6), suggesting that Cys-242-Cys-273, but not Cys-571-Cys-666 and Cys-673-Cys-685, is stably formed without the other two disulfides.

Oxidation of rBAT in the Absence of $b^{0,+}$AT—Misfolded and/or unassembled secretory and membrane proteins are degraded via the endoplasmic reticulum-associated degradation (ERAD) pathway. rBAT is degraded via ERAD in the absence of $b^{0,+}$AT (27). It is believed that this is due to its unassembled state and that it is $b^{0,+}$AT assembly *per se* that prevents rBAT degradation. However, it is not known whether unassembled rBAT is folded. To test this, we performed pegylation experiments in HeLa cells expressing rBAT in the presence or absence of $b^{0,+}$AT and $b^{0,+}$AT alone. If rBAT were to be fully oxidized in the absence of $b^{0,+}$AT, a major band with two mPEGs attached (to Cys-18 and Cys-114) was expected. In fact, pegylated rBAT bands corresponding to one to four mPEGs attached were found. In contrast, the major rBAT band had one mPEG attached when $b^{0,+}$AT was present (Fig. 7*A*, compare *lanes 2–4* with *lanes 6–8* and see also Figs. 2 and 6). Five and six mPEGs attached to unassembled rBAT were observed in some experiments but with much less intensity (data not shown). The major pegylated bands in unassembled rBAT had three and four mPEGs (Fig. 7*A*, *lanes 2–4*). This implied that, even if two of the pegylated cysteines were Cys-18 and Cys-114 (a reasonable guess), at least one intramolecular disulfide was not present in unassembled rBAT. Experiments performed in stable MDCK cells expressing much lower amounts of rBAT alone or rBAT together with $b^{0,+}$AT (25, 27) gave similar results (data not shown). Between 60 and 75% of the unassembled rBAT molecules did not form disulfide-linked homodimers or aggregates, as observed when NEM-treated or pegylated samples from HeLa cells expressing only rBAT were run in non-reducing SDS-PAGE (supplemental Fig. 2). The pegylation of unassembled rBAT did not change during the chase, and the signal decreased evenly in intensity because of degradation (Fig. 7*A*, *lanes 2–4*). For comparison, the fate of pegylated wild-type and C571S-C666S rBAT together with

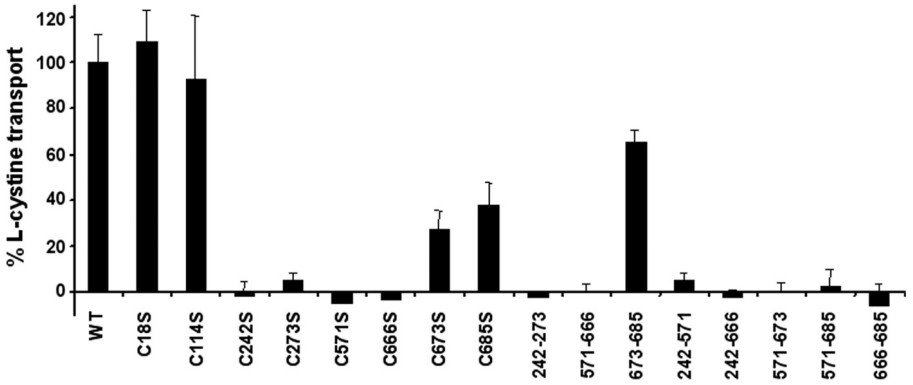

FIGURE 5. **Transport activity of cysteine rBAT mutants.** HeLa cells were transfected with $b^{0,+}AT$ and the wild type or rBAT mutants, and after 36 h cystine transport was measured for 2 min (see "Experimental Procedures"). Data were calculated as the difference between the uptake in each group minus the uptake in cells transfected with $b^{0,+}AT$ alone (which was not different from the transport in vector-transfected cells). The percentage of transport activity compared with wild-type rBAT of a representative experiment is shown. Data are the mean ± S.E. of four replicas per group. Three independent experiments gave similar results.

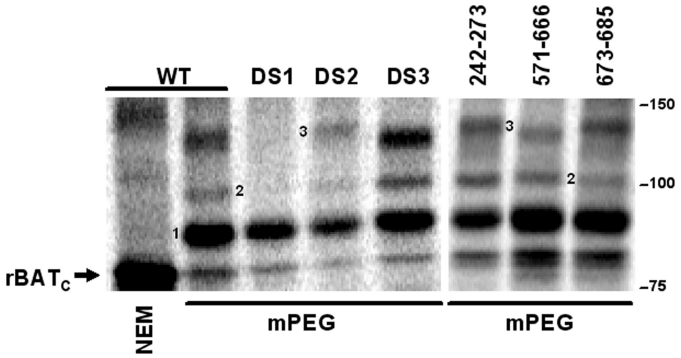

FIGURE 6. **Pegylation of rBAT disulfide mutants (DS) in the presence of $b^{0,+}AT$.** HeLa cells were transfected with WT or mutant rBAT together with $b^{0,+}AT$. After 36 h the cells were labeled, pelleted immediately, and lysed in denaturing solution with either 4 mM mPEG or 20 mM NEM. For clarity, only WT with NEM is shown. The results for the mutants were the same). After incubation for 30 min at 30 °C, the lysates were immunoprecipitated with the anti-$b^{0,+}AT$ antibody, and the precipitates were run under reducing conditions. *Lanes 1–5* and *lanes 6–8* belong to two different experiments. For each mutant, at least four experiments were done, and all gave similar results. Numbers *1* to *3* highlight the pegylated bands. *rBAT$_C$*, core-glycosylated rBAT; *DS1*, *DS2*, *DS3*, rBAT mutants with only Cys-242 and Cys-273, Cys-571 and Cys-666, Cys-673 and Cys-685, respectively, together with Cys-18 and Cys-114. In *lanes 6–8*, the double mutants have the indicated Cys-to-Ser mutations. Bands 1 to 3 were quantified. The relative amount of pegylated bands 2 plus 3 compared with the total amount of pegylated bands (bands 1, 2, and 3) was 4.5 ± 0.9% for DS1; 34.3 ± 3.4% for DS2; 39.1 ± 4% for DS3; 29.2 ± 1.6% for WT; 42.9 ± 3.5% for C242S-C273S; 26.2 ± 3.6% for C571S-C666S; and 27.5 ± 1.3% for C673S-C685S. The data are mean ± S.E. of at least four experiments for each rBAT species. There were significant differences when the value for DS1 was compared with any of the other six rBAT species (unpaired Student's *t* test, $p < 0.005$).

$b^{0,+}AT$ is shown. Pegylation of C571S-C666S remained similar during the chase, the signal decreasing evenly because of degradation (Fig. 7*A*, *lanes 9–11*). In contrast, the major band carrying one mPEG in wild-type rBAT linked to $b^{0,+}AT$ was maintained and matured because of traffic through the Golgi (Fig. 7*A*, *lanes 7–8*). The minor bands with no, two, and three mPEGs attached disappeared during the chase, most likely because of oxidation of the reduced cysteines to render the mature rBAT band with one mPEG (Fig. 7*A*, *lanes 6–8*).

We increased the time window for rBAT oxidation by inhibiting its degradation. ER-mannosidases are essential for ERAD (37). The ER-mannosidase inhibitor dMNJ inhibits rBAT degradation. This inhibition does not allow ER exit of unassembled rBAT (27). Inhibition of ERAD by dMNJ did not change the pegylation of unassembled rBAT in the absence of $b^{0,+}AT$ (Fig. 7*B*), suggesting that a longer time in the ER environment was not sufficient for folding of rBAT alone. We concluded that unassembled rBAT remained within the ER as an ensemble of different, mainly monomeric, redox species, unable to oxidize its ectodomain.

Posttranslational Oxidative Folding of rBAT in the Presence of $b^{0,+}AT$—We attempted to monitor the oxidative folding pathway of rBAT in the presence of $b^{0,+}AT$ performing short pulses (3 min, within the time range needed to synthesize full-length rBAT) followed by a short chase (supplemental Fig. 3). rBAT was disulfide-linked with $b^{0,+}AT$ immediately after the pulse. Moreover, rBAT was completely oxidated at 1 min of chase, and no intermediates were detected, suggesting that both assembly and ectodomain oxidation occurred either cotranslationally or shortly after translation. Then, we explored the related question of whether rBAT was able to oxidize its ectodomain and to associate with $b^{0,+}AT$ in a posttranslational manner. To this end, we did the pulse in the presence of DTT and the chase without the reducing agent (Fig. 8, *lanes 3–6*, *8*, and *10*). This strategy recapitulates (at least qualitatively) the oxidative folding of other proteins (30, 38). After the pulse, rBAT was detected as a totally reduced molecule (Fig. 8, see the 8-pegylated band in *lane 5*) not disulfide-linked with $b^{0,+}AT$ (Fig. 8, *lanes 3–5*). After 1 h of chase, rBAT was fully oxidized, as judged by the pegylation pattern, and linked with $b^{0,+}AT$ (Fig. 8; *lane 6*). A chase as short as 1 min also allowed detection of fully oxidized $b^{0,+}AT$-linked rBAT without the apparent presence of intermediates (data not shown). $b^{0,+}AT$-associated rBAT matured similar to rBAT synthesized in the absence of DTT (Fig. 8, compare *lanes 7–10*). Thus, reduced rBAT was able to posttranslationally associate with $b^{0,+}AT$, form three intramolecular disulfides, and mature efficiently.

DISCUSSION

We have examined 1) the number and identity of the intramolecular disulfides of rBAT in the presence of $b^{0,+}AT$; 2) the role of these disulfides and of the individual cysteine residues in stability and traffic of the transporter; and 3) whether the oxidative folding of rBAT differs between its unassembled and

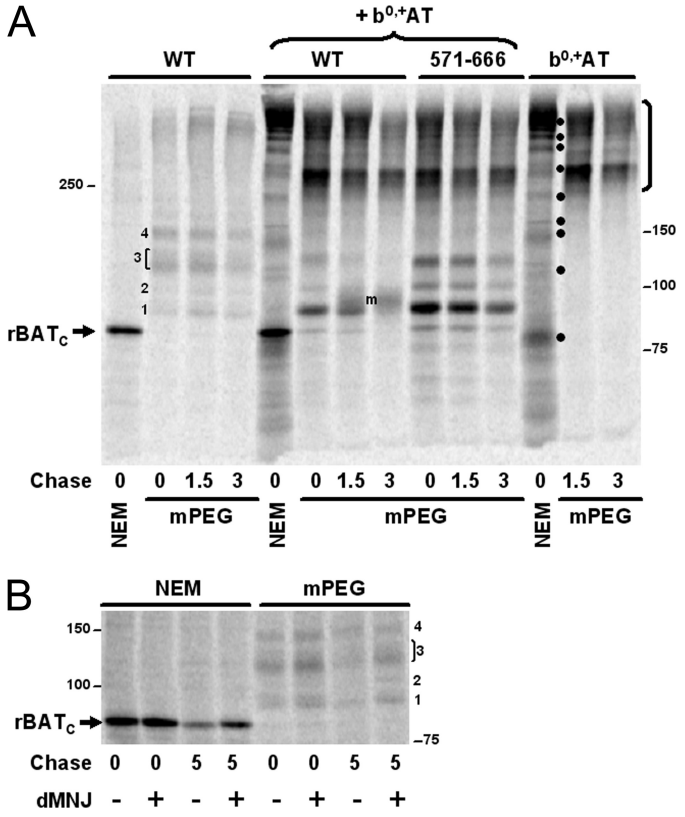

FIGURE 7. **Pegylation of rBAT in the absence of $b^{0,+}$AT.** *A*, HeLa cells were transfected with WT rBAT alone, $b^{0,+}$AT alone, or WT or the C571S-C666S mutant together with $b^{0,+}$AT. After 36 h the cells were labeled, chased for 3 h, and immediately pelleted and lysed in denaturing solution containing either 4 mM mPEG or 20 mM NEM. (The result of C571S-C666S with NEM was the same as for WT). After incubation for 30 min at 30 °C, the lysates were immunoprecipitated with the anti-$b^{0,+}$AT antibody or the anti-rBAT antibody (WT alone group), and the precipitates were run under reducing conditions. One representative experiment of three is shown. Numbers *1* to *4* correspond to the rBAT alone-pegylated bands. Observe that band 3 runs as a smear. The letter *m* indicates mature glycosylated rBAT band with 1 mPEG attached. ● highlight bands that are not rBAT-specific, as they appear both in rBAT together with $b^{0,+}$AT and in the $b^{0,+}$AT alone samples (compare *lanes 5* and *12*). The lower of these bands is a $b^{0,+}$AT dimer. The *bracket* encompasses bands common to *lanes 6–11* and *13-14* which, therefore, are not rBAT-specific. Bands marked with ● and *brackets* were also observed, as expected, in Fig. 2. $rBAT_C$, core-glycosylated rBAT. *B*, HeLa cells were transfected only with wild-type rBAT. After 36 h the cells were labeled, chased for 5 h, and immediately pelleted and lysed in denaturing solution containing either 4 mM mPEG or 20 mM NEM. After incubation for 30 min at 30 °C, equivalent amounts of radioactivity incorporated into protein were immunoprecipitated with the anti-rBAT antibody, and the precipitates were run under reducing conditions. $rBAT_C$ was observed. dMNJ (1 mM) was present throughout the pulse-chase. Numbers on the right side mark pegylated rBAT bands. One representative experiment of two is shown.

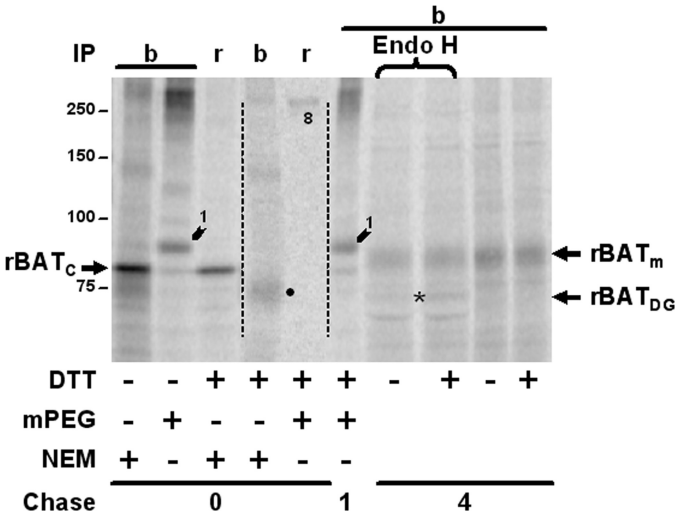

FIGURE 8. **Posttranslational oxidative folding of rBAT in the presence of $b^{0,+}$AT.** HeLa cells were transfected with wild-type rBAT and $b^{0,+}$AT. After 36 h the cells were labeled in the presence or absence of 5 mM DTT (*DTT* ±) and chased without DTT. Immediately after labeling or after 1 h of chase, the cells were pelleted and lysed in denaturing solution containing either 4 mM mPEG or 20 mM NEM (only the NEM samples at 0 h chase are shown), and incubated for 30 min at 30 °C. Cells chased for 4 h were processed as in Fig. 4*A*. They were treated (*lanes 7* and *8*) or not treated (*lanes 9* and *10*) with endoglycosidase H (*Endo H*), immunoprecipitated (*IP*) with the anti-$b^{0,+}$AT (*b*) or the anti-rBAT (*r*) antibody, and run under reducing conditions. A representative experiment of three is shown. The intensity of *lanes 4* and *5* was linearly increased with ImageQuant (*dashed line*). Numbers *1* and *8* mark the corresponding pegylated bands. Number *8* represents reduced and pegylated wild-type rBAT. ● highlights dimeric $b^{0,+}$AT as in Fig. 7*A*. The *asterisk* marks $rBAT_{DG}$ (deglycosylated rBAT). $rBAT_m$, mature glycosylated rBAT; $rBAT_C$, core-glycosylated rBAT.

assembled states. We used cysteine pegylation to tag reduced cysteines in rBAT and pulse-chase and functional studies to analyze stability and trafficking.

The ectodomain of rBAT has three consecutive disulfide bonds. Cys-242-Cys-273 is in the B-domain, an ~90-residue-long globular insertion between the third β-strand (Aβ3) and the third α-helix (Aα3) of the TIM barrel A-domain. Modeling of domain B with the *Bacillus cereus* α-1,6-glucosidase as a template suggested the presence of this disulfide (20). Domain B is present in most α-amylases and forms the substrate-binding cleft together with the central domain A (39, 40). Some α-amylases have a disulfide in domain B, which might be important for enzyme stability (40). In this sense, the double mutant C242S-C273A and the single mutants C242S and C273A are rapidly degraded, indicating a destabilizing effect (Figs. 3 and 5). Pegylation of C242S-C273A and wild-type rBAT is similar, suggesting that C242S-C273A does not influence formation of the other two disulfides. However, the single mutants C242S and C273A (and combinations of C242S with C571S, C666S, and C673S) cause the prevalence of more reduced $b^{0,+}$AT-linked rBAT forms (Fig. 2, *A* and *B*). This is surprising because domains B and C are located at opposite sites of the central TIM barrel (20, 39), and the other two disulfides are Cys-571-Cys-666, joining the C-domain and the C-terminal tail, and Cys-673-Cys-685 in the C-terminal tail. The absence of the Cys-242-Cys-273 disulfide may cause misfolding of domain B but not misfolding of more C-terminal regions unless Cys-242 or Cys-273 are unpaired. Without its native partner, these cysteines may disturb formation of the C-terminal disulfides. The domain B disulfide may form first, preventing Cys-242 and Cys-273 from making contact with more C-terminal, as yet unfolded, regions.

The rBAT tail has no homology to known sequences. Cys-571-Cys-666 connects domain C with this tail. Cys-571 lies within the β1 strand of domain C (Cβ1). Cβ1, Cβ2, and Cβ3 may form the mainly hydrophobic contacts between the C and the A domains (Aα6 to Aα8) (20). Stabilization of the tail closer to domain C and the A-C interface by the Cys-571-Cys-666 disulfide seems to be essential for biogenesis because Cys-571 and Cys-666 single and double mutants are quickly degraded (Fig. 3). Cys-673-Cys-685 is not important *per se* for biogenesis (Figs. 4 and 5). Although it shows at least a 30% decrease in

transport activity, it is difficult to ascertain, using transient transfections, whether this is significant. Strikingly, the single mutants do show reduced stability, maturation, and function compared with wild-type and C673S-C685S rBAT, although they clearly differ from the much more dramatic effects of the other cysteine mutants analyzed (Figs. 3, 4, and 5). In the context of the stabilization role of the Cys-571-Cys-666 disulfide, the 11-residue loop within the Cys-673-Cys-685 disulfide could be important for a late folding event, perhaps related to the ER exit of the transporter (see the compromised maturation of the C673S and C685S transporters in Fig. 4). This loop might still be stable enough in the context of C673S-C685S but not in C673S and C685S. The importance of this loop is highlighted by the fact that deletion of Cys-673 to Cys-685 leads to fast degradation, no maturation and no induction of transport activity[3].

The results point to a possible oxidative folding pathway for rBAT-$b^{0,+}$AT. Given that Cys-114 is the first extracellular cysteine from rBAT, and that it is far away from the next one, Cys-242, it is likely that the intermolecular disulfide between rBAT and $b^{0,+}$AT forms first and cotranslationally. This is supported by the very fast detection of the disulfide-linked heterodimer (supplemental Fig. 3 and (27)). However, it is not needed for oxidation of the intramolecular disulfides because the C114S mutant and wild-type rBAT look alike in the analysis, and C114S does not decrease transport activity. Therefore, non-covalent interactions between rBAT and $b^{0,+}$AT suffice for a functional complex. The pegylation of C242S-C273A, C571S-C666S, and C673S-C685S is very similar (Fig. 2*B*), suggesting that any one of the three disulfides could form independently of the others. However, to avoid non-native contacts between unpaired Cys-242 or Cys-273 with more C-terminal cysteines, formation of Cys-242-Cys-273 may initiate the intramolecular oxidation pathway. This is strongly supported by the fact that Cys-242-Cys-273 is completely oxidized in the absence of the other two disulfides (Fig. 6). In contrast, pegylation of Cys-571-Cys-666 and Cys-673-Cys-685 in the absence of the other two intramolecular disulfides is very similar to wild-type rBAT and double cysteine mutants (Figs. 6, 2*B*, and 7*A*). These results suggest that, after the complete oxidation of Cys-242-Cys-273, the oxidation of Cys-571-Cys-666 and/or Cys-673-Cys-685 in wild-type rBAT is posttranslationally stabilized (see also Fig. 7*A*). Actually, pegylation of C571S-C673S and C666S-C685S is also similar to the *native* disulfide mutants C571S-C666S and C673S-C685S, indicating the presence of non-native disulfides in C571S-C673S and C666S-C685S, most likely between the corresponding unpaired cysteines (Fig. 2*B*). The presence of non-native disulfides within the folding on-pathway of some disulfide-rich proteins has been reported both *in vitro* and *in vivo* (38, 41, 42). Together, these data raises the possibility that $b^{0,+}$AT posttranslationally controls the connectivity of C-domain and tail cysteines, irreversibly shifting oxidative folding toward native disulfides Cys-571-Cys-666 and Cys-673-Cys-685. If so, assembly with $b^{0,+}$AT may stabilize the interactions of the rBAT tail with the A-C interdomain interface and the C domain.

[3] M. Rius and J. Chillarón, unpublished data.

Earlier studies showed that rBAT expressed alone (unassembled rBAT) is degraded *via* the ERAD pathway, and that heterodimerization blocks degradation (27). $b^{0,+}$AT could mask an exposed region in unassembled rBAT acting as a degradation determinant, similar to unassembled TCRα (43). An alternative and non-exclusive hypothesis is that unassembled rBAT is recognized as an unfolded polypeptide. Here we show that this is also a possibility because unassembled rBAT does not complete the oxidative folding of its ectodomain (Fig. 7*A*). The pegylation shifts from the more prominent three and four mPEG bands in unassembled rBAT to the more intense one mPEG band in $b^{0,+}$AT-associated rBAT. The pegylated bands 1 to 4 (and the minor ones 5 and 6) reflect the presence within the ER of several unassembled rBAT redox species, which could be in equilibrium. In fact, the major bands with three and four mPEGs attached indicate that at least one intramolecular disulfide is not present. It is tempting to speculate that the ensemble of different redox species in rBAT expressed alone represents the *in vivo* equivalent of the ensemble of redox intermediates detected in folding studies of small disulfide-rich proteins *in vitro* (42).

There is evidence for *in vivo* post-assembly folding of selected subunits in other heteromeric protein complexes (11, 12, 44, 45). More challenging is to analyze, for a given heteromeric complex A-B, what the role of one subunit is, *e.g.* A, in the folding of the other. Subunit B folding may be completely dependent on assembly with A. On the other hand, subunit A may just facilitate folding of subunit B (that could proceed in the absence of A with properly modified conditions *in vivo*). Actually, this question has recently been convincingly solved only for the Ig heavy chain C_H1 domain. C_H1 folding strictly depends on the association with the Ig light chain C_L domain (44). In an initial approach to the problem, we show that the redox state of rBAT in the absence of $b^{0,+}$AT does not change during the chase (Fig. 7*A*, *lanes 2–4*). More importantly, the same happened when rBAT degradation was delayed (Fig. 7*B*). This suggests that folding and degradation of unassembled rBAT are not competing events and that $b^{0,+}$AT assembly, besides providing more time for wild-type rBAT folding, may have a more active role in that process. Analogous to the C_L-dependent folding of C_H1 (44), assembly with $b^{0,+}$AT might be mandatory for oxidation of the rBAT ectodomain.

Recently, Sakamoto and coworkers (46) described an ER exit signal at the cytoplasmic C terminus of $b^{0,+}$AT, active only after association with rBAT. That study, together with this report and our previous one (27), permits the proposal of a working model on how biogenesis events in $b^{0,+}$AT and rBAT are coordinated to render an ER exit-competent native complex: 1) $b^{0,+}$AT folds within the ER and remains stable; 2) fast, probably cotranslational, assembly with unfolded rBAT prevents degradation of this subunit and promotes oxidative folding of its ectodomain (folding may also depend on the calnexin system (27)); and 3) the $b^{0,+}$AT ER exit signal is *activated*, facilitating traffic of the complex to the plasma membrane. Future studies should address the detailed description of the oxidative and non-oxidative folding pathways of this heteromeric transporter and how end stages of rBAT ectodomain folding may be coupled with activation of the ER exit signal within $b^{0,+}$AT.

Acknowledgments—We thank Robin Rycroft for editorial support. We also thank the laboratory of Prof. Manuel Palacín (Institute for Research in Biomedicine, Barcelona, Spain), and especially Dr. Marta Pineda, for materials and infrastructure support in the beginning of this project.

REFERENCES

1. Abramson, J., Smirnova, I., Kasho, V., Verner, G., Kaback, H. R., and Iwata, S. (2003) Structure and mechanism of the lactose permease of *Escherichia coli*. *Science* **301,** 610–615
2. Gao, X., Lu, F., Zhou, L., Dang, S., Sun, L., Li, X., Wang, J., and Shi, Y. (2009) Structure and mechanism of an amino acid antiporter. *Science* **324,** 1565–1568
3. Yamashita, A., Singh, S. K., Kawate, T., Jin, Y., and Gouaux, E. (2005) Crystal structure of a bacterial homologue of Na+/Cl-dependent neurotransmitter transporters. *Nature* **437,** 215–223
4. von Heijne, G. (2011) Introduction to theme "membrane protein folding and insertion." *Annu. Rev. Biochem.* **80,** 157–160
5. Khushoo, A., Yang, Z., Johnson, A. E., and Skach, W. R. (2011) Ligand-driven vectorial folding of ribosome-bound human CFTR NBD1. *Mol. Cell* **41,** 682–692
6. Shao, S., and Hegde, R. S. (2011) A flip turn for membrane protein insertion. *Cell* **146,** 13–15
7. Tatu, U., Braakman, I., and Helenius, A. (1993) Membrane glycoprotein folding, oligomerization and intracellular transport. Effects of dithiothreitol in living cells. *EMBO J.* **12,** 2151–2157
8. Wang, N., Daniels, R., and Hebert, D. N. (2005) The cotranslational maturation of the type I membrane glycoprotein tyrosinase. The heat shock protein 70 system hands off to the lectin-based chaperone system. *Mol. Biol. Cell* **16,** 3740–3752
9. Gajewski, C., Dagcan, A., Roux, B., and Deutsch, C. (2011) Biogenesis of the pore architecture of a voltage-gated potassium channel. *Proc. Natl. Acad. Sci. U.S.A.* **108,** 3240–3245
10. Wanamaker, C. P., and Green, W. N. (2007) Endoplasmic reticulum chaperones stabilize nicotinic receptor subunits and regulate receptor assembly. *J. Biol. Chem.* **282,** 31113–31123
11. Chapman, D. C., and Williams, D. B. (2010) ER quality control in the biogenesis of MHC class I molecules. *Semin. Cell Dev. Biol.* **21,** 512–519
12. Mitchell, W. B., Li, J., Murcia, M., Valentin, N., Newman, P. J., and Coller, B. S. (2007) Mapping early conformational changes in αIIb and β3 during biogenesis reveals a potential mechanism for αIIbβ3 adopting its bent conformation. *Blood* **109,** 3725–3732
13. Penn, A. C., Williams, S. R., and Greger, I. H. (2008) Gating motions underlie AMPA receptor secretion from the endoplasmic reticulum. *EMBO J.* **27,** 3056–3068
14. Palacín, M., and Kanai, Y. (2004) The ancillary proteins of HATs. SLC3 family of amino acid transporters. *Pflugers Arch.* **447,** 490–494
15. Verrey, F., Closs, E. I., Wagner, C. A., Palacin, M., Endou, H., and Kanai, Y. (2004) CATs and HATs. The SLC7 family of amino acid transporters. *Pflugers Arch.* **447,** 532–542
16. Bröer, S., and Palacín, M. (2011) The role of amino acid transporters in inherited and acquired diseases. *Biochem. J.* **436,** 193–211
17. D'Angelo, J. A., Dehlink, E., Platzer, B., Dwyer, P., Circu, M. L., Garay, J., Aw, T. Y., Fiebiger, E., and Dickinson, B. L. (2010) The cystine/glutamate antiporter regulates dendritic cell differentiation and antigen presentation. *J. Immunol.* **185,** 3217–3226
18. Ishimoto, T., Nagano, O., Yae, T., Tamada, M., Motohara, T., Oshima, H., Oshima, M., Ikeda, T., Asaba, R., Yagi, H., Masuko, T., Shimizu, T., Ishikawa, T., Kai, K., Takahashi, E., Imamura, Y., Baba, Y., Ohmura, M., Suematsu, M., Baba, H., and Saya, H. (2011) CD44 variant regulates redox status in cancer cells by stabilizing the xCT subunit of system xc(-) and thereby promotes tumor growth. *Cancer Cell* **19,** 387–400
19. Kowalczyk, L., Ratera, M., Paladino, A., Bartoccioni, P., Errasti-Murugarren, E., Valencia, E., Portella, G., Bial, S., Zorzano, A., Fita, I., Orozco, M., Carpena, X., Vázquez-Ibar, J. L., and Palacín, M. (2011) Molecular basis of substrate-induced permeation by an amino acid antiporter. *Proc. Natl. Acad. Sci. U.S.A.* **108,** 3935–3940
20. Fort, J., de la Ballina, L. R., Burghardt, H. E., Ferrer-Costa, C., Turnay, J., Ferrer-Orta, C., Usón, I., Zorzano, A., Fernández-Recio, J., Orozco, M., Lizarbe, M. A., Fita, I., and Palacín, M. (2007) The structure of human 4F2hc ectodomain provides a model for homodimerization and electrostatic interaction with plasma membrane. *J. Biol. Chem.* **282,** 31444–31452
21. Chillarón, J., Estévez, R., Mora, C., Wagner, C. A., Suessbrich, H., Lang, F., Gelpí, J. L., Testar, X., Busch, A. E., Zorzano, A., and Palacín, M. (1996) Obligatory amino acid exchange via systems bo,+-like and y+L-like. A tertiary active transport mechanism for renal reabsorption of cystine and dibasic amino acids. *J. Biol. Chem.* **271,** 17761–17770
22. Fernández, E., Carrascal, M., Rousaud, F., Abián, J., Zorzano, A., Palacín, M., and Chillarón, J. (2002) rBAT-b(0,+)AT heterodimer is the main apical reabsorption system for cystine in the kidney. *Am. J. Physiol. Renal Physiol.* **283,** F540–F548
23. Bauch, C., and Verrey, F. (2002) Apical heterodimeric cystine and cationic amino acid transporter expressed in MDCK cells. *Am. J. Physiol. Renal Physiol.* **283,** F181–F189
24. Pineda, M., Wagner, C. A., Bröer, A., Stehberger, P. A., Kaltenbach, S., Gelpí, J. L., Martín Del Río, R., Zorzano, A., Palacín, M., Lang, F., and Bröer, S. (2004) Cystinuria-specific rBAT(R365W) mutation reveals two translocation pathways in the amino acid transporter rBAT-b0,+AT. *Biochem. J.* **377,** 665–674
25. Reig, N., Chillarón, J., Bartoccioni, P., Fernández, E., Bendahan, A., Zorzano, A., Kanner, B., Palacín, M., and Bertran, J. (2002) The light subunit of system b(o,+) is fully functional in the absence of the heavy subunit. *EMBO J.* **21,** 4906–4914
26. Chillarón, J., Font-Llitjós, M., Fort, J., Zorzano, A., Goldfarb, D. S., Nunes, V., and Palacín, M. (2010) Pathophysiology and treatment of cystinuria. *Nat. Rev. Nephrol.* **6,** 424–434
27. Bartoccioni, P., Rius, M., Zorzano, A., Palacín, M., and Chillarón, J. (2008) Distinct classes of trafficking rBAT mutants cause the type I cystinuria phenotype. *Hum. Mol. Genet.* **17,** 1845–1854
28. Font, M. A., Feliubadaló, L., Estivill, X., Nunes, V., Golomb, E., Kreiss, Y., Pras, E., Bisceglia, L., d'Adamo, A. P., Zelante, L., Gasparini, P., Bassi, M. T., George, A. L., Jr., Manzoni, M., Riboni, M., Ballabio, A., Borsani, G., Reig, N., Fernández, E., Zorzano, A., Bertran, J., and Palacín, M., and International Cystinuria Consortium (2001) Functional analysis of mutations in SLC7A9, and genotype-phenotype correlation in non-Type I cystinuria. *Hum. Mol. Genet.* **10,** 305–316
29. Tansey, W. P. (2007) Denaturing protein immunoprecipitation from mammalian cells. *CSH Protoc.* doi:10.1101/pdb.prot4619
30. Braakman, I., Helenius, J., and Helenius, A. (1992) Manipulating disulfide bond formation and protein folding in the endoplasmic reticulum. *EMBO J.* **11,** 1717–1722
31. Chillarón, J., Roca, R., Valencia, A., Zorzano, A., and Palacín, M. (2001) Heteromeric amino acid transporters: biochemistry, genetics, and physiology. *Am. J. Physiol. Renal Physiol.* **281,** F995–1018
32. Deora, A. B., Ghosh, R. N., and Tate, S. S. (1998) Progressive C-terminal deletions of the renal cystine transporter, NBAT, reveal a novel bimodal pattern of functional expression. *J. Biol. Chem.* **273,** 32980–32987
33. Guo, Z. Y., Chang, C. C., Lu, X., Chen, J., Li, B. L., and Chang, T. Y. (2005) The disulfide linkage and the free sulfhydryl accessibility of acyl-coenzyme A:cholesterol acyltransferase 1 as studied by using mPEG5000-maleimide. *Biochemistry* **44,** 6537–6546
34. Bisceglia, L., Purroy, J., Jiménez-Vidal, M., d'Adamo, A. P., Rousaud, F., Beccia, E., Penza, R., Rizzoni, G., Gallucci, M., Palacín, M., Gasparini, P., Nunes, V., and Zelante, L. (2001) Cystinuria type I. Identification of eight new mutations in SLC3A1. *Kidney Int.* **59,** 1250–1256
35. Egoshi, K. I., Akakura, K., Kodama, T., and Ito, H. (2000) Identification of five novel SLC3A1 (rBAT) gene mutations in Japanese cystinuria. *Kidney Int.* **57,** 25–32
36. Font-Llitjós, M., Jiménez-Vidal, M., Bisceglia, L., Di Perna, M., de Sanctis, L., Rousaud, F., Zelante, L., Palacín, M., and Nunes, V. (2005) New insights into cystinuria: 40 new mutations, genotype-phenotype correlation, and digenic inheritance causing partial phenotype. *J. Med. Genet.* **42,** 58–68
37. Kanehara, K., Kawaguchi, S., and Ng, D. T. (2007) The EDEM and Yos9p

families of lectin-like ERAD factors. *Semin. Cell Dev. Biol.* **18,** 743–750
38. Jansens, A., van Duijn, E., and Braakman, I. (2002) Coordinated nonvectorial folding in a newly synthesized multidomain protein. *Science* **298,** 2401–2403
39. Fitter, J. (2005) Structural and dynamical features contributing to thermostability in α-amylases. *Cell Mol. Life Sci.* **62,** 1925–1937
40. Janecek, S., Svensson, B., and Henrissat, B. (1997) Domain evolution in the α-amylase family. *J. Mol. Evol.* **45,** 322–331
41. Arias-Moreno, X., Arolas, J. L., Aviles, F. X., Sancho, J., and Ventura, S. (2008) Scrambled isomers as key intermediates in the oxidative folding of ligand binding module 5 of the low density lipoprotein receptor. *J. Biol. Chem.* **283,** 13627–13637
42. Chang, J. Y. (2011) Diverse pathways of oxidative folding of disulfide proteins: underlying causes and folding models. *Biochemistry* **50,** 3414–3431
43. Bonifacino, J. S., Cosson, P., and Klausner, R. D. (1990) Colocalized transmembrane determinants for ER degradation and subunit assembly explain the intracellular fate of TCR chains. *Cell* **63,** 503–513
44. Feige, M. J., Groscurth, S., Marcinowski, M., Shimizu, Y., Kessler, H., Hendershot, L. M., and Buchner, J. (2009) An unfolded CH1 domain controls the assembly and secretion of IgG antibodies. *Mol. Cell* **34,** 569–579
45. van Lith, M., and Benham, A. M. (2006) The DMα and DMβ chain cooperate in the oxidation and folding of HLA-DM. *J. Immunol.* **177,** 5430–5439
46. Sakamoto, S., Chairoungdua, A., Nagamori, S., Wiriyasermkul, P., Promchan, K., Tanaka, H., Kimura, T., Ueda, T., Fujimura, M., Shigeta, Y., Naya, Y., Akakura, K., Ito, H., Endou, H., Ichikawa, T., and Kanai, Y. (2009) A novel role of the C-terminus of b 0,+ AT in the ER-Golgi trafficking of the rBAT-b 0,+ AT heterodimeric amino acid transporter. *Biochem. J.* **417,** 441–448
47. Watanabe, K., Hata, Y., Kizaki, H., Katsube, Y., and Suzuki, Y. (1997) The refined crystal structure of *Bacillus cereus* oligo-1,6-glucosidase at 2.0 A resolution. Structural characterization of proline-substitution sites for protein thermostabilization. *J. Mol. Biol.* **269,** 142–153

The carrier subunit of a plasma membrane transporter is required
for the oxidative folding of its helper subunit

Mònica Rius and Josep Chillarón

SUPPLEMENTAL DATA

Supplementary Figure 1. Accessibility of mPEG to rBAT cysteines. HeLa cells were transiently transfected with wild type (WT), C18S rBAT or with vector alone (-), and after 36 h the cells were labeled with [^{35}S]Met/Cys in the absence (lanes 10 to 12) or presence of 5 mM DTT (lanes 1 to 9; + DTT). The cells were pelleted immediately and lysed in denaturing solution with either 4 mM mPEG (lanes 1, 2, 10 and 12), 20 mM NEM (lane 11), or 4 mM PEG with increasing concentrations of NEM (lanes 3 to 9; black triangle). After incubation for 30 min at 30ºC, the lysates were immunoprecipitated with the anti-rBAT antibody and the precipitates run under reducing conditions. The numbers (0 to 8) point to the unpegylated (0) and pegylated (1 to 8) rBAT bands. mPEG alone produced a maximum increase in size greater than that expected for either wild type (8 Cys) or C18S (7 Cys) rBAT (compare lanes 1, 2 and 11). Lanes 10 and 11 show pegylation of rBAT synthesized in the absence of DTT, shown here only for comparison: for discussion see Fig. 7A and the text. Pegylated band 3 in rBAT alone (square bracket) is observed as a smear (see Fig. 7A, B and Supplementary Figure 2) or as a closely spaced doublet of bands (this Figure). The gel was run a longer time in order to observe a better separation of the ladder of bands. This is the reason why the unpegylated band was at the bottom of the gel. Cracking of a part of the bottom of the gel during drying caused the broken appearance of the unpegylated band (number 0) in lanes 8-11. A representative experiment from n = 5 is shown.

Supplementary Figure 2. Unassembled rBAT in reducing and non-reducing SDS-PAGE. HeLa cells were transfected with wild type rBAT or with vector (-) alone. After 36 h the cells were labeled and immediately pelleted and lysed in denaturing solution containing either 4 mM mPEG or 20 mM NEM (only the NEM WT sample is shown). After 30 min incubation at 30ºC, lysates were immunoprecipitated with the anti-rBAT antibody and the precipitates were run under reducing (r) or non-reducing (nr) conditions. One representative experiment from three is shown. The numbers (1 to 4) point to the rBAT-pegylated bands. The asterisk marks homodimeric rBAT. The disulfide-linked aggregated material observed in the mPEG-treated sample in non-reducing conditions is shown between brackets. $rBAT_C$: core-glycosylated rBAT.

Supplementary Figure 3. Rapid oxidation of rBAT in the presence of $b^{0,+}$AT. HeLa cells were transfected with wild type rBAT and $b^{0,+}$AT. After 36 h the cells were labeled with 400 μCi/ml [^{35}S]Met/Cys for 3 min and chased for the indicated times. The cells were immediately pelleted and lysed in denaturing solution containing either 4 mM mPEG or 20 mM NEM (only the NEM zero sample is shown). After 30 min incubation at 30ºC, lysates were immunoprecipitated with the anti-$b^{0,+}$AT antibody and the precipitates were run under reducing conditions. Number 1 marks the band with 1 mPEG attached. One representative experiment from two is shown.

Supplementary Figure 1

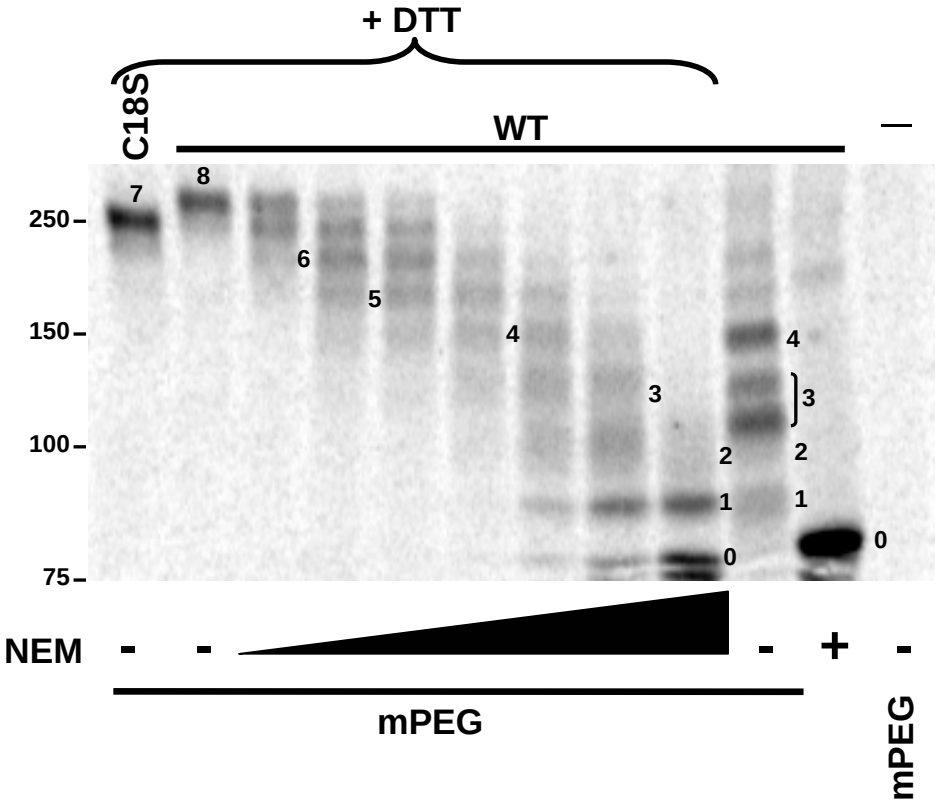

Supplementary Figure 2

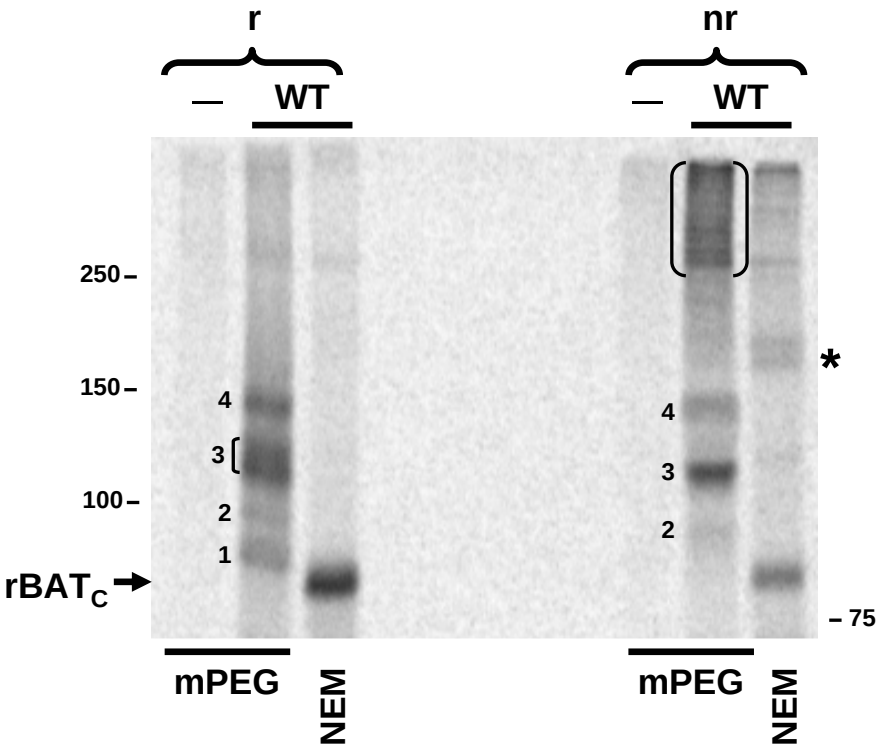

Supplementary Figure 3

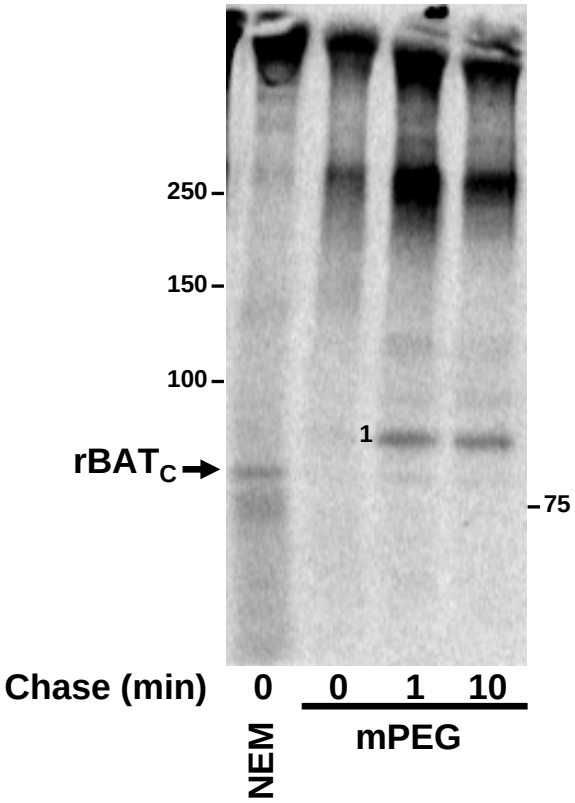

Appendix II

- P. Bartoccioni, M. Rius, A. Zorzano, M. Palacín and J. Chillarón. "Distinct classes of trafficking rBAT mutants cause the type I cystinuria phenotype", *Human Molecular Genetics*, **2008**, 17, 1845.

These results are part of the background of this thesis. M. Rius contributed by performing the experiments required by the referees of the journal (results labeled as "not shown" in the publication).

Human Molecular Genetics, 2008, Vol. 17, No. 12 ***1845–1854***
doi:10.1093/hmg/ddn080
Advance Access published on March 10, 2008

Distinct classes of trafficking rBAT mutants cause the type I cystinuria phenotype

Paola Bartoccioni[1,3,4], Mònica Rius[1,2,3], Antonio Zorzano[1,3], Manuel Palacín[1,3,4,†] and Josep Chillarón[1,2,3,†,*]

[1]Department of Biochemistry and Molecular Biology and, [2]Department of Animal Physiology, Faculty of Biology, University of Barcelona, Barcelona, Spain, [3]Institute for Research in Biomedicine, Barcelona Science Park, Barcelona, Spain and [4]CIBERER, Barcelona, Spain

Received December 20, 2007; Revised and Accepted March 9, 2008

Most mutations in the rBAT subunit of the heterodimeric cystine transporter rBAT-$b^{0,+}$AT cause type I cystinuria. Trafficking of the transporter requires the intracellular assembly of the two subunits. Without its partner, rBAT, but not $b^{0,+}$AT, is rapidly degraded. We analyzed the initial biogenesis of wild-type rBAT and type I cystinuria rBAT mutants. rBAT was degraded, at least in part, via the ERAD pathway. Assembly with $b^{0,+}$AT within the endoplasmic reticulum (ER) blocked rBAT degradation and could be independent of the calnexin chaperone system. This system was, however, necessary for post-assembly maturation of the heterodimer. Without $b^{0,+}$AT, wild-type and rBAT mutants were degraded with similar kinetics. In its presence, rBAT mutants showed strongly reduced (L89P) or no transport activity, failed to acquire complex N-glycosylation and to oligomerize, suggesting assembly and/or folding defects. Most of the transmembrane domain mutant L89P did not heterodimerize with $b^{0,+}$AT and was degraded. However, the few [L89P]rBAT-$b^{0,+}$AT heterodimers were stable, consistent with assembly, but not folding, defects. Mutants of the rBAT extracellular domain (T216M, R365W, M467K and M467T) efficiently assembled with $b^{0,+}$AT but were subsequently degraded. Together with earlier results, the data suggest a two-step biogenesis model, with the early assembly of the subunits followed by folding of the rBAT extracellular domain. Defects on either of these steps lead to the type I cystinuria phenotype.

INTRODUCTION

Cystinuria (OMIM 220100) is an autosomal recessive disease of renal reabsorption and intestinal absorption of cystine and dibasic amino acids. Cystine precipitates and forms calculi which ultimately produce renal insufficiency. Two cystinuria phenotypes are distinguished: type I, where the obligate heterozygotes have normal urinary excretion; and non-type I, where the obligate heterozygotes have moderate to high excess of urinary excretion of cystine and dibasic amino acids (1). All but one mutations in *SLC3A1*, encoding rBAT, cause type I cystinuria (2,3). Mutations in *SLC7A9*, encoding $b^{0,+}$AT, cause non-type I phenotype and also some type I cases (3). A gene dosage effect can explain non-type I cystinuria, since *SLC7A9*$^{+/-}$ mice express already the phenotype (4). It is not known why type I heterozygotes are silent.

rBAT is a type II membrane glycoprotein with a large glucosidase-like extracellular domain. $b^{0,+}$AT is a non-glycosylated, polytopic membrane protein. Their co-expression induces the transport system $b^{0,+}$-*like*, an obligatory exchanger that physiologically mediates the influx of cystine and dibasic amino acids and the efflux of neutral amino acids (5,6). Intracellular assembly of rBAT with $b^{0,+}$AT to form a disulfide-linked heterodimer is required for functional expression. When expressed alone, rBAT remains endoglycosidase H sensitive and is degraded, whereas $b^{0,+}$AT is stable (7,8). In contrast, $b^{0,+}$AT expressed alone is stable and can be recovered in a functional form from its intracellular location (7–9). The rBAT-$b^{0,+}$AT heterodimer oligomerizes into a stable heterotetramer expressed in the brush border membranes of the epithelial cells of the renal proximal

*To whom correspondence should be addressed at: Department of Animal Physiology, Faculty of Biology, University of Barcelona, Av. Diagonal, 645, E-08028 Barcelona, Spain. Tel: +34 934034700/9385; Fax: +34 934110358; Email: jchillaron@ub.edu
†M.P. and J.C. share last authorship.

tubule (10). System $b^{0,+}$-*like* is the main apical reabsorption system for cystine in kidney (6).

From the more than 60 rBAT mutations found in type I cystinuria patients, all are located in the extracellular domain, with the exception of the transmembrane mutants L89P and I105R (3,11). The few pathogenic rBAT mutants which have been examined showed reduced or absent transport activity (8,12,13). For the M467T and M467K mutations expressed in *Xenopus* oocytes, a trafficking defect was suggested, although function was recovered with higher protein expression, specially for the M467T mutant (12), raising doubts about the situation *in vivo*. Only the R365W mutation has been expressed in a mammalian cell system and its traffic was also impaired (8). However, the mechanism underlying these putative trafficking defects has not been addressed.

Here we report the basic features of the biogenesis of the rBAT-$b^{0,+}$AT heterodimer in mammalian cells. We show that, without $b^{0,+}$AT, rBAT is an ERAD (Endoplasmic Reticulum-Associated Degradation) substrate. Maturation of the rBAT-$b^{0,+}$AT heterodimer requires interaction with the calnexin chaperone system, suggesting that folding of rBAT is not completed before assembly. We compare the fate of wild-type and type I cystinuria rBAT mutants L89P, T216M, R365W, M467K and M467T, with or without wild-type $b^{0,+}$AT. T216M and M467T are the most common rBAT missense mutations, representing 6.4 and 26.4% of the alleles, respectively, of the International Cystinuria Consortium (3). The transmembrane domain L89P mutant is assembly-defective, but not folding-defective. The extracellular domain rBAT mutants are degraded after efficient assembly with $b^{0,+}$AT, indicating misfolding, but not assembly impairment.

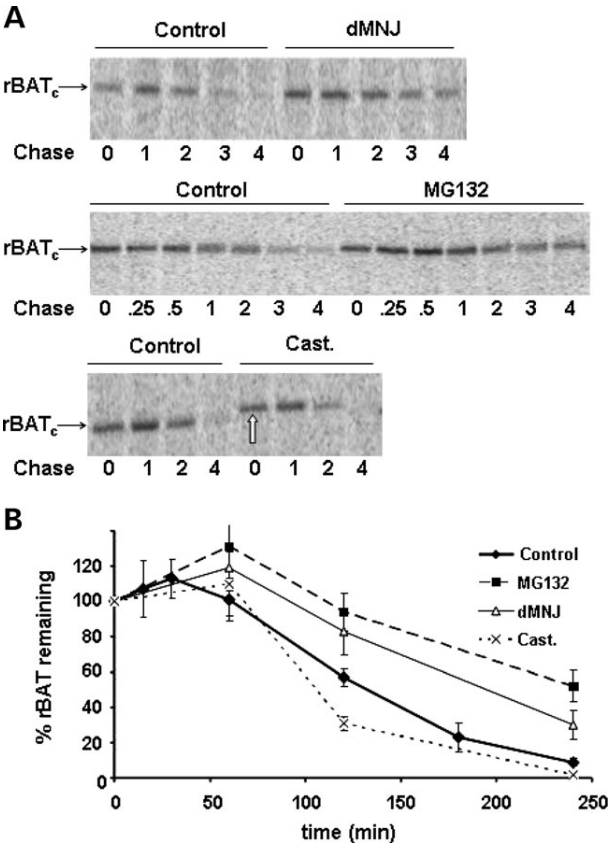

Figure 1. Fate of rBAT in the absence of $b^{0,+}$AT. (**A**) MDCK cells stably expressing human rBAT were labeled for 15 min with ^{35}S-Met/Cys and chased with excess Met/Cys up to 4 h. Equivalent amounts of radioactivity incorporated into protein were immunoprecipitated with the anti-rBAT antibody. The precipitates were run under reducing conditions. The core-glycosylated rBAT band (rBAT$_c$, ~90 kDa) is observed. dMNJ (1 mM) and castanospermine (Cast., 1 mM) were present during all the experiment, whereas MG132 (30 μM) was added immediately after the pulse. The white arrow points out the effect of castanospermine on rBAT mobility, due to the inhibition of glucose trimming. Representative experiments are shown. (**B**) The quantifications (mean ± SEM) of at least three independent experiments for each condition are shown. The value at each point of the chase was divided by the value at point zero, which was set to 100.

RESULTS

Our aim was to examine the early biogenesis of wild-type human rBAT, $b^{0,+}$AT and the rBAT-$b^{0,+}$AT heterodimer and compare it with type I cystinuria rBAT mutants. HeLa and MDCK cells are good models to study these proteins (7–10,14,15). We used previously documented stable MDCK cell lines expressing wild-type rBAT, $b^{0,+}$AT or both proteins together (9). Only cells co-expressing rBAT and $b^{0,+}$AT elicited cystine transport activity (9).

Unassembled rBAT is an ERAD substrate

We set-up pulse-chase experiments followed by immunoprecipitation with specific antibodies [(6,15) and see Materials and Methods] directed against N-terminal peptides of rBAT and $b^{0,+}$AT. In MDCK cells expressing only rBAT, this protein ran as a ~90 kDa endoglycosidase-H sensitive band (consistent with its intracellular localization) (7,8), which, after a *lag* phase of ~1 h, disappeared with a half-life of $\tau_{1/2} = 54 \pm 4$ min (Fig. 1). In contrast, in MDCK cells expressing only $b^{0,+}$AT, more than 60 and 30% of the pulse-labeled ~40 kDa band of $b^{0,+}$AT was detected after 8 and 24 h of chase, respectively (data not shown). We further characterized rBAT degradation. The proteasome inhibitors MG132 (Fig. 1) and lactacystin (not shown) delayed degradation, and so did the ER-mannosidase inhibitor dMNJ (Fig. 1). Therefore, rBAT disposal is mediated, at least in part, by the proteasome and ER-mannosidase-dependent ERAD pathway (16,17). The *lag* phase suggests that rBAT is initially retained in the calnexin chaperone system (16). Castanospermine inhibits glucose trimming mediated by the ER-glucosidases I and II (see the mobility shift of the rBAT band in Fig. 1), avoiding the generation of monoglucosylated N-glycans required for interaction with calnexin/calreticulin. The drug accelerated disposal (Fig. 1, see the chase point 2 h), suggesting that interaction with the calnexin chaperone system delays rBAT degradation (16). However, the *lag* phase was not reduced (Fig. 1, see the chase point 1 h). Neither the lysosomal degradation inhibitor leupeptin nor the secretory pathway inhibitor brefeldin A had any effect on rBAT disposal (not shown).

Assembly and maturation of rBAT and $b^{0,+}AT$

Pulse-chase experiments were performed in MDCK cells co-expressing rBAT and $b^{0,+}AT$. The proteins were immunoprecipitated with anti-rBAT and anti-$b^{0,+}AT$ antibodies separately and run under reducing and non-reducing conditions (Fig. 2A). Immediately after the pulse, rBAT ran as a ~90 kDa endoglycosidase H sensitive band under reducing conditions (7,8) (Fig. 2A, +DTT panel). This band co-precipitated with the anti-$b^{0,+}AT$ antibody, indicating that assembly took place within the ER and that it was a fast event (Fig. 2A; +DTT panel, anti-$b^{0,+}AT$ IP, time zero lane). Assembly was mediated by a disulfide bridge (Fig. 2A; −DTT panel; the ~135 kDa heterodimer band). Most of the labeled rBAT was co-precipitated with the anti-$b^{0,+}AT$ antibody (Fig. 2A; compare the rBAT bands with both immunoprecipitating antibodies in the +DTT panel). Consistently, rBAT was mainly found in the ~135 kDa band (Fig. 2A, −DTT panel, anti-rBAT IP, time zero lane). During the chase, virtually all rBAT matured to a ~96 kDa endoglycosidase H resistant band (7,8) in a precursor-product fashion (Fig. 2A, +DTT panel). The maturation half-time was ~1 h. Maturation of the heterodimer could also be observed (Fig. 2A, −DTT panel). In spite of the similar amounts of rBAT detected with anti-rBAT and anti-$b^{0,+}AT$ antibodies, a stronger $b^{0,+}AT$ signal was seen with anti-$b^{0,+}AT$ (Fig. 2A, +DTT panel), indicating that much of the precipitated $b^{0,+}AT$ is not associated with rBAT, and that $b^{0,+}AT$ is present in great excess over rBAT. Moreover, the signal of the co-precipitated $b^{0,+}AT$ was much less intense than the rBAT signal, suggesting that newly synthesized rBAT was associated mainly with unlabeled $b^{0,+}AT$ (Fig. 2A; anti-rBAT IP, +DTT panel). The group of Verrey observed a similar scenario (7).

Next, we used castanospermine to examine the relevance of glucose trimming in assembly and maturation of rBAT-$b^{0,+}$AT (Fig. 2B). When added during all the experiment, labeled rBAT molecules remained untrimmed (Fig. 2B, Cast. all; see the mobility shift). Inhibition of glucose trimming did not affect assembly of the heterodimer *via* a disulfide bridge (Fig. 2B, Cast. all, and data not shown), and did not induce degradation of rBAT (compare with Fig. 1, Cast.). When castanospermine was added only during the chase (Fig. 2B, Cast. chase), no labeled untrimmed rBAT molecules were detected. In these conditions, we can measure the effect of inhibition of the glucosidase II-mediated trimming of the last glucose of N-glycans. This trimming facilitates dissociation of glycoproteins from calnexin/calreticulin (18). Maturation of rBAT was delayed (Fig. 2B; observe the persistence of the endoglycosidase H sensitive rBAT band in the Cast. chase compared to the Control group), suggesting that the folding of rBAT is not complete before assembly of both subunits, and that it is facilitated by the calnexin chaperone system.

Type I cystinuria rBAT mutants are trafficking-defective

We used transient transfections in HeLa cells to study the biogenesis of type I cystinuria rBAT mutants localized either to the transmembrane or the TIM-barrel domains (Fig. 3A). We

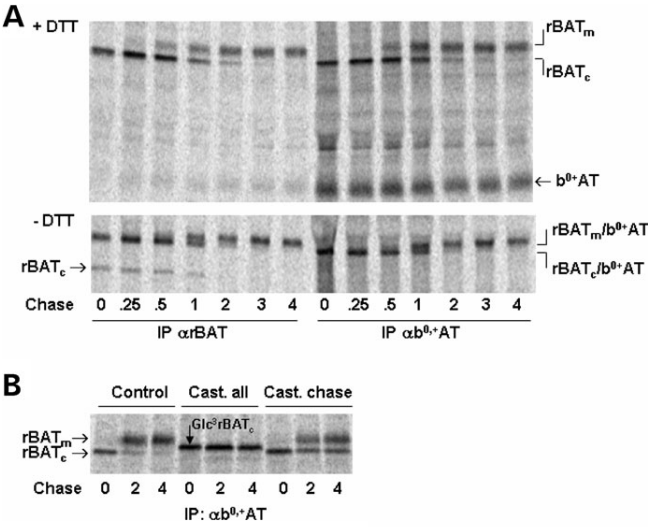

Figure 2. Assembly and maturation of the rBAT-$b^{0,+}$AT heterodimer. MDCK cells stably expressing human rBAT and $b^{0,+}AT$ were labeled for 15 min and chased as above. (**A**) Immunoprecipitations (IP) were performed with anti-rBAT (left) and anti-$b^{0,+}AT$ (right) antibodies, and the precipitates were run both under reducing (+ DTT, upper panel) and non-reducing (−DTT, bottom panel) conditions. In reducing conditions, core-glycosylated rBAT ($rBAT_c$; ~90 kDa), mature rBAT ($rBAT_m$; ~96 kDa) and the $b^{0,+}AT$ band ($b^{0,+}AT$; ~40 kDa) are observed. In non-reducing conditions, core-glycosylated ($rBAT_c/b^{0,+}AT$) and mature ($rBAT_m/b^{0,+}AT$) heterodimers are also distinguished, and unassembled $rBAT_c$ is observed disappearing during the chase. (**B**) Here only the co-precipitated rBAT bands with the anti-$b^{0,+}AT$ antibody are shown in reducing conditions. The results with the anti-rBAT antibody are similar (not shown). Pulse-chase experiments were as above but castanospermine (1 mM) was included in all the experiment (Cast. all) or only in the chase (Cast. chase). Observe the mobility shift of rBAT (Cast. all; Glc^3rBAT_c), indicating that the trimming of the synthesized rBAT has been blocked. Representative data of at least $n = 4$ experiments are shown.

have already used these cells to analyze the transport activity of the rBAT-$b^{0,+}AT$ heterodimer, its functional and structural units, and to report initial data on the R365W rBAT mutant (8,10,15).

We confirmed the main results obtained in MDCK cells. In the absence of $b^{0,+}AT$, rBAT was degraded, after a *lag* phase of ~2 h, with a half life of $\tau_{1/2} = 106 \pm 18$ min, and degradation was at least in part mediated by the proteasome (Supplementary Material, Figure A). We monitored assembly of rBAT and $b^{0,+}AT$ with transfection conditions which allow that almost all pulse-labeled rBAT co-precipitates with the anti-$b^{0,+}AT$ antibody (see Materials and Methods). The results were also comparable to MDCK cells. The endoglycosidase H resistant rBAT band was detected as a smear just above the endoglycosidase H sensitive band (Supplementary Material, Figure B and also Fig. 8). For this reason, maturation was followed directly with endoglycosidase H assays. After 8 h, all the pulse-labeled rBAT had complex N-glycosylation. The maturation half-time was ~2 h (Supplementary Material, Figure B). Inhibition of glucose trimming with castanospermine did not disturb assembly (not shown).

We transfected wild-type rBAT and type I cystinuria rBAT mutants in the presence of $b^{0,+}AT$ in HeLa cells and measured cystine transport. Only the L89P mutant showed a significant transport function (Fig. 3B). Loss of function was not due to

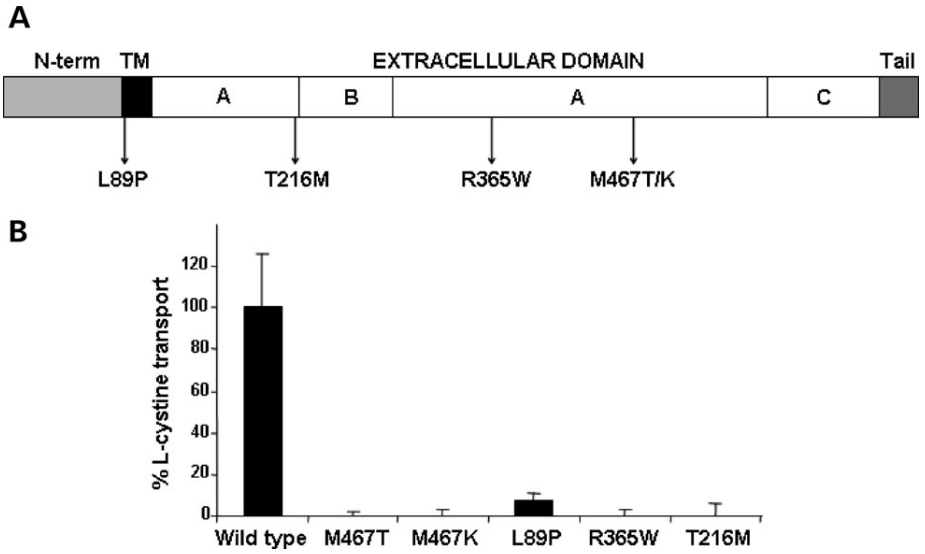

Figure 3. Transport activity of type I cystinuria rBAT mutants. (**A**) The scheme depicts the position of the rBAT mutations, in scale. The structural alignment with the extracellular domain of the homologue 4F2hc (20) and with the oligo-1,6-glucosidase of *Bacillus cereus* (34) shows that the extracellular domain of rBAT is composed of a $(\beta/\alpha)_8$ TIM-barrel (domain A), the subdomain B, an antiparallel 8-stranded β-sheet (domain C) and a short C-terminal tail. All the mutations of the extracellular domain that have been analyzed lie in the TIM-barrel. TM: transmembrane domain. (**B**) HeLa cells were transiently transfected with $b^{0,+}$AT and the wild-type or the different rBAT mutants, and after 36 h cystine transport activity was measured for 1 min (see Materials and Methods). The transport activity was calculated as the difference between the measured uptake in each group minus transport activity measured in cells transfected with $b^{0,+}$AT alone (which was not different from the transport in vector-transfected cells). The percentage of transport activity compared to the wild-type rBAT of a representative experiment is shown. Data are the mean ± SEM of four replicas per group. Two more independent experiments gave similar results.

decreased expression levels of the mutants compared to the wild-type (Fig. 4A). The percentages of transfected cells (see Materials and Methods) and $b^{0,+}$AT expression (data not shown) were similar. However, most of the mutant proteins remained endoglycosidase H sensitive, consistent with retention in an intracellular location (most likely the ER) (Fig. 4B). Only a small but significant amount of the L89P rBAT acquired endoglycosidase H resistance (Fig. 4B); and, in some experiments, we observed the same for the M467T mutant. The rBAT mutants formed heterodimers with $b^{0,+}$AT (Fig. 4C) as judged by the presence of the ∼135 kDa band (rBAT/$b^{0,+}$AT) under non-reducing conditions. To our surprise, this band was clearly diminished in the L89P mutant. A ∼250 kDa band appeared also under non-reducing conditions, which may correspond to the heterotetramer [rBAT-$b^{0,+}$AT]$_2$ (6,10). This band was not detected in the mutants (with the exception of the L89P mutant and, in some experiments, the M467T mutant), suggesting failure to oligomerize (Fig. 4C). We measured directly the amount of heterotetrameric rBAT-$b^{0,+}$AT by blue native-PAGE followed by western blot, where [rBAT-$b^{0,+}$AT]$_2$ runs at ∼500 kDa (10). We detected this band in the wild type and also in L89P, but at much lower amounts. Even less heterotetramer was present in the R365W and M467T lanes (Fig. 5). All mutants were detected as aggregates (operationally defined as material that did not enter the stacking gel and/or that ran as a smear at the top of the running gel), with the exception of the M467T. We suggest that these aggregates contain both unassembled rBAT and single heterodimers, since: (i) bands with a size consistent with these species are not detected in blue native gels [data not shown and (10)]; (ii) they are observed in SDS–PAGE western blots (Fig. 4C); and (iii) unassembled rBAT is also seen as aggregates in blue native gels (Fig. 5; see the asterisk). Interestingly, $b^{0,+}$AT expressed alone was also detected as aggregated material in blue native gels (not shown). Assembly and oligomerization might dissolve rBAT and $b^{0,+}$AT aggregates [which contain functional $b^{0,+}$AT (9)], similar to the association of the chaperone Shr3p with the General Amino acid Permease from yeast (19).

The L89P mutant assembles inefficiently with $b^{0,+}$AT

We seek to find the molecular mechanism for the trafficking defects. We examined the degradation kinetics of the different rBAT species in the absence of $b^{0,+}$AT and found no significant differences between the wild type and the mutants (Fig. 6). Notice that there is no mobility change in the T216M mutant (Fig. 6, the asterisks). T216 lies in an N-glycosylation consensus site. The result indicates that this site is not used *in vivo*. The structural alignment of rBAT with the X-ray structure of the extracellular domain of the rBAT homologue 4F2hc shows that T216 is an internal residue located very close to the putative active cleft, explaining why this site is not N-glycosylated (20). Next, we measured the assembly of wild-type and mutant rBAT with $b^{0,+}$AT. Under our experimental conditions, more than 80% of the rBAT and $b^{0,+}$AT expressed is immunoprecipitated with the specific antibodies (not shown). We compared the amounts of pulse-labeled rBAT immunoprecipitated by the anti-rBAT antibody with that co-precipitated by the anti-$b^{0,+}$AT antibody, under reducing conditions (Fig. 7A). In HeLa cells, there is a great excess of $b^{0,+}$AT over rBAT and most

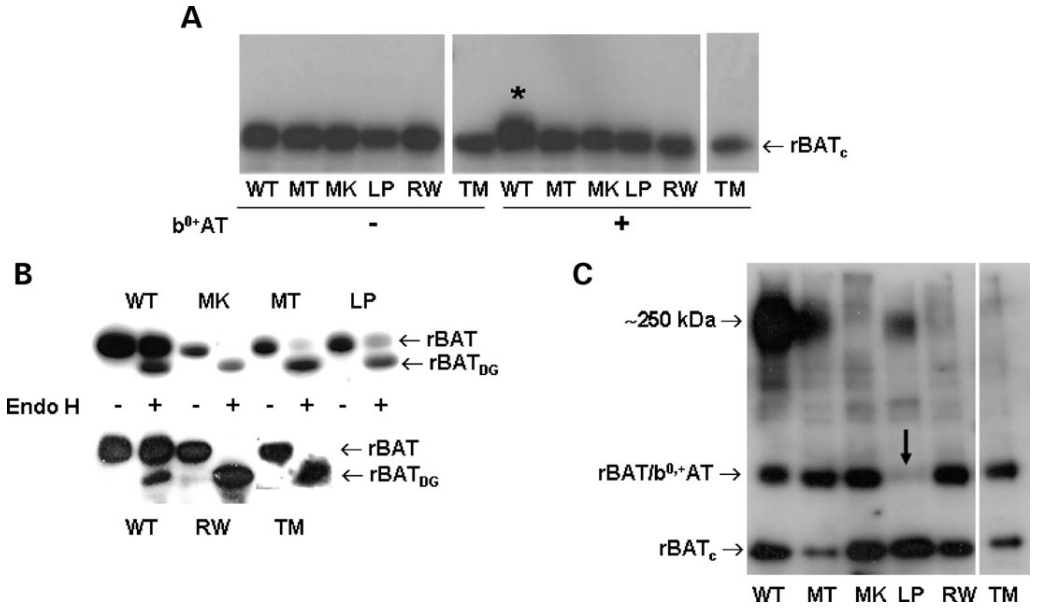

Figure 4. Wild-type and mutant rBAT expression and maturation in HeLa cells. In (**A**) and (**C**), aliquots of the same cells used for the transport experiment shown in Figure 3 were used for western blot analysis. Total membranes from the transfected cells were loaded for SDS–PAGE. Ten micrograms of protein were loaded per lane. Proteins were transferred to PVDF membranes and decorated with the anti-rBAT antibody. (A) Comparison of the expression levels of wild-type and mutant rBAT, in the presence and absence of $b^{0,+}$AT, under reducing conditions. The asterisk (*) marks the mobility shift of the wild-type rBAT in the presence of $b^{0,+}$AT, indicating maturation of N-glycans. $rBAT_c$: ~90 kDa core-glycosylated rBAT. (**B**) Endoglycosidase H (endo H) assays of wild-type and mutant rBAT in the presence of $b^{0,+}$AT. Total membranes were obtained from HeLa cells transfected with $b^{0,+}$AT and the wild-type and mutant rBAT species. Ten micrograms of protein were digested or not with the enzyme, and run in SDS–PAGE under reducing conditions. Proteins were transferred to PVDF membranes and decorated with the anti-rBAT antibody. A representative experiment (of at least $n = 4$ for all the rBAT species) is shown. $rBAT_{DG}$: de-glycosylated rBAT. (C) The same samples of (A) (with $b^{0,+}$AT) were run under non-reducing conditions. The arrow marks the few amount of L89P mutant in the heterodimeric form. rBAT/$b^{0,+}$AT: ~135 kDa heterodimer. Observe the ~250 kDa band. In (A) and (C), all lanes belong to the same gel and membrane. WT, wild-type rBAT; MT, M467T; MK, M467K; LP, L89P; RW, R365W; TM, T216M.

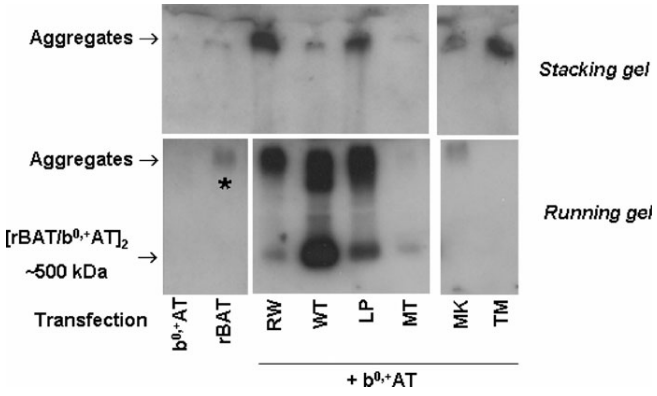

Figure 5. Blue native-PAGE analysis of wild-type and mutant rBAT. HeLa cells were transfected with $b^{0,+}$AT and wild-type or mutant rBAT species. After 36 h, total membranes were solubilized with digitonin and 30 μg were loaded in 4–20% linear blue native gels. Proteins were transferred and decorated with anti-$b^{0,+}$AT (not shown) and anti-rBAT antibodies. The 3% stacking gel is also presented. Data are from a representative experiment of $n = 4$. The exposure time to detect rBAT alone (asterisk) is longer (>10-fold) than for the rest of the gel. Wild-type and mutant rBAT are abbreviated as in Figure 4.

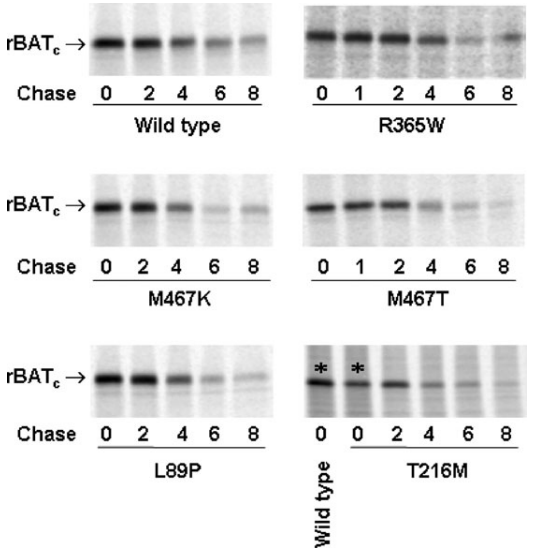

Figure 6. Decay kinetics of wild-type and mutant rBAT in the absence of $b^{0,+}$AT. HeLa cells transiently expressing wild-type or mutant rBAT were labeled for 30 min with ^{35}S-Met/Cys and chased with excess Met/Cys up to 8 h. Equivalent amounts of radioactivity incorporated into protein were immunoprecipitated with the anti-rBAT antibody. The precipitates were run under reducing conditions. The core-glycosylated rBAT band ($rBAT_c$, ~90 kDa) is observed. The asterisks mark the identical size of wild-type rBAT and the T216M mutant. Representative experiments of at least $n = 4$ for each rBAT species are shown.

of the labeled rBAT is associated with unlabeled $b^{0,+}$AT (data not shown), as in MDCK cells (Fig. 2A). Therefore, under non-reducing conditions most of the radioactivity associated with the ~135 kDa heterodimer band comes from labeled

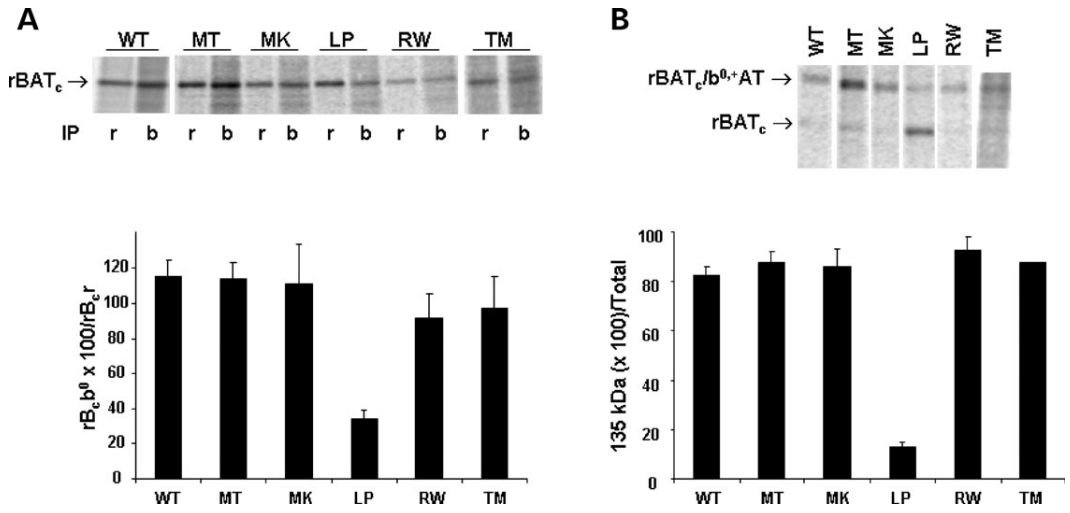

Figure 7. Assembly of wild-type and mutant rBAT with $b^{0,+}$AT. HeLa cells transiently transfected with $b^{0,+}$AT together with wild-type or mutant rBAT were pulse-labeled for 30 min and lysed. Equivalent amounts of radioactivity incorporated into protein were immunoprecipitated with the anti-rBAT (IP, r) and the anti-$b^{0,+}$AT (IP, b) antibodies, and run under reducing (**A**) and non-reducing conditions (**B**; here only the anti-rBAT immunoprecipitations are presented). Representative experiments are shown. (A) For quantification, the $rBAT_c$ band signal in the anti-$b^{0,+}$AT immunoprecipitation (rB_cb^0) was multiplied by 100 and divided by the $rBAT_c$ band signal in the anti-rBAT immunoprecipitation (rB_cr). The results (mean ± SEM of at least $n = 4$ experiments for each rBAT species) are given as the percentage of total pulse-labeled $rBAT_c$ co-precipitated with the anti-$b^{0,+}$AT antibody. (**B**) For quantification, the $rBAT_c/b^{0,+}$AT (~135 kDa) band signal was multiplied by 100 and divided by the total rBAT signal ($rBAT_c$ plus $rBAT_c/b^{0,+}$AT bands) in the anti-rBAT immunoprecipitation. The results (mean ± SEM of at least $n = 4$ experiments for each rBAT species, with the exception of T216M, $n = 1$) are given as the percentage of total rBAT found in the $rBAT_c/b^{0,+}$AT band (assembled rBAT). See text for further explanations. Wild-type and mutant rBAT are abbreviated as in Figure 4.

rBAT molecules. We obtained another estimation of assembly efficiency by comparing the ~90 kDa band with the ~135 kDa band in anti-rBAT immunoprecipitates under non-reducing conditions (Fig. 7B). Both estimations indicated that only the L89P mutation had an assembly defect, because only between 10 and 30% of the labeled L89P mutant did heterodimerize with $b^{0,+}$AT.

rBAT mutants of the TIM-barrel are degraded after assembly with $b^{0,+}$AT

We followed the fate of wild-type and mutant rBAT in the presence of $b^{0,+}$AT. A decay of the rBAT signal co-precipitated with the anti-$b^{0,+}$AT antibody was observed for the T216M, R365W, M467K and M467T mutants (Fig. 8 and data not shown), indicating that the TIM-barrel mutants of rBAT are directed for disposal after assembly with $b^{0,+}$AT. Endoglycosidase H assays confirmed that no maturation of rBAT mutants occurred during the chase (data not shown). In the case of the L89P mutant, we were able to detect low amounts of heterodimer, which remained stable throughout the chase (Fig. 9; compare with wild-type and M467T heterodimers). These results suggest that mutants of the TIM-barrel domain of rBAT either delay or disrupt post-assembly folding of the rBAT extracellular domain. In striking contrast, the transmembrane domain L89P mutation may affect only the assembly step.

DISCUSSION

Biogenesis of the wild-type transporter

We measured for the first time the turnover rates and maturation half-times of the human subunits of the system $b^{0,+}$-*like*, rBAT and $b^{0,+}$AT, expressed alone or together. We show that unassembled rBAT is an ERAD glycoprotein substrate with a characteristic kinetic behavior: a *lag* phase, where unassembled rBAT may wait for $b^{0,+}$AT while being retained by chaperones, followed by a degradation phase (16,21,22). Contrary to other ERAD glycoprotein substrates (16,23), the retention was not by-passed by inhibition of glucose trimming in MDCK cells. In contrast, preliminar results show that castanospermine decreases the *lag* phase and accelerates the degradation phase of rBAT in HeLa cells (data not shown). We could only speculate about the difference between the two cell types. It is likely that the order and the kinetics of interactions between distinct chaperone complexes and rBAT during the *lag* phase are not the same. The most relevant interaction (related to degradation) between the calnexin chaperone system and rBAT during the *lag* phase may occur later in MDCK cells as compared with HeLa cells.

rBAT degradation is blocked by heterodimerization in the ER. This step is fast. Some labeled rBAT associates with $b^{0,+}$AT after a 2.5 min pulse (not shown). This time is within the range needed to synthesize full-length rBAT (24), suggesting that it can assemble co-translationally with already synthesized $b^{0,+}$AT. Assembly might be independent of the calnexin chaperone system, as it is not impaired by the inhibition of the formation of monoglucosylated N-glycans. In contrast, preventing the deglucosylation of monoglucosylated N-glycans (which slows dissociation of glycoproteins from calnexin/calreticulin), delays maturation of rBAT-$b^{0,+}$AT (Fig. 2B). This result indicates that maturation of rBAT within the heterodimer depends on interactions with the lectins. We propose that there are some post-assembly folding steps of the extracellular domain of rBAT, which are

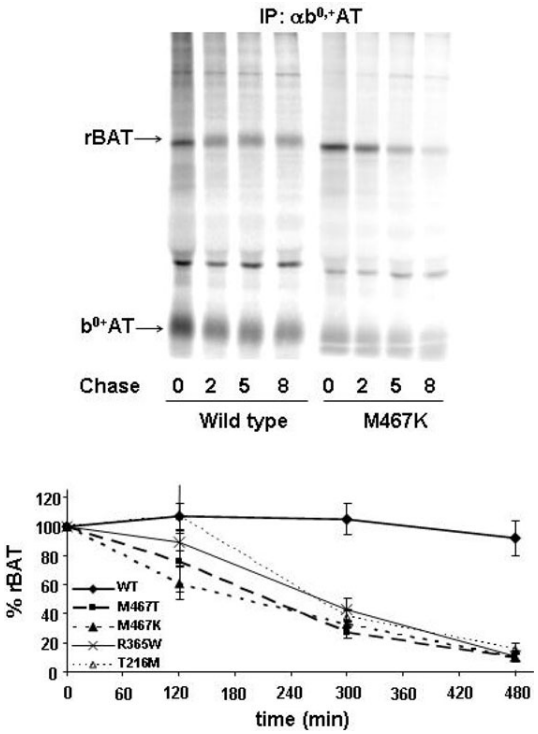

Figure 8. Post-assembly degradation of the extracellular domain rBAT mutants. HeLa cells transiently expressing $b^{0,+}AT$ together with wild-type or mutant rBAT were labeled for 30 min with ^{35}S-Met/Cys and chased with excess Met/Cys up to 8 h. Equivalent amounts of radioactivity incorporated into protein were immunoprecipitated with the anti-$b^{0,+}AT$ antibody. The precipitates were run under reducing conditions. The results of a representative experiment with the wild-type and the M467K mutant are presented. The wild-type and M467K samples are from the same experiment and have been processed in parallel (although in two different gels). The two dried gels were exposed simultaneously in the same intensifying screen. The quantification of the rBAT signal co-precipitated with the anti-$b^{0,+}AT$ antibody is shown. This signal corresponds to the sharp endoglycosidase H-sensitive band together with the diffuse endoglycosidase H-resistant rBAT species appearing only at 2, 5 and 8 h chase points in the wild type (see also Supplementary Material, Figure B). Data are the mean ± SEM of at least three independent experiments for each rBAT species.

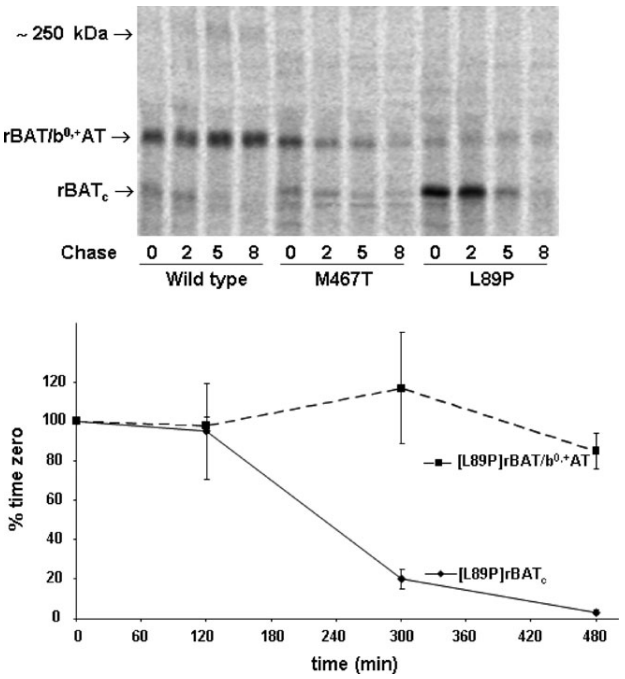

Figure 9. [L89P]rBAT-$b^{0,+}AT$ heterodimers are stable. HeLa cells transiently expressing $b^{0,+}AT$ together with wild-type, M467T or the L89P rBAT mutant were labeled for 30 min with ^{35}S-Met/Cys and chased with excess Met/Cys up to 8 h. Equivalent amounts of radioactivity incorporated into protein were immunoprecipitated with the anti-rBAT antibody (upper panel). The precipitates were run under non-reducing conditions. Only the result of a representative experiment is shown. Two more experiments gave similar results. The quantification of the L89P rBAT-containing bands is shown at the bottom panel. Data are the mean ± SEM of $n = 3$ experiments.

facilitated by the calnexin chaperone system. Whether $b^{0,+}AT$ is mandatory for post-assembly folding of rBAT remains an open question. $b^{0,+}AT$ folding seems to be independent of rBAT, because it is functional in its absence (9). Our data are compatible with models proposed for other oligomeric protein complexes, such as potassium channels and acetylcholine receptors, where biogenesis proceeds through interspersed folding and assembly steps (25,26).

Biogenesis of type I cystinuria rBAT mutants

Wild-type biogenesis provides the framework to study type I cystinuria rBAT mutations. In *Xenopus* oocytes, the M467T, M467K and T216M mutants showed reduced transport activity (12,13). Amino acid uptake increased and even reached wild-type levels upon higher expression (12), raising doubts about the situation *in vivo*. Instead, the R365W mutant was not functional in HeLa cells [(8) and Fig. 3B]. Here we demonstrate that the mutants tested lack function in human cells and none of them acquires complex N-glycosylation (but see below). Therefore, the absence of transport activity is primarily due to strong trafficking defects.

The heterotetramer [rBAT-$b^{0,+}AT]_2$ is the structural unit of this transporter at the plasma membrane and the single heterodimer is the functional unit (10). The small, but significant, transport measured in the L89P mutant correlates with the few heterotetramers and mature L89P molecules detected. The even lower levels of M467T heterotetramers and mature molecules may be not enough to detect significant uptake (Figs 4B and 5). In fact, all the mutants tested fail, to different extents, to form stable heterotetramers. They are instead detected as aggregates in blue native gels (with the exception of M467T). Our solubilization conditions may allow resolution only of heterotetramers, but not heterodimers or monomers. Aggregation could be also due to the presence of high molecular weight complexes containing ER-resident chaperones or ERAD machinery (27,28). In any case, the aggregation suggests a folding and/or assembly defect that hinders formation of mutant heterotetramers. Dimerization of the heterodimer may be needed for ER-exit. Oligomerization can be one of the final quality control steps of the biogenesis of rBAT-$b^{0,+}AT$, as shown for other proteins (29,30).

From the mutations studied here, L89P is in the transmembrane domain and the rest lie in the $(\beta/\alpha)_8$ TIM-barrel of the

extracellular domain [(20) and Fig. 3A]. We do not know how these mutations affect the folding and/or assembly of rBAT. However, they do not lead to a new phenotype in the absence of $b^{0,+}$AT, since unassembled wild-type and mutant rBAT disappear with similar kinetics (Fig. 6). There are other examples of this behavior, as $K_{IR}6.2$ mutations of K_{ATP} channels when expressed without the sulfonylurea receptor (SUR) subunit (31). Only co-expression with $b^{0,+}$AT discriminates between wild-type rBAT and mutants. The mutants fail to exit the ER and are directed to disposal, strongly suggesting a defect in early biogenesis, like many other mutant proteins in the secretory pathway (17,32). Most of the L89P molecules do not stably assemble with $b^{0,+}$AT. L89 is the putative second residue of the transmembrane segment. The L89P mutant is fully N-glycosylated, suggesting a correct insertion in the membrane. Proline may induce a kink in the transmembrane domain or directly interfere with interactions with $b^{0,+}$AT. The assembly defect of the L89P mutant agrees with the proposed dominant role of the N-terminal and transmembrane domains of rBAT in the association with $b^{0,+}$AT (33). Despite the assembly defect, some [L89P]rBAT-$b^{0,+}$AT heterodimers and heterotetramers form and are functional (Figs 3B, 5 and 9). This may be due to overexpression. However, the stability and functionality of the L89P heterodimers suggest that, in contrast to the TIM-barrel mutants (see below), the L89P mutation does not cause misfolding.

The TIM-barrel mutants show a trafficking defect of different origin. They assemble efficiently with $b^{0,+}$AT, but are subsequently degraded, suggesting misfolding of the extracellular domain. It is interesting also to compare the ratio 135/$\sim$250 kDa bands between wild-type, L89P and M467T mutants in Figure 4C. This ratio is similar for the wild-type and the L89P mutant, but it clearly differs from that of the M467T mutant. This suggests that, once the heterodimer is formed, both the wild-type and the L89P mutant can readily form the heterotetramer. In contrast, for the M467T mutation, only a few heterodimers can oligomerize, arguing again for a folding defect. Therefore, at least two different classes of pathogenic rBAT mutants exist: assembly defective (L89P) and folding-defective (TIM-barrel mutants). At our level of analysis, these two classes are mutually exclusive, but lead to the same type I cystinuria phenotype. It is unlikely that the correlation between the position of the mutants within the rBAT protein and their molecular effects is just a mere coincidence.

Summary model

The data are consistent with a minimal working model for the biogenesis of the rBAT-$b^{0,+}$AT transporter. Fast interactions of the N-terminal and transmembrane domains of rBAT with folded $b^{0,+}$AT determine formation of the heterodimer, which is impaired in the L89P mutant. Assembly with $b^{0,+}$AT blocks rBAT degradation. These early steps do not require the calnexin chaperone system. After assembly, the rBAT extracellular domain folds within that chaperone system. Heterotetramerization proceeds immediately after completion of rBAT folding, or interspersed within the final folding steps. Only the heterotetramers exit the ER to the Golgi complex. Mutations of the extracellular domain of rBAT disrupt or delay the post-assembly folding of rBAT, hindering stable oligomerization and leading to its degradation.

MATERIALS AND METHODS

Reagents and antibodies

Reagents were purchased from Sigma unless otherwise indicated. Pro-mix l-[^{35}S] *in vitro* cell labeling mix (L-[35S]Methionine and L-[35S]Cysteine), D-MEM media without L-Methionine and L-Cystine, and Dialyzed FBS, were from GE Healthcare. Antibodies against the N-termini of human $b^{0,+}$AT and rBAT are described elsewhere (6,15).

cDNA constructs

The vectors for mammalian cell expression of human rBAT and $b^{0,+}$AT have been described elsewhere (15). The construction of the R365W, M467T and M467K rBAT mutants is detailed in (8,12). To express the M467T and M467K rBAT mutants in mammalian cells, the cDNAs in pSPORT were removed with EcoRI and XbaI and cloned into pCDNA3 cut with the same enzymes. The L89P and T216M mutants were obtained by site-directed mutagenesis (QuickChangeTM, Stratagene) of pCDNA3-rBAT, using the mutagenic oligonucleotides (only sense oligonucleotides are shown): 5′-ATACCTCGGGAGATCCCCTTCTGGCTCACAGTG-3′, and 5′-CATACCAAACCACATGAGTGATAAACATATTT GGTTTC-3′, respectively. All mutations were confirmed by DNA sequencing using the d-Rhodamine dye Terminator Cycle Sequencing Ready Reaction Kit (Perkin Elmer Applied Biosystems). The sequence reactions were analysed with an Abi Prism 377 DNA Sequencer.

Cell culture and transfection

MDCK-IIJ and HeLa cells were grown in Dulbecco's modified Eagle's medium (Gibco) supplemented with 10% fetal calf serum (heat-inactivated), 100 U/ml penicillin (Gibco) and 0.1 mg/ml streptomycin (Gibco), at 37°C in a humidified atmosphere containing 5% CO_2. Stably transfected MDCK-derived cell lines (9) were supplemented with the appropriate selection agent (400 μg/ml geneticin and/or 100 μg/ml hygromycin B). Calcium phosphate transient transfection of HeLa cells was performed as described (12,15). The efficiency of transfection was above 70% in all experiments. For transient transfections, 10 cm diameter plates were incubated with a mixture of DNA containing 2 μg of pEGFP (green fluorescence protein; Clontech), 6 μg of pCDNA3-rBAT (wild-type or the different mutants) and 12 μg of pCDNA3-$b^{0,+}$AT as described (12,15). In these conditions, more than 80% of the labeled wild-type rBAT molecules in pulse-chase studies were assembled with $b^{0,+}$AT (data not shown). When rBAT or $b^{0,+}$AT were transfected alone, 12 or 6 μg of pCDNA3 were added, respectively.

Membrane preparation, SDS–PAGE, western blot and blue native gel electrophoresis

We have published detailed procedures for these methods elsewhere (6,10). Protein quantitation was performed with the BCA method (Pierce).

Transport measurements

Influx rates of 50 μM L-[^{3}H]arginine (ARC) and 20 μM L-[^{35}S]cystine (Amersham) in transfected HeLa cells were performed as described (9,15).

Endoglycosidase H assay

The enzyme was obtained from New England Biolabs and was used following the manufacturer protocol.

Pulse-chase and immunoprecipitation protocols

Cells were transfected and seeded in 3.5 cm diameter plates at 60–70% confluence. The following day cells were incubated for 30 min in pre-warmed L-Methionine/L-Cystine free media containing 10% dialyzed FBS. Subsequently, cells were labeled for 15 (MDCK) or 30 min (HeLa) with a mixture of [^{35}S]methionine/cysteine (120 μCi/ml) and, after removal of the labeling media, incubated with pre-warmed media supplemented with 5 mM unlabeled L-methionine/L-cysteine. At the indicated times, cells were washed twice with cold phosphate-buffered saline (PBS) and once with cold PBS containing 20 mM *N*-ethylmaleimide for 5 min. Cells were collected and lysed on a rotating wheel in 0.2 ml of NET buffer (150 mM NaCl, 5 mM EDTA, 50 mM Tris, pH 7.4, 0.5% NP-40) with the protease inhibitors aprotinin, leupeptin, phenylmethylsulfonyl fluoride, and pepstatin, and 20 mM NEM. After 30 min at 4°C, a postnuclear supernatant was obtained by 10 min of 10 000 g centrifugation at 4°C. Inhibitors [25 μM lactacystin, 30 μM MG132, 1 mM castanospermine (Cast.), 1 mM 1-deoxymannojirimycin (DMNJ), 10 μg/ml Brefeldin A, and 200 μg/ml leupeptin] and control vehicles were included from the beginning of the starving period to the end of the chase, except for castanospermine in some experiments, and for MG132, which was added after the end of the pulse. All inhibitors were from Calbiochem.

Immunoprecipitations were performed from equivalent amounts of radioactivity incorporated into proteins, by adding an equal volume of immunoabsorbent buffer (200 mM H_3BO_3, 50 mM $Na_2B_4O_7$, 150 mM NaCl, 1% NP-40 and 0.1% ovalbumin, pH 8.3) with the same protease inhibitors as the lysis buffer, and polyclonal antibodies to rBAT or $b^{0,+}$AT, in combination with protein A-Sepharose. Precipitates were washed four times with borate-NaCl buffer (0.5% NP-40, 0.3 M NaCl, 25 mM $Na_2B_4O_7$ and 0.1 M H_3BO_4, pH 8.3) and twice with 40 mM HEPES, pH 8. Samples were run on SDS–PAGE under reducing or non-reducing conditions. Gels were stained with Coomassie brilliant blue to control for precipitating antibodies, dried and put on an intensifying screen for quantification with a Phosphoimager Typhoon 8600 (Molecular Dynamics).

Preliminar immunoprecipitation experiments were performed to control for the efficiency and the specificity of the immunoprecipitating antibodies. In our experimental cell system and pulse-chase conditions, the antibodies almost quantitatively immunoprecipitated all the pulse-labeled rBAT and $b^{0,+}$AT molecules (more than 80%; data not shown). Co-precipitation of rBAT and $b^{0,+}$AT with the anti-$b^{0,+}$AT antibody, and of $b^{0,+}$AT and rBAT with the anti-rBAT antibody did not occur when lysates from cells expressing rBAT alone and $b^{0,+}$AT alone were mixed before immunoprecipitation (Supplementary Material, Figure C).

Data analysis

The relative intensities of the labeled bands were determined using phosphorimaging, as follows: each band was outlined by a rectangle (as tightly-fitting to the band as possible) and a rectangle of identical size was drawn in the closest area without any band in the lane. The relative positions of band and background rectangles were maintained within the experiment and among similar experiments. The value for each rectangle was calculated using the Local Average Background Correction of the ImageQuant software. The final value of the band was the difference between the value of the rectangle band and the value of the rectangle background. The data were plotted as intensity values of the fraction remaining obtained by dividing by the zero time value, if not otherwise indicated. The decay data were fitted to an initial time in a Plateau followed by a single exponential function. The Plateau period and the half-life results are given as mean ± SEM. The maturation values were fitted to a four-parameter logistic equation (with bottom and top values set of 0 and 100, respectively).

SUPPLEMENTARY MATERIAL

Supplementary Material is available at HMG Online.

ACKNOWLEDGEMENTS

We thank Susanna Bial (Institute for Research in Biomedicine and CIBERER, Barcelona) for technical assistance and Robin Rycroft for editorial support.

Conflict of Interest statement. None declared.

FUNDING

This study was supported by the grants BFU2006-06788/BMC (to J.C.) and BFU2006-14600 (to M.P.); by the European Community project grant 502802 EUGINDAT, and by Generalitat de Catalunya grant 2005 SGR00947. P.B. was a recipient of a predoctoral fellowship from the Spanish Ministry of Education and Science, and is currently supported by the CIBERER (Centro de Investigación Biomédica en Red de Enfermedades Raras), Barcelona.

REFERENCES

1. Palacin, M., Nunes, V., Font-Llitjos, M., Jimenez-Vidal, M., Fort, J., Gasol, E., Pineda, M., Feliubadalo, L., Chillaron, J. and Zorzano, A. (2005) The genetics of heteromeric amino acid transporters. *Physiology*, **20**, 112–124.
2. Calonge, M.J., Gasparini, P., Chillaron, J., Chillon, M., Gallucci, M., Rousaud, F., Zelante, L., Testar, X., Dallapiccola, B., Di Silverio, F. *et al.* (1994) Cystinuria caused by mutations in rBAT, a gene involved in the transport of cystine. *Nat. Genet*, **6**, 420–425.
3. Font-Llitjos, M., Jimenez-Vidal, M., Bisceglia, L., Di Perna, M., de Sanctis, L., Rousaud, F., Zelante, L., Palacin, M. and Nunes, V. (2005) New insights into cystinuria: 40 new mutations, genotype-phenotype correlation, and digenic inheritance causing partial phenotype. *J. Med. Genet.*, **42**, 58–68.
4. Feliubadalo, L., Arbones, M.L., Manas, S., Chillaron, J., Visa, J., Rodes, M., Rousaud, F., Zorzano, A., Palacin, M. and Nunes, V. (2003) Slc7a9-deficient mice develop cystinuria non-I and cystine urolithiasis. *Hum. Mol. Genet.*, **12**, 2097–2108.
5. Chillaron, J., Estevez, R., Mora, C., Wagner, C.A., Suessbrich, H., Lang, F., Gelpi, J.L., Testar, X., Busch, A.E., Zorzano, A. and Palacin, M. (1996) Obligatory amino acid exchange via systems bo,+-like and y+L-like. A tertiary active transport mechanism for renal reabsorption of cystine and dibasic amino acids. *J. Biol. Chem.*, **271**, 17761–17770.
6. Fernandez, E., Carrascal, M., Rousaud, F., Abian, J., Zorzano, A., Palacin, M. and Chillaron, J. (2002) rBAT-b(0,+)AT heterodimer is the main apical reabsorption system for cystine in the kidney. *Am. J. Physiol. Renal Physiol.*, **283**, F540–F548.
7. Bauch, C. and Verrey, F. (2002) Apical heterodimeric cystine and cationic amino acid transporter expressed in MDCK cells. *Am. J. Physiol. Renal Physiol.*, **283**, F181–F189.
8. Pineda, M., Wagner, C.A., Broer, A., Stehberger, P.A., Kaltenbach, S., Gelpi, J.L., Martin, D.R., Zorzano, A., Palacin, M., Lang, F. and Broer, S. (2004) Cystinuria-specific rBAT(R365W) mutation reveals two translocation pathways in the amino acid transporter rBAT-b0,+AT. *Biochem. J.*, **377**, 665–674.
9. Reig, N., Chillaron, J., Bartoccioni, P., Fernandez, E., Bendahan, A., Zorzano, A., Kanner, B., Palacin, M. and Bertran, J. (2002) The light subunit of system b(o,+) is fully functional in the absence of the heavy subunit. *EMBO J.*, **21**, 4906–4914.
10. Fernandez, E., Jimenez-Vidal, M., Calvo, M., Zorzano, A., Tebar, F., Palacin, M. and Chillaron, J. (2006) The structural and functional units of heteromeric amino acid transporters. The heavy subunit rBAT dictates oligomerization of the heteromeric amino acid transporters. *J. Biol. Chem.*, **281**, 26552–26561.
11. Guillen, M., Corella, D., Cabello, M.L., Gonzalez, J.I., Sabater, A., Chaves, J.F. and Hernandez-Yago, J. (2005) Identification of novel SLC3A1 gene mutations in Spanish cystinuria families and association with clinical phenotypes. *Clin. Genet.*, **67**, 240–251.
12. Chillaron, J., Estevez, R., Samarzija, I., Waldegger, S., Testar, X., Lang, F., Zorzano, A., Busch, A. and Palacin, M. (1997) An intracellular trafficking defect in type I cystinuria rBAT mutants M467T and M467K. *J. Biol. Chem.*, **272**, 9543–9549.
13. Saadi, I., Chen, X.Z., Hediger, M., Ong, P., Pereira, P., Goodyer, P. and Rozen, R. (1998) Molecular genetics of cystinuria: mutation analysis of SLC3A1 and evidence for another gene in type I (silent) phenotype. *Kidney Int.*, **54**, 48–55.
14. Bauch, C., Forster, N., Loffing-Cueni, D., Summa, V. and Verrey, F. (2003) Functional cooperation of epithelial heteromeric amino acid transporters expressed in madin-darby canine kidney cells. *J. Biol. Chem.*, **278**, 1316–1322.
15. Font, M.A., Feliubadalo, L., Estivill, X., Nunes, V., Golomb, E., Kreiss, Y., Pras, E., Bisceglia, L., d'Adamo, A.P., Zelante, L. *et al.* (2001) Functional analysis of mutations in SLC7A9, and genotype-phenotype correlation in non-Type I cystinuria. *Hum. Mol. Genet.*, **10**, 305–316.
16. Molinari, M. (2007) N-glycan structure dictates extension of protein folding or onset of disposal. *Nat. Chem. Biol.*, **3**, 313–320.
17. McCracken, A.A. and Brodsky, J.L. (2005) Recognition and delivery of ERAD substrates to the proteasome and alternative paths for cell survival. *Curr. Top. Microbiol. Immunol.*, **300**, 17–40.
18. Parodi, A.J. (2000) Protein glucosylation and its role in protein folding. *Annu. Rev. Biochem.*, **69**, 69–93.
19. Kota, J. and Ljungdahl, P.O. (2005) Specialized membrane-localized chaperones prevent aggregation of polytopic proteins in the ER. *J. Cell Biol.*, **168**, 79–88.
20. Fort, J., de la Ballina, L.R., Burghardt, H.E., Ferrer-Costa, C., Turnay, J., Ferrer-Orta, C., Uson, I., Zorzano, A., Fernandez-Recio, J., Orozco, M. *et al.* (2007) The structure of human 4F2hc ectodomain provides a model for homodimerization and electrostatic interaction with plasma membrane. *J. Biol. Chem*, **282**, 31444–31452.
21. de Virgilio, M., Kitzmuller, C., Schwaiger, E., Klein, M., Kreibich, G. and Ivessa, N.E. (1999) Degradation of a Short-lived Glycoprotein from the Lumen of the Endoplasmic Reticulum: the role of N-linked glycans and the unfolded protein response. *Mol. Biol. Cell*, **10**, 4059–4073.
22. Le, A., Graham, K.S. and Sifers, R.N. (1990) Intracellular degradation of the transport-impaired human PiZ alpha 1- antitrypsin variant. Biochemical mapping of the degradative event among compartments of the secretory pathway. *J. Biol. Chem.*, **265**, 14001–14007.
23. Ruddock, L.W. and Molinari, M. (2006) N-glycan processing in ER quality control. *J. Cell Sci.*, **119**, 4373–4380.
24. Braakman, I., Hoover-Litty, H., Wagner, K.R. and Helenius, A. (1991) Folding of influenza hemagglutinin in the endoplasmic reticulum. *J. Cell Biol.*, **114**, 401–411.
25. Deutsch, C. (2002) Potassium channel ontogeny. *Annu. Rev. Physiol.*, **64**, 19–46.
26. Wanamaker, C.P., Christianson, J.C. and Green, W.N. (2003) Regulation of nicotinic acetylcholine receptor assembly. *Ann. N. Y. Acad. Sci.*, **998**, 66–80.
27. Meunier, L., Usherwood, Y.K., Chung, K.T. and Hendershot, L.M. (2002) A subset of chaperones and folding enzymes form multiprotein complexes in endoplasmic reticulum to bind nascent proteins. *Mol. Biol. Cell*, **13**, 4456–4469.
28. Molinari, M., Galli, C., Piccaluga, V., Pieren, M. and Paganetti, P. (2002) Sequential assistance of molecular chaperones and transient formation of covalent complexes during protein degradation from the ER. *J. Cell Biol.*, **158**, 247–257.
29. Keith, N., Parodi, A.J. and Caramelo, J.J. (2005) Glycoprotein tertiary and quaternary structures are monitored by the same quality control mechanism. *J. Biol. Chem.*, **280**, 18138–18141.
30. Salahpour, A., Angers, S., Mercier, J.F., Lagace, M., Marullo, S. and Bouvier, M. (2004) Homodimerization of the {beta}2-adrenergic receptor as a prerequisite for cell surface targeting. *J. Biol. Chem.*, **279**, 33390–33397.
31. Crane, A. and Aguilar-Bryan, L. (2004) Assembly, maturation, and turnover of KATP channel subunits. *J. Biol. Chem.*, **279**, 9080–9090.
32. Sitia, R. and Braakman, I. (2003) Quality control in the endoplasmic reticulum protein factory. *Nature*, **426**, 891–894.
33. Franca, R., Veljkovic, E., Walter, S., Wagner, C.A. and Verrey, F. (2005) Heterodimeric amino acid transporter glycoprotein domains determining functional subunit association. *Biochem. J.*, **388**, 435–443.
34. Watanabe, K., Hata, Y., Kizaki, H., Katsube, Y. and Suzuki, Y. (1997) The refined crystal structure of Bacillus cereus oligo-1,6-glucosidase at 2.0 a resolution: structural characterization of proline-substitution sites for protein thermostabilization. *J. Mol. Biol.*, **269**, 142–153.

SUPPLEMENTARY MATERIAL

Supplementary Legends to Figures

Figure A. Decay kinetics of wild type rBAT and effect of lactacystin

1. Hela cells transiently transfected with rBAT were pulse-chased, lysed and immunoprecipitated with the anti-rBAT antibody as stated under Materials and Methods. The precipitates were run under reducing conditions. A representative experiment of n = 12 is shown. **2.** Hela cells transiently transfected with rBAT were incubated with 25 μM lactacystin or with DMSO (vehicle) for 10 h. Cell lysates (20 μg) were loaded in SDS-PAGE under reducing conditions. Proteins were transferred to PVDF membranes and decorated with the anti-rBAT antibody. A representative experiment of n = 3 is shown.

Figure B. Assembly and maturation of wild type rBAT

HeLa cells transiently expressing wild type rBAT and $b^{0,+}AT$ were pulse-labeled, chased, lysed and immunoprecipitated as stated under Materials and Methods. After immunoprecipitation with anti-rBAT, half of the precipitate was digested with endoglycosidase H. Precipitates were run under reducing conditions. Observe the smear of labeled rBAT detected first at the 2 h chase point and the de-glycosylated rBAT molecules ($rBAT_{DG}$).

Figure C. Control immunoprecipitations

HeLa cells transfected with rBAT, $b^{0,+}$AT, co-transfected with both expression vectors (rBAT/$b^{0,+}$AT), or untransfected (-), were pulse-labeled, lysed and immunoprecipitated (IP) with the indicated antibodies or only with Protein A-Sepharose beads (∅), as stated under Materials and Methods. In the **Mix** lanes, the same amounts of lysate used for the rBAT alone and $b^{0,+}$AT alone samples were mixed after lysis, and immunoprecipitated. All lanes belong to the same gel.

Sup. Figure A

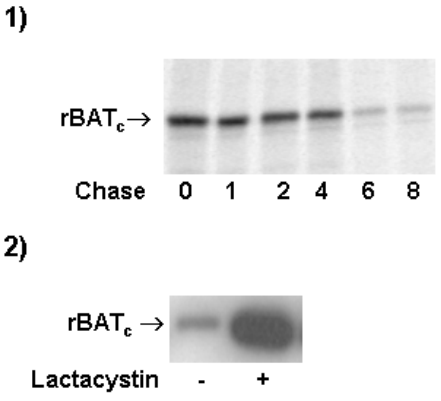

Sup. Figure B

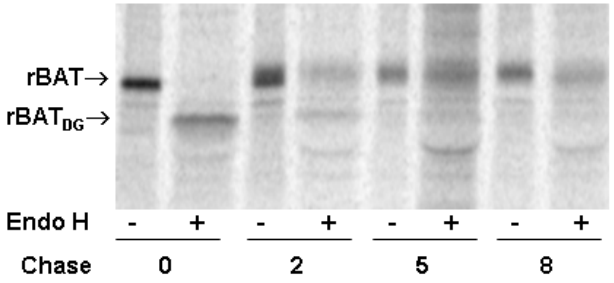

Sup. Figure C

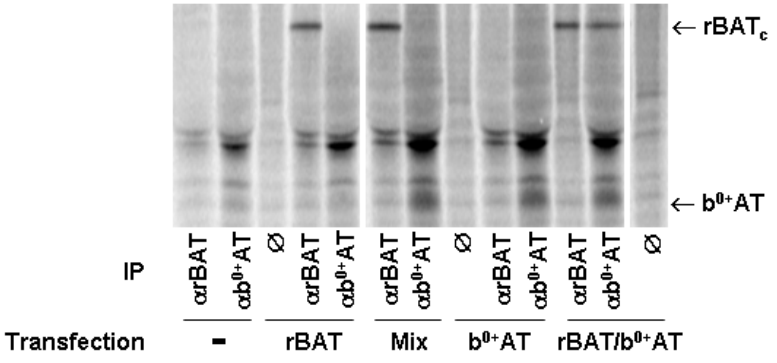
← rBAT$_c$
← b^{0+}AT
IP
αrBAT
αb^{0+}AT
Ø
αrBAT
αb^{0+}AT
αrBAT
αb^{0+}AT
Ø
αrBAT
αb^{0+}AT
αrBAT
αb^{0+}AT
Ø
Transfection
-
rBAT
Mix
b^{0+}AT
rBAT/b^{0+}AT